HAVcR-1 and the Prevention of Metastatic Disease in Human Prostate Cancer

by
Emily Jacqueline Ann Telford

A Dissertation Submitted to Cardiff University in Candidature for the Degree of
Doctor of Philosophy

Cardiff- China Medical Research Collaborative (CCMRC)
Cardiff University
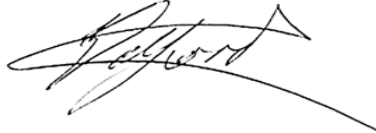Henry Welcome Building
Heath Park
CF14 4XN
United Kingdom

March 2019

Declaration and Statements

DECLARATION

This work has not been submitted in substance for any other degree or award at this or any other university or place of learning, nor is being submitted concurrently in candidature for any degree or other award.
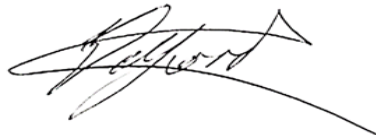
Signed .... Date: 14/03/2019

STATEMENT 1

This thesis is being submitted in partial fulfilment of the requirements for the degree of PhD

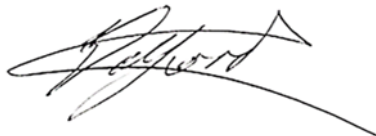Signed .... Date: 14/03/2019

STATEMENT 2

This thesis is the result of my own independent work/investigation, except where otherwise stated, and the thesis has not been edited by a third party beyond what is permitted by Cardiff University's Policy on the Use of Third-Party Editors by Research Degree Students. Other sources are acknowledged by explicit references. The views expressed are my own.

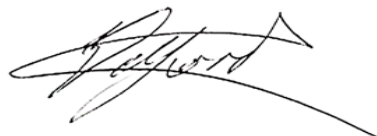Signed .... Date: 14/03/2019

STATEMENT 3

I hereby give consent for my thesis, if accepted, to be available online in the University's Open Access repository and for inter-library loan, and for the title and summary to be made available to outside organisations.

Signed .... Date: 14/03/2019

Acknowledgments

Publications

Abstracts

Martin TA, Telford E and Jiang WG. HAVCR1 is a potential prognostic factor in human breast cancer. *Anticancer Research*. 2015 July; 35 (7) :4327.

Reviews

Telford EJA, Jiang WG and Martin TA. HAVcR-1 involvement in cancer progression. Histology and Histopathology. 2017 Feb; 32 (2): 121-128

Conference Attendance

Poster Presentations

China UK Cancer (CUKC) Conference in Cardiff in July 2015

Cancer Research Wales 50th Anniversary Symposium in Cardiff in March 2016

Oral Presentations

Capital International Cancer Conference 2015 in Beijing in October 2015

CUKC Conference in Beijing in April 2017

Abbreviations

(cc)RCC	(clear cell) Renal Cell Carcinoma
ACTH	Adrenocorticotropic Hormone
ADAM	A disintegrin and metalloprotease
ADC	Antibody Drug Conjugate
ADT	Androgen Deprivation Therapy
AF	Activation Function
AGMK	African green monkey kidney cells
AJs	Adherens Junctions
ANOVA	Analysis of Variance
AP2	Activator Protein-2
AR	Androgen Receptor
AR-Vs	Androgen Receptor Splice Variants
ATAD2	ATPase family AAA domain-containing protein 2
ATCC	American Tissue Culture Collection
ATP	Adenosine Triphosphate
BAD	BCL-2 antagonist of cell death
bFGF	Basic Fibroblast Growth Factor
BM40	Basement Membrane Protein 40
BPE	Benign Prostatic Enlargement
BPE	Bovine Pituitary Extract
BPH	Benign Prostatic Hyperplasia
BRCA1/2	Breast cancer susceptibility gene 1/2
BSA	Bovine Serum Albumin

CAPZB	Capping Actin Protein of Muscle Z-Line Beta Subunit
CAR	Coxsackievirus and Adenovirus Receptor
c-Cbl	casitas B-lineage lymphoma
CCL21	C-C motif ligand 21
CCR7	C-C motif chemokine receptor 7
CD44	Cluster of Differentiation 44
CE	Cryptic Exon
CHEK2	Checkpoint kinase 2
CPE	*Clostridium perfringens* enterotoxin
CPPS	Chronic Pelvic Pain Syndrome
CRH	Corticotropin-releasing hormone
CRPC	Castrate Resistant Prostate Cancer
CT scan	Computerised Tomography Scan
CT	Calcitonin
C-terminus	Carboxyl-terminus
CTL	Cytotoxic T-leucocyte
CXCL12	C-X-C motif ligand 12
CXCR4	C-X-C chemokine receptor 4
CYP17	Cytochrome p17
DAPI	4',6-diamidino-2-phenylindole
DBD	DNA Binding Domain
dEP1	density enhance phosphatase 1
DEPC	Diethylpyrocarbonate
DHT	Dihydrotestosterone

DMEM	Dulbecco's modified Eagle's medium
DMSO	Dimethylsuphoxide
DNA	Deoxyribonucleic acid
DRE	Digital Rectal Examination
DS	Desmosomes
EC	Extracellular
E-Cadherin	Epithelial Cadherin
ECIS	Electric Cell-Substrate Impedance Sensing
ECM	Extracellular Matrix
EDTA	Ethylenediaminetetracetic acid
EGF	Epidermal Growth Factor
EGFR	Epidermal Growth Factor Receptor
ELISA	Enzyme-Linked Immunosorbent Assay
EMT	Epithelial to Mesenchymal Transition
EPAC2	Exchange protein directly activated by cAMP2
EPLIN	Epithelial Protein Lost In Neoplasm
ERK	Extracellular Regulated Kinases
ERSPC	The European Randomised Study for Prostate Cancer
E-selectin	endothelial selectin
ETs	E-twenty-six
F-actin	Filamentous Actin
FCS	Foetal Bovine Serum
FITC	Fluorescein isothiocyanate
FlnA	Filamin-A

GAP	GTPase activation Proteins
GEF	Guanine Nucleotide Exchange Factor
GEO	Gene Expression Omnibus
GJs	Gap Junctions
GK	Guanylate kinase
GnRH	Gonadotropin Releasing Hormone
GSK-3β	Glycogen Synthase Kinase 3 beta
GTP	Guanosine Triphosphate
HAV	Hepatitis A virus
HAVcR-1	Hepatitis A virus cellular receptor (HAVcR-1)
HGF	Hepatocyte Growth Factor
HIF-1	Hypoxia Inducible Factor 1
HIFU	High Intensity Focused Ultrasound
HIV	Human immunodeficiency virus
HLA	Human Leucocyte Antigen
HPC1	Hereditary Prostate Cancer 1
HPV	Human Papilloma Virus
HRE	Hormone Response Elements
HSP	Heat Shock Protein
IF	Immunofluorescent
Ig	Immunoglobulin
IGF	Insulin-like growth factor
IHC	Immunohistochemical
IL	Interleukin

JAMs	Junctional Adhesion Molecules
JNK	c-Jun N-terminal Kinase
KIM-1	Kidney injury molecule 1
KLK2	Kallikrein Related Peptidase 2
LB	Liquid Broth
LBD	Ligand Binding Domain
LH	Luteinizing Hormone
LLG1	Lethal Giant Larvae 1
LRP5/6	Low-density Lipoprotein receptor-related protein 5
MAGUK	Membrane-Associated Guanylate Kinase
MAPK	Mitogen-activated Protein Kinase
MET	Mesenchymal to Epithelial Transition
MBD	Met Binding Domain
MEK1	MAPK/ERK kinase 1
MMP	Matrix Metalloproteases
MRI	Magnetic Resonance Imaging
MSR1	Macrophage Scavenger Receptor 1
MT1	Membrane-type 1
MUC1	Mucin 1
N-Cadherin	Neural Cadherin
NES	Nuclear Export Signal
NLS	Nuclear Localisation Signal
N-selectin	neuronal selection
NTD	N-Terminal Transactivation Domain

N-terminus	Amino-terminus
Pax3	Paired Box 3
P-box	Permutation box
PBS	Phosphate Buffer Saline
P-Cadherin	Placental Cadherin
PCP	Paracellular Permeability
PCR	Polymerase Chain Reaction
PEDGF	Platelet Derived Growth Factor
PKA/C/G	Protein Kinase A/C/G
PMA	Propidium Monozide
PMH	Phenyl-Methylene Hydantoin
PON1	Paraoxonase 1
PP1/2A/2B	Protein Phosphatase 1/2A/2B
ProtecT	Prostate Testing for Cancer and Treatment
PSA	Prostate Specific Antigen
PTB	Phosphotyrosine Binding
PTP	Protein tyrosine phosphatases
PVDF	Polyvinylidene Fluoride
qPCR	Quantitative Polymerase Chain Reaction
Rac	Ras-related C3 botulinum toxin substrate
Ras	Rat Sarcoma
R_b	Barrier Resistance
R-Cadherin	Retinal Cadherin
Rho	Ras homology

RNA	Ribonucleic Acid
RNASEL	Ribonuclease L
ROCK	Rho-associated protein Kinase
RPMI	Roswell Park Memorial Institute
RT	Reverse Transcriptase
SDS	Sodium Dodecyl Sulphate
SEM	Standard Error of the Mean
SF	Scatter Factor
SFM	Serum Free Medium
SH3	Src Homology 3
SHBG	sex hormone binding globulin
sLe	sialyl Lewis
SPARC	Secreted Protein Acidic and Cysteine Rich
SPH	Serine Proteinase Homology
TAU	Transcriptional Activation Units
TBE	Tris-Borate-EDTA
Tcf-4	Transcription Factor 4
TER	Transepithelial/Transendothelial Resistance
TF	Transcription Factor
TGF-β	Transforming Growth Factor β
TIM-1	T-cell immunoglobulin and mucin domain containing molecule 1
TJs	Tight Junctions
TM	Transmembrane

TMPRSS2	Transmembrane protease serine 2
TNM staging	Tumour, Lymph Node and Metastasis staging
TPBS	Tween PBS
TPR	Translocating promoter region
TRITC	Tetramethylrhodamine isothiocyante
TRUS	Trans-rectal Ultrasound
TURP	Transurethral Resection of the Prostate
VEGF	Vascular Endothelial Growth Factor
WB	Western Blotting Analysis
WCB	Wales Cancer Bank
ZO	Zonula Occludin
ZONAB	ZO-1 Associated Nucleic Acid-Binding Protein

Summary

Introduction: Prostate cancer is a significant burden in the UK, despite continuing research our understanding of disease progression and at present treatment options are still limited. In small studies, Hepatitis A virus cellular receptor (HAVcR-1) has been linked to cancer aetiology and may regulate junctional complexes. Its role in prostate cancer remains unexplored. This study aimed to investigate the expression of HAVcR-1 in prostate cancer samples and explore the cellular and molecular impact of HAVcR-1, with particular focus on junctional complexes, using *in vitro* models.

Methods: Clinical serum samples from prostate cancer patients were tested for HAVcR-1 ectodomain levels through enzyme-linked immunosorbent assay. Clinical prostate cancer samples were tested for the expression of HAVcR-1 through immunohistochemistry. Cell models based on bone metastatic site prostate cancer (PC-3) and normal prostate epithelia (PZ-HPV-7) were employed to evaluate the influence of HAVcR-1 on cellular functions involved in cancer aetiology by use of in *vitro* functional assays. Cell signalling changes were explored by was or Kinex™ antibody microarray, western blotting analysis, immunofluorescence and polymerase chain reaction (PCR)

Results: Levels of HAVcR-1 ectodomain in the serum of patients decreased in the serum of prostate cancer patients compared to healthy controls. Within prostate cancer patients ectodomain levels had no correlation to Gleason score. Histologically, total protein and gene expression of HAVcR-1 were increased in prostate cancer. Manipulation of HAVCR-1 levels within PC-3 cells had no impact on cell growth, invasion, adhesion, transepithelial resistance (TER) and paracellular permeability (PCP). Increased HAVcR-1 expression did however result in decrease PC-3 wound healing. Both increased as well as decreased HAVcR-1 expression increased constrain on current flow beneath cells during initial attachment and spreading as well as decreased barrier function resistance during electrical wound healing. Overexpression of HAVcR-1 in PZ-HPV-7 cells increased invasive potential, adherence to a cell matrix, whilst no changes in migration, TER, PCP and barrier function resistance were observed. At a protein level phosphorylation of β-catenin Y333 was observed in PZ-HPV-7 cells overexpressing HAVcR-1. Further analysis revealed HAVcR-1 overexpression decreased membranous E-cadherin, increased nuclear β-catenin and increased Cyclin D1 protein expression within PZ-HPV-7 cells.

Conclusion: This study preliminary shows HAVcR-1 expression and ectodomain release coincides with the presence of prostate cancer thus indicating a potential of HAVcR-1 as a biomarker to aid in diagnostics. Furthermore, it also potentially indicates the involvement ofHAVcR-1 in cancer development, altering cancer associated cellular behaviours. Initial evidence from this study implicates HAVcR-1 in the process of EMT and the dysregulation of junctional complexes. Therefore, highlighting the potential involvement of HAVcR-1 in prostate cancers development and metastatic potential. Differences between cell models may suggest differences in signalling pathways that involve HAVcR-1 and thus further research is required to characterize HAVcR-1 signalling.

Figures

Tables

Contents

Chapter I:

Introduction

1.1 Prostate cancer

1.1.1 The Prostate Gland

The prostate is an exocrine gland found exclusively in mammals, it is comparable to a walnut in shape and size; being approximately 4 cm long and 2 cm wide. The prostate is located dorsally to the symphysis pubis at the base of the bladder where it surrounds a portion of the urethra, known as the prostatic urethra, and the two ejaculatory ducts (See Figure 1.1). The prostate is composed of a smooth muscle capsule and numerous smooth muscle partitions that radiate inwards towards the urethra [1]. A layer of pseudostratified columnar secretory epithelial cells cover these muscular partitions forming ducts with non-secretory basal epithelial cells interspaced along the basal lamina (See Figure 1.1) [2, 3]. These prostatic ducts originate from the urethra and radiate peripherally to completely surround the urethra. The stromal component of the prostate is not fully composed of smooth muscle cells but of all cellular and extracellular elements outside of the epithelial basal lamina, including fibroblasts, blood vessels and associated pericytes, wandering connective tissue cells, nerve terminals and lymphatics, all of which are embedded in a loose collagenous extracellular matrix [3].

A main role of the prostate is in male ejaculation via the production of the fluid components of semen [2]. During ejaculation prostatic secretions are discharged from prostatic ducts into the prostatic urethra and transported down the urethra by muscular contractions [3]. Prostate secretions have a relatively high pH which aids in the neutralisation of the acidic urethra and secretions of the testes and vagina. These secretions contain clotting factors resulting in the transient coagulations of semen

via the conversion of fibrinogen, secreted from the seminal vessels, into fibrin. This coagulation keeps the semen as a single mass for a few minutes after ejaculation, at which time fibrinolysis occurs resulting in the dissolution of the coagulum and the release of sperm cells [1].

There are three main conditions which affect the prostate: benign prostatic hyperplasia (BPH), prostatitis and prostate cancer. BPH, also termed enlarged prostate and benign prostatic enlargement (BPE), is the most common. Mainly occurring in men after the age of 50, BPH is associated with restricted urination. Prostatitis by comparison can affect men of any age; however, it is most typical in men between aged 30 and 50. Prostatitis describes the set of symptoms thought to be caused by infection or inflammation and can be divided into four types: chronic pelvic pain syndrome (CPPS), acute bacterial prostatitis, chronic bacterial prostatitis and asymptomatic prostatitis. Similarly to BPH, prostatitis commonly results in restriction of urination however, pain and discomfort around the testis, rectum or lower abdomen may also occur [4]. The third condition is prostate cancer, which is the main focus of this study and will be explained in detail in the upcoming sections.
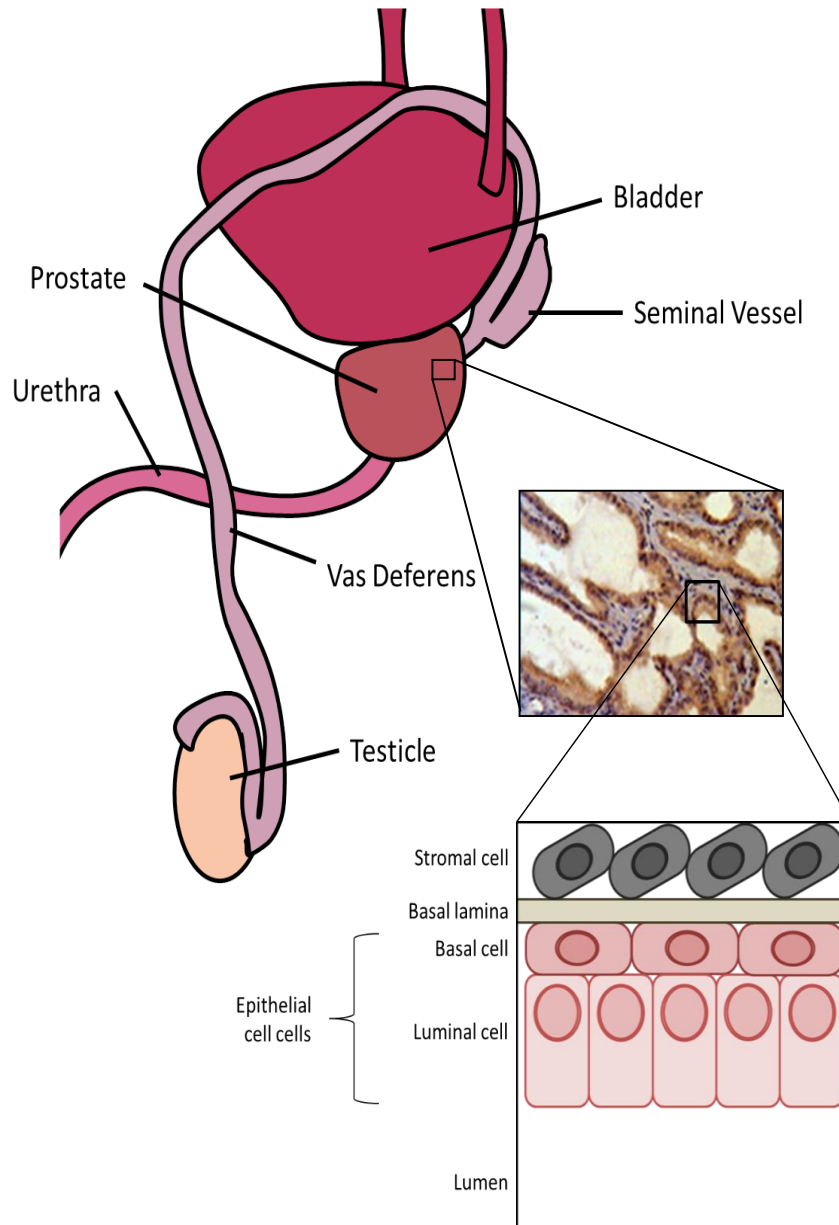
Figure 1.1. The Prostate Gland.
Adapted from [2, 3]. Representation of the prostate gland: location, appearance at a cellular level and cellular components.

1.1.2 Prostate Cancer Statistics

1.1.2.1 UK Statistics

In the United Kingdom (UK), prostate cancer is the most common cancer in males and the fourth most common cause of deaths due to cancer. Prostate cancer accounts for approximately a quarter of cancer cases in males, there are 46689 diagnoses of and 11287 deaths due to prostate cancer per year in the UK (See Figure 1.2.A) [5]. The disease generally occurs in men over 50 years of age, with only 0.1 % of cases occurring in males under 50 years of age and 85 % of cases occurring in males aged 65 and above [6-8]. There is therefore a correlation between age and incidence of prostate cancer (See Figure 1.2.B). Over time there has been a shift towards a younger diagnostic age, with the percentage of cases being diagnosed in males aged 75 and above decreasing from 46 % in 1979-1981 to 36 % in 2010-2012. However, rather than an earlier onset this is most likely to be due to earlier diagnosis of prostate cancer [8]. Prostate cancer incidence has been increasing over time with a 147 % increase in the UK between 1979-1981 and 2010-2012 and this can also be somewhat attributed to better diagnostics as well as an aging population (See Figure 1.2.C) . Prostate cancer mortality rates are also strongly associated with age, with 99 % of prostate cancer deaths occurring in men aged 55 and older and 75 % occurring in men aged 75 and older (See Figure 1.2.B) [9]. This mortality rate has been decreasing since the peak in the late 1980's/ early 1990's, with a 21 % decrease between 1991-1993 and 2010-2012. This is also attributed to earlier diagnosis as well as improved treatment (See Figure 1.2.C) [10].

1.1.2.2 European Statistics

In Europe, prostate cancer is the most common cancer in males, the third most common cancer overall and is the sixth most common cause of cancer death [11]. There are approximately 400364 diagnoses and 92328 deaths of prostate cancer per year [12].

1.1.2.3 Worldwide Statistics

Worldwide, prostate cancer is the second most common cancer in males and the fifth most common cancer overall [13]. In terms of mortality prostate cancer is the fourth most common cause of cancer deaths in males and the eighth most common cause of cancer death overall. There are approximately 1278106 new cases and 358989 deaths per year worldwide [14].

A

Prostate Cancer Incidences and Deaths by Country in the UK

B

Prostate Cancer Age Related Incidence and Mortality Rates in the UK

C

Prostate Cancer Year Specific Incidence and Mortality Rates in the UK
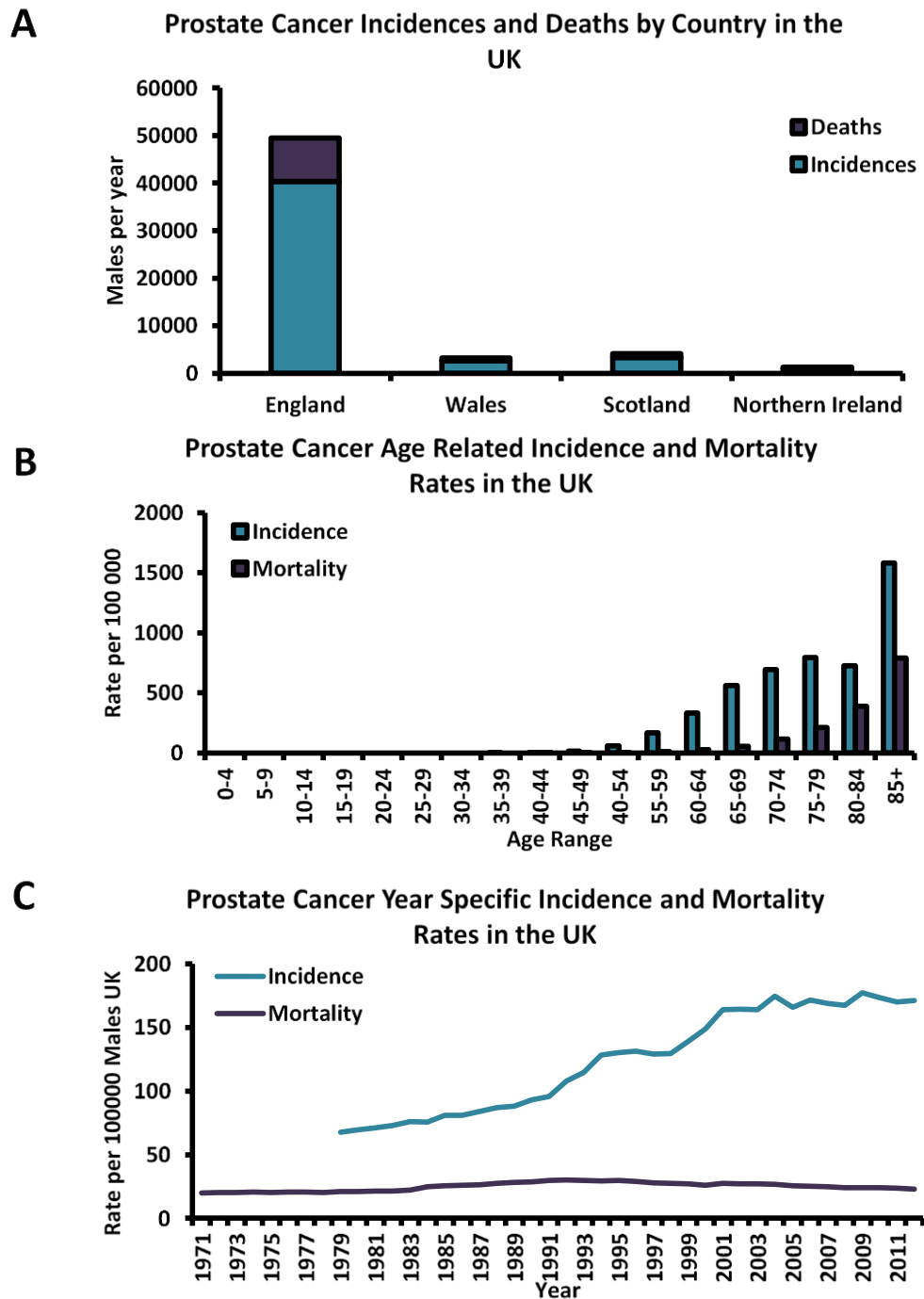
Figure 1.2 Prostate Cancer Statistics.
Adapted from [15]. **A** Graph showing number of prostate cancer incidences and deaths in each country of the UK in 2012. **B** Graph showing prostate cancer incidence and mortality rates per 100000 in the UK in 2012 separated into age range. **C** Graph showing yearly prostate cancer incidence and mortality rate per 100000 males in the UK.

1.1.3 Risk and Preventative Factors

There is a 1 in 8 lifetime risk of prostate cancer in the UK [16]. As previously discussed, incidence of prostate cancer is strongly correlated to age. However, age is not the only risk factor, others are detailed below.

1.1.3.1 Family History, Genetics and Ethnicity

Inherited factors are thought to explain an estimated 5-10 % of prostate cancer cases [17]. The risk of prostate cancer increases if a first degree relative (father, brother or son) has been previously been diagnosed [18]. Although generally associated with breast cancer, an increased risk of prostate cancer has also observed with BRCA1 and BRCA2 gene mutations [19, 20].

The lifetime risk of developing prostate cancer increases to 1 in 4 in black men (black African, black Caribbean and black other but not black mixed) [16]. Age standardised rates for white males is 97 in every 100000 men and this increases in black males to 203 in every 100000 men [7].

Other genetic variations implicated in prostate cancer include: HPC1, EPAC2, RNASEL, MSR1, HPCX, HPC20 and vitamin D receptor [21]. Interestingly, genetic polymorphisms have also been reported as important in androgen metabolism including: genes for the androgen receptor, 5α reductase type 2 and steroid hydroxylase [22].

1.1.3.2 Other Risk Factors

Being overweight has also been linked to increased risk of advanced prostate cancer, though this may be due to late diagnosis. Other risk factors include dietary factors

(animal fat and calcium), smoking, alcohol consumption as well as previous vasectomy [21].

1.1.3.3 Preventative Factors

Contrary to black males, men of Asian ethnicity have a decreased risk of developing prostate cancer; with age standardised rates decreasing from 97 per 100000 men for white males to 49 per 100000 men for Asian males [7].

1.1.4 Prostate Cancer Aetiology

1.1.4.1 Androgen Signalling Cascade

Androgens are the male sex hormone of the steroid hormone family, which are mainly produced in the testes, ovaries and adrenals [23]. Testicular androgen is imperative for the male phenotype differentiation process as well as the maintenance of male reproductive function and gender dependent parameters including: bone and muscle mass and behaviour [23]. Testosterone, the androgenic steroid, is the precursor for dihydrotestosterone (DHT) and oestrogens. Both testosterone and DHT are ligands for the androgen receptor (AR), a nuclear transcription factor and member of the steroid hormone receptor superfamily of genes [23, 24].

The human AR is a 110 kDa protein consisting of approximately 919 amino acids, however this may vary due to variable length stretches of poly-glutamine and poly-glycine. The AR is encoded by a single copy number gene, consisting of 8 exons, located on the X chromosome (q11-12) [23, 25]. The AR is composed of four domains: an N-terminal transactivation domain (NTD), a DNA binding domain (DBD), hinge region and a C-terminal ligand binding domain (LBD) (See Figure 1.3.A). The NTD is encoded by exon 1 and is thought to be constitutively active, it contains transcription

activation function (AF-1) composed of two transcriptional activation units (TAU): TAU 1 and TAU 5. TAU5 is responsible for the majority of constitutive activity and is able to remain active even with LBD deletion [24, 26]. The DBD is encoded by exons 2 and 3 and contains two zinc finger motifs. The first contains a P-box motif that makes base specific contacts thus co-ordinating gene specific nucleotide contacts within the DNA groove, whilst the second contains a D-box motif functioning as a DBD/DBD binding site for DNA- dependent receptor homo-dimerization. The hinge region is a flexible linker between the DBD and LBD containing the nuclear localisation sequence (NLS). Filamin-A (FlnA), a cytoskeletal protein interacts with DBD, hinge region and LBD facilitating AR translocation to the nucleus. There also exist Ran and importin/ β-dependent NLS in the DBD and importin/ β-independent NLS in the NTD and LBD. The ligand binding domain facilitates ligand binding to the AR. It also contains an AF-2, which interacts with co-regulators [23, 24].

The AR is held inactive in the cytoplasm by association with heat shock proteins (HSP) and activation results from the binding of androgens. Testosterone is mainly produced in the testes with a small contribution from the adrenal glands. It is secreted into the circulatory system where the majority is bound to albumin and sex hormone binding globulin (SHBG). A minority of testosterone is freely dissolved in the serum and can enter the prostate where 90 % of it is converted to the more active metabolite DHT by 5α-reductase. Both DHT and testosterone can bind to the AR causing a conformational change and leading to the dissociation of HSP and receptor phosphorylation and thus activation [27, 28]. This activation allows the dimerization and translocation of AR into the nucleus, where, via interactions hormone response elements (HRE), commonly located within the regulatory regions of target genes, as

well as interactions with co-factors, the AR induces the formation of a stable pre-initiation complex near to the transcription start site, resulting in the expression of these genes [26, 29]. Ligand dissociation occurs and the AR is shuttled back to the cytoplasm where it can re-associate with HSP and process can repeat [30]. The genes transcribed due to AR signalling include: PSA, TMPRSS2, KLK2 and ATAD2 [31]. PSA is a kallikrein-related serine protease which is secreted into the blood and increased tumour burden correlates with increased detectable serum PSA, making PSA the key biomarker in the clinical monitoring of prostate cancer development and progression [32, 33]. ATAD2 is an AR co-factor possessing both an AAA-type ATPase domain and a bromodomain which recognise acetylated histones to permit control of androgen-induced gene expression [34, 35]. ATAD2 overexpression promotes cell survival and proliferation and thus is tumorigenic in a number of prostate cancer subtypes (See Figure 1.3.B) [36]. Androgens and the activation of the androgen receptor are important in normal prostate gland growth, development and function as well as in prostate carcinogenesis and progression to androgen- independent disease [24, 37].
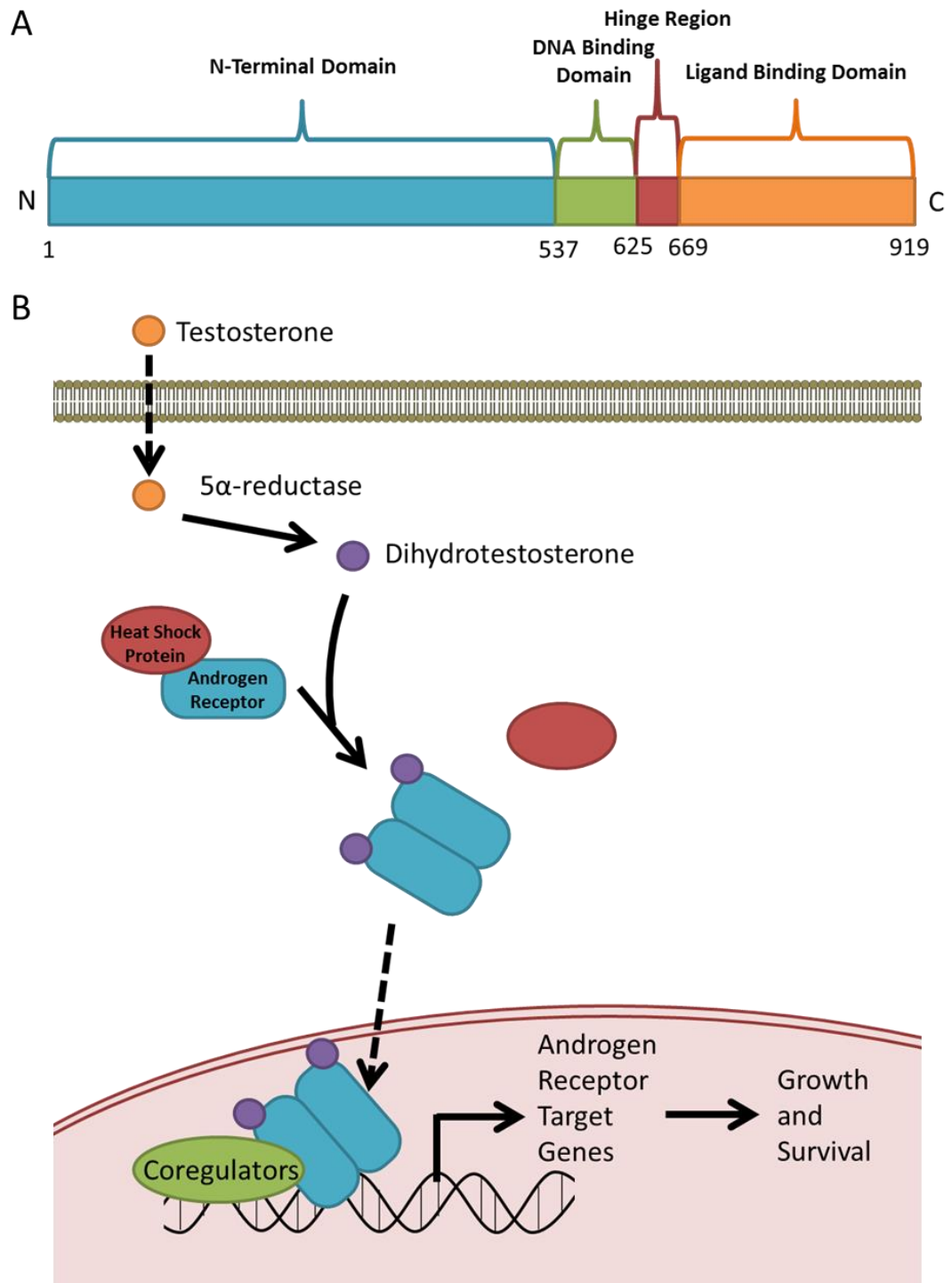
Figure 1.3. The Androgen Receptor.
Adapted from [24].**A** Representation of androgen receptor protein. **B** Major androgen signalling cascade

1.1.4.2 Progression to Castrate Resistant Prostate Cancer

The AR is expressed in the majority of primary prostate tumours and the majority of tumours are dependent on androgens at time of diagnosis [37, 38]. Androgens are the main regulators of the ratio of cells proliferating and those dying by stimulating proliferation and inhibiting apoptosis, thus prostate cancer depends on a crucial level of androgen signalling for growth and survival. Therefore, a possible treatment option of prostate cancer involves the reduction of the androgen signalling cascade resulting in cancer regression due to a decrease in proliferation and increased in apoptosis [28]. Unfortunately these therapies eventually fail in a median time of 12 to 18 months and the tumour progresses to a lethal, hormone refractory state, known as castrate resistant prostate cancer (CRPC) [28, 37, 39].

This progression from clinically localised naïve cancer to CRPC is due to aberrant AR signalling and can develop via a number of pathways involving a complex interplay of a network of signalling molecules. These pathways can be separated into four types: hypersensitivity, promiscuous, outlaw and splice variant (See Figure 1.4) [28]. The hypersensitivity pathways involves the overactivation of androgen signalling via AR amplification/overexpression, increased AR sensitivity, stability and nuclear localisation, co-regulator amplification or increased DHT production [28, 40-43]. The promiscuous pathways involve mutation of the AR, leading to decreased specificity and resulting in inappropriate activation by alternative ligands including: non-androgen steroids and AR antagonists [28, 41, 44]. Steroid hormone receptors that are activated by ligand independent mechanisms are referred as outlaw receptors, thus the outlaw pathway involves activation via phosphorylation of the AR due to cytokines and growth factors activating intracellular signalling cascades [24, 28, 37,

44]. AR splice variants (AR-Vs) have been found where by the native LBD is replaced by variant specific peptide sequences encoded by cryptic exons (CE) 1, 2, 3 and 2b. Due to the lack of a LBD, they exhibit ligand independent activity and thus are constitutively active [25, 45-47]. These pathways result in the reestablishment of AR signalling therefore allow the tumour to progresse and metastasize to secondary sites [28].
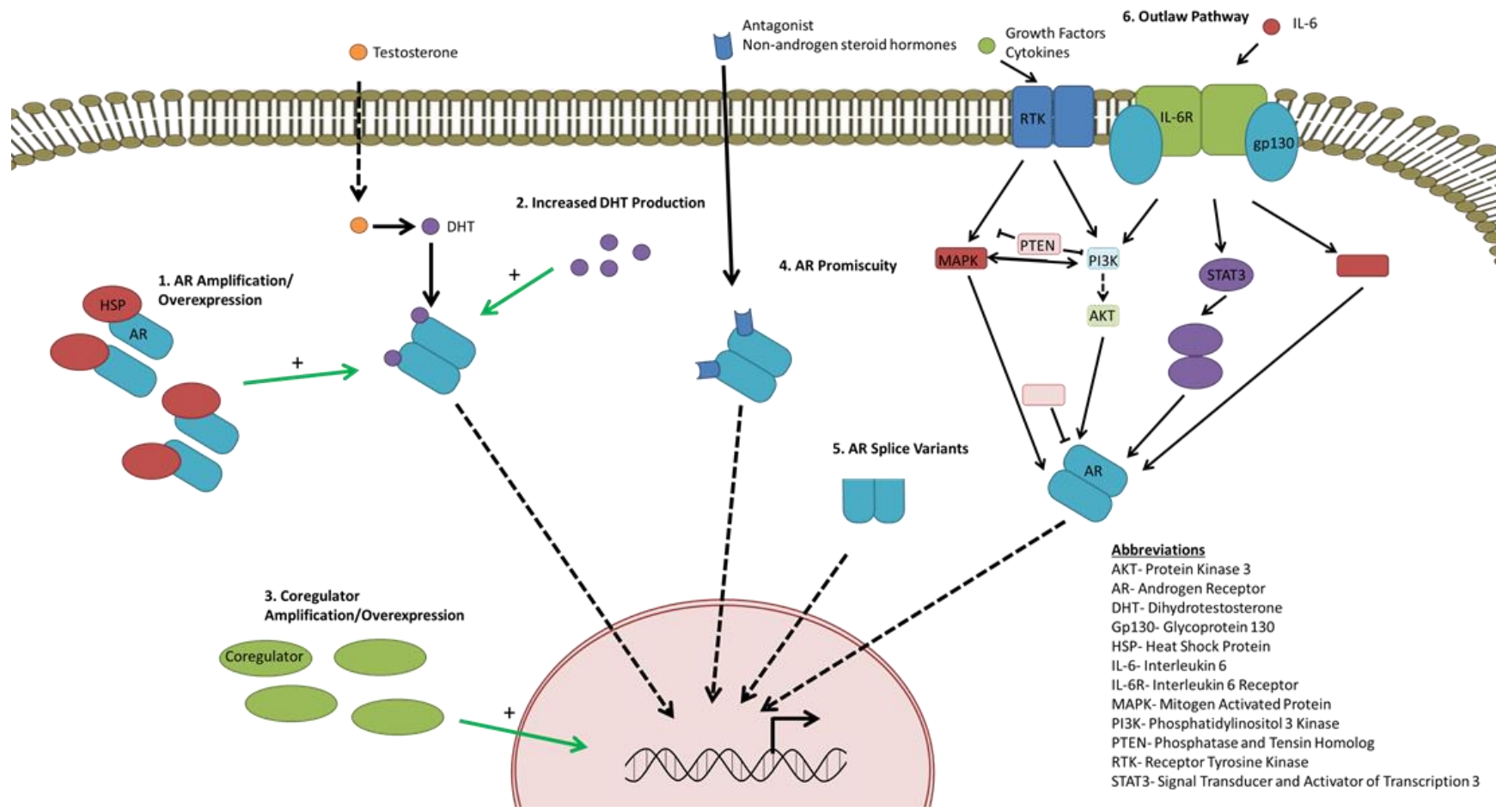
Figure 1.4 AR Signalling in CRPC.
Adapted from [28]. Representation of gain of AR signalling activity in CRPC

1.1.4.3 Prostate Cancer Metastasis

Metastasis is the process by which malignant cells leave the primary tumour and travel to distant sites to establish a secondary tumour [48]. Metastatic disease is responsible for approximately 90 % of cancer related deaths, however the process is in reality quite inefficient, with only ≤0.01 % of cancer cells that leave the primary tumour developing into metastases in animal models [49-51]. The progression from a localised primary tumour to metastatic cancer is reliant on an evolutionary process involving a series of mutations resulting in six alterations in cell physiology: self-sufficiency in growth signals, insensitivity to growth-inhibitory signals, evasion of apoptosis, limitless replicative potential, sustained angiogenesis and tissue invasion and metastasis [50]. There are three routes that cancer cells can take to metastasize: the circulatory system (haematogenous), lymphatic system (lymphatic) or body cavities (transcoelomic) (See Figure 1.5) [52]. The hematogenous route involves a series of steps: angiogenesis, cell dissemination, migration and invasion of stroma surrounding primary site, intravasation, circulation, extravasation, colonization and angiogenesis in secondary site [53].
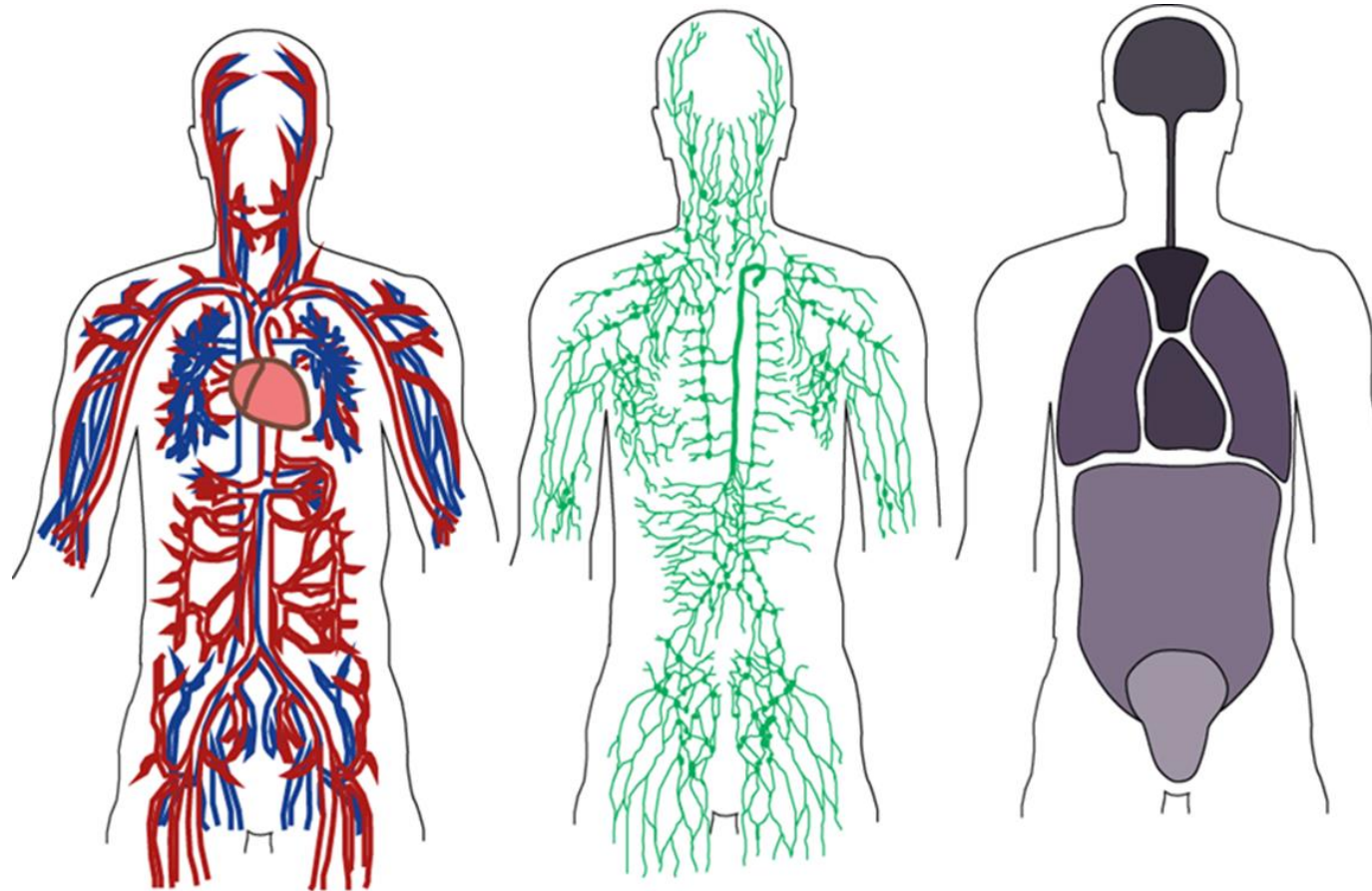
Figure 1.5. Routes of Metastasis.
Adapted from [52, 54, 55]. Representation of the three possible routes of metastasis: haematogenous, lymphatic and body transcoelomic respectively.

Angiogenesis

A tumour can only grow to a size of 1 mm in diameter due to diffusion distance from the circulatory system before angiogenesis is required to support its metabolic requirements [48, 56]. The hypoxic microenvironment of these tumours can then activate angiogenesis via the up regulation of hypoxia-inducible factor-1 (HIF-1) and other molecules, creating an imbalance in angiogenic factors. This imbalance is established by cancer cells, surrounding stromal cells, tumour associated macrophages and other components of the extracellular matrix (ECM) [48, 57]. The result is an increase in pro-angiogenic factors including: vascular endothelial growth factor (VEGF), basic fibroblast growth factor (bFGF), hepatocyte growth factor (HGF) and platelet-derived growth factor (PDGF) as well as a decrease in anti-angiogenic factors including: angiostatin and thrombospondin-1 [48, 58]. Thus angiogenesis can occur via the partial degradation of the surrounding ECM, endothelial cell proliferation and migration, vascular loop formation and basement membrane development (See Figure 1.6) [48].

Pro-angiogenic Factors:
Vascular endothelial growth factor (VEGF),
basic fibroblast growth factor (bFGF),
platelet-derived growth factor (PDGF)

Anti-angiogenic Factors:
Angiostatin, Thrombospondin-1

Hypoxia

1 mm tumour

Extracellular
Matrix
Degradation

Proliferation

Migration

Tube
Formation

Loop
Formation
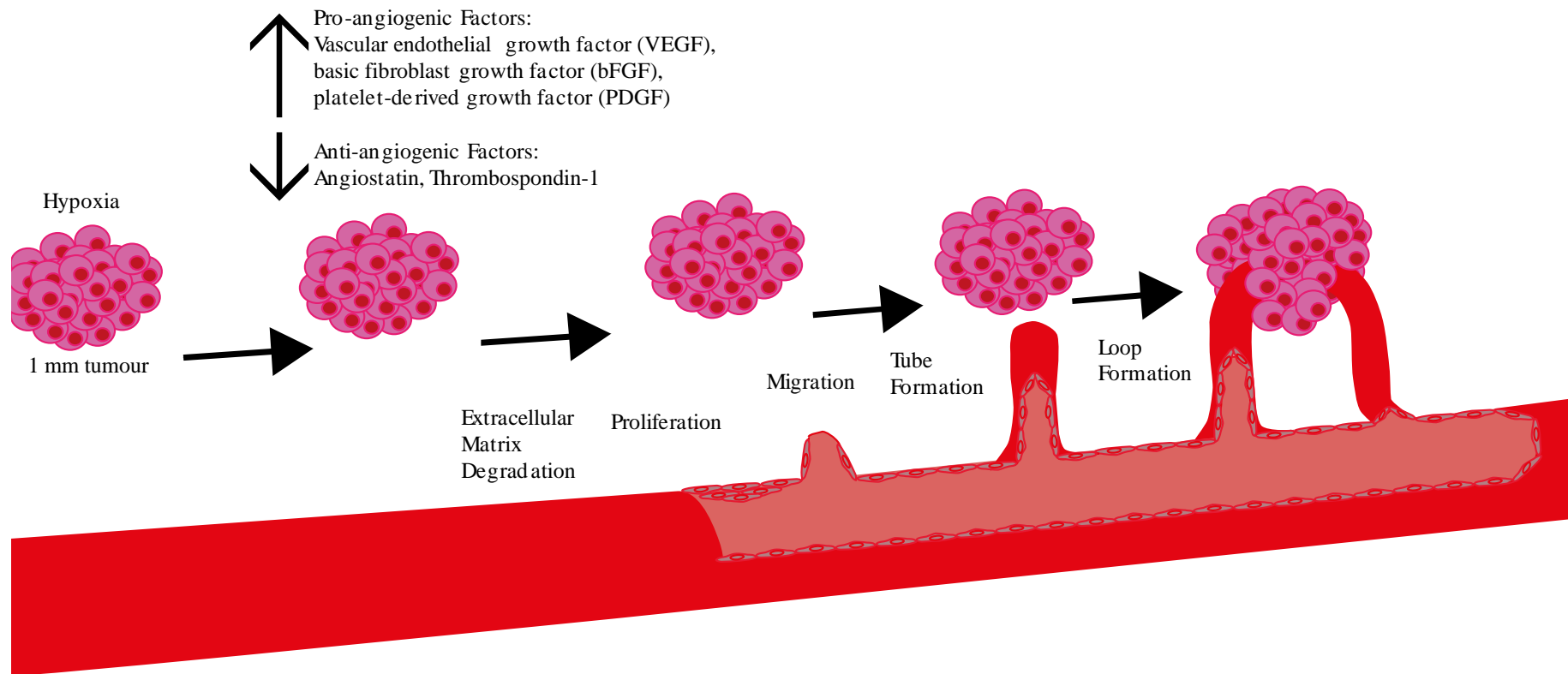
Figure 1.6. Angiogenesis.
Adapted from [59]. Representation of the stages of angiogenesis

Metastasis

The next step in metastasis is cancer cell dissemination from the tumour, local migration and invasion [48]. Epithelial cell have a restricted migratory capability partly due to the basement membrane as well as cell-cell adhesion which is maintained by junctions including adherens junctions (AJs) and tight junctions (TJs) [53]. This adhesion between neighbouring cancer cells must be overcome; however adhesion mechanisms are required for migration, thus adhesion mechanisms are not lost but disordered in these cancer cells [48, 60]. This is achieved via the reduced expression of adhesion molecules required for epithelial -epithelial cell adhesion such as epithelial (E)-cadherin but with a concurrent increased expression of adhesion molecules required for cancer cell-ECM adhesion such as integrin α6β1 [48, 53, 61, 62]. Depending on the environment the migration of single cells occur via two modes: elongated/ mesenchymal migration or rounded/ amoeboid migration, however they can also migrate as a cell group [63-65]. The Rho family of GTPases are key regulators of cell adhesion, with Rac1 promoting the formation of large membrane protrusions called lamellipodia that drive motility and Rho A and Rho C can recruit the ROCK family of kinases that phosphorylate cytoskeletal proteins promoting actin stress fibre production and resulting in the generation of contractile force [66-68]. Local invasion, whereby cancer cells extend and penetrate neighbouring tissues, is a prerequisite for cancer metastasis [69]. Local invasion requires the degradation of the surrounding stroma, mainly the basement membrane and interstitial connective tissue which is achieved via the use of proteases including: matrix metalloproteinases (MMPs), serine proteinases, cysteine proteinases and aspartyl proteinases [48, 53].

Cells enter the circulation by migrating through the vessel wall, this is known as intravasation, which can be separated into two types: paracellular intravasation where the cell migrates between endothelial cells which requires disruption of endothelial junctions and transcellular intravasation whereby the cell migrates through the endothelial cell body [65]. The new blood vessels generated by angiogenesis generally have weak cell-cell junctions and factors including: VEGF and transforming growth factor β (TGFβ) decrease the barrier function allowing for the transient disruption of junctions and the paracellular intravasation of cancer cells [65, 70].

Once within the circulatory system cancer cells must survive physical damage from hemodynamic shear force as well as evade the immune system [49, 52]. Cancer cells may evade the immune system by decreasing the amount of class 1 human leucocyte antigen (HLA) expressed and preventing cytotoxic T-leucocyte (CTL) mediated killing [48]. Cells circulate as part of a fibrin clot surrounded by other tumour cells and platelets and leukocytes forming a microembolis which aids in protection against sheer stress and obstructs capillaries, facilitating arrest in the microvasculature [48, 52]. The interaction between cancer cells and endothelial cells is thought to be comparable to leucocyte trafficking and extravasation at inflammatory sites via the 'dock and lock' mechanism [71]. Cells arrest on endothelium by low-affinity binding between E-selectin and ligands sialyl Lewis a or x (sLe^a or sLe^x) or CD44 as well as neuronal selectin (N-selectin) homophilic interactions. Firmer cell adhesion is achieved by integrins, CD44 and mucin 1 (MUC1). Cells can then extravasate, which similarly to intravasation can be transendothelial or paracellular [48, 65]. The cancer cell must then invade the basement membrane, penetrate the local parenchyma and

establish a microenvironment conducive to tumour survival and proliferation [52, 56, 65].

Extravasation could theoretically occur in any organ, however cancer types generally show organ specific metastasis patterns, with prostate cancer metastasising to the liver, lungs, pleura, adrenal glands, brain, lymph nodes and most predominantly to the bone (See Figure 1.7) [51-53, 56, 72]. Organ specificity was first explained by Stephen Paget's 'seed and soil' model, whereby the cancer cell (seed) will only metastasise to specific organs (soil) well suited for tumour growth [73]. This model was contested by James Ewing who proposed a mechanical model in which the metastatic pattern was due to circulatory and lymphatic flow from the primary tumour [74]. It is now widely accepted that both mechanical factors and organ suitability are important as well as chemoattractant homing whereby cells move to organs expressing specific molecules [48]. Chemoattractant factors include: the minor bone matrix protein osteonectin (also known as SPARC/ BM40), TGF-β1 secreted by osteoblasts, epidermal growth factor (EGF) expressed by lymph node and medullary bone stroma, insulin like growth factors 1 and 2 (IGF1 and IGF2), HGF acting via the Met receptor and collagen peptides [48, 75-80]. Chemokines have also been implicated in cancer cell homing, they are thought to cooperate with adhesion receptors thus determining cell arrest and extravasation site. CXCL12 and CCL21 are ligands for CXCR4 and CCR7 receptors respectively. Both receptors are expressed on breast cancer cells and distinct tissue distribution of ligands at main metastatic breast cancer sites suggests they may be important in chemotaxis and the localisation of metastasis of breast cancer. CXCL12-CXCR4 chemotaxis has been suggested to also be important in prostate cancer metastasis [48, 52, 81].
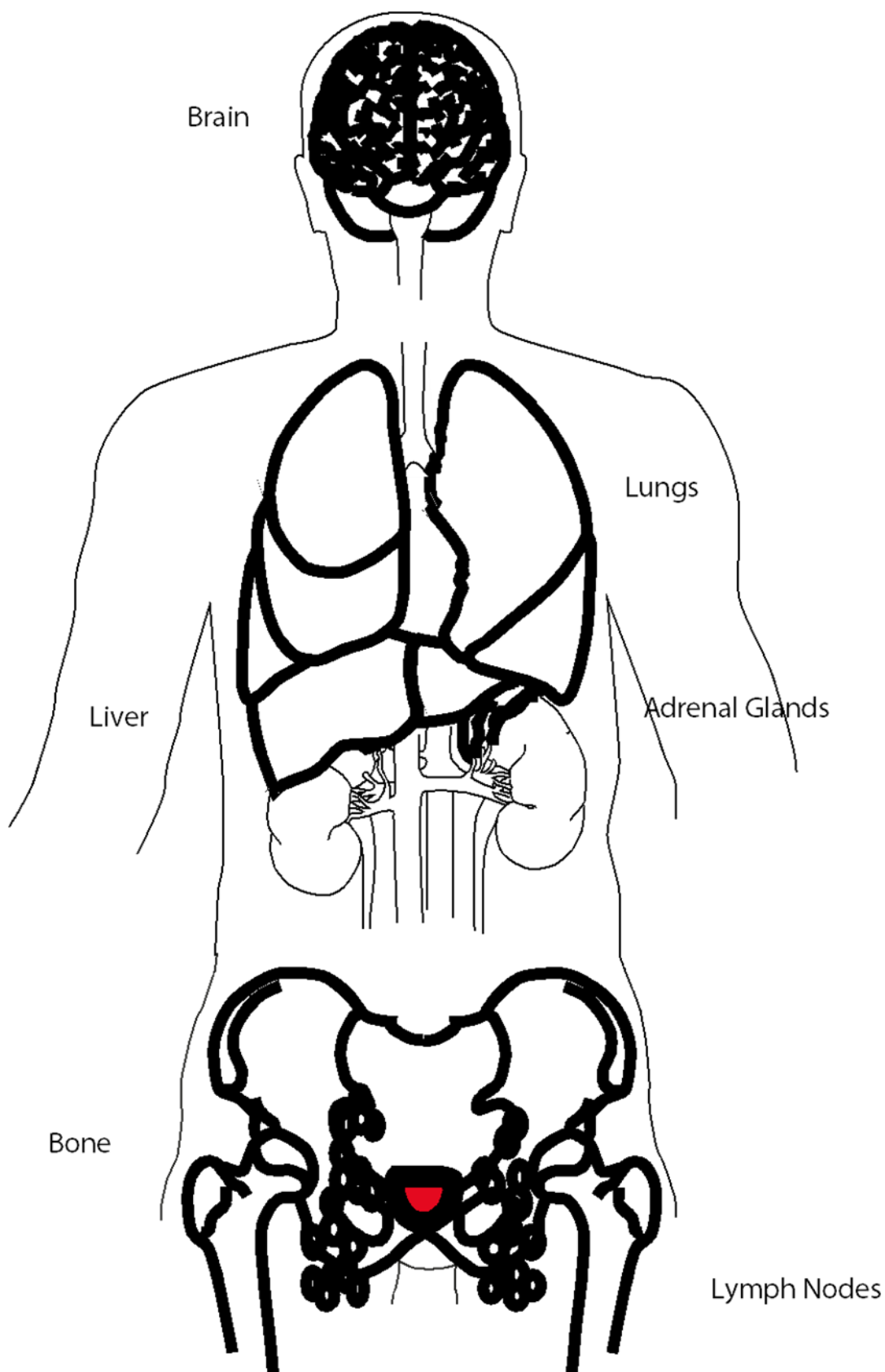
Figure 1.7. Metastasis Sites.
Adapted from [51-53, 56, 72]. Representation of prostate cancer metastasis sites (shown in bold) from primary tumour in the prostate (shown in red)

1.1.5 Prostate Cancer Models

Pre-clinical model systems have been of great value in prostate cancer research, allowing for the increased understanding of the mechanisms involved in carcinogenesis and enabling the identification of therapeutic and preventative measures [82, 83]. These models have many benefits, however due to the complexity of prostate cancer development and progression all models have their limitations and there is no one ideal model system for the research of prostate cancer [82].

Prostate cancer cell lines PC-3, Du145 and LNCaP derived from metastatic sites were the first identified and are still the most commonly used cell lines in published studies [84]. Due to the lack of patients giving rise to immortalised cell there has been numerous cell lines produced via the immortalization human prostate epithelia [85]. These cell lines have their advantages, with them having infinite replicative potential and being easy to handle however they do not represent the diversity of human tumours due to the lack of heterogeneity as well as lacking the microenvironment or immune influence that is present in prostate tumours [83]. Primary cell cultures better reflect the characteristics of the original tumours, however also have their limitations, with them not being as easily assessable as cell lines, having a finite lifespan and specific culture techniques making then harder to handle [85].

Animal models are the bridge between in *vitro* cell models and clinical trials. Prostate cancer research frequently relies on mouse models of which there are multiple types including: xenograft, allograft, knockout and genetically engineered. Whereby xenograft mouse models involve the introduction of human tumour tissues, cell lines or primary cell cultures into an immunocompromised mouse [86]. Allograft mouse

modes differ from xenograft due to introduced cells being from the same inbred immunocompetent mouse strain and thus allow the study of prostate cancer with the immune system present. The site of introduction in xenograft and allograft mouse models can vary depending on the purpose of the study but include subcutaneous, intravenous, orthotropic, tail vein and intracardiac [86-88]. Knockout mouse models involve of the silencing of tumour suppressor genes and genetically engineered mouse models enable flexible manipulation of particular genes, thus can reproduce the stages of prostate cancer through to the metastatic disease [86, 87].

1.1.6 Prostate Cancer Detection and Staging

Prostate cancer is a relatively silent disease, however at advanced stages urinary obstruction and bone pain may occur [2]. Primary diagnostic methods involve a digital rectal examination (DRE) and PSA assay, with irregularities prompting further diagnostic investigations to be carried out, including: biopsy and imaging techniques [2, 89].

1.1.6.1 Digital Rectal Examination (DRE)

DRE is the physical examination of the prostate gland through the wall of the rectum to assess size and textual irregularities [90]. Unfortunately DREs are unreliable as they are subjective as results depend on the experience of the examiner and have poor sensitivity as tumour may arise from a untouchable site of the prostate [89, 91].

1.1.6.2 Prostate Specific Antigen (PSA) Assay

PSA is a 33 kDa glycoprotein of 237 amino acids produced primarily in prostatic secretory epithelium via androgen regulation. PSA is a kallikrein-related serine protease released into the seminal fluid and is believed to have a role in liquefaction

of seminal fluid via the hydrolysis of senenogelin [32, 33]. In normal conditions small

amounts of PSA enter the circulation with serum level ranging from 0.1- 4 ng/mL. The

development of prostate cancer results in the increased disruption of the normal

prostate architecture and elevated levels of PSA are able to enter the serum; serum

levels of >4 ng/mL are indicative of prostate cancer [92]. However, other factors may

cause this increase including: BPH, prostatitis, ejaculation within 3 days prior to

assay, urethral instrumentation such as cystoscopy, thus further diagnostic

investigations are required. This makes PSA a nonspecific biomarker for prostate

cancer which results in approximately 67 % false positives and 15 % false negatives

[32, 33, 89].

1.1.6.3 Biopsy

A needle biopsy is often performed through the rectum using trans-rectal ultrasound

(TRUS) guidance. This involves 10-12 tissue samples being collected under local

anaesthetic, which are then assessed for the presence of cancer and a Gleason score

is given. However, there is the possibility that cancer is missed thus resulting in false

negatives and there are a number of side effects that include: short term bleeding

(rectal, urinary or haemospermia), infection, urine retention and pain [93][92]. A

template biopsy may also be performed to rule out false negatives or are performed

instead of a TRUS needle biopsy [94]. This involves at least 20 tissue samples being

collected, normally under general anaesthetic, via a needle inserted through the

perineum. There is a template on the perineum with holes approximately 5 mm apart

and TRUS is also used to guide the needle into the prostate. Template biopsies have

a decreased risk of false negatives due to increased samples taken but have similar

side effects with decreased risk of serious infection but increased risk of urine

retention [95, 96]. Targeted biopsies are also an option, using the information gathered from imaging techniques to collect samples from abnormal areas [97].

A Gleason score is given based on the biopsies taken. The Gleason score is a sum of the most common Gleason grade in the samples and the highest Gleason grade found in the samples. Gleason grade is given based on how normal the cells appear, where 1 is normal prostate tissue and 5 is extremely abnormal tissue. The Gleason score can therefore range from 2-10 however as most cancers are Gleason grade 3 or more the Gleason score is normally between 6 and 10. The higher the Gleason score the more aggressive the cancer and the increased likelihood of metastasis [98, 99].

1.1.6.4 Imaging

Various imaging techniques can be used to obtain an accurate diagnosis and to assess information on stage and grade of the cancer to facilitate treatment decisions. These techniques include: TRUS, magnetic resonance imaging (MRI), computerised tomography (CT) scans and bone scans and x-rays [100].

1.1.6.5 Staging

Stage describes the spread of prostate cancer. Prostate cancer confined to the prostate gland is known as localised disease. Localised prostate cancer is generally slow-growing and non-aggressive. If the cancer has broken out of the prostate capsule and has spread to the surrounding area including: seminal vessels, bladder, rectum, pelvic wall or local lymph nodes it is known as locally advanced disease. Advanced disease is also known as metastatic disease where prostate cancer has spread to more distant sites of the body. Further staging of prostate cancer uses the

TNM system, which stages the tumour (T), lymph nodes (N) and metastases (M) separately (See Table 1.1) [101].

Table 1.1. The TNM staging system. Adapted from [101].

Tumour Staging			
Localised Disease	T1		Small tumour that is undetectable by imaging or DRE, diagnosed by PSA assay and biopsy
		a	Incidental histological finding in < 5% of tissue
		b	Incidental histological finding in > 5% of tissue
		c	Tumour identified by needle biopsy
	T2		Tumour is confined to the prostate
		a	Tumour in one half of one prostate lobe
		b	Tumour in both halves of one prostate lobe
		c	Tumour in both prostate lobes
Locally Advanced Disease	T3		Tumour extends through the prostate capsule
		a	Tumour broken out of prostate capsule
		b	Tumour spread to seminal vessel
	T4		Tumour spread to local area such as external sphincter, rectum, bladder, levator muscles and pelvic wall
Lymph Node Staging			
	NX		Lymph nodes cannot be checked
	N0		No cancer found in local lymph nodes
	N1		Cancer found in local lymph nodes
Metastasis Staging			
	MX		Metastasis cannot be checked
	M0		No cancer found outside of the pelvis
	M1	a	Cancer found in lymph nodes outside of the pelvis
		b	Cancer found in the bone
		c	Cancer found in other organs

1.1.7 Treatment

There are various treatment options for prostate cancer including: surgery, radiotherapy, hormone therapy, chemotherapy, cryotherapy and steroids. Treatment decisions are based on cancer stage, Gleason score, age, general health, symptoms and prognosis.

1.1.7.1 Monitoring Prostate Cancer

Prostate cancer generally affects older men and is often a slow growing disease thus some patients may never need treatment. Instead of immediate treatment prostate cancer may be monitored and treatment given if disease progresses. This aims to reduce overtreatment and reduce treatment associated physical and psychological morbidity [102, 103]. Monitoring prostate cancer can be separated into two subtypes: active surveillance and watchful waiting.

Active surveillance is the monitoring of low risk localised prostate cancer that is slow growing and unlikely to be causing any symptoms [102]. Regular tests are carried out to assess changes in the cancer they involve PSA assay every 3- 6 months, DREs, biopsies 12 months after diagnosis and imaging. If results suggest cancer progression treatment with a curative aim is given [102, 103]. In comparison, watchful waiting is the monitoring of generally locally advanced or metastatic prostate cancer. Watchful waiting is suitable if the prostate cancer is asymptomatic, there are other health problems that make the patient less able to cope with treatment or the prostate cancer isn't likely to decrease life expectancy [104]. Tests are also used to assess cancer progression, involving PSA assays and DREs, however there is less likelihood of biopsies and more likelihood of bone scans [105]. The main difference in active

surveillance and watchful waiting is that if treatment is required in watchful waiting it is with the aim to control rather than cure the cancer [104-106].

1.1.7.2 Surgery

Radical Prostatectomy

Radical prostatectomy is the removal of the prostate gland. This is either performed as an open surgery via a retropubic or perineal incision or as a laparoscopic surgery, which may be by hand or robotic assisted. The surrounding tissue, local lymph nodes and seminal vessels are also removed and thus depending on the prostate cancer stage this surgery may be curative. Also depending on stage and location of the prostate cancer a nerve sparing surgery may be performed whereby the two nerve bundles that run alongside the prostate, which are important for erectile function, are preserved. Unfortunately, radical prostatectomy can result in mortality (30- day mortality in 0.11-0.13 % of patients), impotence (11-87 % of patients) and incontinence (0-87 % of patients). Although side effect can diminish over time it has been shown that at 52 months post radical prostatectomy 88% of patients report erectile dysfunction and 31% report urinary leakage [102, 107].

Orchidectomy

Orchidectomy is the removal of the testes from the scrotum. This stops testosterone production in the testes resulting in lower testosterone levels and reduced AR signalling thus preventing prostate cancer growth [108]. Although this surgery is effective, it has become less common due the introduction of hormone therapy that reduce AR signalling without surgical risk and recovery time. Possible side effects of orchiectomy include: erectile dysfunction and osteoporotic changes [109].

Transurethral resection of the Prostate (TRUP)

Often used in the treatment of BPH TRUP is performed to alleviate the symptoms of prostate cancer rather than treat the disease. TRUP involves the removal of parts of the prostate causing urinary retention by blocking the urethra [110].

1.1.7.3 Radiotherapy

Radiotherapy is the use of ionising radiation to kill cancer cells. Depending on stage of prostate cancer this may be curative. Radiotherapy includes external, brachytherapy and palliative. Whereby, external radiotherapy involves high doses of radiation being delivered to the prostate. It is usually given daily for up to eight weeks [111]. Also known as internal radiotherapy, brachytherapy is separated into two types: low dose rate brachytherapy and high dose rate brachytherapy. Low dose rate brachytherapy is also known as seed implantation brachytherapy and involves the permanent implantation of between 70 and 150 small radioactive beads into the prostate, under TRUS guidance, via a needle through the perineum. These beads then give off a low dose of radiation with a half-life of 60 days. High dose rate brachytherapy involves the temporary implantation of hollow catheters, under TRUS guidance, into the prostate via the perineum. These catheters are then connected to a brachytherapy machine whereby radioactive seeds travel through the catheters releasing a dose of radiation to the prostate. Side effects include: proctitis, urinary retention, erectile dysfunction, rectal irritation and rectal bleeding [111-114].

Palliative radiotherapy is used to alleviate pain caused by bone metastases. Targeting bone metastases, either by external radiation or by an intravenous injection of radium 223 or strontium 89, causes tumour shrinkage as well as bone strengthening [115-118].

1.1.7.4 Androgen Deprivation Therapy

As previously discussed, androgen signalling is important in prostate cancer development and progression thus therapies have been developed to reduce signalling. These therapies are used to decrease the risk of cancer recurrence or to slow the growth of or shrink advanced prostate cancer. As an alternative to orchidectomy, androgen deprivation therapy can be used to decrease testosterone levels without the risks that come with having surgery. Gonadotrophin Releasing Hormone (GnRH) agonists are one type of hormone therapy. They act to activate GnRH receptors thus creating an initial surge in Luteinizing Hormone (LH) however chronic administration activates a negative feedback mechanism resulting in decreased LH and thus decreased testosterone production [119]. GnRH agonists include: leuprorelin, goserelin acetate, buserelin, triptorelin and histrelin (See Table 1.2) [120]. In contrast the GnRH receptor antagonist degarelix inhibits the GnRH receptor decreasing LH and therefore testosterone levels without the initial surge found with GnRH agonists [119]. Anti-androgens are the third type of hormone therapy currently used, they include: bicalutamide, flutamide and enzalutamide (See Table 1.2). Bicalutamide and flutamide bind the AR allowing for nuclear translocation but prevent co-factor recruitment. Enzalutamide on the other hand inhibits the AR (wild type and T877A and W741C mutants) as well as inhibiting nuclear translocation, DNA binding and co-factor recruitment [121, 122]. The cytochrome p17 inhibitor abiraterone is the final hormone therapy currently used. Abiraterone acts to decrease both testicular and adrenal androgen concentrations (See Figure 1.8) [122].

Table 1.2. Androgen Deprivation Therapies in Clinical Use. Adapted from [120].

Name	Brand Name	Administration Route	Administration Frequency
Gonadotrophin Releasing Hormone (GnRH) Agonists			
Leuprorelin	Prostap/ Lutrate	Subcutaneous/ Intramuscular Injection	Every 3 months
Goserelin acetate	Zoladex/ Novgos	Subcutaneous Injection	Every 4 weeks or 12 if long lasting
Buserelin	Suprefact	Subcutaneous Injection/ Nasal Spray	Injection 3 times a day for 7 days then nasal spray 6 times per day
Triptorelin	Decapeptyl SR/ Gonapeptyl Depot	Subcutaneous/ Intramuscular Injection	1 per month/ 1 per 3 months/ 1 per 6months
Gonadotrophin Releasing Hormone (GnRH) receptor Inhibitor			
Degarelix	Firmagon	Subcutaneous Injection	2 injections then 1 per month
Anti-Androgens			
Bicalutamide	Casodex	Tablet	1 per day
Flutamide	Drogenil	Tablet	3 per day
Enzalutamide	Xtandi/ MDV3100	Tablet	4 tablets once a day
Cytochrome p17 inhibitors			
Abiraterone	Zytiga	Tablet	4 tablets once a day
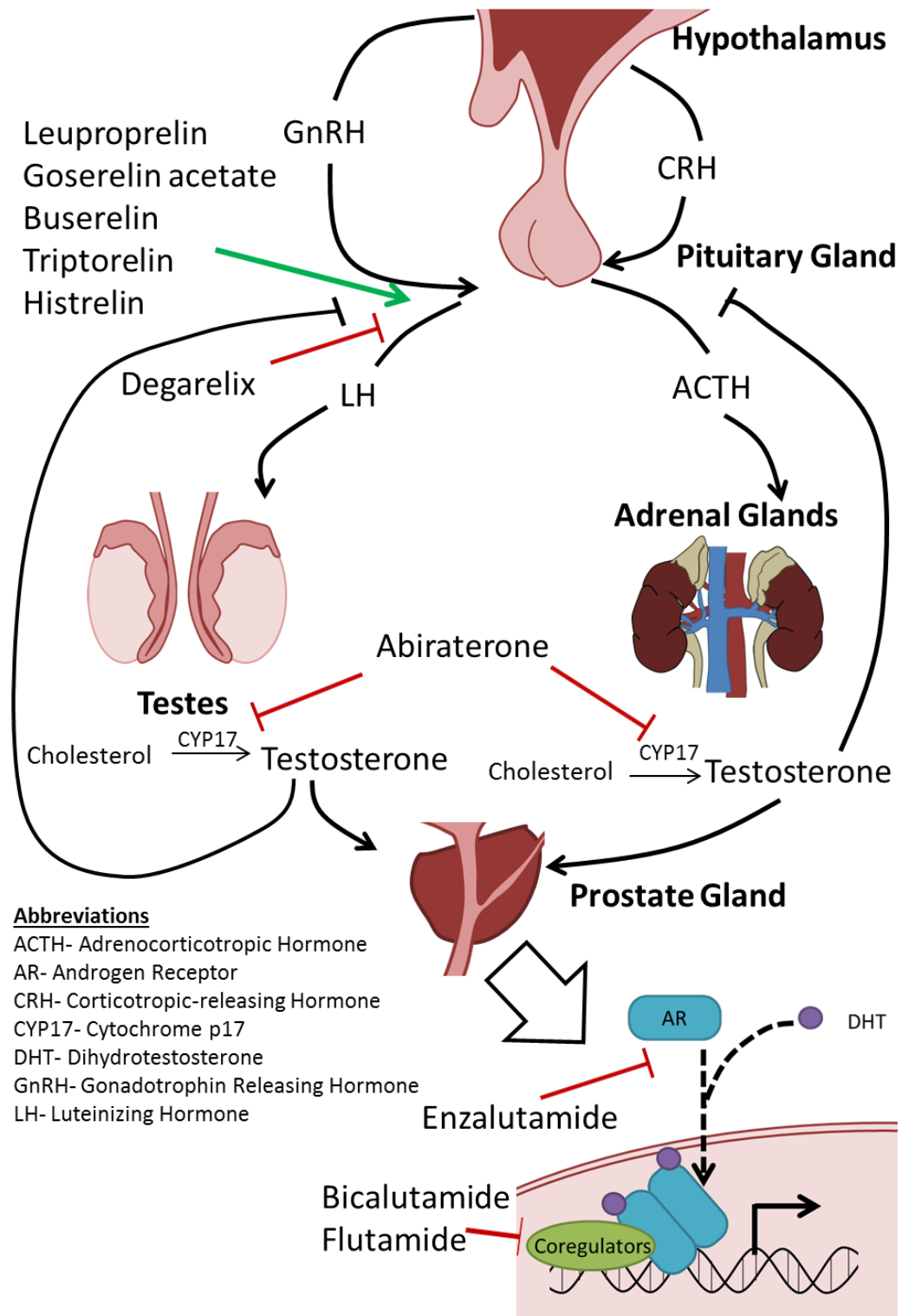
Figure 1.8. Androgen Deprivation Therapy.
Adapted from [122]. Hormone therapy targets in the treatment of Prostate Cancer

1.1.7.5 Chemotherapy

Chemotherapy includes: docetaxel (Taxotere), mitoxantrone, epirubicin, paclitaxel (Taxol) and estramustine. They may be used alongside hormone therapy to treat metastatic prostate cancer or used to treat prostate cancer that isn't responding to hormone therapy. Side effects include: nausea, hair loss, sore mouth and eyes, mouth ulcers and infertility [123].

1.1.7.6 Steroids

Steroids, most commonly dexamethasone, are used to treat prostate cancer that is not responding to hormone therapy and may be used alongside chemotherapy. Side effects include: weight gain, swelling of hands, feet and eyelids and increased blood pressure [124].

1.1.7.7 Cryotherapy

Cryotherapy, also known as cryoablation or cryosurgery, kills cancer cells by freezing. Cryotherapy needles are inserted into the prostate via the perineum under TRUS or x-ray guidance. A warming catheter is inserted into the urethra to protect the urethra during treatment. The treatment involves argon gas being circulated through the needles to freeze the tissue. Side effects include: impotence, incontinence, urinary retention and pelvic pain. Currently cryotherapy is only recommended to be used as part of clinical trials [125].

1.1.7.8 Ultrasound therapy

High intensity focused ultrasound (HIFU) waves are used to heat and kill cancer cells. HIFU waves are produced by ultrasound probe inserted into the rectum. The most common problems reported include: infections in the prostate area and urinary

retention. Currently HIFU therapy is only recommended to be used as part of clinical

trials [126].

1.2 Intercellular Junctions

1.2.1 Epithelial and Endothelial Cell Junctions

Epithelial and endothelial cells make up semi-permeable sheets that line both internal and external surfaces, thus separating internal compartments and separating a multi-cellular organism from the outside environment [127, 128]. Junctional complexes link these cells to one another creating a barrier to enable the maintenance of concentration gradients between compartments and therefore allowing for differentiated fluid environments [129]. This barrier function allows for control of paracellular transport, transcellular transport and is controlled by cell polarization, which unlike the majority of cells that create transient polarisation, in endothelial and epithelial cells is more permanent [127, 128]. The plasma membrane of epithelial cells can be separated into three domains: apical, lateral and basal. The apical membrane domain is typically covered in microvilli and faces lumens or the outside environment. The lateral membrane domain membrane contains junctional complexes joining adjacent cells to one another and the basal membrane domain generally rests on a basal lamina, a type of ECM composed of mainly type IV collagen, laminin and proteoglycans, facing underlying tissue [127, 128]. There are three cell adhesion junctions on the lateral membrane: tight junctions (TJs), adherens junctions (AJs) and desmosomes (DS) as well as gap junctions (GJs) that function in cell communication (See Figure 1.9)[127, 128, 130]. Endothelial membrane structure is similar to that of epithelial cells with membrane domain segregated by junctional complexes however unlike epithelial cells they do not contain DS [131]. All cell-cell junctions contain transmembrane (TM) proteins that join adjacent cells to one

another via homo- or hetero-typic TM protein binding and via scaffolding proteins associate with the actin cytoskeleton which allows for the transduction of signals between cells [128, 130].

Apical
Membrane

Tight Junctions

Adherens
Junctions

Desmosomes

Gap Junctions

Basolateral
Membrane
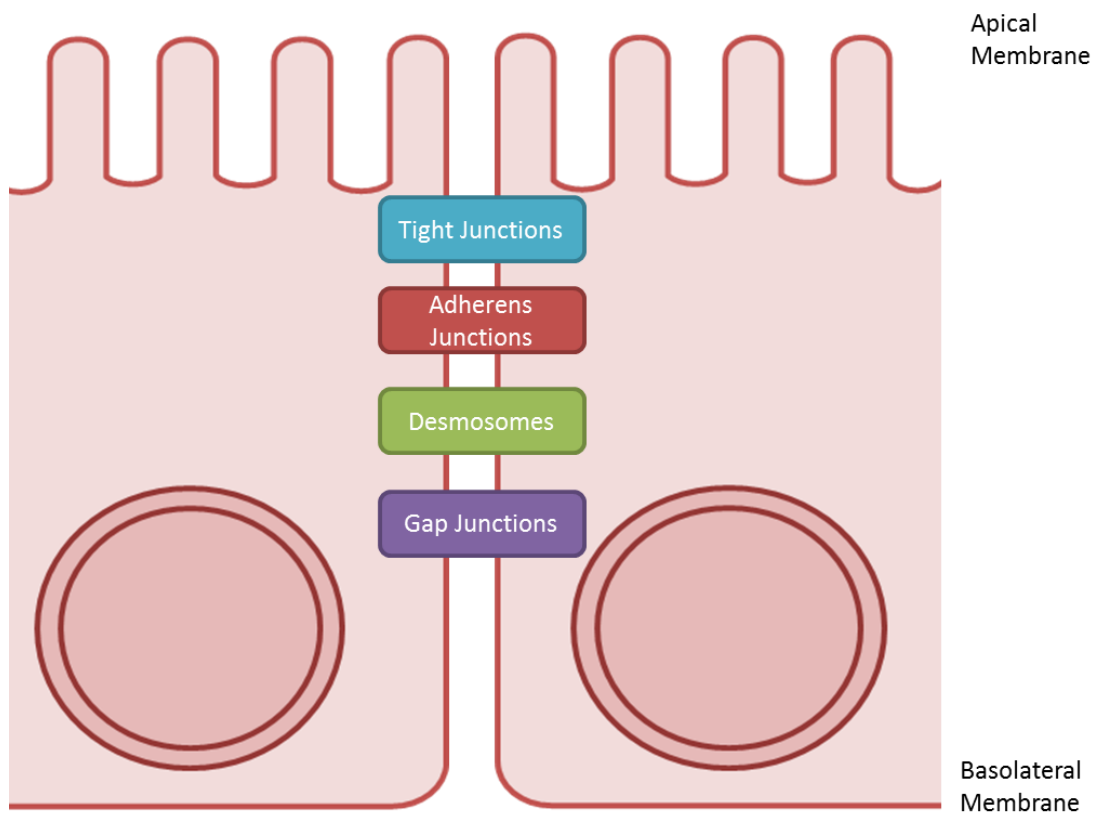
Figure 1.9 Epithelial Junctions.
Adapted from [127]. Diagrammatic representation of junctions within the lateral membrane domain of epithelial cells.

1.2.2 Junctional Location

1.2.2.1 Adherens Junction Location

AJs are observed in a variety of different cell types including myocytes and Schwann cells however, the most well-known example is within polarised epithelial cells [132]. Within polarised epithelia AJs form part of the tripartite junctional complex between adjacent cells and are typically located basally to TJs on the lateral membrane [132-134]. AJs are characterised by parallel plasma membranes of neighbouring cells that are 10-20 nm apart. The intercellular spaces of AJs are occupied by numerous cylinder-like projections that bridge the two membranes [133, 135]. Furthermore, the cytoplasmic aspect of AJs are linked to a contractile bundle of actin filaments and thus link the plasma membrane to the actin cytoskeleton at discrete contact regions and are also known as the adhesion belt due to them completely enclosing cells along the F-actin lining/ circumferential actin belt [132, 134, 136]. In the majority of epithelia, AJs are continuous (belt-like) however, when the tripartite junctional complex is not present AJs are often discontinuous (spot-like) and are located along the entirety of the lateral membrane [133, 136]. In non-epithelial cells, such as neuronal synaptic junctions and mesenchymal tentacle-like processes, AJ are also present as discontinuous structures [137-139]. The importance of these two structures is currently unknown however, it is thought that either they perform different functions or that they are different stages of junctional maturation [140].

1.2.2.2 Tight Junction Location

TJs occur in both epithelial and endothelial membranes, as well as being observed in Schwann cells [141]. TJs are an anastomosing networks of strands that encircle the cell apex, forming belt like structures with continuous intramembrane strands in the

protoplasmic (P)-face with complementary groves in the ectoplasmic (E)-face [142-144]. TJ form gasket-like contacts between adjacent cells, which are seen as discrete sites of fusion (kissing) points between outer leaflets of adjacent cell membranes and result in the obliteration of intercellular space [128, 133, 143, 145-147]. In mammalian epithelia, TJs are typically found at the apical and lateral membrane boundary making them the most apical of the cell-cell junctions [128]. There are however some exceptions for instance in hepatocytes where there apical membrane domain is formed in the lateral membrane domain between two neighbouring cells [148]. Junctional complexes are less well defined in endothelia than in epithelia with AJs and TJs intermingled and GJs also found close to the luminal surface [149].

1.2.3 Junctional Proteins

1.2.3.1 Adherens Junction Proteins

AJs are composed of three classes of proteins: 1) adhesion receptors spanning the intercellular space of the junction and comprising the adhesive bond, 2) cytoskeleton/membrane plaque proteins that link the adhesion receptors with the cytoskeletal network and 3) the cytoskeletal network that anchors the junction (actin) [140].

Intercellular junctions rely on transmembrane proteins that bind homo- or hetero-typically to transmembrane proteins on neighbouring cells and with AJs cadherin proteins are the main adhesion receptor [134]. The cadherin family of transmembrane proteins is composed of multiple subfamilies, one which being the classical cadherins. E-, N-, R- and P-cadherin are members of the classical subfamily that bind in a calcium dependent manner to cadherins on neighbouring cells [150, 151]. Members of the classical cadherin subfamily have similar structures, with the

extracellular domain being broken into five cadherin extracellular (EC) domains section EC1-EC5. Binding of Ca^{2+} to each of the EC domains is important for the correct conformation of the extracellular domain and EC1 at the N-terminus determining binding specificity [126, 151].

Cytoplasmic proteins affect the adhesive action of cadherin extracellular domains altering the strength and stability of the junction [134]. Classical cadherins bind directly and indirectly to numerous cytoplasmic proteins including members of the catenin family [151]. P120-catenin binds cadherins at the juxtamembrane portion of the cytoplasmic domain and this binding stabilises cadherin at the plasma membrane, increases the adhesiveness of the cells as well as regulating motility through the actin cytoskeleton via interactions with the Rho family of GTPases [152-154]. β-catenin and γ-catenin both bind to the C-terminal half of the cadherin cytoplasmic domain [134]. β-catenin binds in a phospho-related manner with phosphorylation of cadherin at serine residues increasing binding affinity however phosphorylation of β-catenin tyrosine residues disrupts binding [151, 155, 156]. Catenin proteins in turn interact with a variety of other proteins such as β-catenin binding to α-catenin to form the β catenin-α catenin complex which joins cadherins to the cytoskeleton through mediators including formin, vinculin and EPLIN [134].

The cadherin/catenin core adhesion complex is the most recognised component of AJs however there is a second complex that constitutes AJs, the nectin/afadin complex [140]. Within this complex the nectin family of four proteins (nectin-1, nectin-2, nectin-3 and nectin-4) are the adhesion receptors which, unlike cadherin proteins, mediate Ca^{2+} independent cell adhesion [150, 157]. Nectins are members of the IgG superfamily with their extracellular domains being comprised of three IgG-

like loops and interacts in a homo- and hetero-typical manner to other nectin or nectin like receptors to form a junction between neighbouring cells. Similarly, to classical cadherin proteins, nectin proteins are single pass transmembrane proteins and the cytoplasmic domain of nectin interacts with plaque proteins that link the adhesion receptors with the cytoskeleton, with afadin being the predominant plaque protein [140, 157, 158]. Afadin binds a PDZ binding motif at the C-terminus of nectins [157]. Afadin is an F-actin binding protein that anchors the nectins to the actin cytoskeleton. Furthermore, nectin can bind a myriad of proteins including cell polarity proteins such as partitioning-defective homolog 3 (Par-3) and therefore ensures the correct spatial and temporal localisation of Par3, a protein crucial for the subsequent establishment of apico-basalateral polarity [150, 157].

1.2.3.2 Tight Junction Proteins

TJs are multiprotein complexes and these proteins can be categorised into three groups: 1) integral membrane proteins, 2) associated scaffold/ plaque anchoring proteins and 3) regulatory proteins [143, 145, 159, 160]. Integral membrane proteins are transmembrane proteins that bridge the intercellular space between adjacent cells and are therefore responsible for cell adhesion. These are then linked to the cytoskeleton, to other transmembrane proteins of the same cell and to signalling cascades via plaque anchoring proteins in conjunction with regulatory proteins [143]. Integral membranes associate with partners in opposing membrane of adjacent cell creating a zipper-like seal [129]. Integral membrane proteins can be separated into two groups: tetraspanning proteins and single spanning proteins. Tetraspanning proteins such as occludin and claudin proteins contain four transmembrane domains, two extracellular loops and cytoplasmic C and N termini. Single spanning proteins

that belong to immunoglobulin superfamily such as JAMs which only contain one transmembrane domain [129].

Occludin was the first TJ integral membrane protein identified and was achieved by the production of monoclonal antibodies against enriched chicken liver membranes [161]. Human occludin was discovered to be a 522 aa protein of 59 kDa. Occludin forms a zipper like seal by the two extracellular loops containing high levels of glycine and tyrosine residues making them hydrophobic and allowing their interaction with occludin extracellular loops on neighbouring cells [147, 161-163]. The claudin family of proteins, 26 of which are present in humans, were later identified as TJ integral membrane proteins. Sharing a similar structure to occludin with two extracellular loops, the first of which being responsible for homotypic binding of claudin extracellular loops on neighbouring cells [164-168]. JAMs belong to the immunoglobulin superfamily and are dissimilar to occludin and claudins having only one transmembrane domain. However, similarly to occludin and claudins, JAMs form homotypic interactions with the extracellular domains of JAMs on neighbouring cells [129, 169].

Plaque anchoring proteins connect integral membrane proteins to the cell cytoskeleton as well as connecting integral membrane proteins of the same cell to one another. Plaque anchoring proteins also link these integral membrane proteins to signalling molecules thus regulating TJ integrity and allowing communication between cells and the external milleu. These proteins include ZO-1, ZO-2, ZO-3, cingulin, MAGI-1, Pals1 and PATJ [143, 170, 171]. Occludin can bind to ZO-1 via the cytoplasmic C terminus [147, 163]. The claudin family also bind plaque anchoring proteins via its cytoplasmic C terminus, these proteins include: ZO-1, -2 and -3, PATJ,

MUPP1 and MAGI-1, -2 and -3 [129, 166, 172]. JAMs that a class I PDZ domain binding motif (the protein binding module that binds C-terminal tripeptide motif S/TXV) are able to bind to ZO-1 and MAGI-1 [129, 169, 173, 174]. JAMs that contain a type II PDZ binding motif (a protein binding module that binds hydrophobic amino acids with the C-terminal) can interact with PDZ domains of TJ plaque anchoring proteins including: AF-6, ASIP/Par3, ZO-1, cingulin [129, 173].

Regulation of TJs is imperative not only for initial assembly and maintenance but in order to change TJ structure and integrity depending on cell requirements. This is achieved by the linking of TJs to signalling molecules to transmit signals between TJs and the rest of the cell. This allows for the regulation of multiple cellular processes as well as the regulation of TJs. TJs therefore associate with kinases, phosphatases, regulators of membrane traffic, guanine nucleotide exchange factors (GEFs) and GTPase activating proteins (GAPs) [175, 176]. GEFs and GAPs are both regulators of small GTPase via activation or inhibition respectively. GTPase activity must be regulated for correct junction assembly, cell-cell contact and junction stabilisation. Plaque anchoring proteins regulate this by recruiting GEFs and GAPs, restricting their localisation or by being the targets of activated GTPases [176]. The Rho family are important GTPases in TJ barrier function. Rho are members of the Ras superfamily of small GTPases and include RhoA, Cdc42 and Rac; with RhoA seemingly the most important. TJ are also regulated by phosphorylation for instances low resistance membranes have greater ZO-1 phosphorylation than higher resistant membranes. Protein kinase C (PKC) is one of the families of kinases that are responsible for TJ protein phosphorylation with novel PKC δ and θ as well as atypical PKC λ and ζ isoforms being associated with TJs. Other kinases include protein kinase A (PKA) and

protein kinase G (PKG) [177]. The reduction of phosphorylation of TJ proteins also affects TJ integrity thus phosphatases are also important regulatory proteins, these include protein phosphatase 1 (PP1), protein phosphatase 2A (PP2A) and protein phosphatase 2B (PP2B) [177].

1.2.4 Junctional Function

1.2.4.1 Adherens Junction Function

AJs preliminarily function to maintain physical association between cells however, they have broader functions as they are important in for the formation of TJs, the regulation of the actin cytoskeleton, intercellular signalling and transcriptional regulation [151].

Cell adhesion is essential for the formation of multicellular organisms and AJs are responsible for the initiation and maintenance of cellular contacts and loss or disruptions of AJs result in the loosening of cell-cell contacts subsequently resulting in the disorganisation of tissue architecture [134, 151].

The formation of AJs can be broken into three stages: 1) transient contacts, 2) formation of stable contacts and 3) extension of stable contacts [178]. During the initial stage of formation spot-like junctions form at the tips of cellular protrusions from adjacent cells whereby nectins and cadherens separately form trans-dimers between cis-dimers on neighbouring cells. It is likely that nectins form the initial clusters which then recruit cadherens. The recruitment and interaction of nectins and cadherens with cytoplasmic proteins link these clusters to the actin cytoskeleton. These spot-like junctions then form more mature AJs [151, 178]. This formation of AJs results in the formation of TJs however once formed AJs are not critical for the maintenance of TJs [151].

From the earliest stages of embryonic development cells of epithelial and mesenchymal in origin are crucial to the structure and function of organs [179]. However, the epithelial and mesenchymal phenotypes are not permanent with cells switching between them. These processes are termed epithelial to mesenchymal transition (EMT) and the mesenchymal to epithelial transition (MET) [179]. AJs are highly dynamic and enable the reorganisation and dispersal of cell such as during EMT and thus molecular hallmarks of EMT include the down regulation of the AJ transmembrane protein E-cadherin as well as the up regulation of N-cadherin as well as the dysregulation of vimentin and fibronectin [151, 180]. Histologically cells that go through EMT become more spindle shaped and lose basal-apical polarity as well as acquiring greater motility and resistance to apoptosis. These characteristics promote normal cell migration and survival during embryogenesis and wound healing. EMT and MET are therefore tightly regulated by epigenetic changes, transcription factors, micro-RNA and signalling pathways including that of AJ protein β-catenin [180].

Activation of β-catenin is classically attributed to Wnt signalling whereby Wnt binds its receptor Frizzled and co-receptors LRP5/6 resulting in the formation of an LRP-Axin-FRAT complex. This complex frees β-catenin from GSK-3β sequestration preventing its degradation and allowing cytoplasmic accumulation and nuclear translocation [180]. However, Wnt-independent beta-catenin signalling also occurs such as via EGFR signalling whereby tyrosine phosphorylation of β-catenin results in the dissociation from E-cadherin and AJs. Within the cytoplasm β-catenin can be degraded or can be translocated to the nucleus. Nuclear β-catenin can regulate the expression of numerous genes including gene involved in cell proliferation (*c-myc* and

Cyclin D1),inhibition of apoptosis (*MDR1/PGP, COX-2, PPARδ*), tumour progression (*MMPs, uPAR, Upa, CD44, Laminin γ2* and *NrCAM*), Growth factors (*c-met, VEGF, WISP-1, BMP-4*), transcription factors (*c-jun, fra-1, ITF-2, Id2* and *AF17*) and negative feedback targets (*conductin, Tcf-1* and *Nkd*) [181].

Therefore, AJs are able to regulate and transduce intracellular junctions, which may result in changes to gene expression. AJs can also regulate the actin cytoskeleton and as they connect to the actin cytoskeleton as well as linking neighbouring cells AJ coordinate movement of cell groups [132, 151].

1.2.4.2 Tight Junction Function

The most documented functions of TJ include: gate function; providing a diffusion barrier selectively regulating the paracellular passage of solutes and fence function; demarcating the apical and basolateral domains of the cell. However TJs are also important as intermediates and transducers of cell signalling important in processes such as differentiation and growth, mediators of cell adhesion and barriers to migration and motility (See Figure 1.10) [142, 143].

Barrier function is essential for multicellular organisms to be able to establish and maintain distinct fluid compartments. Epithelial cells separate tissue spaces and endothelial cells line blood and lymphatic vessels [145, 160, 171, 182]. Epithelial cells and endothelial cells form continuous monolayers which function as selective permeability barriers between compartments by regulating the passage of ions, water and solutes via paracellular movement [145, 183]. This prevents the diffusion of non-specific solutes resulting in the maintenance of the distinct composition of adjacent tissue compartments which requires the paracellular space between adjacent cells to be sealed [171]. These barriers are due to a junction at the most

apical region of this zone, i.e. TJs [147, 171, 184]. The permeability of these barriers can vary considerably with the selection of claudin being expressed within the tissue and the expression being tissue specific [144, 185]. Different claudins have different size and charge selectivity and produce TJs of different tight/ leakiness as determined by the first extracellular loop [184]. Therefore the expression of TJ proteins help to define the overall transport characteristics of each epithelia and endothelia [147].

With TJ selectively blocking paracellular transport it is imperative that there is controlled transcellular movement of molecules [182]. For this to occur, cells need to differentiate their plasma membrane to form specialised domains of distinct protein and lipid compositions, known as cellular polarisation [145]. TJ do not initiate this polarization but form after cell polarization has occurred [128]. However along with other intramembrane fences formed from other junctional complexes, TJs are thought to be important in the maintenance of this polarisation by preventing the free diffusion of proteins and lipids between the apical and basolateral membrane domains. This polarisation is also important for other cell biological processes including: cell adhesion, cell signalling, cell migration, asymmetric cell division and epithelial as well as endothelial barrier formation [128, 145].

TJ are involved in numerous signalling cascades, the extent of which is still being investigated. PKC signalling is important in TJ regulation by phosphorylating TJ proteins with PKC stimulation triggering translocation of TJ proteins to cell borders and PKC inhibition decreasing transepithelial resistance (TER), indicating disruption of TJS. MAPK signalling modulates TJ paracellular transport by up/down regulating the expression of several TJ proteins. There is also crosstalk between PKC and MAPK

signalling in TJ regulation. One example of this is in corneal epithelial cells where activation of PKC results in decreased TER via MAPK activation [177].

It has also been found that certain plaque anchoring proteins have a secondary role in gene expression. There appears to be correlation with subcellular location and confluence/ proliferation, with these proteins being found in the nucleus in proliferating low confluent cells, but at TJs in high confluent non-proliferating cells [176]. ZO-1 is one of these proteins that can shuttle between the nucleus and TJs, localised in the nucleus of low confluent cells and has been found to associate with the Y-box transcription factor ZONAB (ZO-1- associated nucleic acid-binding protein).

In highly confluent cells ZO-1 sequesters ZONAB in the cytoplasm resulting in a decreased nuclear level of CDK4 the regulator of G1/S phase transition; which interacts with ZONAB and colocalises with ZO-1 at TJs. Cytoplasmic ZONAB also results in decreased gene expression of target genes including cyclin D1 and PCNA; which are important in cell cycle control and DNA replication and repair respectively. Other genes regulated by ZONAB include: proteins involved in DNA replication, proteins involved in chromatin remodelling and proteins involved in DNA repair. ZONAB has also been shown to interact with symplekin, a nuclear protein that can associate with TJs. Symplekin is linked to 3'- end processing of pre-mRNA and polyadenylation as well as regulating gene expression of ZONAB target genes including cyclin D1. This ZO-1/ZONAB signalling is controlled by RalA and Apg-2. RalA is a member of the Ras superfamily of small GTPases which are important in actin cytoskeleton remodelling, cell cycle control, cellular transformation and vesicle transport. GTP bound RalA inhibits ZONAB by increasing the levels of cytoplasmic

ZONAB. Apg2 is a heat shock protein that competes for the SH3 domain, ZONAB binding site, of ZO-1 thus is an activator of ZONAB [175, 176].

Other TJ plaque anchoring proteins have been found in the nucleus including: ZO-2, ZO-3, PALS-1, MAGIs, PAR-6, PAR-3 and cingulin and have been shown to interact with transcription factors such as ZO-2 interacting with Fos, Jun and C/ERP [176, 186]. ZO-2 interactions with these transcription factors occurs in the nucleus as well as at TJs, suggesting that ZO-2 also acts to sequester transcription factors away from the nucleus and preventing transcription of target genes in polarised cells [187]. It is therefore possible for TJ to regulate the expression of a variety of genes and thereby regulate a variety of cellular processes.
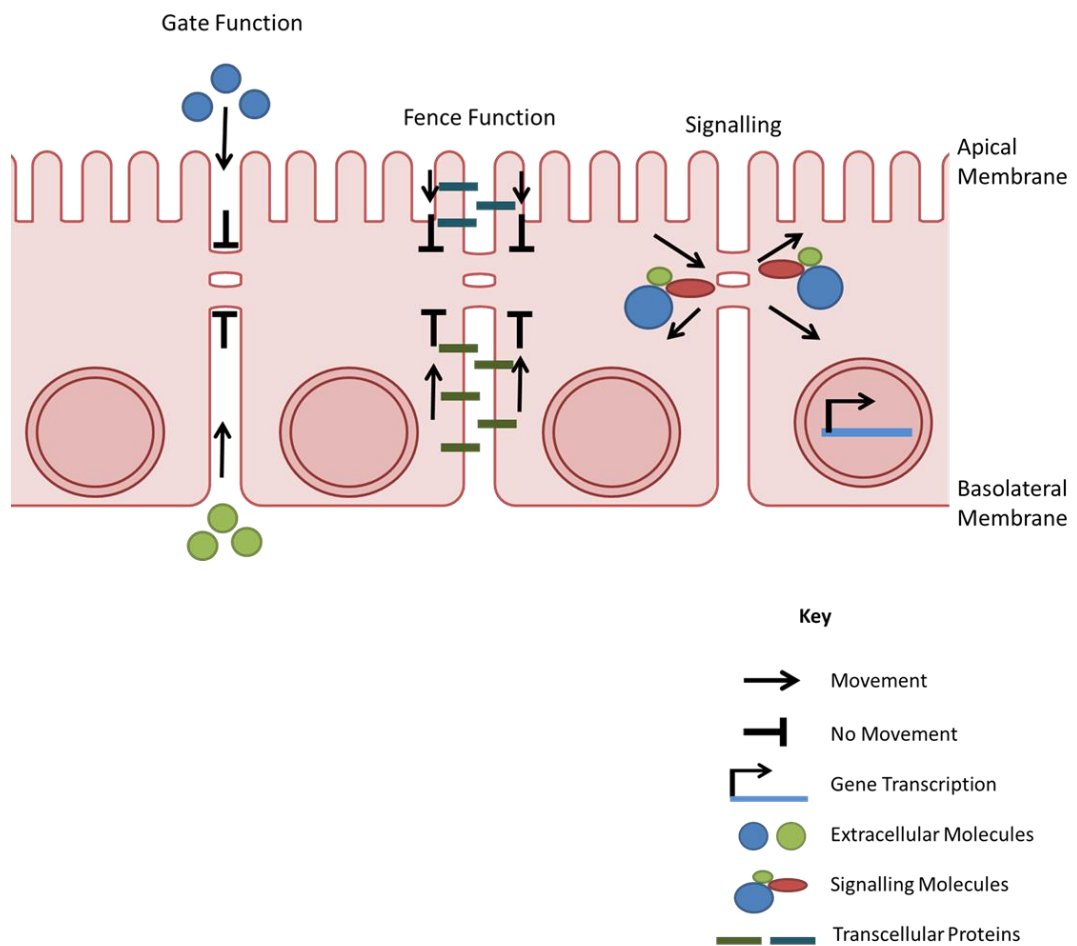
Figure 1.10. Tight Junction Roles.
Adapted from [169]. Systematic representation of the roles of TJs

1.2.5 Junctions and Disease

1.2.5.1 Adherens Junctions and Disease

Cells require the ability to adhere and communicate with other cells and the extracellular environment for morphogenesis and the maintenance of tissue integrity. Cellular junctions are dysregulated in many human disorders either by inherited gene mutation or during disease pathogenesis. Disruptions to AJs or defects in AJ proteins are associated with a variety of diseases including inflammatory bowel disease, hair and skin disorders and cancer [188-191].

Inflammatory bowel diseases such as Crohn's disease and ulcerative colitis are multifactorial diseases resulting in the contribution of both environmental and genetic factors. Inflammatory bowel diseases are characterised by prolonged cytokine stimulation in the gut, dysbiosis of intestinal microbiota and the dysregulation of the mucosal immune system [189]. AJ have been implicated in these diseases with alterations in genes encoding E-cadherin and P-cadherin being important in their development and a decreased E-cadherin staining being observed around ulcerated mucosal regions in Crohn's and ulcerative diseases [189, 192-194]. Decreased E-cadherin is essential to allow for cell regeneration, differentiation and migration. However, in inflammatory bowel disease the absence of E-cadherin expression results in the loss of cell-cell adhesion, impairing the integrity of the mucosal barrier and therefore allowing for the exposure of the lumen to the underlying mucosal immune system and in turn resulting in disease relapse [195, 196]. Other AJ proteins have also been implicated in inflammatory bowel diseases including α-catenin, β-catenin and p120-catenin, which have been shown to be decreased around regions of ulceration [189].

Mutations in the gene encoding P-cadherin (*CDH3*) have also been linked to hypotrichosis with juvenile macular dystrophy, an autosomal disorder characterised by early hair loss and the progressive degeneration of the central retina resulting in blindness. P-cadherin is expressed in hair follicle and retinal pigment epithelium and alterations in this protein via gene mutation is thought to result in loss of cell-cell adhesion [190, 197, 198].

With over 90 % of cancers being epithelial in origin it is unsurprising that factors that promote the normal architecture and functioning of epithelia are altered throughout the development and progression of cancer [199]. Adhesion molecules contribute to various functions including signal transduction, cell growth, differentiation, gene expression, morphogenesis, immunological function, cell motility and inflammation. Therefore adhesion molecules have pivotal role in development of recurrent, invasive, and distant metastasis with some acting as tumour suppressors [200]. The dysregulation of AJ has particular implications in transformation and tumour invasion with EMT being important in cancer progression and metastasis with EMT resulting in drug resistance, cancer stem cell transformation and poor prognosis of numerous cancers [180, 201]. One of the hallmarks of EMT is the loss of E-cadherin and the loss of E-cadherin based cell-cell adhesion has been observed during the progression of a multitude of human cancer [199].

The inactivation of E-cadherin is thought to be an important step in the development of most, if not all, epithelial derived tumour types and loss of E-cadherin is associated with increased invasive and metastatic potential and with a poor clinical outcome [202, 203]. The importance of E-cadherin in cancer development has been demonstrated in mice whereby the loss of E-cadherin drives the transition of

adenomas to carcinomas of pancreatic β-cells expressing SV40 large T antigen and the maintenance of E-cadherin expression resulted in the stalling of these cells at the adenoma stage [203]. In non-small-cell lung cancer reduced E-cadherin is associated with tumour cell dedifferentiation, local invasion, regional metastasis and reduced survival [204]. In bladder cancer loss of membranous E-cadherin staining correlates with high grade, advanced stage and poor prognosis [200]. Furthermore mutations in the E-cadherin gene have been identified in familial gastric cancer [202].

E-cadherin is not the only AJ protein that has been linked to cancer, the dysregulation of cadherin molecules has been strongly associated with cancer metastasis and progression such as in breast cancer whereby an increased P-cadherin expression is related to a worse prognosis [205, 206]. Other AJ proteins are also implicated in cancer progression such as in colorectal cancer with an increased β-catenin nuclear staining and decreased E-cadherin membrane staining being two independent adverse prognostic factors [181].

The dysregulation of AJs and AJ proteins has also been associated with the development and progression of prostate cancer. Expression of E-cadherin, β-catenin, α-catenin and p120 catenin are all decreased in prostate cancer and these decreases correlate to high Gleason grade [207-209]. Cadherin switching was associated with prostate cancer specific death although N-cadherin expression did not correlate with any prognostic parameters. However, P-cadherin expression is associated with a shorter time to skeletal metastasis [209, 210]. Furthermore, it is not only the expression of AJs proteins that is important for prostate cancer aetiology but also their localisation. An increased nuclear staining of β-catenin is associated with higher Gleason grade and β-catenin is thought to contribute to prostate cancer

progression through links with androgen signalling, cell proliferation and cell death [207].

1.2.5.2 Tight junctions and Disease

TJs have been linked to numerous diseases including Crohn's disease whereby variations in claudin expression in intestinal epithelium results in variation in TJ integrity and decreased amounts of TJs which in turn results in an increased intestinal permeability and therefore diarrhoea. Within the blood brain barrier TJ regulate transport of molecules and immune cells from the blood into the brain and vice versa, thus maintaining homeostasis of central nervous system microenvironment. The increased migration of leukocytes in multiple sclerosis has been shown to reorganise the actin cytoskeleton and TJs and decrease ZO-1 and occludin synthesis. Hereditary deafness nonsyndromic recessive deafness DFNB29 can be caused by mutations in cochleal claudin-14 resulting in changes in TJ charge sensitivity. Familial hypomagnesemia with hypercalciuria and nephrocalcinosis may be caused by mutations in claudin-16 which impair TJ functions affecting permeability properties as well as claudin-19. TJs are important in both the inner (endothelial) and outer (epithelial) layers of the blood retinal barrier however in diabetic retinopathy it is the inner layer that is the primary site of vascular leakage resulting in macular oedema; thought to be the directly responsible for vision loss. This may be due to VEGF mediated TJ altering via decreased occludin expression and increased occludin and ZO-1 phosphorylation. Furthermore TJs have been implicated in cancer progression [185].

Multiple cancers originate from epithelia thus TJ exist between cancer cells as well as the endothelium these cells need to get through to metastasise via the circulatory

system. Secondary tumours are responsible for the majority of cancer mortality due to tumour metastasis. There is an emerging interest in TJ involvement in cancer progression and metastasis with numerous TJ proteins having been shown to be important in crucial changes of cell physiology including: evasion of apoptosis, limitless replicative potential, angiogenesis and tissue migration and motility; all of which are required for cancer to progress to metastatic disease as previously discussed in Section 1.1.4.3 [143].

TJs are important in the maintenance of epithelial polarization. In cancer this is important due to polarized epithelia having low proliferation rates and loss of polarization therefore often leads to increased proliferation and is often seen in carcinogenesis [128]. An example of this is in airway epithelia which constitutively produce the growth factor heregulin and its oncogenic receptor tyrosine kinases ErbB2-4. Binding of heregulin to its receptors initiates proliferation, therefore to control this in differentiated airway epithelia heregulin-α is localised to the apical membrane domain as well as airway surface liquid and ErbB2-4 are located at the basolateral membrane domain and are thus physically separated from one another. They only interact when epithelial cell polarisation or TJ integrity is compromised resulting in proliferation [211].

The claudin family of integral membrane proteins are frequently deregulated in cancer and appear to play important roles in multiple carcinogenic alterations in cell physiology. For instance, Claudin-1 down-regulation is seen in several cancers [212]. However, Claudin-1 expression in liver cancer is linked with increased MMP2 activity and activation of c-Abl-PKCδ mediated migration and invasion [213]. Claudin-4

expression in ovarian epithelial cells results in increased gene expression of pro-angiogenic cytokines such as IL-8 [214]. Claudin-6 is reported to act as a tumour suppressor in breast cancer and down regulation results in decreased apoptosis as well as increasing MMP activity thus increasing invasion and transendothelial migration [215]. Claudin-7 down regulation results in increased migration in lung cancer, increased venous invasion and liver metastasis in colorectal and increased invasion in oesophageal cancer. This may be explained by decreased Claudin-7 resulting in decreased E-cadherin expression as well as increased ERK/MAPK signalling pathway activity [216-218].

Other integral membrane proteins have also been implicated in these alterations of cell physiology with decreased occludin levels correlating with dedifferentiation and progression of several cancers and resulting in decreased pro-angiogenic expression [219, 220]. Alterations in JAM family proteins have been shown in several cancers including: breast and renal cancers as well as melanomas [221-223]. JAM-A down regulation results in increased epithelial cell proliferation and appears to be an early event in the development of renal cancer and increases migration of renal cancer cells [222, 224]. However, in certain models decreasing JAM-A has been shown to decrease tumour growth; with JAM-A appearing to inhibit Akt-dependent β-catenin activation [225]. JAM-A overexpression has also been associated with increased breast cancer metastasis [221]. Furthermore JAM-A is required for bFGF induced angiogenesis [226]. JAM-C appears to be required for melanoma cell transendothelial migration and increased JAM-C expression is linked to increased invasion and metastasis, whereas JAM-A impairs melanoma cell transendothelial migration [223].

Plaque anchoring proteins have also been implicated in cancer aetiology. ZO-1 is able to regulate membrane-type 1 (MT1) MMP expression and ZO-1 knockdown in breast cancer cells results in decreased MT1-MMP expression and decreased invasion. Down regulation of the ZO-1 interacting protein Scribble in mammary epithelia resulted in decreased cell polarity, decreased apoptosis and increased dysplasia resulting in cancer after a period of latency [227]. Furthermore, as previously discussed ZO-1/ZONAB signalling is important in the regulation of proliferation thus decreased ZO-1 levels increases nuclear ZONAB levels and in turn increases proliferation [175]. It is therefore not surprising that ZO-1 is down regulated in certain cancers including breast, pancreatic and brain cancers [175].

It is therefore apparent that TJ proteins are imperative in stages of cancer progression, although different proteins may be important in different stages and expression may vary with cancer type. Thus, each cancer may have a different TJ protein expression fingerprint.

Within prostate cancer the expression profiles of some TJ proteins have been investigated (See Table 1.3). Expression of claudin 3 and 4 mRNA was shown to be high in prostate cancer with the distribution of claudin-3 mRNA expression changing from being restricted to glandular epithelia in the normal prostate to also being found in malignant epithelia in prostate adenocarcinoma. As claudin-3 and 4 are capable of binding *Clostridium perfringens* enterotoxin (CPE) to mediate toxin-dependent cytolysis it was found that prostate cancer highly expressing claudin-3 and claudin-4 is sensitive to CPE-mediated cytosis [228]. Similarly, another study found that claudin-3 and claudin-4 expression persisted in prostatic adenocarcinoma in comparison to benign epithelia with expression being similar or increased. This

expression of claudin-3 and claudin-4 correlated with advanced stage tumours and claudin-3 expression with recurrence. They also showed that claudin-1 and claudin-7 expression decreased in prostatic adenocarcinoma in comparison to benign epithelia and that his decrease in claudin-1 and claudin-7 correlated with high tumour grade and decreased claudin-1 with biochemical recurrence [229]. In contrast to this it was shown that claudin-1 and claudin-7 levels were high in prostate cancer samples, in the majority of samples claudin-3 and claudin-4 were high and claudin-2 and claudin-5 levels were low [230]. When comparing prostate adenocarcinoma to BPH claudin-2, claudin-3 and claudin-5 expression was increased, claudin-4 expression was decreased and there was no change in claudin-1 and claudin-7. Increased expression of claudin-3 and claudin-5 was associated with perineural invasion [231]. Claudin-3 expression is also shown to be increased in prostatic intraepithelial neoplasia, prostate cancer and metastatic prostate cancer in comparison to normal epithelia and BPH [232]. Occludin was shown to be lost in unpolarised epithelial cells of Gleason grade 4 and 5 tumours [233]. Calcitonin (CT) and its G-couple receptor (CTR) are both up regulated in metastatic prostate cancer and activated CT-CTR causes increased tumourigenicty and metastatic potential in multiple prostate cell lines. This has been suggested to be due to disrupted TJs as indicated by decreased TER, increased paracellular permeability (PCP) and internalisation of ZO-1 [234]. Investigations into compounds that can reverse these changes led to the identification of phenyl-methylene hydantoin (PMH) as a potential therapeutic [235]. Studies into TJs in prostate cancer are limited and show conflicting results. However, this may be due to studies looking at differences in expression between normal and prostate epithelia, expression levels in prostate cancer epithelia

or comparisons between prostate cancer and BPH which are likely to have a changed expression profile from the normal prostate.

Regulation of TJs in the prostate has been linked to androgen signalling with decreased testosterone or androgen serum levels being associated with decreased claudin-4 and claudin-8 expression in prostate epithelium. Decreased testosterone levels are associated with decreased contact points between adjacent membranes as well as being associated with increased prostate inflammation. It has therefore been proposed that decreased testosterone due to aging results in decreased TJs and increased inflammation, which may contribute to the development and progression of prostate neoplasia [236]. Furthermore, in the LNCaP cell line two forms of claudin-7, full length 211 aa form and C-terminal truncated 158 aa form, are able to regulate PSA expression. They therefore may be involved in androgen regulation in prostate cancer; with increased androgen stimulation leading to increased claudin-7 and increased PSA gene expression [237].

Table 1.3.Changes in TJ protein expression in Prostate Cancer

Protein	Change in Expression	Reference
Claudin-1	Down regulated	[229]
	Up regulated	[230]
	No change	[231]
Claudin-2	Down regulated	[230]
	Up regulated	[231]
Claudin-3	Up regulated	[228]
	No change/ Up regulated	[229]
	Up regulated	[232]
	Up regulated	[231]
Claudin-4	Up regulated	[228]
	No change/ Up regulated	[229]
	Down regulated	[231]
Claudin-5	Down regulated	[230]
	Up regulated	[231]
Claudin-7	Down regulated	[229]
	Up regulated	[230]
	No change	[231]
Occludin	Down regulated	[233]

1.3 Hepatocyte Growth Factor

1.3.1 Hepatocyte Growth Factor Structure

HGF, also known as scatter factor (SF), was identified as the ligand for the oncogene MET [238-242]. HGF gene is located on chromosome 7q21.11 and encodes a large multidomain 728 amino acid protein consisting of six domains: an amino terminal domain , four kringle domains 1-4 and a serine proteinase homology (SPH) domain; which lacks enzymatic activity due to mutations in essential residues [242]. HGF is secreted from mesenchymal cells as an inactive single chain precursor (pro-HGF) which is proteolytically cleaved after the K4 domain, between residues 494 and 495, to form two subunits: heavy (α) subunit of 463 amino acids and light (β) subunit of 234 amino acids. These two subunits are disulphide linked to form the active HGF heterodimer [238, 243-246].

1.3.2 Hepatocyte Growth Factor Receptor

First identified in the 1980s MET is a proto-oncogene located on chromosome 7q21-31 [245, 247]. The *MET* gene encodes the c-Met tyrosine kinase, the receptor for HGF and transcription is regulated by E-twenty six (Ets), paired box 3 (Pax3), activator protein-2 (AP2) and transcription factor 4 (Tcf-4) [246, 248-250]. Similarly to HGF, c-Met is disulphide linked heterodimer formed from proteolytic cleavage of a 1390 amino acid precursor between residues 307 and 308 resulting in an α subunit and β subunit. The α subunit as well as amino acids 308 and 514 of β subunit make up the semaphorin (sema) domain the rest of the β subunit contains the cysteine rich domain, four immunoglobulin domains (Ig1-Ig4), a transmembrane region,

intracellular cytoplasmic juxtamembrane domain and tyrosine kinase domain [245, 251].

1.3.3 Hepatocyte Growth Factor Signalling

HGF binds to c-Met via NK1 and SPH domains interacting with the c-Met Sema domain [251]. HGF binding results in receptor dimerization and transphosphorylation of tyrosine residues, Tyr1234 and Tyr1235, located within the catalytic loop of the tyrosine kinase domain and the subsequent phosphorylation of Tyr 1349 and Tyr1356 within the carboxyl-terminal tail. These residues are docking sites for intracellular adaptor proteins including GAB1, GRB2 and SHC, via Src-homology-1 (SH2) domains, phosphotyrosine binding (PTB) domains or Met binding domains (MBD) [252]. These mediate signal transduction via activation of signalling pathways including: MAPK, PI3K-Akt and STAT-3 to control a variety of cellular processes including: cell proliferation, cell survival, cell motility and differentiation [245, 246, 253, 254].

1.3.3.1 MAPK Cascade

The MAPK cascade is a phospho-relay system in which a series of three protein kinases phosphorylate and activate one another [254]. Met activates Ras, a small GTPase, through the GRB2-SOS complex as well as through SHP2 which dephosphorylates and deactivates GAB1 a protein that normally deactivates Ras. Active GTP bound Ras recruits Raf, a Ser/Thr kinase, promoting a conformational changes and activation of Raf which can then phosphorylate and activate MAPK/ERK kinase 1 (MEK1) or MEK2. MEK1/MEK2 in turn phosphorylates and activates ERK1/ERK2, which then translocates to the nucleus where they phosphorylate and stabilise several transcription factors involved in G1-S cell cycle transition [246, 254].

Met can also activate JNK MAPK cascade via Ras activating Rac1 as well as activation via Gab1-Crk1 [245, 254] . As well as activating the p38 MAPK cascade, both of which can control a range of cellular processes including: cell proliferation, differentiation, transformation and apoptosis [254].

1.3.3.2 PI3K cascade

PI3K can be activated directly by c-Met or indirectly through Ras activation. PI3K activation recruits Akt, a Ser/Thr kinase to the plasma membrane leading to the inactivation of BCL-2 antagonist of cell death (BAD), a pro-apoptotic protein and the activation of MDM2, an E3 ubiquitin protein that promotes degradation of p53, resulting in cell survival. Akt also inactivates glycogen synthase kinase 3β (GSK3β) resulting in the expression of Myc and cyclin D1 important in cell cycle regulation [254].

1.3.3.3 STAT Pathway

STAT3 associates to c-Met directly and indirectly through Gab1 and is phosphorylated by active c-Met. Phosphorylated STAT3 then dislocates from c-Met, forms a homodimer through their SH3 domains, translocates to the nucleus and regulates the expression of several genes involved in proliferation, survival and differentiation [252, 254].

1.3.3.4 c-Met regulation

c-Met activation is tightly regulated to maintain tissue homeostasis, this is achieved by a negative feedback loop resulting in Met degradation via an ubiquitin-proteasome pathway [245, 255]. Activation of c-Met by HGF binding results in the recruitment of casitas B-lineage lymphoma (c-Cbl) via direct binding to Tyr1003 of c-Met and indirectly through association with the N-terminal SH3 domain of Grb2

which in turn associates with Tyr1356 of Met [256]. c-Cbl is a E3 ubiquitin-protein ligase which ubiquitinates c-Met [255, 256]. This leads to c-Met internalisation into endosomes and degradation [257, 258]. c-Met activity is also modulated by dephosphorylation of tyrosine residues. This is accomplished through protein tyrosine phosphatases (PTPs) including: the receptor-type PTPs density enhance phosphatase 1 (dEP1) and leukocyte common antigen-related molecule (LAR) as well as the non-receptor PTPs PTP1B and T-cell protein tyrosine phosphatase [246].

1.3.4 Hepatocyte Growth Factor and Tight Junctions

HGF has been shown to dysregulate TJs in a number of cell lines resulting in decreased cell polarity [259]. HGF treatment changes the expression of TJ proteins expression including decreasing claudin-2 and increasing claudin-3 in MDCK cells, decreasing ZO-1 and claudin-1 in HUVEC cells and decreasing claudin-1 in retinal pigment epithelial monolayers [259-262]. HGF also affects TJ protein distribution within cells with HGF treatment resulting in relocalisation of claudin-1 and occludin to the cytoplasm in retinal pigment epithelial monolayers, decreasing the amount ZO-1 and barmotin/7H6 at the cell membrane in MDCK cells and the amount of ZO-1 at cell membranes in non-tumoral gastric epithelia (IMGE-5) cells [262-264]. Furthermore, HGF treatment results in increased ZO-1 phosphorylation in breast cancer cells as well as occludin phosphorylation in retinal pigment epithelial monolayer and decreases TER as well as increasing PCP in a number of cell types. All of which suggests HGF regulates TJ integrity and HGF signalling results in decreased TJ integrity resulting in decreased polarity and increased migratory potential [261, 262, 264, 265].

1.3.5 Hepatocyte Growth Factor and Cancer

HGF/c-Met signalling controls many cellular processes shown to be deregulated in cancer thus over activation may be imperative in cancer development and/or progression. HGF-c-Met signalling has been shown to be overactive in numerous cancers and this can be due to gene amplification, activation mutations, chromosomal rearrangements, transcriptional upregulation and HGF overexpression [246].

1.3.5.1 Gene Amplification

Amplification of the MET gene results in protein overexpression and increased c-Met activation. Gene amplification has been reported in a number of tumours including: oesophageal adenocarcinoma, gastric adenocarcinoma, medullablastoma and pancreatic adenocarcinoma [246, 266-272]. There is also a link between c-Met gene amplification and tumour grade and prognosis in some cancers [268].

1.3.5.2 Activation Mutations

Activating mutations have been discovered in the c-Met kinase domain in sporadic and inherited forms of human papillary renal carcinoma [246, 272-274]. Mutations have also been identified in the c-Cbl binding site and HGF-binding region of the c-Met Sema domain [246].

1.3.5.3 Chromosomal Rearrangements

c-Met was identified in an osteosarcoma cell line contained the chromosomal rearrangement fusing the tyrosine kinase domain of c-Met to the upstream translocating promoter region (TPR). This creates c-met with constitutive dimerization and activation promoting tumour development [246, 247, 272, 275].

1.3.5.4 Transcriptional Upregulation

Transcriptional upregulation is also seen in the absence of gene amplification resulting in increased protein expression and c-Met over activation. This has been reported in a number of carcinomas including: thyroid carcinoma [246, 272]. Hypoxia has been shown to activate *c-Met* transcription via the transcriptional factor hypoxia inducible factor 1α (HIF1α) [246, 276, 277].

1.3.5.5 HGF Over Expression

HGF has been found to be frequently overexpressed in the reactive stroma of primary tumours which increases c-Met activity in tumour cells [246, 272, 278].

1.3.5.6 Hepatocyte Growth Factor and Prostate Cancer

The prostate gland may be well suited for the model by which HGF is produced in mesenchymal cells and affects nearby epithelial cells expressing c-Met especially in prostate cancer where stromal-epithelial interactions are thought to be important for cancer growth and progression. In cell lines HGF has been shown to be expressed by prostatic stromal myofibroblastic cells but not prostate cancer cell lines (PC-3, Du145 and LNCaP) and c-Met is expressed on some prostate cancer cell lines (PC-3 and Du145) which fits this model. However, c-Met only being expressed on androgen-insensitive cell lines (PC-3 and Du145) but not androgen-sensitive cell lines (LNCaP) as well as expression of c-Met increasing in metastatic prostate cancer in comparison to primary prostate cancer and in rat prostate epithelia after castration suggests HGF/ c-Met signalling is important in prostate cancer progression. Furthermore, in Du145 cells HGF induced dose dependent proliferation and scattering, both of which are important in cancer progression [279]. HGF increased nuclear location and transcriptional activity of NF-κB via PI3K-AKT signalling cascade

in Du145 cells and resulting in antiapoptotic signals and cell protection which are also important in cancer progression [280]. In respect to TJs, HGF causes decreased ZO-1, ZO-2 and ZO-3 at cell junctions in prostate cancer cell lines (PC-3, Du145, PZ-HPV-7 and CA-HPV-10) and decreases TER in these cell lines implying disruption of TJ integrity which has been shown to promote cancer development and progression [281].

1.4 Hepatitis A Virus Cellular Receptor

The Hepatitis A virus cellular receptor (HAVcR-1) is the cellular receptor for *Hepatitis A virus* (HAV) a *Hepatotropic picornavirus*, the cause of acute hepatitis A in humans [282]. HAVcR-1 is also termed T-cell immunoglobulin and mucin domain containing molecule 1 (TIM-1) and kidney injury molecule-1 (KIM-1). HAVcR-1 is expressed on every tested human organ including: liver, small intestine, colon and spleen as well as high expression on the kidney and testis, however the natural function of HAVcR-1 has not been fully investigated [282].

1.4.1 HAVcR-1 Structure

Located on chromosome 5q31.1-32.3 in humans the *HAVCR1* gene is approximately 38.7 kb and consists of 9 exons and 8 introns (See Figure 1.11A) [283]. This encodes a 359 amino acid class I integral glycoprotein which can be roughly broken down into three sections; the extracellular domain, transmembrane domain (TMD) and the cytoplasmic domain (See Figure 1.11B).

The extracellular domain that exists at the N-terminal section of the HAVcR-1 proteins is approximately 272 amino acids and consists of a 109 amino acid cysteine rich region (Ig-like domain) and a 163 amino acid threonine, serine and proline rich region (mucin-like domain) [282]. The Ig-like domain contains six conserved cysteine residues as well as an N-glycosylation site [282, 284]. The mucin-like domain, termed so due to it being characteristic of a mucin-like O-glycosylated protein, contain 13 conserved repeats of the consensus PTTTTL, two conserved N-glycosylation sides as well as a possible N-glycosylated site [282]. The mucin-like domain is therefore predicted to be highly glycosylated , to have an extended conformation and extend

the Ig-like domain away from the cell membrane to form a lollypop on a stick like configuration (See Figure 1.11C) [285, 286]. The TMD is the major hydrophobic region of HAVcR-1, it is 22 amino acids in length and exists between residues 290 and 311. Conserved within the TMD there is a cysteine residue at reside 296 which is thought to allow the addition of fatty acids to aid in the stabilisation of membrane attachment [282].The cytoplasmic domain that exists at the C-terminal end of HAVcR-1 is short in comparison to the extracellular domain only being 48 amino acids in length. This domain contains a tyrosine phosphorylation motif QAENIY starting at residue 350 and may therefore make HAVcR-1 important in signalling events [282, 284].

There are two splice variants of HAVcR-1 termed HAVcR-1a and HAVcR-1b; HAVcR-1b is described above. HAVcR-1a is 334 amino acids and only varies from the described HAVcR-1 structure at the C-terminus whereby the cytoplasmic domain is shorter and is therefore missing the QAENIY tyrosine phosphorylation motif (See Figure 1.11D). The complexity of HAVcR-1 leads to variability in protein size. The gene is expected to encode a 36 kDa protein however due to four possible N-glycosylation sites, multiple possible O-glycosylation sites and possible biotinylation, it can result in the mature protein being approximately 100 kDa as well as the immature protein being 70 kDa or 50 kDa [284]. HAVcR-1 can also undergo cleavage to release an ectodomain as detailed in Section 1.4.2. This ectodomain is approximately 90 kDa and the membrane bound fragment which remains is approximately 14 kDa [287].

A

B

1kb

C

D

324 SVSFSSLQIKALQNAVEKEV**QAEDNIY**IENSLYATD   359aa HAVcR-1b

324 RPHKSCIHQRE   334aa HAVcR-1a
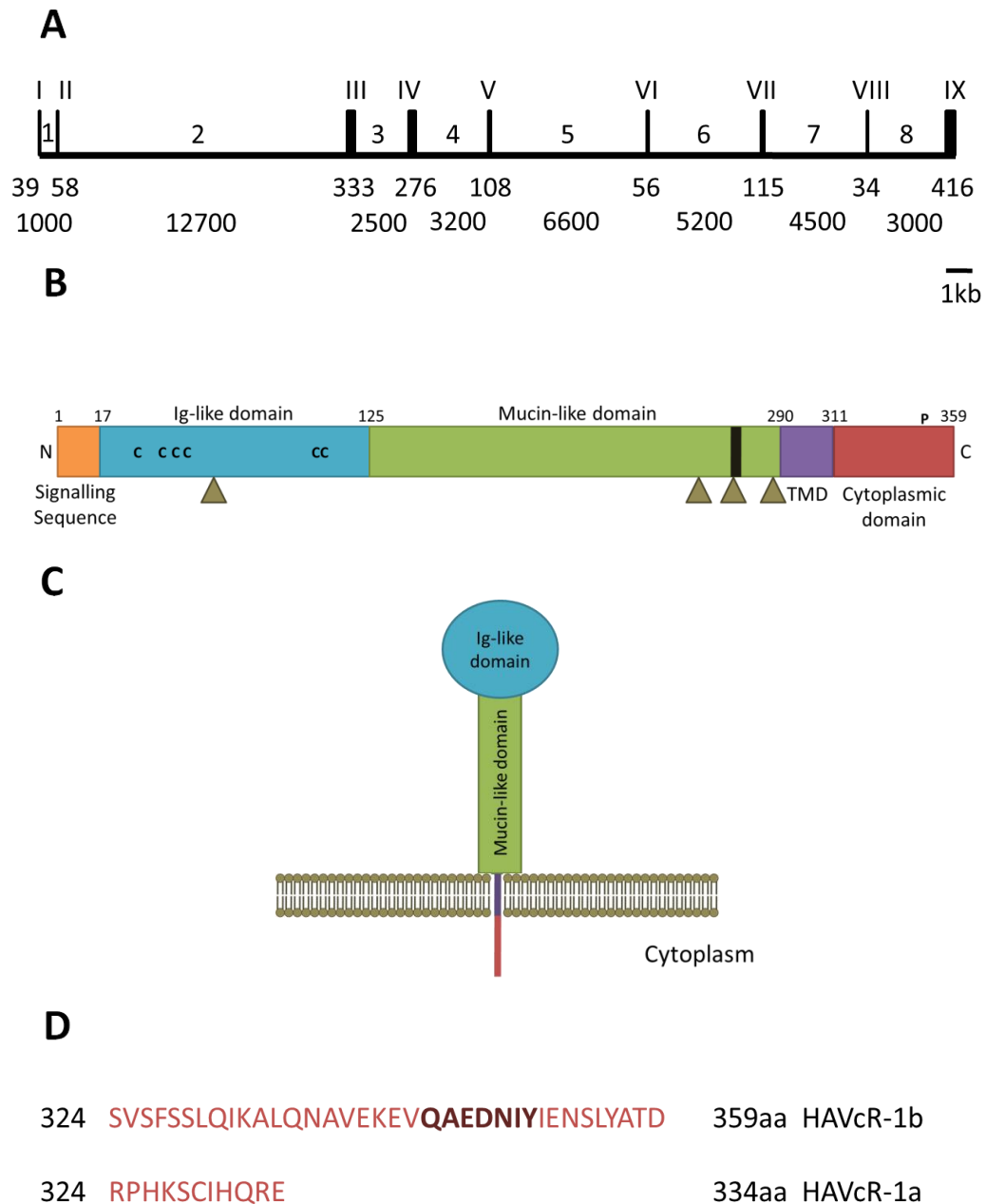
Figure 1.11 HAVcR-1 Gene and Protein Structure.
Adapted from [283, 284]. **A** Representation of the *HAVCR1* gene showing the size in base pairs of the introns number 1- 8 and the exons numbered in roman numerals 1-9. **B** Representation of HAVcR-1b protein showing the size and position of its structural domains, position of cysteine residues in the Ig-like domain represented by (c), position of possible N-glycosylation sites represented by triangles, position of the tyrosine phosphorylation motif QAEDNIY represented by (P) and predicted cleavage site represented by a black box. **C** Predicted secondary structure of HAVcR-1. **D** Amino acid sequence of the cytoplasmic domain of HAVcR-1a and HAVcR-1b.

1.4.2 HAVcR-1 Ectodomain

There is a proteolytic cleavage site in the mucin-like domain near the TMD of HAVcR-1 (See Figure 1.12). Cleavage at this site releases a HAVcR-1 ectodomain into the extracellular space [284, 288]. The site of cleavage is predicted to occur between residues 266 and 278 due to a monoclonal antibody targeting this site (ABE3) blocking cleavage and due to this site being present in both splice variants HAVcR-1a and HAVcR-1b are both believed to be equivalent substrates for proteases [284, 289]. The p38 signalling cascade is thought to regulate cleavage. This is because activating p38 and ERK-MAPK signalling via pervanadate treatment promotes cleavage and the use of SB202190, a p38 inhibitor, inhibiting this pervanadate induced cleavage but the MEK1 and MEK2 inhibitor U0126 having no effect on pervanadate induced cleavage [289]. The cleavage event has been attributed to metalloproteases of the matrix metalloprotease (MMP) family or the a desintegrin and metalloprotease (ADAM) family due to batimastat (BB-94) and ilomastat (GM6001) inhibiting and propidium monoazide (PMA) promoting HAVcR-1 cleavage [284, 289].

Metalloproteinases:
-ADAM
-MPP

Proteolytic Cleavage

Promoters of Cleavage
- Pervanadate
- PMA

Inhibitors of Cleavage
- Bitamastat (B4-94)
- Ilomnastat (GM6001)
- SB202190 (p38 Inhibitor)
- mAb ABE3
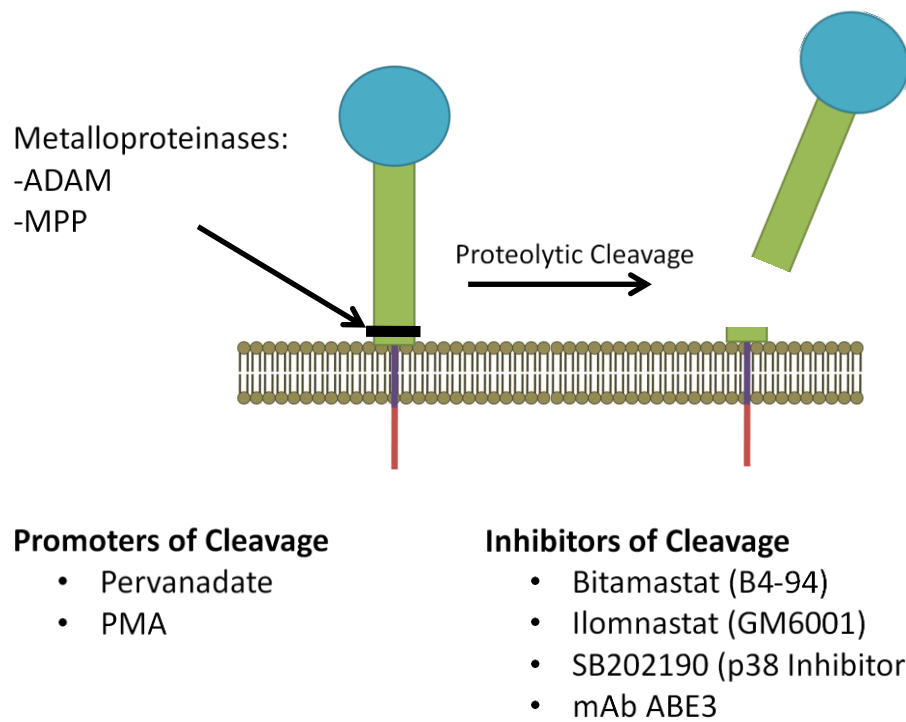
Figure 1.12 HAVcR-1 Ectodomain
Adapted from [287]. Representation of HAVcR-1 cleavage proximal the membrane by metalloproteases to release a HAVcR-1 ectodomain. Treatments that are known to promote or inhibit this cleavage event are listed.

1.4.3 HAVcR-1 in Hepatitis A infection

HAVcR-1 was first identified due to monoclonal antibodies protecting African green monkey kidney cells (AGMK) from Hepatitis A via blocking binding of the *Hepatitis A virus* (HAV) to the cells [290]. HAV has a positive-strand genomic RNA of approximately 7.5 kb. This RNA is covalently linked at its 5' to a small virus protein VPg and contains a poly (A) tail at its 3' [291]. The mature capsid of HAV is formed by 60 copies of at least three viral proteins VP1, VP2 and VP3 and a small unmyristoylated protein, VP4, plays a signal role in the assembly of this capsid [292]. Currently the mechanisms of HAV entry into the cell are elusive with no receptor binding site found on this capsid [293]. However it is known that the Ig-like domain and its N-glycosylation site of HAVcR-1 is required for HAV binding and the Ig-like domain as well as the mucin-like domain is required to induce alteration and uncoating of HAV [294-296].

1.4.4 HAVcR-1 in Kidney Repair

After injury to the proximal tubular epithelium, cells lose their polarity and epithelial cell apoptosis occurs. Surviving epithelia are then required to dedifferentiate, proliferate, migrate over the denuded basement membrane, redifferentiate and repolarise [297]. HAVcR-1 expression is low in the healthy kidney however this is increased in the renal proximal epithelial cells when injured and regenerating after ischemic and toxic kidney injury [298]. This is important as HAVcR-1 is a phosphatidylserine receptor and HAVcR-1 binding phosphatidylserine on the surface of apoptotic cells and mediates the epithelial phagocytosis of these apoptotic cells. Thus HAVcR-1 transforms kidney proximal epithelial cells into semi-professional

phagocytes, resulting in the clearance of injured cells without the need of the immune system and therefore down regulates innate immunity and inflammation [299-301]. HAVcR-1 overexpression after injury also promotes cell migration and proliferation, both of which are crucial for kidney regeneration as previously mentioned [302]. Therefore HAVcR-1 plays a crucial role in the process of kidney repair.

Interestingly the metalloproteinase cleavage of HAVcR-1 proximal to the membrane in these cells releases the HAVcR-1 ectodomain into the urine [284, 289, 298]. Urinary HAVcR-1 is therefore a promising biomarker in kidney injury with it being increased in both acute and chronic kidney injury [303-306]. Levels of the HAVcR-1 ectodomain in the plasma was also increased with acute and chronic kidney injury thus there is a possibility of a blood test for HAVcR-1 [306]. Furthermore, there is a possibility of HAVcR-1 to be used as a biomarker in donor kidneys where acute kidney injury could lead to transplant rejection with donor urine HAVcR-1 levels being higher in kidneys that displayed post-transplant dysfunction. Therefore, a lateral flow detection system for urinary HAVcR-1 (RenaStick™; BioassayWorks, Ijamsville, MD, USA) has been developed to allow simple point of care diagnostic test [307]. Initial testing of this device has been promising with RenaStick™ results being able to rapidly detect kidney injury [308].

1.4.5 HAVcR-1 in Atopy

Atopy including asthma, allergic rhinitis and atopic dermatitis (eczema) arises from environmentally induced immune responses in genetically susceptible individuals. HAVcR-1 has been found to be a gene that increases asthma susceptibility with

HAVcR-1 being expressed on CD4+ T cells, which play important roles in the pathogenesis of asthma and HAVcR-1 transcription occurring during antigen stimulation [309]. It is currently hypothesised that HAVcR-1 is important in regulating cytokine production in T-cells and it is due to this that a hypoallergenic response occurs [310]. HAVcR-1 is expressed on activated CD4+ T cells and this expression is maintained in TH2 cells but not TH1 cells. Activation of CD4+ T cells with a TIM-1 mAb and T cell receptor ligation increased proliferation and IL-4 and IFN-γ. In TH2 cells activation increased proliferation and the production of IL-4 leading to increased pulmonary inflammation in response to antigen challenge [311].

Interestingly there is thought to be correlation in asthma occurrence and the decline in HAV infection, with HAV seropositivity protecting against atrophy when certain HAVcR-1 variants are present [312]. It is thought that HAV infection reduces Th2 cell differentiation and therefore decreases the risk of developing atrophy. This fits the hygiene hypothesis whereby the rise in atrophy is explained by the increased standards of hygiene removing the exposure to protective infections in early life due [313].

1.4.6 HAVcR-1 in Cancer

The correlation between total HAVcR-1 and urinary HAVcR-1 levels and kidney injury led to investigations to assess whether HAVcR-1 could be used as a biomarker in renal cell carcinoma (RCC) [314, 315]. RCC is the most common type of kidney cancer in adults being responsible for approximately 80 % of cases it is frequently diagnosed late making fatality rates high. The most common histological type of RCC, accounting for 75-80 %, is clear cell RCC (ccRCC) [316]. HAVcR-1 has been found to be

overexpressed by 2- 12 fold in 8/13 of ccRCC but interestingly expression is decreased in benign oncocytomas [283]. 60 % of ccRCC contain duplications in chromosome 5 which has been mapped to Ch5q22 and Ch531.1 which contains the gene locus of HAVcR-1, explaining the increased expression of HAVcR-1 however transcriptional control, mRNA processing, mRNA export and protein stability may also contribute [283, 290]. Both the chromosomal location and overexpression of HAVcR-1 implicate it in the development of RCC and it is now thought that HAVcR-1 may be a susceptibility gene for RCC [283, 317].

Urinary HAVcR-1 levels also show a potential to distinguish between benign renal tumours and renal cancer as well as between clear cell renal carcinoma and other histological types of the disease [315, 318]. Urinary HAVcR-1 levels also showed a correlation between renal tumour size and grade [315, 317]. This is of importance as the late presentation of ccRCC leads to high mortality rates and highlights the possibility of HAVcR-1 being clinically important in cancer diagnosis. Urinary HAVcR-1 levels are also shown to be increased in prostate cancer thus highlighting the possibility of HAVcR-1 to be a biomarker of a multitude of cancers and opens up the possibility for the RenaStick™ to be used in cancer diagnosis as well as in the detection of kidney injury [315].

Total HAVcR-1 levels have also been shown to be increased in a multitude of cancers including breast, colorectal, ovarian and prostate [283, 319, 320]. This overexpression has led to investigations into the role of HAVcR-1 in cancer aetiology. HAVcR-1 has been linked to TJs, which have an important role in the prevention of cancer metastasis. Evidence currently suggests that the HAVcR-1 overexpression seen in cancer is linked to TJ disruption and therefore links HAVcR-1 to cancer

metastasis [319]. A number of virus receptors have been found to be associated with junctional structures including TJs and AJs and investigations into the association of HAVcR-1 with junctional structures found via immunoprecipitation that the 50 kDa HAVcR-1 associates with the C terminal of ZO-1 and to a lesser extent ZO-2 as well as the N-terminal of occludin and RhoC [143]. Due to the importance of these molecules in TJs it is possible that HAVcR-1 is also involved in the TJ complex in endothelial and epithelial cells. Overexpression and knockdown analysis of HAVcR-1 in a human umbilical cord cell line (HECV cells) suggests the importance of HAVcR-1 expression in the HGF mediated breakdown of TJ as show by decreased TER in HAVcR-1 overexpressed HECV cells in comparison to HAVcR-1 knockdown HECV endothelial cells when treated with HGF. Dual immunofluorescence of HAVcR-1 and ZO-1 showed an increased expression and concentrated disruption of ZO-1 in cell-cell junctions in knockdown HECV cells in comparison to wild type HECV cells when treated with HGF. Therefore it has appears likely that both HGF and HAVcR-1 act on the same pathway responsible for the integrity and maintenance of TJs [143]. Overexpression of HAVcR-1 in cell lines results in decreased TJs, HAVcR-1 overexpression in cancer is likely to also result in decreased TJs which may mediate metastasis. HAVcR-1 may therefore be a target for anti-metastatic cancer therapies. HAVcR-1 overexpression has also been shown to prevent differentiation and altered the expression of other members of the family that are associated with differentiation and de-differentiation events in kidney renal cell adenocarcinoma (769-P) and immortalised normal proximal tubular cell (HK-2) cell lines thus linking HAVcR-1 to these events [283]. *In vitro* HAVcR-1 overexpression and knockdown experiments using kidney renal cell adenocarcinoma (769-P) cells also revealed

delayed and increased migration as well as increased and decreased proliferation respectively [321]. HAVcR-1 may therefore play an important role in the regulation of multiple processes in cancer aetiology.

Ig-like domains are implicated in mediating protein-protein interactions and if at cell surface especially cell-cell and cell-extracellular matrix interactions [322]. The mucin domain which extends Ig-like domain away from surface like a stalk could have a role in configuration and protection as well as cell adhesion [286, 322]. It is also possible that similarly to other cell surface mucins such as MUC1 the mucin-like domain of HAVcR-1 may act in an anti-adhesive manner by preventing interactions between cells as well as between cells and the extracellular matrix [323, 324]. This may be a mechanism to allow detachment of cancer cells from primary tumours, a critical step in metastasis [324].

HAVcR-1 may therefore be a novel target for therapeutics in a variety of cancers and it has been shown that the monoclonal antibody 190/4 (mAb 190/4) binds HAVcR-1 and is internalized into the cell making it ideal for generation of an immunotoxin either by its conjugation with a toxin or its use in conjunction with a secondary antibody conjugated with a toxin [283, 325]. The use of the mouse mAb 190/4 followed by a secondary anti-mouse antibody conjugated to the toxin saporin was shown to effectively kill the kidney cell line GL37 via the HAVcR-1 receptor, making it a possible anti-cancer treatment [283]

Furthermore, the HAVcR-1 ectodomain has been shown to increase IL-6 expression which activates the STAT-3 pathway leading to increased HIF-1α [321]. High levels of IL-6 are present in patients with metastatic RCC and are correlated with poor survival. IL-6 binds the ligand binding receptor gp80 which leads to the phosphorylation of

tyrosine residues of the transducing receptor gp130. This allows for the docking and phosphorylation of the activator of transcription STAT-3 [326]. STAT-3 transcriptionally activates genes involved in tumour proliferation, apoptosis inhibition and angiogenesis including HIF1A, a key protein in promoting hypoxia induced angiogenesis [327]. HAVcR-1 shedding may therefore mediate angiogenesis and metastasis by regulating adhesion, migration and HIF-1α levels thus could be targeted as therapeutic target. The production of soluble HAVcR-1 can be inhibited by small molecule inhibitors of metalloproteases. However similarly to Herceptin (Transtuzamab) blocking the proteolytic cleavage of HER2 in breast cancer, therapeutic monoclonal antibodies blocking the cleavage site of HAVcR-1 may be a more specific therapeutic in HAVcR-1 positive cancers [284, 328].

1.5 Hypothesis and Aims

HAVcR-1 is a transmembrane protein that has been found to be overexpressed in breast, colorectal, renal and prostate cancer [283, 319]. Cleavage of HAVcR-1 proximal to the membrane leads the release of the HAVcR-1 ectodomain of which levels in urine of ccRCC is increased and correlates with tumour size and grade. This therefore proposes the HAVcR-1 ectodomain as a potential non-invasive biomarker for certain cancers [315, 317].

Links between HAVcR-1 and cellular junctions have been identified with HAVcR-1 overexpression disrupting TJ integrity [319]. Furthermore, HAVcR-1 has been linked to HGF mediated breakdown of TJ and therefore poses an exciting opportunity to explore HAVcR-1 as an anti-metastatic therapeutic target [143].

The role of HAVcR-1 in cancer development and progression is an active area of research however the role of HAVcR-1 in prostate cancer has not been fully investigated. Therefore, the main hypotheses of this study are that HAVcR-1 and/or the HAVcR-1 ectodomain will provide an effective biomarker for prostate cancer diagnosis and that through dysregulation of epithelial cell adhesion HAVcR-1 contributes to the development and progression to metastatic disease of prostate cancer.

The following aims will be addressed throughout the following chapters with the overall focus towards evaluating whether there is a potential to use HAVcR-1 is a prostate cancer biomarker and/or a viable therapeutic option to prevent/ treat prostate cancer metastasis.

- To explore the expression of HAVcR-1 in prostate cancer in comparison to normal prostate tissue.

- To explore the levels of the HAVcR-1 ectodomain in the serum of prostate cancer patients in comparison to healthy controls.

- To assess the expression profile of HAVcR-1 in prostate cancer cell lines.

- To establish stable HAVcR-1 overexpression and knockdown cell models.

- To investigate the effects of HAVcR-1 expression on cellular adhesion complexes.

- To investigate the effects of HAVcR-1 expression on cellular behaviour including: growth, invasion, migration and adhesion.

- To investigate the effects of HGF in conjunction with HAVcR-1 expression on cellular adhesion complexes and cellular behaviour.

85

Chapter II:

Materials and Methods

2.1 Materials

2.1.1 Mammalian Cell Lines

This study used PZ-HPV-7 an immortalised prostate epithelial cell line, CA-HPV-10 immortalised prostate adenocarcinoma cell line and LNCaP, PC-3 and Du145 metastatic prostate cancer cell lines. In addition, the HECV vascular endothelial cell line was used. PZ-HPV-7, CA-HPV-10, LNCaP, PC-3 and Du145 cell lines were purchased from the American Tissue Culture Collection (ATCC) (Manassas, VA, USA) and the HECV cell line was purchased from Interlab Cell Line Collection (Genova, Italy) at the commencement of this study and further details about these cell lines can be found in Table 2.1.

Table 2.1 Cell Lines Used In This study

Information regarding the source, morphology, growth properties and medium of cell lines used throughout this study.

Cell Line	Organism	Tissue	Disease/Cell Type	Age (Years)	Gender	Morphology	Growth Medium
PC-3	*Homo-Sapiens* (Human)	Prostate: Derived from Metastatic Site: Bone	Grade IV Adenocarcinoma	62	Male	Epithelial	DMEM
Du145	*Homo-Sapiens* (Human)	Prostate: Derived from Metastatic Site: Brain	Grade IV Carcinoma	69	Male	Epithelial	DMEM
LNCaP	*Homo-Sapiens* (Human)	Prostate: Derived from Metastatic Site: Lymph Node	Grade IV Carcinoma	50	Male	Epithelial	RPMI 1640
CA-HPV-10	*Homo-Sapiens* (Human)	Prostate	Human Papilomavirus 18 (HPV-18) Transformed Adenocarcinoma	63	Male	Epithelial	Keratinocyte -SFM
PZ-HPV-7	*Homo-Sapiens* (Human)	Prostate: Epithelial	Human Papilomavirus 18 (HPV-18) Transformed Epithelium	70	Male	Epithelial	Keratinocyte -SFM
HECV	*Homo-Sapiens* (Human)	Umbilical Code	Endothelium	0	Female	Endothelial	DMEM

DMEM- Dulbecco's modified Eagle's medium, RPMI- Roswell Park Memorial Institute, SFM- Serum free medium, HPV-Human papilloma virus

2.1.2 Primers

Primers used were designed using the Primer-BLAST programme available from NCBI. Reverse primers used for quantitative polymerase chain reaction (qPCR) included the addition of a z-sequence on the 5' end of the primer. Custom designed primers were synthesised by Sigma-Aldrich (Gillingham, Dorset, UK), diluted to 100 µM in PCR H_2O and stored at -20 °C. Forward and reverse primers for polymerase chain reaction (PCR) as well as forward primers for qPCR were further diluted 1:10 before use. Reverse qPCR primers were further diluted 1:100 before and all diluted primers were temporarily stored at 4 °C. Full sequences are given in Table 2.2 and Table 2.3.

Table 2.2 Primer Sequences Used in PCR

Target genes, sequences of primer pairs, cycle number and product size are detailed within this table.

Target Gene	Forward (F) and reverse (R) Primer Sequences 5'-3'	Cycle Number	Size (bp)
HAVCR1	F: CAACAACAAGTGTTCCAGTG	35	436
	R: GCATTTTGCAAAGCTTTAAT		
GAPDH	F: GGCTGTTTTAACTCTGGTA	25	475
	R: GACTGTGGTCATGAGTCCTT		
ZO1	F: CCACATACAGATACGAGTCCTC	30	533
	R: TGGCTTATGCTGAGATGAAGG		
ZO2	F: CTGACATGGAGGAGCTGA	30	844
	R: GAGACCATACTCTTCGTTCG		
CLDN1	F: ATGGCCAACGCGGGGC	30	636
	R: TCACACGTAGTCTTTCC		
CLDN2	F: TATAGCACCCTTCTGGGCCT	30	432
	R: CCTTGGAGAGCTCCTTGTGG		
CLDN3	F: ATGCAGTGAAGGTGTACGA	30	403
	R: TGGTGGCCGTGTACTTCTTC		
CLDN4	F: TGGGAGGGCCTCTGGATGAA	30	422
	R: TGGTGGCCGTGTACTTCTTC		
CLDN7	F: ATAACCCTTTGATCCCTACC	30	113
	R: ACTGAACCTGACCGTACAACAGG		
CLDN9	F: CTTCATCGGCAACAGCATCG	30	339
	R: AAGTCCTGGATGATGGCGTG		
JAMA	F: AACAAGATCACAGCTTCCTA	30	600
	R: CTTACTCGAAGTCCCTTTCT		
OCLN	F: ATGTCATCCAGGCCTC	30	579
	R: ATAGACAATTGTGGCA		
CTNNA1	F: CACAGAGAAGGTTCTGGAAG	30	518
	R: CCGATGTATTTTTGAGTGGT		
CTNNB1	F: AAAGGCTACTGTTGGATTGA	30	649
	R: TCCACCAGAGTGAAAAGAAC		
CCND1	F: CGGTGTCCTACTTCAAATGT	30	721
	R: ACCTCCTCCTCCTCCTCT		
EPLIN	F: TCAAACTAAGATTCTCCGGG	30	875
	R: TCGGGGCATCTTCTACC		
GSK3β	F: ATGTTTCGTATATCTGTT	30	534
	R: GGTGGAGTTGGAAGCTGATG		

Table 2.3 Primer Sequences Used in qPCR.
Target gene and sequences of primer pairs are detailed within this table. Reverse primer z-sequences are highlighted in bold.

Target Gene	Forward (F) and Reverse (R) Primer Sequences 5'-3'	Product Size (bp)
HAVCR1	F: GACAATGTTTCAACGA	99
	R: **ACTGAACCTGACCGTACA**TGGAGGAACAAA	
GAPDH	F: CTGAGTACGTCGTGGAGTC	93
	R: **ACTGAACCTGACCGTACA**CAGAGATGATGACCCTTTTG	

2.1.3 Antibodies

2.1.3.1 Primary antibodies

Primary antibodies were diluted to 40 µg/mL in 0.1 % BSA (Bovine Serum Albumin) in PBS and aliquoted to 50 µL and stored at -20 °C. These were diluted for use for western blotting, immunohistochemistry or immunofluorescence as stated in Table 2.4. The supplier, manufacturer's code and species produced in are also given in Table 2.4.

2.1.3.2 Secondary Antibodies

Secondary antibodies were stored at 4 °C ready for use. Supplier, manufacturer's code, species produced in and dilution of secondary antibodies used in western blotting, immunohistochemistry and immunofluorescence are given in Table 2.4. Also included are details on DAPI.

Table 2.4 Primary Antibodies Used In This Study.
Primary antibodies used in western blotting (WB), immunohistochemistry (IHC) and immunofluorescence (IF) are detailed in this table.

Target Protein	Supplier	Manufacture's code	Species	Dilution
HAVcR-1	Abnova, Heyford, Oxfordshire, UK	Pab13202	Rabbit	1:200 (WB)
TIM-1 (HAVcR-1)	R & D Systems, Abingdon, Oxfordshire, UK	AF1817	Mouse	1:500 (IHC)
TIM-1 (N-13) (HAVcR-1)	Santa Cruz, Insight Biotechnology Limited, Middlesex, UK	SC47495	Goat	2 µg/mL (IF)
GAPDH	Santa Cruz, Insight Biotechnology Limited, Middlesex UK	SC32233	Mouse	1:1000 (WB)
Cld-1	Santa Cruz, Insight Biotechnology Limited, Middlesex UK	SC17658	Goat	2 µg/mL (IF)
Cld-7	Santa Cruz, Insight Biotechnology Limited, Middlesex UK	SC17670	Goat	2 µg/mL (IF)
Occludin	Santa Cruz, Insight Biotechnology Limited, Middlesex UK	SC8145	Goat	2 µg/mL (IF)
ZO-1	Santa Cruz, Insight Biotechnology Limited, Middlesex UK	SC8146	Goat	2 µg/mL (IF)
α-Catenin	BD Transduction Laboratories, San Jose, CA, USA	C1620	Mouse	2 µg/mL (IF) 1:4000 (WB)
β-Catenin	Sigma-Aldrich, Gillingham, Dorset, UK	SC8415	Rabbit	2 µg/mL-IF 1:4000 (WB)
E-Cadherin	R & D Systems, Abingdon, Oxfordshire, UK	17029	Mouse	2 µg/mL (IF) 1:200 (WB)
EPLIN	Bethyl Lab, Montgomery, TX, USA	A300-103A	Rabbit	1:1000 (WB)
PKM2	Santa Cruz, Insight Biotechnology Limited, Middlesex UK	SC65176	Goat	1:200 (WB)
Cyclin D1	Santa Cruz, Insight Biotechnology Limited, Middlesex UK	Sc753	Rabbit	1:200 (WB)

Table 2.5 Secondary Antibodies Used In This Study

Secondary antibodies used in western blotting (WB), immunohistochemistry (IHC) and immunofluorescence (IF) are detailed in this table.

Antibody	Supplier	Manufacture's code	Species Produced In	Dilution
Anti-Mouse IgG (whole molecule)-Peroxidase	Sigma-Aldrich, Gillingham, Dorset, UK	A4416	Goat	1:1000 (WB)
Anti-Rabbit IgG (whole molecule)-Peroxidase	Sigma-Aldrich, Gillingham, Dorset, UK	A6154	Goat	1:1000 (WB)
Anti-Goat IgG (whole molecule)-Peroxidase	Sigma-Aldrich, Gillingham, Dorset, UK	A5420	Rabbit	1:1000 (WB)
Biotinylated anti- Mouse IgG	Vector Laboratories, Orton Southgate, Peterborough, UK	BA 2020	Goat	1:50 (IHC)
AlexaFluor 488	Thermo Fisher Scientific, Cramlington, England, UK	Anti-Rabbit A21206 Anti-Mouse A21202 Anti-Goat A11055	Donkey	1:500 (IF)
AlexaFluor 594	Thermo Fisher Scientific, Cramlington, England, UK	Anti-Rabbit A21207 Anti-Goat A11058	Donkey	1:500 (IF)
DAPI	Thermo Fisher Scientific, Cramlington, England, UK	D1306	N/A	1:1000 (IF)

2.1.4 Plastic- and Culture- Ware

All plastic culture-ware including: flasks (T25 T75), plates (6, 24 and 96 well) and centrifuge tubes were obtained from Greiner Bio-One Ltd. (Gloucestershire, UK) unless otherwise stated.

2.1.5 Serum Samples

2.1.5.1 Prostate Cancer Serum Samples

Prostate cancer serum samples (n=236) taken at time of surgery and were obtained from Wales Cancer Bank (WCB). Table 2.6 details prostate cancer grade and age of the patient at time of collection further details can be found in the Chapter VIII Appendix in Table 8.1.

2.1.5.2 Healthy Control Serum Samples

Whole Blood (n=9) was obtained from the Welsh Blood Service or obtained from male volunteers with informed consent (n=5). Serum from volunteers was extracted via centrifugation at 1500 g for 10 min and stored at -80 $^{\circ}$C.

Table 2.6 Prostate Cancer Serum Samples Information

Gleason Grade	Sample Number	Age at Collection
6	44	63.0±0.95
7	91	63.5±0.66
8	47	64.2±1.11
9	48	64.9±1.27
10	6	70.8±5.45

2.1.6 Patient Tissue Samples

Prostate cancer samples (n=2) and normal control samples (n=2) were collected at the University Hospital of Wales by the team led by Mr RA Hurle between January 2003 and 2006. Sections were collected with informed patient consent and with ethical approval from the South East Wales Research Ethics Committee (Panel C) under the project title "Hepatocyte growth factor (HGF) and its regulators on the behaviour of invasive/metastatic prostate cancer". Ethics no: 03/5048.

2.1.7 Solutions and Reagents

2.1.7.1 General Solutions and Reagents

Phosphate buffer saline (PBS)

Phosphate buffered saline 10 X concentrate (Sigma-Aldrich, Gillingham, Dorset, UK) diluted 1:10 in dH_2O. PBS was stored at room temperature.

Distilled H_2O (dH_2O)

H_2O purified using the Elix ® Water Purification System (Merck Millipore, Sigma-Aldrich, Gillingham, Dorset, UK) and stored in 60 L Polyethylene Storage Tank (TANKPE060, Merck Millipore, Sigma-Aldrich, Gillingham, Dorset, UK) with a Vent Filter (TANKMPK01, Merck Millipore, Sigma-Aldrich, Gillingham, Dorset, UK) to protect against airborne contaminants.

2.1.7.2 Cell Culture Solutions and Reagents

Antibiotic Antimycotic Solution- 100 X

Antibiotic Antimycotic Solution 100 X (A5955, Sigma-Aldrich, Gillingham, Dorset, UK) aliquoted to 5 mL and stored at -20 $^{\circ}$C

Trypsin Ethylenediaminetetracetic acid (Trypsin-EDTA)

Trypsin-EDTA 10 X (T4174, Sigma-Aldrich, Gillingham, Dorset, UK) diluted 1:10 dH$_2$O, aliquoted to 25 mL and stored long term at -20 ^{o}C or short term at 4 ^{o}C.

Freezing Medium

DMEM supplemented with 10 % (v/v) Dimethylsuphoxide (DMSO) (Sigma-Aldrich, Gillingham, Dorset, UK). Freezing medium was stored at 4 °C and used at room temperature.

Maintenance Medium

Cell medium containing 0.5 µg/mL of Blasticidin S. (Melford Laboratores Ltd., Suffolk, UK). All maintenance mediums were stored at 4 °C and used at room temperature.

Selection Medium

Cell medium containing 5 µg/mL of Blasticidin S. (Melford Laboratores Ltd., Suffolk, UK). All selection mediums were stored at 4 °C and used at room temperature.

DMEM

Dulbecco's modified Eagle's medium (DMEM) nutrient mixture F-12 HAM with 15 mM HEPES, NaHCO$_3$, pyridoxine and L-Glutamine medium (Sigma-Aldrich, Gillingham, Dorset, UK) supplemented with 10 % (v/v) heat inactivated foetal bovine serum (FCS) (Sigma-Aldrich, Gillingham, Dorset, UK), 1 % (v/v) Antibiotic Antimycotic Solution (A5955, Sigma-Aldrich, Gillingham, Dorset, UK). DMEM was stored at 4 °C and used at room temperature.

Keratinocyte Serum Free Medium (SFM)

Keratinocyte serum free medium supplemented with 0.05 mg/mL Bovine Pituitary Extract BPE and 5 ng/mL EGF (Thermo Fisher Scientific, Cramlington, England, UK). Keratinocyte-SFM was stored at 4 °C and used at room temperature.

RPMI-1640

RPMI-1640 medium (Sigma-Aldrich, Gillingham, Dorset, UK) supplemented with 10 %

(v/v) heat inactivated FCS (Sigma-Aldrich, Gillingham, Dorset, UK), 1 % (v/v) Antibiotic

Antimycotic Solution (A5955, Sigma-Aldrich, Gillingham, Dorset, UK). RPMI-1640 was

stored at 4 °C and used at room temperature.

2.1.7.3 Bacteriology Solutions and Reagents

Liquid Broth (LB)

Tryptone (10 g), NaCl (10 g) and Yeast extract (5 g) in 1 L distilled H_2O

Liquid Broth Agar

Typtone (10 g), NaCl (10 g), Yeast extract (5 g) and Agar (15 g) dissolved in 1 L of

distilled H_2O

TBE

TBE 10 X concentrate (Sigma-Aldrich, Gillingham, Dorset, UK) diluted 1:10 in dH_2O.

2.1.7.4 mRNA Detection Solutions and Reagents

Diethylpyrocarbonate (DEPC) H_2O- 0.05%

DEPC (250 μL) in 500 mL dH_2O

PCR H_2O

Autoclaved and UV treated dH_2O

Reverse Transcription (RT) master mix- 2X

RT 10 X buffer (2 μL), 25 XdNTP mix (0.8 μL), 10 X RT random primers (2 μL),

multiscribe reverse transcriptase (1 μL), RNase inhibitor (1 μL), nuclease free H_2O

(3.2 μL).

2.1.7.5 Protein Detection Solutions and Reagents

Ponceau S

Ponceau S (0.1 %) in 5 % acetic acid

5 % (w/v) Milk

Milk powder (2.5 g) (Marvel, London, UK) in 50 mL TPBS

1 % (w/v) Milk

Milk powder (0.5 g) (Marvel, London, UK) in 50 mL TPBS

Running Buffer

Tris-Glycine SDS Buffer 10 X concentrate (1 L) (Sigma-Aldrich, Gillingham, Dorset, UK)

made up to 10 L in dH_2O

SDS- 10 % (w/v)

SDS (10 g) in 100 mL distilled H_2O

Tween PBS (TPBS)- 0.05 % (v/v)

Tween (0.5 mL) made up to 1 L in PBS

Transfer buffer

Tris Glycine Buffer 10 X concentrate (1 L) (Sigma-Aldrich, Gillingham, Dorset, UK) and

2 L methanol made up to 10 L in distilled H_2O.

Western blotting Lysis buffer

NaCL (150 mM), Tris, 0.02 % Sodium azide (50 mM), Sodium deoxycholate (0.5 %)

and Triton X-100 (1.5 %) made up to 1 L in dH_2O. A cOmplete™, EDTA-free protease

inhibitor cocktail tablet (Sigma-Aldrich, Gillingham, Dorset, UK) was also added and

buffer stored at -20 °C.

Kinexus™ Antibody array Lysis Buffer

A cOmplete™, EDTA-free protease inhibitor cocktail tablet (Roche Diagnostics,

Mannheim, Germany), 10 % (v/v) 2-mercaptoethanol, 1 % (v/v) nonidet P-40 and

50 mM NaF in Tris buffer (0.04 % w/v Tris powder in dH_2O). Stored at -20 °C.

In Vitro Functional Assays Solutions and Reagents

10 % (v/v) Acetic Acid

Acetic Acid ≥99.7 % (320099, Sigma-Aldrich, Gillingham, Dorset, UK) diluted to 1:10 in dH_2O and stored at room temperature.

4 % (v/v) Formalin

Formalin 10 % (HT501128, Sigma-Aldrich, Gillingham, Dorset, UK) diluted to 4 % in dH_2O and stored at room temperature.

2.2 Methods

2.2.1 Mammalian Cell Culture

2.2.1.1 Routine Cell Culture

All cell work was carried out aseptically using a Class II Laminar Flow Cabinet with sterile and autoclaved equipment and consumables. PC-3, Du145 and HECV cell lines were maintained in DMEM medium. LNCaP clone FGC cell line was maintained in RPMI-1640 medium. PZ-HPV-7 and CA-HPV-10 cell lines were maintained in Keratinocyte-SFM. Transfected cell lines containing the pEF6 plasmid vector were cultured in selection medium for 10 to 14 days prior to culture in maintenance medium. Cells were cultured in 25 cm² (T25) culture flasks with 4.5 mL medium or in 75 cm² (T75) culture flasks with 15 mL medium at 37 °C in a 95 % (v/v) humidified atmosphere of 5 % (v/v) CO_2. Cell media was replaced approximately every three days after a PBS wash and passaged at approximately 80 % confluence via trypsinisation.

2.2.1.2 Trypsinisation

Cells were trypsinised to detach cells adhered to the flask. This was performed for routine maintenance, sub-culture, freezing and seeding. Medium was aspirated and

cells were washed with 1 mL or 3 mL PBS for a T25 or T75 respectively to remove excess FCS and thus improve efficacy of trypsin-EDTA. PBS was then aspirated and 1 mL or 3 mL of sterile trypsin-EDTA was added to the T25 or T75 respectively. Flasks were incubated at 37 °C in a 95 % (v/v) humidified atmosphere of 5 % (v/v) CO_2 for approximately 5-10 min until cells were detached. Trypsin-EDTA was then neutralised using 4 mL or 7 mL DMEM due to it containing FCS and mixture transferred into a sterile universal. Cells grown in keratinocyte-SFM required centrifugation at 12000 g for 5 min prior to re-suspension in keratinocyte-SFM. Cells were then counted and diluted prior to being transferred to further flasks for re-culturing and cell maintenance or into plates and other culture ware for experiments as described later in this chapter.

2.2.1.3 Cell counting

After trypsinisation and re-suspension in recommended growth media, 10 µL of cell suspension was transferred to a 0.1 mm depth cell counting chamber and counted with Neubauer Ruling (Hawksley, Sussex, UK) at 100 X magnification using an inverted light microscope (Reichert, Austria). This gave cell number per mL via equation shown below.

$$\frac{(Cell\ Number)}{mL} = Number\ of\ cells\ counted\ X\ 10^4$$

The cell suspension was then diluted to give required cells per mL; this number changed depending on assay undertaken. The equation for this is shown below.

$$\frac{Number\ of\ Cells\ Required/mL}{Number\ of\ Cells\ in\ Cell\ Solution/mL}\ X\ Volume\ Required\ (mL) = Volume\ of\ Cell\ Solution\ (mL)$$

2.2.1.4 Cell Storage

Cells were trypsinised as previously described, centrifuged at 12000 g for 5 min to give a cell pellet which was then re-suspended in 1 mL or 3 mL freezing medium of a T25 or T75 respectively. The suspension was immediately divided into 1 mL aliquots in 1 mL CRYO.S™ tubes and stored overnight in a -20 °C freezer prior to short term storage in a -80 °C freezer or long-term storage in liquid nitrogen tanks.

2.2.1.5 Cell Revival

Frozen stocks were rapidly thawed in CRYO.S™ tubes using a water bath. The cell solution was then transferred into a sterile universal. DMEM was then added to make the solution up to 5 mL prior to centrifugation at 12000 g for 5 min to obtain a cell pellet. The supernatant containing DMSO was removed, cell pellet re-suspended in 5 mL DMEM, transferred into a T25 flask and incubated at 37 °C in a 95 % (v/v) humidified atmosphere of 5 % (v/v) CO_2. Cells were then subjected to routine cell culture.

2.2.1.6 Mycoplasma Testing

Mycoplasma Testing was undertaken every 3 months on every cell line using the EZ-PCR Mycoplasma Test Kit (Geneflow, Staffordshire, UK). Media was removed from cell culture prior to passaging. Cellular debris was removed via centrifugation at 500 rpm for 2 min and supernatant centrifuged at 16000 g for 10 min to pellet potential mycoplasma. Pellet was re-suspended in 25 μL Buffer Solution prior to heating to 95 °C for 3 min. The reaction mixture for PCR is then prepared using 2.5 μL resuspended pellet, 5 μL reaction mix and 17.5 μL sterile H_2O. PCR was then carried out on samples alongside a positive control provided using the thermocycler geneAmp PCR system 2700 (Applied Biosystems, Carlsbad, CA, USA); parameters are

shown in Table 2.7. PCR products alongside a PCR Ranger 100 bp DNA ladder (Geneflow, Staffordshire, UK) were then separated on 2 % (w/v) agarose (A9539, Sigma-Aldrich, Gillingham, Dorset, UK) gel via electrophoresis at 120 V, 100 mA and 50 kW. Bands at 270 bp show a positive test at which point cells were discarded.

Table 2.7 Mycoplasma Testing PCR parameters

Temperature	Time	Cycles
94 °C	30secs	1
94 °C	30secs	
60 °C	2 min	35
72 °C	1min	
94 °C	30secs	1
60 °C	2 min	1
72 °C	5 min	1

Table 2.7 Mycoplasma Testing PCR parameters

2.2.2 Generation of Plasmids

2.2.2.1 PCR Amplification of HAVcR-1 Ribozyme

Ribozymes were amplified using PCR using GoTaq Green mater mix (Promega, Southampton, UK). Each reaction consisted of the following ingredients:

- 12 µL 2 X GoTaq G2 GREEN master mix

- 5 µL of 500 nM HAVcR-1 ribozyme forward primer (ACTAGTGGAGAGGAGGTCCATCCATCTGTTTCGTCCTCACGGACT)

- 5 µL of HAVcR-1 ribozyme reverse primer (CTGCAGTAGTGGCAGGGTAGTGTCTGATGAGTCCGTGAGGA)

- 2 µL PCR H$_2$0

This mixture was transferred to an RNase free PCR tube and placed in the thermocycler geneAmp PCR system 2700 (Thermo Fisher Scientific, Cramlington, England, UK). The parameters of this are specified in Table 2.8. PCR products were then visualised using gel electrophoresis to ensure expected product size of approximately 200 bp. Products were then stored short term at 4 °C.

Table 2.8 PCR Parameters for HAVcR-1 Ribozyme Amplification

Temperature	Time	Cycles
94 °C	5 min	1
94 °C	20 secs	8
70 °C	30 secs	
72 °C	30 secs	
94 °C	20 secs	8
65 °C	30 secs	
72 °C	30 secs	
94 °C	20 secs	8
60 °C	30 secs	
72 °C	30 secs	
94 °C	20 secs	8
55 °C	30 secs	
72 °C	30 secs	
94 °C	20 secs	8
50 °C	30 secs	
72 °C	30 secs	
72 °C	7 min	1

2.2.2.2 Production of pEF6 Ribozyme Plasmids

The ribozyme insert was cloned into the plasmid using the pEF6/V5-His TOPO TA expression kit (Invitrogen, Paisley, Scotland, UK). Each reaction consisted of the following ingredients:

- 4 μL of ribozyme PCR product

- 1 μL salt solution

- 1 μL TOPO vector

This mixture was combined in a sterile microfuge tube and incubated at room temperature for 5 min. This was then used to transform 50 mL One Shot TOP10 Chemically Competent *Escherichia coli (E. coli)* (Invitrogen, Paisley, Scotland, UK).

2.2.2.3 Transformation of *E. coli*

One Shot TOP10 Chemically Competent *E.coli* (Invitrogen, Paisley, Scotland, UK) (50 mL) were transformed with plasmid produced as described in 2.2.2.2. The was achieved via the heat-shocked method whereby the *E.coli* and plasmid were mixed by gentle pipetting then incubated at 42 °C for 30 seconds prior to a 5 min incubation on ice. This was then added to 250 μL of SOC media (Invitrogen, Paisley, Scotland, UK) and cells were left to shake for an hour at 37 °C.

2.2.2.4 Plasmid selection and orientation analysis

Transformed *E.coli* were spread on agar plates (12 mL LB agar with 100 μg/mL ampicillin) with plates split in half and 100 μL or 150 μL spread on each side. Agar plates were then incubated upside down overnight at 37 °C. Ribozyme insert orientation with the plasmid was checked using PCR (See Table 2.9). Colonies were

picked twice and either mixed with primer mixes for correct or incorrect orientation.

Correct orientation mix consisted of:

- 10 μL 2 X GoTaq G2 GREEN master mix (Promega, Southampton, UK)

- 2 μL of 500 nM T7 forward primer (TTAATACGCTCACTATAGGG)

- 2 μL of 500 nM RB RMR primer (TTCGTCCTCACGGACTCATCAG)

- 5 μL sterile H_2O

Whereas the incorrect orientation mix consisted of:

- 10 μL 2 X GoTaq G2 GREEN master mix (Promega, Southampton, UK)

- 2 μL of 500 nM T7 forward primer(TTAATACGCTCACTATAGGG)

- 2 μL of 500 nM RB TPF primer (CTGATGAGTCCGAGGACGAA)

- 5 μL PCR H_2O.

PCR products were then electrophoresed alongside a PCR Ranger 100 bp DNA ladder (Geneflow, Staffordshire, UK) on a 1 % (w/v) agarose (A9539, Sigma-Aldrich, Gillingham, Dorset, UK) gel at 120 V, 100 mA and 50 kW. Bands for both orientations were approximately 400 bp. Colonies with correct orientation were then picked and incubated in 5 mL of LB overnight at 37 °C on a Stuart Orbital Shaker (SSLI, Stuart, Staffordshire, UK).

Table 2.9. Plasmid orientation analysis PCR parameters

Stage	Sub-stage	Temperature	Time
Initial denaturation		94 °C	10 min
PCR cycle	Denaturation	94 °C	30 sec
	Anneal	55 °C	30 sec
	Elongation	72 °C	30 sec
Final extension		72 °C	7 min
Hold		4 °C	∞

2.2.2.5 Plasmid Purification

Plasmids were extracted and purified using GenElute Plasmid Miniprep Kit (Sigma-Aldrich, Gillingham, Dorset, UK). After the overnight culture of 5 mL of transformed *E.coli* in LB (See Section 2.2.2.3) cells were pelleted via centrifugation at 12000 g for 1 min. Cells were then re-suspended in 200 μL of Re-suspension solution and lysed using 200 μL Lysis solution. This lysis reaction was allowed to occur for less than 5 min prior to neutralization via the addition of 350 μL of Neutralization/ Binding solution and gentle inversion. The cell debris was then precipitated by centrifugation at 12000 g for 10 min. Cleared lysate (supernatant) was then transfered to a previously prepared column. Column preparation involved the addition of 500 μL of Column Preparation solution and the centrifugation at 12000 g for 1 min. The column containing the supernatant was then centrifuged at 12000 g for 1 min and flow-through discarded. The column was then washed twice to remove residual salts and other contaminants using 750 μL of diluted Wash solution and centrifugation at 12000 g for 1 min. The plasmid was then eluted by the addition of 100 μL Elution solution to the column and centrifugation at 12000 g for 1 min. Purified plasmids were then stored at -20 °C.

2.2.2.6 Electroporation of cell lines

Mammalian cell lines were washed with PBS, detached from growth surface using Trypsin-EDTA and diluted in medium so that there was 1×10^6 cells/mL. This cell suspension was then transferred into a sterile electroporation cuvette so that there was 800 μL of cell suspension and 4 μg of plasmid was added. Cells were then electroporated alongside a control containing no plasmid using the Gene Pulser Xcell Electroporation System (BioRad, Hertfordshire, UK) (See Table 2.10). Electroporated

cells were then transferred into a T25 flask with 4 mL of cell medium. After 24 hours

cells are grown in selection medium for up to 2 weeks, until all control cells had died,

before the medium was changed to maintenance medium.

Table 2.10. Electroporation Parameters

Cell line	Voltage (V)	Capacitance (μF)
PC-3	310	1500
PZ-HPV-7	290	1000

2.2.3 mRNA Detection

2.2.3.1 RNA Extraction

Cells were lysed and RNA extracted using EZ-RNA kit (Geneflow, Staffordshire, UK). Medium was aspirated and cells washed with PBS. Denaturing Solution was added at 0.5 mL per 10 cm² culture dish area and cells were scraped using 28 cm length Cell Scrapers (Greiner Bio-One Ltd., Gloucestershire, UK) to maximize harvest. Cells were passed through a 1 mL pipette tip several times to produce a homogenate lysate and transferred into RNase free 1.5 mL microfuge tubes. To this lysate 0.5 mL of Extraction Solution per 0.5 mL of Denaturing Solution was added, vortexed for 15 seconds and incubated at room temperate for 10 min. This was then centrifuged at 12000 g for 15 min at 4 °C. The colourless aqueous upper phase containing RNA was then transferred into a fresh RNAsase free 1.5 mL microfuge tube, washed with 0.5 mL of isopropanol (propan-2-ol) (Fisher Scientific, Loughborough, UK) per 0.5 mL of Denaturing Solution, mixed via inversion and incubated at room temperature for 10 min. This was then centrifuged at 12000 g for 8 min at 4 °C. The supernatant was then discarded and the RNA pellet was washed with 75 % (v/v) ethanol (Fisher Scientific, Loughborough, UK). This was them centrifuged at 7500 g for 5 min at 4 °C. The supernatant was discarded and the RNA pellet was dried at room temperature for approximately 5 min and then re-suspended via pipetting in 20-100 μL DEPC H_2O. Concentration and purity was then measured using a nanophotometer™ (Geneflow, Staffordshire, UK) at 260/280 OD. Extracted RNA was then stored at -80 °C.

2.2.3.2 Reverse Transcription (RT)

RNA was reverse transcribed to cDNA using the GoScript™ Reverse Transcription System (Promega, Southampton, UK). RNA was diluted in DEPC H_2O to produce

500 ng RNA per 4 μL. In a thin walled PCR tube or well of a 96 well PCR plate 1 μL

(0.5 μg) of Primer Oligo(dT)$_{15}$ reagent was then added the RNA dilution. Samples

were then heated to 70 ^{o}C for 5 min, incubated on ice for 5 min and centrifuged for

10 seconds. RT reaction mix was then added to the samples at 15 μL per reaction.

The final 20 μL mix was then incubated at 25 ^{o}C for 5 min, 42 ^{o}C for 60 min and 70 ^{o}C

for 15 min. cDNA was then diluted 1:4 in PCR H$_2$O and stored at -20 ^{o}C.

2.2.3.3 Conventional Polymerase Chain Reaction (PCR)

PCR was carried out using GoTaq Green Master Mix (Promega, Southampton, UK)

with specific primers detailed in Table 2.2. A PCR mix consisted of the following

components:

- 8 μL 2 X GoTaq G2 GREEN Master Mix

- 1 μL 500 nM forward primer

- 1 μL 500 nM reverse primer

- 1-4 μL cDNA made up to 6 μL with PCR H$_2$O

All genes were normalised to the *GAPDH* housekeeping gene thus for every cDNA

sample a PCR reaction with primers specific for *GAPDH* was carried out. Furthermore,

for every primer set a negative control PCR reaction was carried out whereby the PCR

mix contained no cDNA. The reaction mix was formulated in a RNase free thin walled

200 μL PCR tube or a well of a 96-well PCR plate, which were then briefly centrifuged

and placed in the thermocycler geneAmp PCR system 2700 (Thermo Fisher Scientific,

Cramlington, England, UK). PCR conditions are described in Table 2.11 and the

number of PCR cycles was primer dependent and are stated in See Table 2.2. PCR

products were then visualised using gel electrophoresis as described in Section

2.2.3.4.

Table 2.11 Parameters for PCR

Stage		Temperature	Time
Initial denaturation		94 °C	5 min
PCR cycle	Denaturation	94 °C	30 sec
	Anneal	55 °C	30 sec
	Elongation	72 °C	30 sec
Final extension		72 °C	7 min
Hold		4 °C	∞ - until collection

2.2.3.4 Gel Electrophoresis

Agarose gel electrophoresis was used to separate DNA fragments according to size. Samples were loaded onto a 2 % (w/v) agarose gel. Agarose gel was made by adding 1 g or 3 g agarose (A9539, Sigma-Aldrich, Gillingham, Dorset, UK) into 50 mL or 150 mL 1 X TBE buffer respectively. This mixture was then heated in a microwave until powder had fully dissolved to leave a transparent solution and this was then allowed to cool to approximately 70 °C. SYBR safe DNA gel stain (Invitrogen, Paisley, Scotland, UK) was then added, 5 µL for a 50 mL gel and 10 µL for a 15 mL gel. The gel mixture was the poured into prepared casting trays with assembled plastic combs (SCIE-PLAS, Cambridge, UK) and allowed to set at room temperature. Once the gel was set it was submerged in 1 X TBE buffer, combs were removed and PCR products were loaded into the wells at 10-15 µL per well alongside 5 µL PCR Ranger 100 bp DNA ladder (Geneflow, Staffordshire, UK). PCR products were electrophoresed at 120 V, 100 mA and 50 kW using an EV243 power consort (Wolf Laboratories, York, UK) for approximately 30 min or until separation was sufficient. Bands created were then visualised and images were taken under UV light produced by the U:Genius System (Syngene, Cambridge, UK).

2.2.3.5 Quantitative Polymerase Chain Reaction (qPCR)

Precision FAST 2 X qPCR Master Mix with ROX (Primer Design, Southampton, UK) and Amplifuor™ Uniprimer™ Universal System (Intergen Company®, NY, USA) was used to carry out qPCR. A qPCR reaction mix consisted of the following:

- 5 µL of precision FAST 2 X qPCR Master Mix with ROX

- 0.3 µL Amplifuor™ Uniprimer™

- 0.3 µL forward primer

- 0.3 μL reverse Z primer

- 1-4 μL cDNA made up to 4μL in PCR H$_2$0

qPCR was carried out for each sample using primers specific to the house keeping gene *GAPDH*; which was then used for normalising. The qPCR mixes were compiled in triplicate in a microamp® Fast Optical 96 well reaction plate with barcode (Applied Biosystems, Carlsbad, CA, USA) and covered with MicroAmp® Optical Adhesive film (Thermo Fisher Scientific, Cramlington, England, UK). qPCR was carried out using the StepOne Plus Real-Time PCR System (Thermo Fisher Scientific, Cramlington, England, UK). The conditions for qPCR are detailed in Table 2.12.

The Amplifuor™ Uniprimer™ consists of a 3' complementary sequence that pairs with the z-sequence (ACTGAACCTGACCGTACA) present on qPCR reverse primers as well as a 5' hairpin loop labelled with a fluorophore reporter (FAM). When this hairpin loop is intact the 5' reporter is in close proximity to the quencher (DABSYL) and thus the fluorescent signal is quenched. During the first amplification cycle the z-sequence containing reverse primer anneals and amplifies target mRNA. The Amplifuor™ Uniprimer™ can then anneal via the 3' sequence to the amplified mRNA 5' z-sequence and is then extended. This extended Amplifuor™ Uniprimer™ now contains the template for the forward primer which anneals and extends disturbing the hairpin loop, which separates the reporter from the quencher and results in a fluorescent signal. The hairpin structure therefore stays intact when the Amplifuor™ Uniprimer™ is free in solution as well as during the first and second amplification round; fluorescence only occurs during extension of the Amplifluor™ Uniprimer™ by the forward primer. The cycle at which the fluorescent signal reached a particular

threshold, known as the C_T value was then given and this was then analysed using $\Delta\Delta$

C_T normalised to the *GAPDH* housekeeping gene.

Table 2.12 Parameters for qPCR

Stage		Temperature	Time
Initial denaturation		94 °C	10 min
PCR cycles (100 cycles)	Denaturation	94 °C	10 sec
	Anneal	55 °C	30 sec
	Elongation	72 °C	10 min

2.2.4 Protein Detection

2.2.4.1 Protein Extraction

Cells media was aspirated and cells were washed with PBS before being lysed with lysis buffer. The amount of lysis buffer used depended on culture size; 40 μL was used per well of a 6 well pate and 150 μL per 10 cm dish. Cell lysates were then incubated on ice for 5 min, collected to one area using 28 cm length Cell Scrapers (Greiner Bio-One Ltd., Gloucestershire, UK) and transferred to 1.5 mL microfuge tubes. Cell lysates were then rotated for 30 min on a Labinoco LD79 Test-tube Rotator (Wolf Laboratories, York, UK) prior to centrifugation at 12000 g for 15 min at 4 °C. Supernatant (protein lysate) was then transferred into a fresh 1.5 mL microfuge tube, it was then either stored at -20 °C ready for protein sample quantification or equal volumes of LaemmLi 2 X Concentrate (Sigma-Aldrich, Gillingham, Dorset, UK) added prior to boiling at 100 °C for 10 min.

2.2.4.2 Protein Sample Quantification

The Bio-Rad DC™ Protein Assay Kit (BioRad, Hertfordshire, UK) was used for protein sample quantification. A standard curve using bovine serum albumin (BSA) was set up so that BSA concentration was 0, 0.25, 0.5, 1, 1.0, 1.5, 2, 2.5, 3, 3.5, 4, 4.5 and 5 mg/mL. Samples and standards were set up in duplicate with 5 μL per well of a 96-well plate. Reagent A and S mix was prepared so that reagent S was diluted 1:50 in reagent A and 25 μL of this reagent A and S mix was added to each well containing sample or standard, alongside 200 μL reagent B. The plate was then agitated via a shaker and incubated at room temperature for 5 min to allow colorimetric reaction to occur. The plate was then read on an ELx800 Absorbance Reader (BioTek, Swindon, UK) at 630 nm. The absorbance of the standards was used to create a standard curve

and enabled the concentration of samples to be calculated. Samples were then diluted to desired concentration in lysis buffer and added an equal volume of LaemmLi 2 X concentrate (Sigma-Aldrich, Gillingham, Dorset, UK) prior to boiling at 100 °C for 10 min. Protein samples were stored at -20 °C ready for use.

2.2.4.3 SDS Polyacrylamide Gel Electrophoresis (SDS-PAGE)

SDS-PAGE was undertaken on an acrylamide gel composed of a 10 % (v/v) running gel and 5 % (v/v) stacking gel in an OmniPAGE VS10DYS Vertical Electrophoresis System (OmniPAGE, Cleaver Scientific Ltd., Rugby, UK). The reagents to make up resolving and stacking gels are detailed in Table 2.13. Approximately 5 mL of resolving gel mixture was loaded between 2 glass slide that had been assembled in a loading cassette, the top was then covered with isopropanol (2-propanol) (Fisher Scientific, Loughborough, UK) and the gel was left to polymerise at room temperature for approximately 30 min. Once gel had polymerised the isopropanol was removed and approximately 2 mL of stacking gel mixture was loaded on top of the resolving gel, a well-forming Teflon comb inserted into the stacking gel and the stacking gel was left to polymerise at room temperature for approximately 30 min. The loading cassette was then transferred into an electrophoresis tank, running buffer was added so that the central reservoir was filled and the area surrounding the loading cassette was half filled and Teflon combs were removed. Samples were then loaded into wells so that there was 15-20 µL of sample per well depending on well size. Samples were resolved alongside a BLUeye Prestained Protein ladder (Geneflow, Staffordshire, UK). Protein samples were electrophoresed at 100 V, 150 mA and 50 W for approximately 1.5 hours or until sufficient separation had occurred using an EV243 Power Consort (Wolf Laboratories, York, UK)

Table 2.13 Components of Resolving and Stacking Acrylamide Gels for SDS-PAGE

Components	15 mL 10 % Running Gel Volume (mL)	5 mL 5 % Stacking Gel Volume (mL)
Acrylamide 30 % (Sigma-Aldrich)	5.0	0.83
dH_2O	5.9	3.4
1.5M TRIS pH 8.8 (Bio-Rad Laboratories)	3.8	-
0.5M TRIS pH 6.8 (Bio-Rad Laboratories)	-	0.63
10 % SDS	0.15	0.05
10 % APS	0.15	0.05
TEMED (Sigma-Aldrich)	0.006	0.005

2.2.4.4 Western Blot Transfer of Proteins to Polyvinylidene Fluoride (PVDF) Membrane

Samples were then transferred from the acrylamide gel to a PVDF Transfer Membrane (Merck Millipore, Sigma-Aldrich, Gillingham, Dorset, UK) using the Mini Trans-Blot® Cell (BioRad, Hertfordshire, UK) wet transfer system. Western blot transfer required the following per gel:

- 1 piece of PVDF Transfer Membrane

- 6 pieces of filter/ western blotting paper

- 2 foam pads

The PVDF Transfer Membrane was prepared by soaking it in 100 % methanol (Thermo Fisher Scientific, Cramlington, England, UK) for 30 secs and then submersion in transfer buffer whereas the filter paper and foam pads were only submerged in transfer buffer. On completion of the stacking gel component was discarded and the transfer cassette prepared. The transfer cassette was then prepared so that the black side of the cassette was the base and placed in order on top of this was a foam pad, 3 pieces of filter paper, the acrylamide gel, the PVDF Transfer Membrane, 3 pieces of filter paper and the second foam pad. The transfer cassette was transferred to a Mini Trans-Blot Central Core which was then placed inside of a transfer tank along with an ice cooling unit and this was filled with transfer buffer. Electrophoresis was carried out at 100 V, 150 mA and 50 W for approximately 1 hr using an EV243 Power Consort (Wolf Laboratories, York, UK)

2.2.4.5 Immunoprobing

Upon completion of western blot transfer of proteins, the PVDF Transfer Membrane was stained with Ponceau S. (Sigma-Aldrich, Gillingham, Dorset, UK) to verify

124

successful protein transfer. Ponceau S. staining was then removed washing with dH$_2$O. The PVDF Transfer Membrane was then transferred into a 25 mL Falcon Tube so that the protein faced inwards and blocked in 12.5 mL of 5 % (w/v) milk for 1 hr at room temperature on a Stuart Roller Mixer SRT2 (Stuart, Staffordshire, UK) to prevent non-specific antibody binding. Following this the 5 % (w/v) milk was discarded and 4 mL primary antibody diluted in 1 % (w/v) milk was added to the Falcon Tube and membranes incubated at 4 °C on a Stuart Roller Mixer SRT2 (Stuart, Staffordshire, UK) overnight. Primary antibody dilution specifications are detailed in Table 2.4. Following primary antibody incubation membranes were washed 3 times in 5 mL TPBS for 5 min per wash. HRP-conjugated secondary antibodies diluted in 1 % (w/v) milk were then added to falcon tube and membranes incubated in this at room temperature for 1 hr on a Stuart Roller Mixer SRT2 (Stuart, Staffordshire, UK). Secondary antibody specificity and dilution specifications are described in Table 2.5. Secondary antibody specificity chosen was based on the species of which the primary antibody was produced as detailed in Table 2.4. After the secondary antibody incubation, membranes were washed 3 times in TPBS for 5 min per wash and 1 time in PBS for 5 min.

2.2.4.6 Protein Visualisation

EZ-ECL Chemiluminescent Detection Kit (Geneflow, Staffordshire, UK) was used for protein visualisation. Per membrane, 1 mL of EZ-ECL solution, consisting of equal parts EZ-ECL solution A and B, was used. The EZ-ECL solution was made up and left in the dark at room temperature for 5 min. The EZ-ECL solution was then applied directly to the PVDF Transfer Membrane so that the membrane was covered and then incubated in the dark at room temperature for 5 min. Excess EZ-ECL solution

was then removed from the membrane and the chemiluminescent signal was detected and imaged using the G:Box Chemi RxQ Imaging System (Syngene, Cambridge, UK). Semi-quantitative analysis was then carried out on images obtained using ImageJ software, whereby integrated density was used to assess protein expression which was then normalised to the house keeping protein GAPDH.

2.2.4.7 Protein Preparation for the Kinexus™ Antibody Microarray

In preparation for a Kinexus™ Anibody Microarray PZ-HPV-7^{pEF6} and PZ-HPV-7$^{HAVcR-1EXP}$ cells were cultures in 10 cm dishes. When confluent cells were washed twice in PBS, 100 µL Kinexus™ Antibody array lysis buffer was added to lyse cells and cell lysates were collected to an area of the plate using 28 cm length Cell Scrapers (Greiner Bio-One Ltd., Gloucestershire, UK). Cell lysates were then transferred into a 1.5 mL microfuge tubes and rotated for 40 min on a Labinoco LD79 Test-tube Rotator (Wolf Laboratories, York, UK). Samples were then centrifuged at 14000 g for 30 min and the supernatant was transferred to a fresh microfuge.

Protein was quantified using fluorescamine reagent (F9015, Sigma-Aldrich, Gillingham, Dorset, UK). Fluorescamine was dissolved to 3 mg/mL in absolute acetone (Fisher Scientific, Loughborough, UK) in a glass vial. BSA standards described in Section 2.2.4.2 were used in triplicate in a 96 well plate. Protein samples were diluted 1:10 in PBS and transferred in triplicate into the 96 well plate at 150 µL per well. Dissolved fluorescamine was added to BSA standards and protein samples at 50 µL per well and plate was shaken for 1 min. The fluorescent signal was then measured with a 365 nm excitation and 410-460 nm emission filter using the GloMax®- Multi Microplate Multimode Reader (Promega, Southampton, UK). The signal from BSA standards was used to create a standard curve which was then used

to calculate the concentration of the protein samples. Protein samples were then diluted to 4 mg/mL using Kinexus™ Antibody array lysis buffer to a final volume of 300 µL. Samples were then stored at -20 °C prior to being shipped to Kinexus Bioinformatics, Vancover, Canada for the Kinexus™ Antibody Microarray.

2.2.4.8 Kinexus™ Antibody Microarray

The Kinexus™ KAM880 Protein Array service provided by Kinexus Bioinformatics Ltd. (Vancouver, Canada) was utilised for this project. The Kinexus™ KAM880 Protein Array uses microarray chips which contain two sets of 877 antibodies, of which 518 are pan-specific and 359 are phosphosite -specific, therefore allowing for two samples to be tested on the same chip and antibodies cover a wide array of cell signalling proteins and pathways. Antibodies are covalently bound to the array chip, the conditions of which ensure high bind efficiency and specificity. Each antibody has a loading control to ensure constant protein loading. Proteins are fluorescently labelled and the amount of protein present is measured via the amount of fluorescent signal produced. This is done with the ImaGene 8.0 system by Kinexus Bioinformatics Ltd.; which has predetermined settings for spot segmentation and background correction. Background corrected data is then globally normalised to the sum of the intensities of all net signal median values. The percentage change from control (%CFC) was then calculated as follows; whereby treated refers to PZ-HPV-$7^{\text{HAVcR-1EXP}}$ and control refers to PZ-HPV-7^{pEF6}

$$\%CFC = \frac{Globally\ normalised\ treated - Globally\ normalised\ control}{Globally\ normalised\ control} \times 100$$

Percentage error, Z-scores and Z-ratios were also calculated and returned within a Microsoft Excel spreadsheet. Significance was based on z-values of $\leq$-1.65 or $\geq$1.65.

2.2.4.9 Immunofluorescence

Cell were seeded into 8 well glass Millicell EZ slides (Merck Millipore, Sigma-Aldrich, Gillingham, Dorset, UK) at 5 X 10^4 cells per well in 500 µL medium. Slides were then incubated at 37 °C in a 95 % (v/v) humidified atmosphere of 5 % (v/v) CO_2 until cells were confluent. Once confluent culture medium was removed and cells were washed with PBS and fixed in 500 µL 100 % ice cold ethanol per well and left at -20 °C for a minimum of overnight and a maximum of 2 weeks. Ethanol was then removed and cells were wash 3 times with PBS for 5 min per wash and permeabilised by adding 500 µL 0.1 % Triton X-100 (Sigma-Aldrich, Gillingham, Dorset, UK) per well for 1-5 min, depending on protein of interest, at room temperature. Cells were then washed 3 times in PBS for 5 min per wash and blocked using blocking buffer, consisting of 7.5 % (v/v) donkey serum (D9663, Sigma-Aldrich, Gillingham, Dorset, UK) in PBS, at 300 µL per well for 6 hours at room temperature. Blocking buffer was then removed and cells were incubated in 250 µL of primary antibodies diluted to 2 µg/mL in blocking buffer overnight at 4 °C; primary antibodies are detailed in Table 2.4. The primary antibody was then removed and cells were washed 3 times in PBS for 5 min per wash and incubated with 250 µL secondary antibody solution per well for 2 hours in the dark at room temperature. The secondary antibody solution contained secondary antibodies diluted 1:500 and DAPI diluted 1:1000 in blocking buffer. The secondary antibody used was based on the species the primary antibodies had been produced in as detailed in Table 2.4 and secondary antibodies as well as DAPI are detailed in Table 2.5. Cells were then washed 3 times in PBS for 5 min per wash, the plastic chamber removed from slide and slides were mounted with FluorSave™ (345789, Sigma-Aldrich, Gillingham, Dorset, UK) and a cover slip. Slides were then left

to set in the dark at 4 °C overnight and visualised/imaged using the Hamamatsu Orca ER digital camera and the Olympus BXSA microscope at 100 X magnification. Merged images were then created using Adobe Photoshop software.

2.2.4.10   Immunohistochemical Staining (IHC)

Cryosections were stored at -80 °C. These were allowed to thaw at room temp for approximately 15 min prior to being fixed with dried acetone (10162180, Fisher Scientific, Loughborough, UK) for 15 min, air dried for 15 min and washed 3 times with PBS for 5 min per wash. Cryosections were then incubated with blocking diluent (0.1 % (v/v) BSA, 0.01 % (v/v) Marvel, 10 % (v/v) horse serum and 90 % (v/v) PBS) for 1 hour in a humidified box at room temperature. Sections were then incubated in a humidified chamber for 1 hour in primary antibody diluted in blocking diluent to a final concentration of 2 µg/mL or blocking diluent for negative controls. Section were again washed 3 times in PBS for 5 min per wash and then incubated for 30 min in ABC biotinylated secondary antibody diluted in blocking diluent in a humidified chamber for 30 min. Sections were washed 3 times in PBS for 5 min per wash, incubated in a humidified chamber for 30 min in ABC reagent provided in the Vectastastain Universal Elite ABC kit (Vector, Peterborough, UK), washed 3 times in PBS and developed with diaminobenzidine substrate (DAB) (Abcam, Cambridge, UK) (90 % (v/v) 10 % (v/v) DAB and 6 µL Hydrogen peroxide for 10 min). Sections were then washed in H_2O, counterstained in Erhlich's Haematoxylin for 5-10 min and washed in H_2O. To dehydrate, sections went through a series of sequential 5 min washes in 50 % (v/v) ethanol, 70 % (v/v) ethanol, 90 % (v/v) ethanol, 100 % (v/v) ethanol, 100 % (v/v) ethanol, 50 % (v/v) ethanol, 50 %(v/v) xylene and 100 % (v/v) xylene. Dehydrated

sections were then mounted with Distyrene Plasticizer Xylene (DPX) (Sigma-Aldrich, Gillingham, Dorset, UK) and air dried prior to imaging.

Visualisation and imaging of sections was performed using the Leica DM10000LED microscope with a MC120 HD camera and Leica Application Suite (version 3.0.0) software (Leica Microsystems, UK). Localisation and intensity of staining was judged blindly by two people independently of one another.

2.2.4.11 Collection of Cell Media

Cells were grown in 6 well plates until confluent. Cell medium was changed to FCS and Abx free DMEM 24 hours prior to collection. Media was then transferred to an microfuge tube and centrifuged at 12000 g for 5 min to remove free cells and stored at -80 °C.

2.2.4.12 Enzyme -Linked Immunosorbent Assay (ELISA)

ELISA was performed using Human TIM-1 (HAVCR1) ELISA Kit (Thermo Fisher Scientific, Cramlington, England, UK). Serum samples were diluted 1:2 in Diluent B and 100 µL of each sample and provided standards were placed into appropriate wells of the provided 96 well plate. Wells were covered and the plate was incubated at room temperature for 2.5 hours. Solutions were discarded and wells were washed 4 times with 300 µL of 1 X Wash buffer per well. 100 µL of 1 X biotinylated antibody was added to each well and plates were incubated at room temperature for 1 hour. Solution was discarded and wells were washed 4 times with 300 µL 1 X Wash buffer per well. 100 µL of Streptavidin-HRP solution was added to each well and plate incubated at room temperature for 45 min. The solution was discarded and wells were washed 4 times with 300 µL of 1 X Wash buffer per well. TMB substrate was added at 100 µL per well and the plate was incubated at room temperature in dark

for 30 min. Reaction was stopped using 50 μL of the provided Stop Solution. The absorbance was measured on an ELx800 Absorbance Reader (BioTek, Swindon, UK) at 450nm. The absorbance of standards was then used to form a four-parameter logistical standard curve and this was used to calculate the protein concentration of samples.

2.2.5 *In Vitro* Functional Assays

2.2.5.1 Growth Assay

Cells were seeded in triplicate into 24 well plates at $1X10^3$ cells per well in 1 mL of cell medium and incubated at 37 °C in a 95 % (v/v) humidified atmosphere of 5 % (v/v) CO_2 for 1, 3 and 5 days. After incubations cells were washed with PBS and then fixed, stained and imaged as described in Section 2.2.5.4. Cell growth was presented as the fold change in cell number from the 1 day time point.

2.2.5.2 Adhesion Assay

Matrigel™ basement membrane (BD Biosciences, Oxford, UK) was diluted to 0.05 mg/mL in cell medium and 100 μL was loaded into each well of a 96 well plate. This was then dehydrated at 56^oC for 2 hours and stored at 4^oC ready for use. The Matrigel™ was then rehydrated using 100 μL cell medium for 30 min. Medium was then removed and cells were seeded at 5000 cells per well in 200 μL of cell medium and incubated for 30 min at 37 °C in a 95 % (v/v) humidified atmosphere of 5 % (v/v) CO_2. The cell medium was the discarded, the cells were washed with PBS and stained using crystal violet as detailed in Section 2.2.5.4. The experimental set up is shown in Figure 2.1.
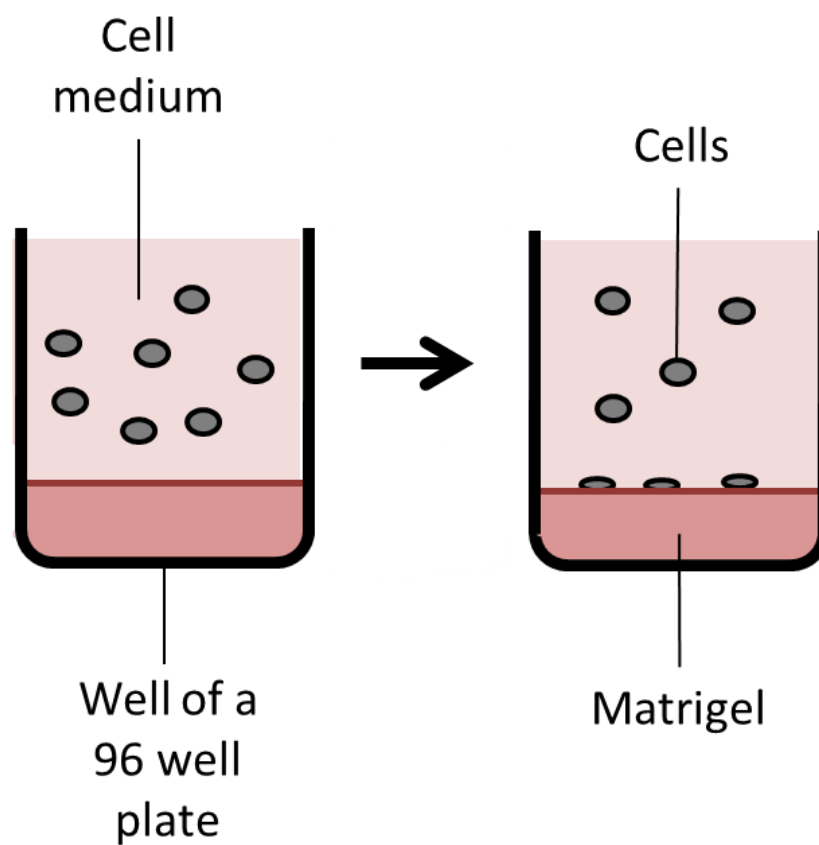
Figure 2.1 Adhesion Assay Experimental Set Up
Schematic of adhesion assay showing a well of a 96 well plate with a Matrigel™ layer
at its base. Cells are added to wells and the number of cells that had adhered to the
Matrigel™ layer in 30 min was quantified.

2.2.5.3 Invasion Assay

Invasion assays used 8 μm pore ThinCert™ 24 well plate inserts (Greiner Bio-One Ltd., Gloucestershire, UK). Matrigel™ basement membrane (BD Biosciences, Oxford, UK) was diluted in serum free medium to 0.5 mg/mL and 100 μL loaded into each insert to replicate the extracellular matrix. This was then dehydrated at 56 ^{o}C for 2 hours and stored at 4 ^{o}C ready for use. The Matrigel™ layer was then rehydrated using 200 μL serum free medium for 30 min, medium was removed prior to cell seeding at 3X10^4 cells per insert in 500 μL of serum free medium. The wells containing these inserts contained 1 mL of cell medium. Cells were then incubated at 37 °C in a 95 % (v/v) humidified atmosphere of 5 % (v/v) CO_2 for 3 days. Post incubation medium was discarded and wells as well as inserts were washed using PBS. The Matrigel™ layer and any cells that had not invaded through this layer were then removed using a cotton bud. Cells that had invaded the Matrigel™ layer and had migrated through to the underside of the ThinCert™ 24 well plate inserts stained using crystal violet as described in Section 2.2.5.4. The experimental set up is shown in Figure 2.2.
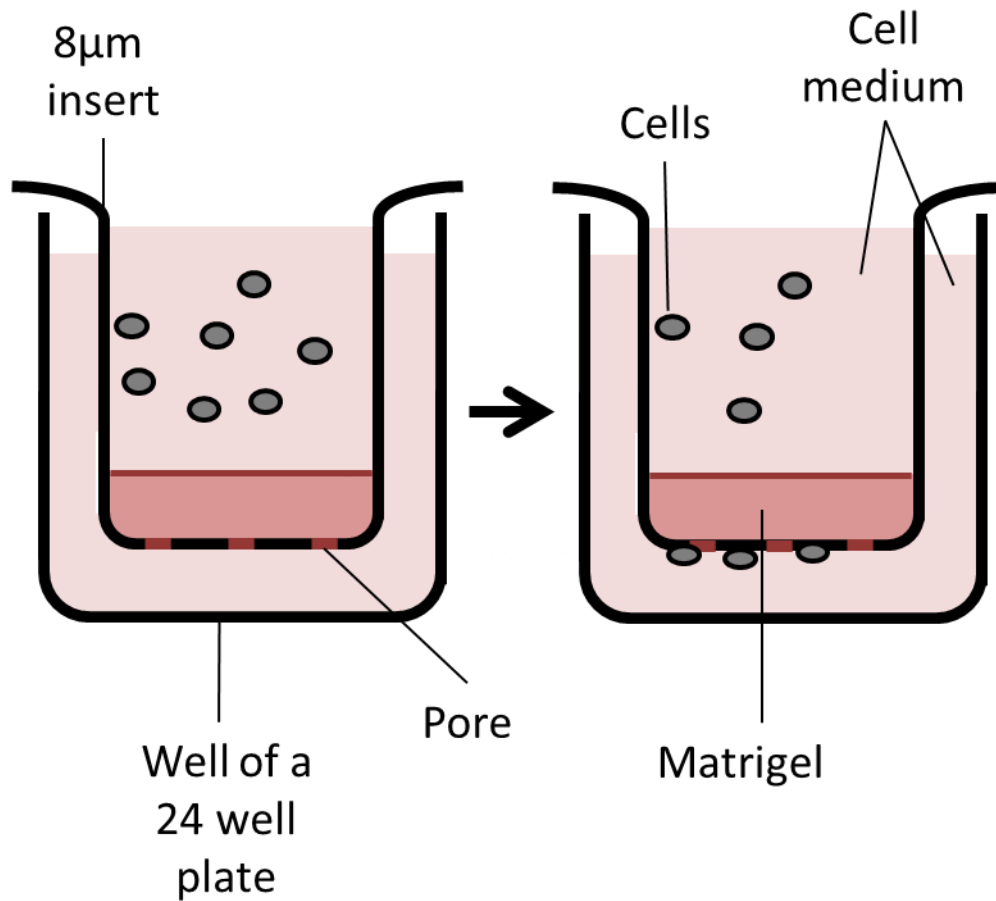
Figure 2.2 Invasion Assay Experimental Set Up
Schematic of invasion assay showing a 8 μm pore ThinCert™ insert within a well of a 24 well plate with a Matrigel™ layer at the base of the insert. Cells were seeded into the insert and number of cells that had invaded through to the underside of the ThinCert™ insert within 3 days was quantified.

2.2.5.4 Crystal Violet Staining

Growth, adhesion and invasion assays were all fixed with formalin and stained with crystal violet for visualisation. After cells were washed with PBS, they were fixed using 200 µL of 4 % (v/v) Formalin; for the invasion assay this was placed in the well outside of the insert. Plates were then incubated at room temperature for 1 hour and washed with dH_2O. Cells were then stained using 200 µL of crystal violet solution (V5265, Sigma-Aldrich, Gillingham, Dorset, UK) per well, with this being outside of the insert in the case of invasion assays and plates were incubated at room temperature for 30 min. Cells were then washed with dH_2O to remove excess crystal violet and dried at 56 °C for approximately 20 min. Images were taken at 5 X magnification and cells were counted. In the case of invasion assays the bottom of each insert was removed and placed on a glass slide for imaging before being returned to the plate. Crystal violet staining was then dissolved using 200 µL 10 % (v/v) Acetic Acid per well with a room temperature incubation of 5 min. The solution was then transferred into 96 well plates and absorbance were measured at 540 nm using the ELx800 Absorbance Reader (BioTek, Swindon, UK).

2.2.5.5 Transepithelial Resistance (TER)

TER used 0.4 µm pore ThinCert™ 24 well plate inserts (Greiner Bio-One Ltd., Gloucestershire, UK) in 24 well plates. Cells were seeded into inserts at $5X10^3$ cells per insert in 500 µL of cell medium with 1.5 mL medium in the well outside of the insert. Cells were incubated at 37 °C in a 95 % (v/v) humidified atmosphere of 5 % (v/v) CO_2 until confluent. Media was then replaced and resistance across the membrane was then measured in triplicate immediately afterwards using the EVOM² Epithelial Volt/Ohm Meter (World Precision Instruments, Hitchin, Hertfordshire, UK).

Where treatments were applied resistance was also measured every hour after the initial measurement for 10 hours. Data was then converted to $\Omega . cm^2$ by the multiplication of measured resistance by the surface area of the ThinCert™ 24 well plate inserts (0.336 cm^2) as detailed below.

$$^{R}Tissue(\Omega) = \ ^{R}Total(\Omega) - \ ^{R}Blank(\Omega)$$

$$TER(\Omega.cm^2) = \ ^{R}Tissue(\Omega) \times \ ^{M}Area(cm^2)$$

With single measurements TER were taken immediately after media change and analysed as fold change from pEF6 controls. With time point measurements TER were analysed as normalised to 0 hour time point via the subtraction of TER ($\Omega . cm^2$) at 0 hours from the TER ($\Omega . cm^2$) at every subsequent time point.

2.2.5.6 PCP (Paracellular permeability)

PCP used 0.4 µm pore ThinCert™ 24 well plate inserts (Greiner Bio-One Ltd., Gloucestershire, UK) in 24 well plates. Cells were seeded into inserts at $5X10^3$ cells per insert in 500µL of medium with 1.5 mL medium in the well outside of the insert. Cells were incubated at 37 °C in a 95 % (v/v) humidified atmosphere of 5 % (v/v) CO_2 until confluent. Cell medium was then replaced and 0.2 mg/mL of Tetramethylrhodamine isothiocyante (TRITC)-dextran conjugate with an average molecular weight of 40 kDa (42874, Sigma-Aldrich, Gillingham, Dorset, UK) and 0.2 mg/mL of Fluorescein isothiocyanate (FITC)-dextran conjugate with an average molecular weight of 10 kDa (FD10S, Sigma-Aldrich, Gillingham, Dorset, UK) was added to each insert. Immediately after media change and every hour thereafter until 10 hours, 20 µL of cell medium from outside of the inserts was transferred into a black 96 well cell culture microplate (Greiner Bio-One) in duplicate. Fluorescence was then measure using the GloMax® Multi Detection System (Promega,

Southampton, UK) at excitation 520 and emission 580-640 for TRITC-dextran and excitation 940 and emission 510-570 for FITC-dextran. Measurements were then normalised to the 0 hour time point measurement via subtraction and statistical analysis performed. The experimental set up is shown in Figure 2.3.
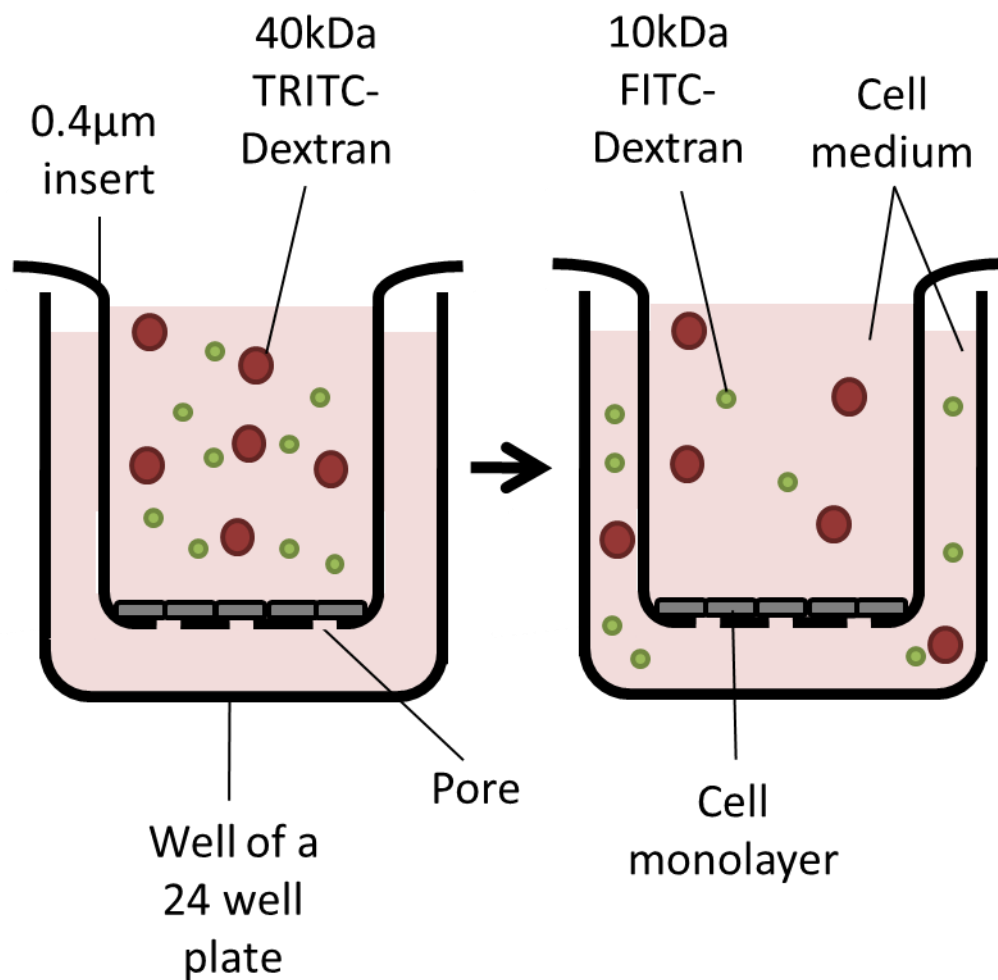
Figure 2.3 Paracellular Permeability Experimental Set Up
Schematic of PCP showing 0.4 µm pore ThinCert™ insert within a well of a 24 well plate with a cell monolayer at the base of the insert. 40 kDa TRITC-Dextran and 10 kDKa FITC-Dextran was added into the insert and the amount that moved to the outside of the insert was quantified every hour by measuring the amount of fluorescence produced from samples of cell medium.

2.2.5.7 Wound Healing Scratch Migration Assay

Cells were seeded in quadruplicate into 24 well plates at $5X10^3$ cells per well in 1 mL of cell media. Plates were then incubated at 37 °C in a 95 % (v/v) humidified atmosphere of 5 % (v/v) CO_2 until confluent. The cell medium was then removed and the cells were washed in 1 mL PBS. A scratch was then made manually using 200 μL pipette tips. Cell debris was removed by a second PBS wash and 1 mL fresh medium used per well. Images were then taken at 5 X magnification to give the 0 hour time point. Images were then taken every hour after this up to 10 hours. Between acquiring images plates were incubated at 37 °C in a 95 % (v/v) humidified atmosphere of 5 % (v/v) CO_2. As images were taken manually after their acquisition images from the same well at different time points were overlaid and aligned using Adobe Photoshop and cropped to ensure the same area of the well was analysed per well. Images were then analysed using ImageJ software to give wound area this was then used to percentage change in area from the 0 hour time point (presented as percentage wound closure)

2.2.5.8 Electric Cell-substrate Impedance Sensing (ECIS)

ECIS was performed using 96W1E+ plates (ECIS Cultureware™, IBIDI, Martinsried, Germany) and the ECIS® Z-theta model instrument (IBIDI, Martinsried, Germany). Prior to experimental runs, wells were stabilised with 200μL cell medium to clean the gold electrodes and reduce impedance drift during the experimental run. Wells were then inoculated with $5X10^4$ cells per well in 300 μL recommended cell medium. The behaviour for cell monolayers were then electrically monitored at 7 predefined frequencies (1, 2, 4, 8, 16, 32 and 64 kHz). At 25 hours an electrical wound of 60000 Hz and 3000 μA was applied to the cell monolayers for 30 secs. This was set

up using the Elevated Field Module which can create a high electric field sufficient to form pores in cell membranes and when applied for longer time period results in cell wounding and cell death of cells situated on the electrode. The resulting changes to the cell monolayers were continuously monitored, at the frequencies stated previously, during wounding and for 17 hours post wounding.

ECIS measures the impedance at numerous time points and at the 7 predefined frequencies however the ECIS® Z-theta model instrument also measures the phase difference between voltage and current thus allowing the impedance measurements to be broken down into its resistance and capacitance components. This enables the measurement of different functional and structural properties of the cells cultured during initial attachment and spreading as well as during wound healing. At different frequencies the current flow varies, at low frequencies the majority of the current flows within the paracellular space, thus flowing underneath and between cells, the resistance at low frequencies (<4 kHz) is therefore representative of cell contacts, both cell- cell and cell-plate. At high frequencies the majority of the current flows through the cells themselves and thus capacitance at high frequencies (>32 kHz) is indicative of cell coverage. The ECIS® Z-theta model instrument can also be used to apply the ECIS model, a mathematical model that calculates the resistance between cells/ barrier function resistance (R_b), cleft resistance/ constraint on current flow beneath the cell (alpha) and the membrane capacitance (Cm) and thus giving more insight into the changes that are occurring to the cells. Therefore, the data collected was analysed as fold change from time 0 hours for initial attachment and spreading and from time 25 hours for wound healing for resistance and capacitance at 1 kHz and 64 kHz respectively as well as well as for R_b and alpha.

2.2.5.9 HGF Treatment

Functional assays where HGF treatment as used cells were either treated with 40 ng/mL HGF or an equal amount of 0.1 % BSA in PBS as the control. Treatment was done at time 0 in all cases with this being at seeding for growth, invasion and adhesion, immediately after scratch formation with migration, at the same time as fluorescent dextran conjugates for PCP and immediately after base line (time 0 hr) readings for TER.

2.3 Statistical Analysis

Microsoft Excel was used for statistical analysis of data utilising a two-tailed unpaired Student's t-test. For patient serum samples Graphpad Prism (version 6, GraphPad Software Inc., CA, USA) whereby a D'Agostino &Pearson omnibus K2 normality test was performed on columns to assess normality. If data was of a normal distribution a two-tailed, unpaired Student's t-test for the comparison of two data sets or a one-way ANOVA for the comparison of three or more data sets. If data was not of a normal distribution a Mann-Whitney U test was performed for the comparison of two data sets or a Kruskal-Wallis test was performed for the comparison of three or more data sets. Mixed-design analysis of variance model (mixed ANOVA) was performed using IBM SPSS Statistics 24 software. This was used for any assay where two treatments were given and data was collected at different time points, these assays include scratch, TER, ECIS and PCP assays. In all cases p values of <0.05 was considered significant and represented on graphs by *. Where p<0.01, p<0.001 or p<0.0001 the representation of **, *** or **** was used respectively.

Chapter III:

HAVcR- 1 Expression in

Prostate Cancer Patient

Samples and Cell Lines

3.1 Introduction

Prostate cancer is the second most common cancer in males worldwide and the most common cancer in males in the UK with approximately 1278106 and 46689 new cases per year respectively [5, 14]. Diagnostic techniques however are still reliant on the inherently flawed PSA blood test. The PSA blood test is a low level invasive test and therefore has limited associated risk in comparison to other invasive testing, such as prostate biopsies, which may result in subsequent infection and urinary incontinence [329, 330]. However, the PSA test is inaccurate, with 67 % false positive and 15 % false negative results due to PSA not being a cancer specific protein marker [329]. It is therefore important to identify novel biomarkers that can be used to improve the accuracy of low invasive testing.

Of greater significance is the current inability to differentiate between low-risk progression and high-risk progression prostate cancer at an early curable stage [86]. Low-risk progression prostate cancers are those that are unlikely to grow or metastasise outside of the prostate for many years and therefore have limited risk of morbidity or mortality, whilst high-risk progression prostate cancer are those that are likely to grow and progress to metastatic disease resulting in increased morbidity and mortality [331]. The problem with not being able to identify high-risk progression prostate cancer is that it results in overtreatment of low-risk progression prostate cancer and the unnecessary associated morbidity [86]. Data from The European Randomised Study for Prostate cancer (ERSPC) suggested that for one prostate cancer death to be prevented 37 men would need to be treated for prostate cancer and thus 36 of which would be treated but have no benefit [82, 86]. This has severe implications when side effects of prostate cancer treatment are taken into

consideration, such as incontinence and impotence due to radical prostatectomy, as it means that the people who are receiving unnecessary treatment not only gain no survival benefit but potentially have a decreased quality of life [88]. This highlights the necessity of identifying biomarkers to categorise tumours that are likely to progress at an early stage to ensure treatment is provided. It is also just as imperative to identify tumours that are unlikely to progress and thus advocate the "watch and wait" treatment method. Active surveillance and watchful waiting are methods to combat this problem, whereby prostate cancer is monitored but remains untreated until cancer progression occurs [332, 333]. These approaches have a clinical benefit due to the decreased treatment associated morbidity whilst not affecting survival. This was demonstrated by The National Institute for Health Research-supported Prostate Testing for Cancer and Treatment (ProtecT) trial whereby there was no 10 yr survival benefit with radical prostatectomy or radiotherapy in comparison to active surveillance of clinically localised prostate cancer [334]. However, the monitoring of prostate cancer involves invasive testing including prostate biopsies, and their associated risks as well as the PSA blood test, which as previously discussed is unreliable [332]. Therefore, biomarkers that can be detected by low invasive methods are necessary to improve this monitoring process.

Unsurprisingly due to the large number of cases, prostate cancer is the cause of a large number of deaths. It is the eighth most common cause of cancer related deaths worldwide and the fourth most common cause of cancer related deaths in the UK, with 358989 and 11287 deaths per year respectively [5, 14]. Metastasis is the cause of approximately 90 % of cancer related deaths [84]. Therefore, studies into the metastatic process are required to improve understanding with the aim of novel

target identification to treat or prevent metastatic disease and improve patient survival.

HAVcR-1 has been found to be up-regulated in certain cancers, including: breast, ovarian, colon and renal [283, 319, 320]. HAVcR-1 is therefore a molecule of interest for cancer diagnosis and as a potential target for cancer therapies. HAVcR-1 is proteolytically cleaved proximal to the cell membrane to release an ectodomain [284, 288]. This HAVcR-1 ectodomain can be secreted into urine from certain tissue types and this release is increased in RCC (renal cellular carcinoma) [315]. The HAVcR-1 ectodomain is therefore a potential biomarker for certain cancers. HAVcR-1 expression and ectodomain release in cancer is still poorly categorised. There is little known about its usefulness as a biomarker for prostate cancer diagnosis, progression and prognosis. Furthermore, there is a lack of study into the release of the HAVcR-1 ectodomain into the circulation and the use of this as a potential biomarker for the use in a blood test for cancer diagnosis and monitoring.

This chapter therefore aimed to determine levels of HAVcR-1 ectodomain in prostate cancer patient serum and to evaluate possible correlations between these levels and prostate cancer development and/or progression. It also aimed to assess and evaluate total HAVcR-1 protein levels in prostate cancer tissue sections and *HAVCR1* gene expression. Furthermore, it set out to assess total HAVcR-1 and ectodomain levels from prostate cell lines to ensure they are viable *in vitro* model systems for further study.

3.2 Materials and Methods

3.2.1 Collection of Prostate Cancer Patient Serum Samples

Prostate cancer serum samples (n=236) were obtained from Wales Cancer Bank (WCB). (See Section 2.1.5.1)

3.2.2 Collection of Control Serum Samples

Whole Blood (n=9) was obtained from the Welsh Blood Service or obtained from male volunteers with informed consent (n=5) and serum was extracted (See Section 2.1.5.2)

3.2.3 Collection of Tissue Samples

Prostate cancer samples (n=2) and background control samples (n=2) were collected at the University Hospital of Wales (See Section 2.1.6)

3.2.4 Mammalian Cell Culture

All cell lines were obtained from the ATCC (Middlesex, UK), maintained in recommended media (See Table 2.1) as described in Section 2.2.1.

3.2.5 Collection of Cell Media

Cells were grown in 6 well plates until confluent. Cell medium was collected and prepared as described in Section 2.2.4.11.

3.2.6 Enzyme-Linked Immunosorbent Assay (ELISA)

ELISA was performed on serum and cell medium samples using the Human TIM-1 (HAVCR1) ELISA Kit (Thermo Fisher Scientific, Cramlington, England, UK). The methodology is detailed in Section 2.2.4.12.

3.2.7 RNA Extraction from Cell Culture, PCR and qPCR

Cells were seeded into 6 well plates and cultured until confluent. RNA was then extracted using the EZ-RNA kit (Geneflow, Staffordshire, UK) as detailed in Section 2.2.3.1. Of this total RNA 500 ng was used to synthesise cDNA using Primer Design Precision Nanoscript 2 Reverse Transcription kit (Primer Design, Southampton, UK) as detailed in Section 2.2.3.2. PCR was then carried out using GoTaq G2 Green master mix (Promega, Southampton, UK) as detailed in Section 2.2.3.3 and primers listed in Table 3.1. PCR products were subjected to gel electrophoresis on a 2 % agarose gel as detailed in Section 2.2.3.4.

cDNA was also used for qPCR, using Precision FAST 2 X qPCR Master Mix with ROX (Primer Design, Southampton, UK). qPCR methodology is detailed in Section 2.2.3.5 and primers used within this chapter are detailed in Table 3.1.

3.2.8 Protein Extraction from Cell Culture and SDS PAGE and Western Blotting Analysis

Cells were seeded into 6 well plates and cultured until confluent. Protein was then extracted using protein lysis as detailed in Section 2.2.4.1. Protein samples were then subjected to SDS-PAGE and western blotting as detailed in Section 2.2.4.3 and Section 2.2.4.4. Immunoprobing and protein visualisation was carried out as described in Section 2.2.4.5 and Section 2.2.4.6 with specific antibodies detailed in Table 3.2.

3.2.9 Immunofluorescent (IF) Staining of Cell Lines

Cells were seeded at $5X10^4$ cells per well of a Millicell EZ-8-well chamber slide (Merck Millipore, Sigma-Aldrich, Gillingham, Dorset, UK) until confluent prior to being immunofluorescently stained as detailed in Section 2.2.4.9. Primary and secondary antibodies used are described in Table 3.2.

3.2.10 Immunohistochemical (IHC) Staining of Tissue Samples

IHC staining of cryogenically frozen tissue samples is detailed in Section 2.2.4.10. Antibodies used are detailed in Table 3.2

3.2.11 Statistical Analysis

PCR and western blot analysis bands were quantified using Image J, this data as well as q-PCR data was then statistically analysed utilising the Student's t-test on Microsoft Excel; $p < 0.05$ was considered statistically significant. Statistical analysis on ELISA data was performed using Graphpad Prism (version 6, GraphPad Software Inc., CA, USA). First a D'Agostino & Pearson omnibus normality test was performed on columns to assess normality and if data was of a normal distribution a two-tailed was performed for the comparison of two data sets or a one-way ANOVA for the comparison of more than three data sets. If data was not of a normal distribution a Mann-Whitney U test was performed for the comparison of two data sets or a Kruskal-Wallis test was performed for the comparison of more than three data sets. In all cases values $p < 0.05$ was considered statistically significant. ImageJ was used to quantify staining in IHC as representative of protein concentration. For each tissue

section 15 areas were quantified prior to the Student's t-test being carried out on

Microsoft Excel; $p < 0.05$ was considered statistically significant.

Table 3.1 Chapter III PCR and qPCR Primers

	Target	Primer Name	Sequence 5'-3'	Number of Cycles	Product Size (bp)
PCR	*HAVCR1*	HAV1F9	CAACAACAAGTGTTCCAGTG	35	436
		HAV1R9	GCATTTTGCAAAGCTTTAAT		
	GAPDH	GAPDHF8	GGCTGCTTTTAACTCTGGTA	25	475
		GAPDHR8	GACTGTGGTCATGAGTCCTT		
qPCR	*HAVcR-1*	HAVR1F1	GACAATGTTTCAACGA	100	99
		HAV1ZR	**ACTGAACCTGACCGTACA** TGGAGGAACAAA		
	GAPDH	GAPDHR2	CTGAGTACGTCGTGGAGTC	100	93
		GAPDH ZR2	**ACTGAACCTGACCGTACA** CAGAGATGATGACCCTTTTG		

Table 3.2 Chapter III Protein Detection Antibodies

Antibody	Animal Source	Company	Concentration
HAVcR-1	Rabbit	Abnova, Heyford, Oxfordshire, UK	1:200- WB
TIM-1 (HAVcR-1)	Mouse	R & D Systems, Abingdon, Oxfordshire, UK	1:500- IHC
TIM-1 (N-13) (HAVcR-1)	Goat	Santa Cruz, Insight Biotechnology Limited, Middlesex UK	2µg/ml- IF
GAPDH	Mouse	Santa Cruz, Insight Biotechnology Limited, Middlesex UK	1:1000- WB
Anti- Mouse IgG (whole molecule)- Peroxidase antibody	Rabbit	Sigma-Aldrich, Gillingham, Dorset, UK	1:1000-WB
Anti- Rabbit IgG (whole molecule)- Peroxidase antibody	Goat	Sigma-Aldrich, Gillingham, Dorset, UK	1:1000-WB
Biotinylated anti- Mouse IgG	Goat	Vector Laboratories, Orton Southgate, Peterborough, UK	1:50-IHC
Anti- Goat AlexaFluor 594	Donkey	Thermo Fisher Scientific, Cramlington, England, UK	1: 500- IF

3.3 Results

3.3.1 Serum HAVcR-1 Ectodomain Levels Decrease with Prostate Cancer

To investigate the release of the HAVcR-1 ectodomain into the circulation with the occurrence of prostate cancer HAVcR-1 ectodomain levels were assessed in serum samples from patients with prostate cancer and from healthy controls using ELISA. HAVcR-1 ectodomain levels were decreased in serum samples from the prostate cancer patient group (64.53 pg/mL) compared with serum samples from the healthy control group (154.4 pg/mL). Statistical analysis revealed this decrease was significant (p<0.0001) (See Figure 3.1.).
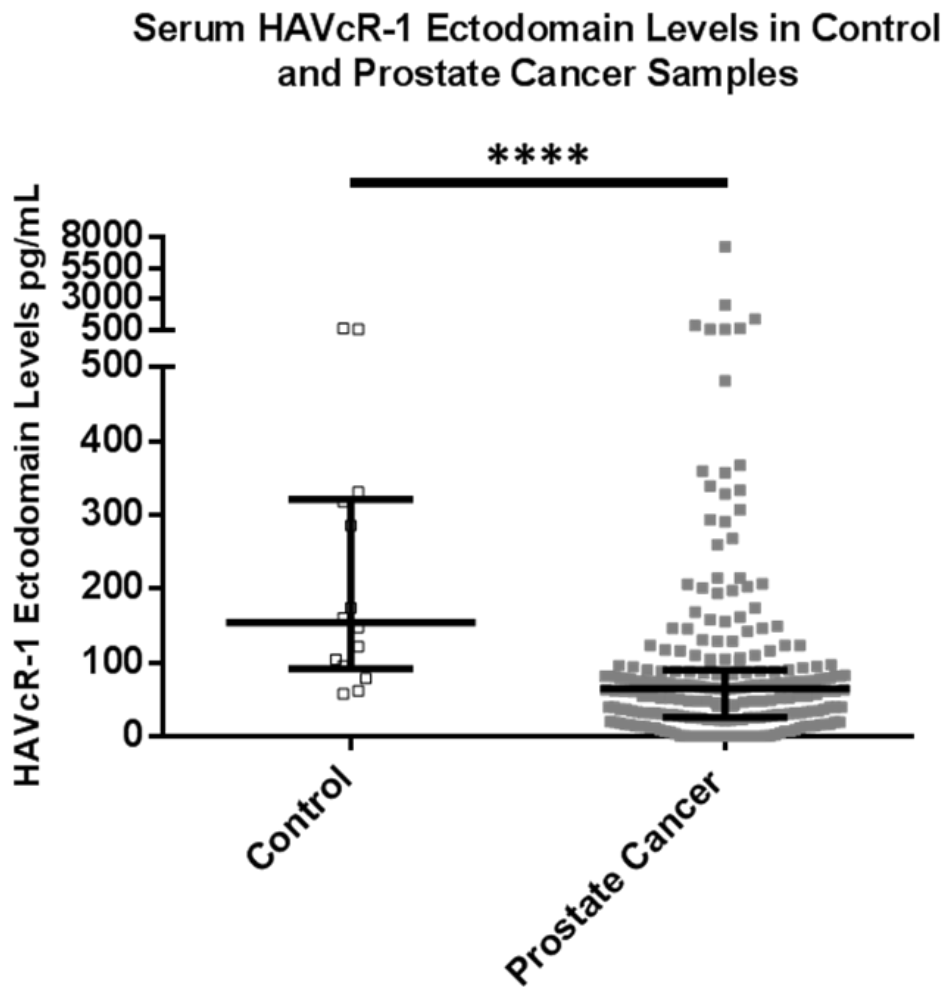
Figure 3.1. Serum HAVcR-1 Ectodomain Levels in Cancer in Comparison to Control
Prostate cancer and control serum samples were analysed for HAVcR-1 Ectodomain using Human TIM-1 (HAVCR1) ELISA Kit. Graph shows the difference in medians of levels between healthy controls and prostate cancer patients. Statistical analysis was then performed using the Mann Whitney test, utilising Graphpad Prism software and p<0.05 was considered significant. p<0.0001 is represented by **** and error bars show interquartile range.

3.3.2 Serum HAVcR-1 Ectodomain Levels are Independent of Gleason Score

Serum samples were collected with pathophysiological parameters, including Gleason score, therefore allowing for more in-depth analysis of serum HAVcR-1 ectodomain levels to be performed. This was to identify potential trends between HAVcR-1 ectodomain levels and prostate cancer progression. Gleason scores 6, 7, 8, 9 and 10 prostate cancer serum samples as well as healthy control serum samples were compared.

This showed significant decreases between the healthy control group (154.4 pg/mL) and Gleason score 6 (48.88 pg/mL; $p<0.0001$), Gleason score 7 (66.94 pg/mL; $p<0.0001$), Gleason score 8 (48.38 pg/mL; $p<0.0001$) and Gleason score 9 (68.21 pg/mL; $p=0.0095$). However, there was no significant change in serum HAVcR-1 ectodomain levels between he healthy control group (154.4 pg/mL) and Gleason score 10 (89.57 pg/mL; $p=0.2599$) (Figure 3.2A).

When analysed without the healthy control group there was no trend in serum HAVcR-1 ectodomain levels with Gleason score; with the Kruskal-Wallis One Way Analysis on Ranks revealing no significant differences in the medians of each Gleason score ($p=0.2688$). Furthermore, when prostate cancer patient serum samples were separated into low grade (Gleason score 6 and 7) and high grade (Gleason score 8, 9 and 10) there was no significant change in serum HAVcR-1 ectodomain levels between low-grade samples (63.94 pg/mL) and high-grade samples (64.53 pg/mL) ($p=0.6811$) (See Figure 3.2B).

A

B
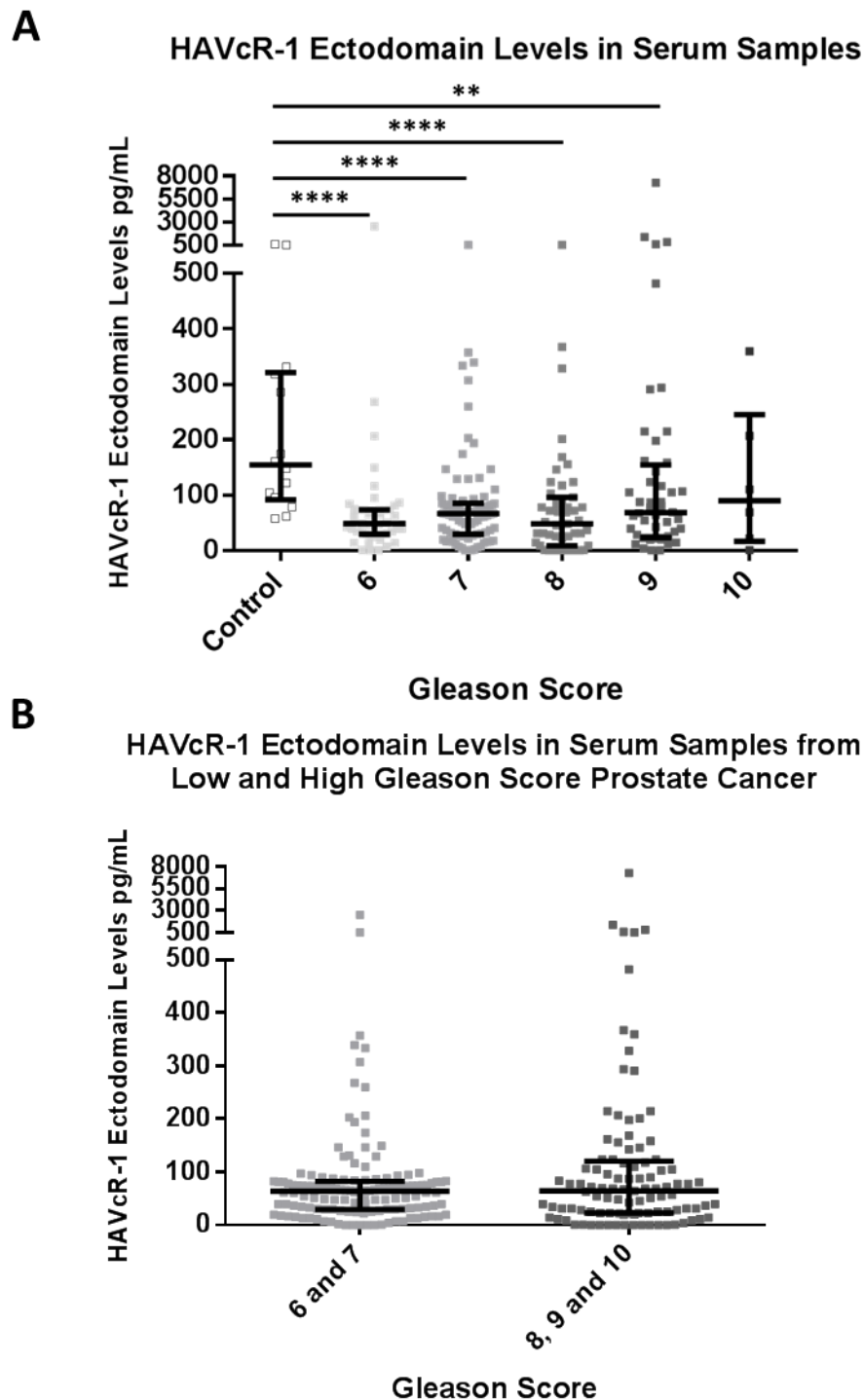
Figure 3.2 Serum HAVcR-1 Ectodomain Levels with Gleason Scores
Serum samples were analysed for HAVcR-1 Ectodomain levels via ELISA. Results were then analysed to assess differences in levels in serum samples between **A** control group and Gleason score 6, 7, 8, 9 and 10 prostate cancer and **B** between low Gleason score (6 and 7) and high Gleason score (8, 9 and 10). Statistical analysis performed using Mann-Whitney U Test (Graphpad Prism software) whereby. $p<0.05$ was considered significant and $p<0.01$ and $p<0.0001$ are represented by ** and **** respectively. Graphs show the medians with error bars showing interquartile range.

3.3.3 High HAVcR-1 Protein Expression in Prostate Cancer Tissues

Total HAVcR-1 protein expression was then assessed to investigate the relationship between total expression and serum ectodomain levels. To achieve this as well as to investigate the localisation of HAVCR-1 in prostate tissue, total HAVcR-1 in prostate cancer (n=2) and background control (n=2) tissue samples was stained via IHC.

This revealed that the HAVcR-1 protein is expressed in prostate glandular epithelia. Analysis of staining intensity, as representative of HAVcR-1 expression, revealed a significant increase in HAVcR-1 total protein expression in malignant prostate epithelia in comparison to control prostate epithelia (p=0.0006) (See Figure 3.3).
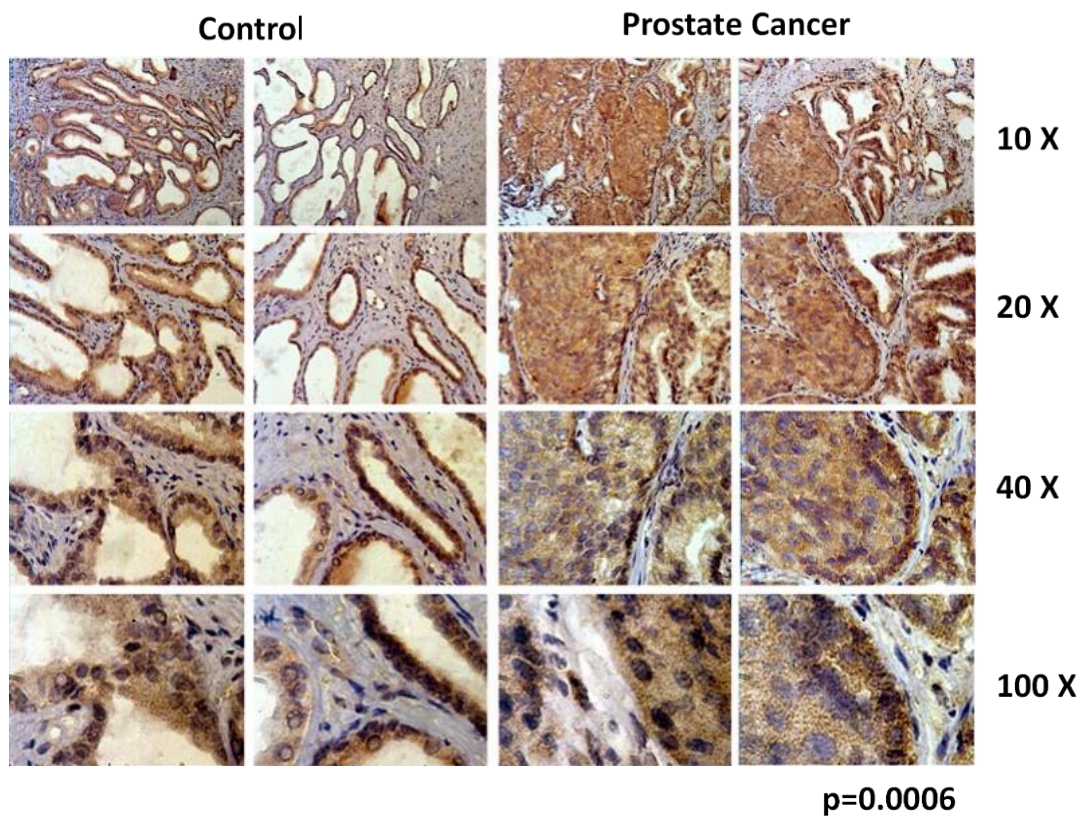
Figure 3.3 Prostate Tissue Staining for Total HAVcR-1 Levels
Tissue samples stained for HAVcR-1 protein expression using IHC. HAVcR-1 expression in malignant prostate epithelia in comparison to normal prostate epithelia was quantified via ImageJ software and statistical analysis was performed via the Student's t-test using Microsoft Excel software; $p<0.05$ was considered significant and the p value stated next to images.

3.3.4 High *HAVCR1* Gene Expression in Prostate Cancer

HAVCR1 gene expression was then investigated. Unfortunately, patient sample RNA was unavailable thus data available on the Gene Expression Omnibus (GEO) (www.ncbi.nlm.nih.gov/geo/) repository, in particular the GSE55945 (www.ncbi.nlm.nih.gov/geo/query/acc.cgi?acc=GSE55945) and GSE6919 (www.ncbi.nlm.nih.gov/geo/query/acc.cgi) GEO DataSets, were utilised to evaluated total *HAVCR1* gene expression in tissues.

The GSE55945 GEO DataSet assessed differences in gene expression between benign prostate tissue (n=8) and malignant prostate tissue (n=13). When utilised for *HAVCR1* gene expression there was a significant increase in expression in malignant prostate tissue in comparison to benign prostate tissue (p=0.047) (See Figure 3.4A). The GSE6919 GEO DataSet was used to assess for differences in *HAVCR1* gene expression between normal prostate tissue free of any pathological alteration (n=18) and primary prostate tumour samples (n=65). This showed an increase of *HAVcR1* gene expression in primary tumours however significance was not reached (p=0.185) (See Figure 3.4B).
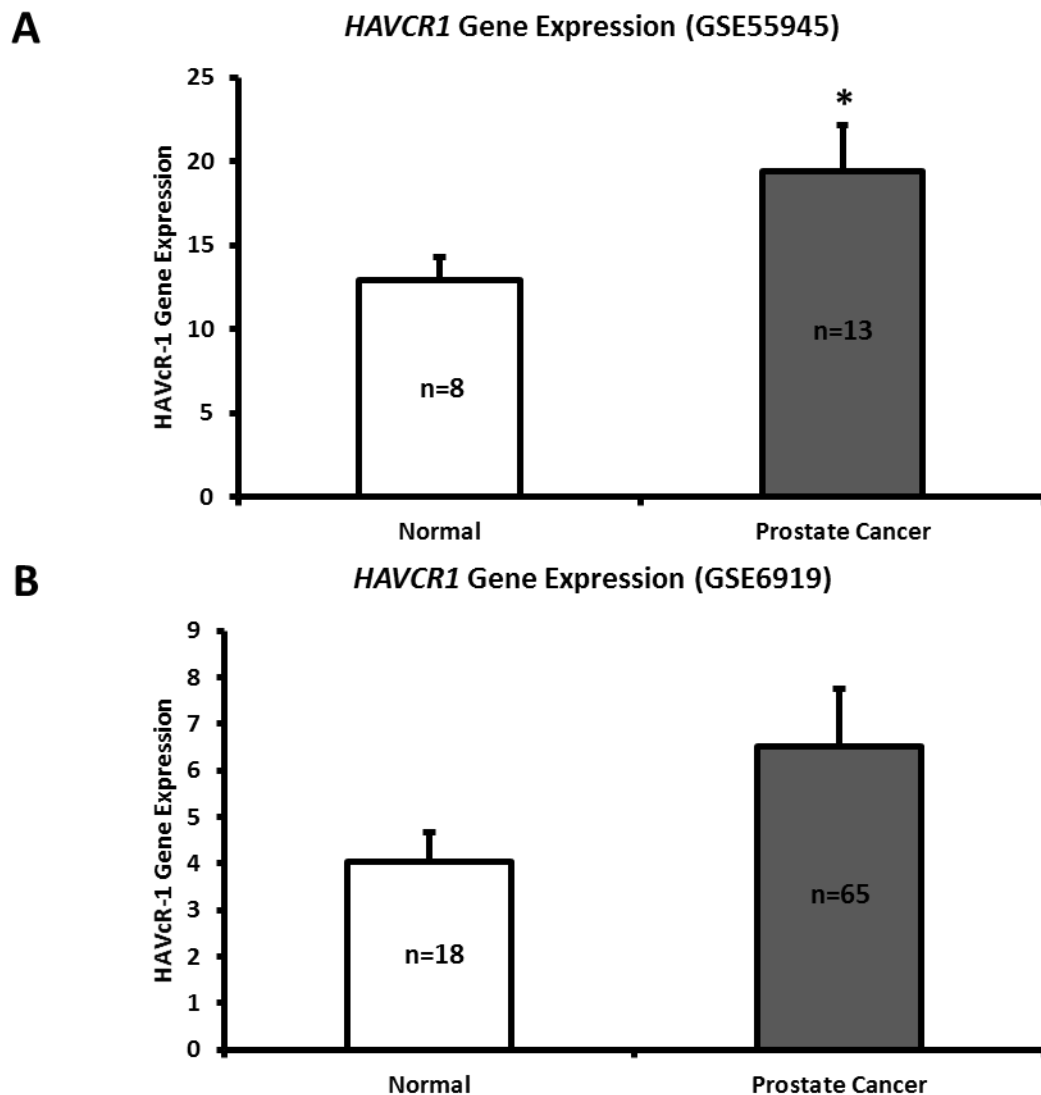
Figure 3.4 GEO DataSets Analysis of *HAVCR1* Gene Expression in Prostate Cancer
GEO datasets utilized to identify changes in *HAVCR1* gene expression between normal and prostate cancer tissue samples in GEO DataSets (www.ncbi.nlm.nih.gov/geo/) **A** GSE55945 and **B** GSE6919. Data shown are the means with error bars showing SEM and n numbers are shown within bars. Statistical analysis preformed via Graphpad Prism software D'Agostino & Pearson omnibus normality test revealed, **A** data was of Gaussian distribution thus the parametric t-test with Welch's correction was utilised and $p < 0.05$ was considered significant and represented by * and **B** data was not of Gaussian distribution thus the non-parametric Mann-Whitney U Test was utilised and significance ($p < 0.05$) was not reached

3.3.5 Prostate Cell Lines Release Constant Levels of HAVcR-1 Ectodomain

Levels of HAVcR-1 ectodomain released from prostate cell lines *in vitro* were measured to assess whether they showed a similar trend to that of serum HAVcR-1 ectodomain levels. The amount of HAVcR-1 ectodomain secreted from various cell lines within 24hours were assessed via ELISA on collected cell media (See Figure 3.5). These were analysed as fold change relative to the HECV positive control.

This revealed that there was no significant difference between HAVcR-1 ectodomain levels from the cell media of PC-3 cells (0.11± 0.025), Du145 cells (0.11± 0.032), LNCaP cells (0.08±0.014), CA-HPV-7 cells (0.08± 0.01) or PZ-HPV-7 cells (0.07 ± 0.013).
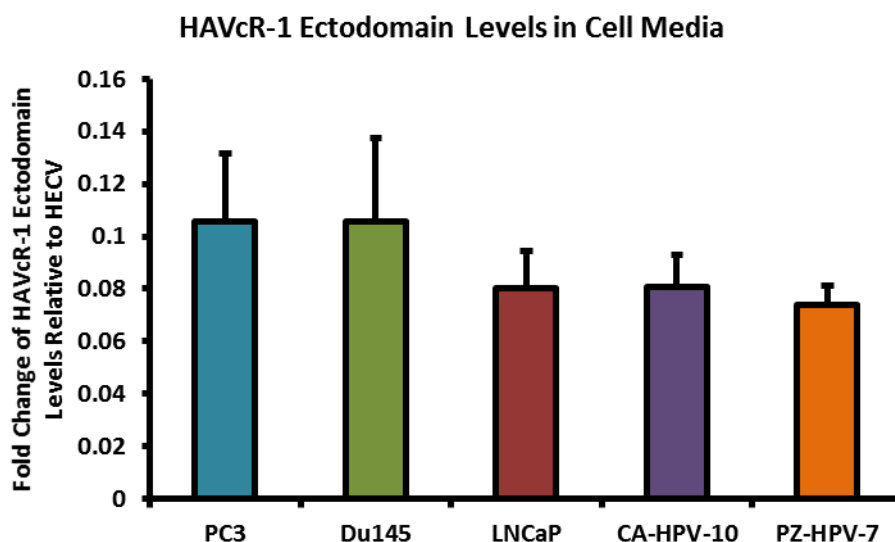
Figure 3.5 HAVcR-1 Ectodomain Release from Prostate Cell Lines
Cells lines were grown in 6 well plates in recommended media, media was changed to FCS and Abx free DMEM 24 hours prior to 100 % confluency and media was collected at 100 % confluency. This media was then analysed for HAVcR-1 levels using Human TIM-1 (HAVCR1) ELISA Kit. Results were then analysed to assess differences HAVcR-1 ectodomain level between different cell lines and shown as fold change relative to HECV positive control (not shown on graph). Statistical analysis was performed using Student's t-test however significance ($p < 0.05$) was not reached. Graph shows the means of three independent experiments with error bars showing SEM

3.3.6 HAVcR-1 Protein Expression Varies in Prostate Cell Lines

The expression of HAVcR-1 mature and immature (~100 kDa and ~70 kDa respectively) cellular protein levels were assessed in various prostate cell lines, alongside the HECV cell line as a positive control, using western blot analysis as well as IF staining. Band intensity as well as fluorescent intensity, as representative of protein expression, was then quantified via ImageJ software and analysed as fold change relative to the HECV positive control.

A similar trend was seen in the expression of both the mature and immature protein with a greater expression in metastatic tumour derived cell lines PC3, Du145 and LNCaP than in the immortalised cell lines CA-HPV-10 and PZ-HPV-7. The highest expression was in LNCaP cells and the lowest in PZ-HPV-7 cells however, significance was not reached (See Figure 3.6).

Total HAVcR-1 staining also showed greater protein expression in PC3, Du145 and LNCaP cells lines than the CA-HPV-10 cell line and this in turn was greater than the expression in the PZ-HPV-7 cell line (See Figure 3.7).
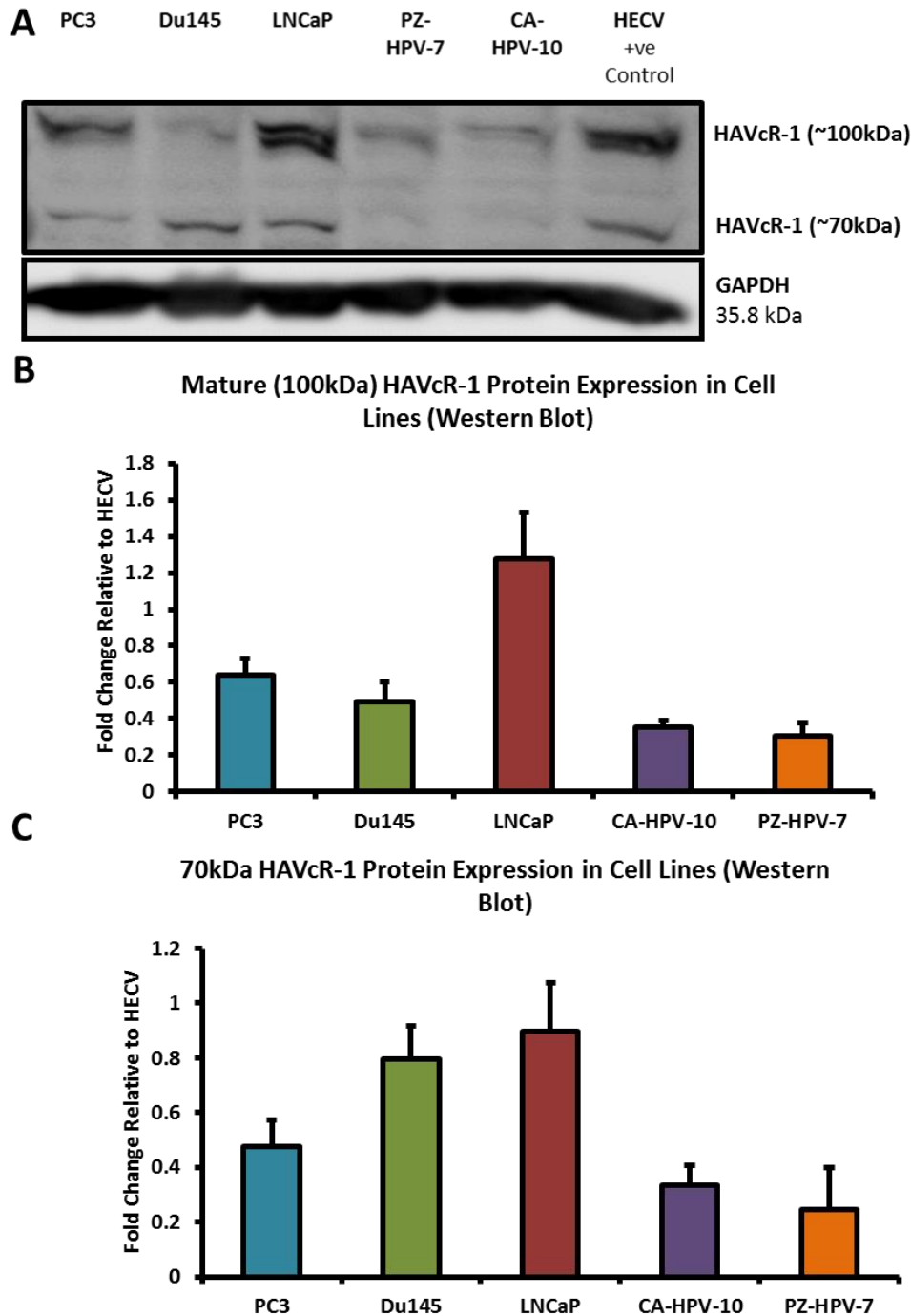
Figure 3.6 HAVcR-1 Protein Expression in Prostate Cell Lines
Cell lines grown in supplemented medium and harvested at 100 % confluence. Data shown are the means of three independent experiments and error bars show SEM. HAVcR-1 protein expression was assessed using **A** SDS PAGE and western blot analysis where the blot is representative of three independent experiments. **B** and **C** Graphs show band intensity as quantified by ImageJ software for **B** the ~100 kDa mature protein and **C** the ~70 kDa immature protein. **B** and **C** HAVcR-1 protein expression was normalised to GAPDH and is shown as fold change relative to HECV positive control (not shown). Student's t-tests were performed and significance of $p<0.05$ was not reached

A

	HAVcR-1	DAPI	Merge
PC-3			
Du145			
LNCaP			
CA-HPV-10			
PZ-HPV-7			
HECV			100 X

B

HAVcR-1 Staining Intensity
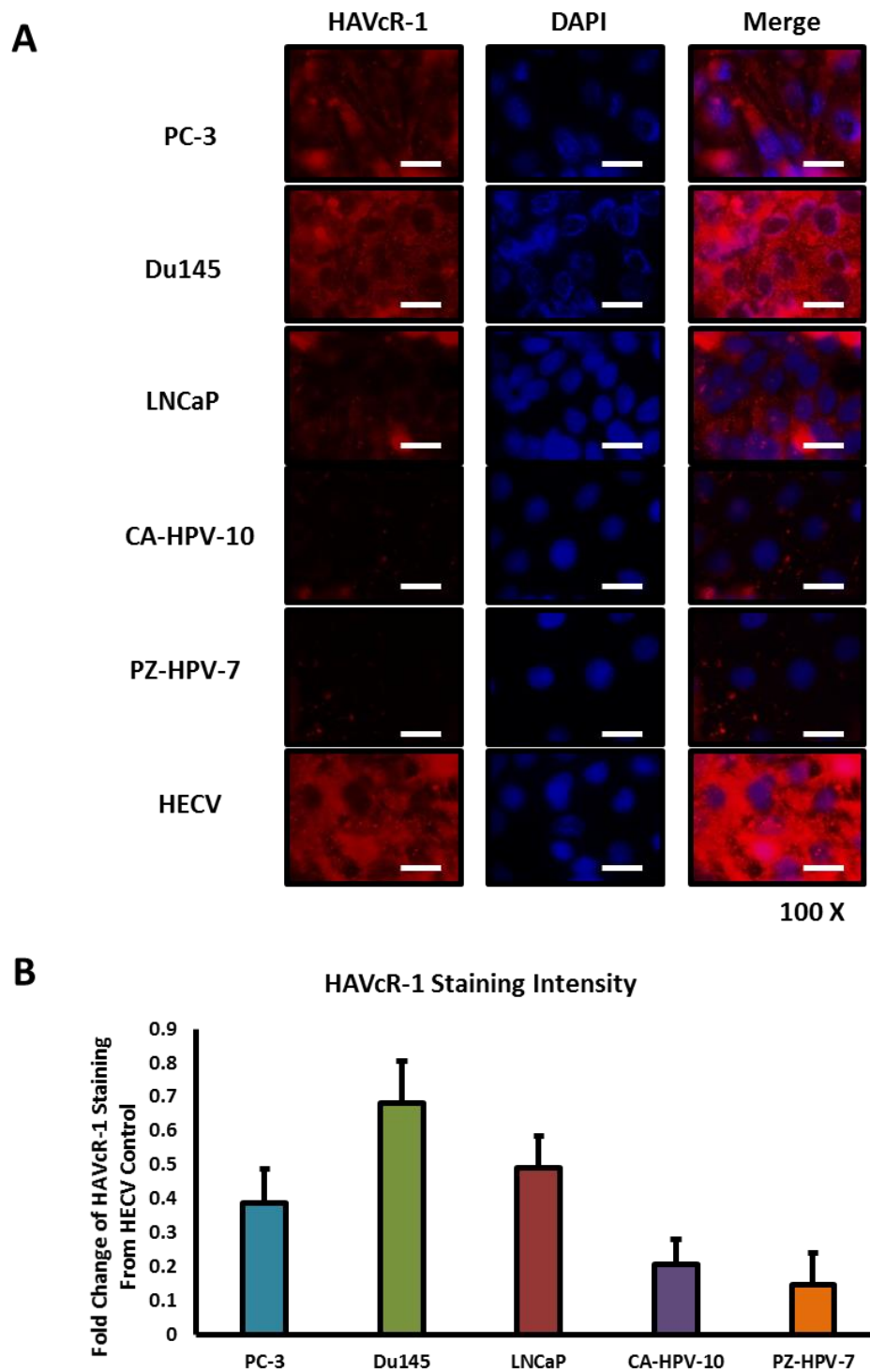
Figure 3.7 HAVcR-1 Protein Staining in Prostate Cell Lines

Cell were grown in 8 well chamber slides in supplemented media and subjected to immunofluorescence at 100 % confluence with HAVcR-1 and nuclear staining. Images were taken at 100 X magnification. Scale bars are representative of 20 μm. **A** Images are representative of three independent experiments and show fluorescence emission correlating to HAVcR-1 expression or nuclear staining and a merged image of both. **B** Graph shows quantitative analysis of immunofluorescent staining of HAVcR-1

3.3.7 *HAVCR1* Gene Expression Varies in Prostate Cell Lines

HAVCR1 gene expression of several prostate cell lines was assessed using PCR and qPCR. PCR band intensity as representative of gene expression was then quantified via ImageJ software. Data for both PCR and qPCR were analysed as fold change relative to the HECV positive control.

PCR revealed a significantly higher *HAVCR1* gene expression in PC3 cells than in LNCaP (p=0.005), CA-HPV-10 (p=0.019) and PZ-HPV-7 (p=0.009) cell lines. Although not significant, *HAVCR1* gene expression appears to be highest in the Du145 cell line and lowest in the PZ-HPV-7 cell line (See Figure 3.8A and B). qPCR revealed the same trend with the highest *HAVCR1* gene expression seen in Du145 cell and the lowest in PZ-HPV-7 cells however significance was not reached (See Figure 3.8C).
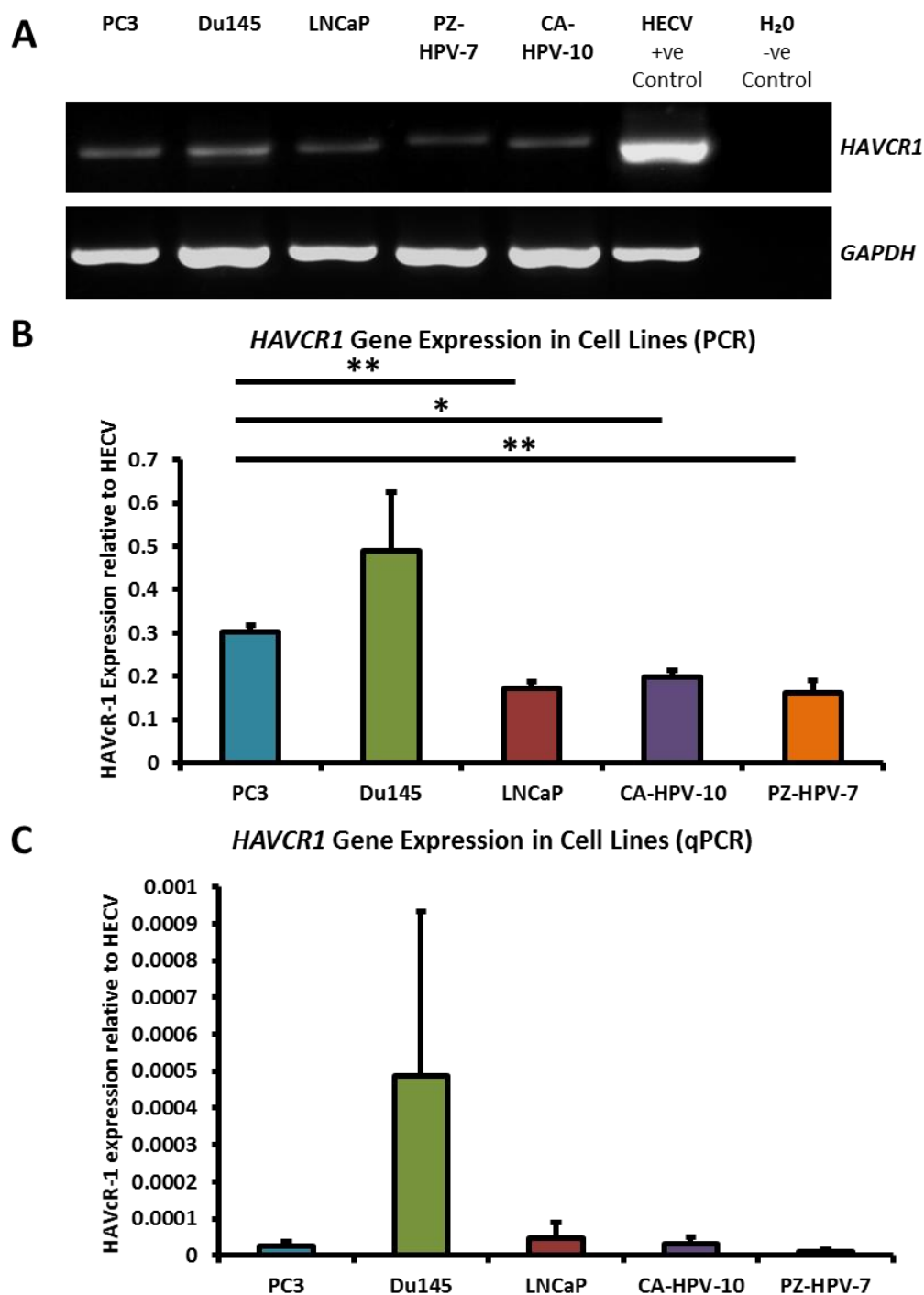
Figure 3.8 *HAVCR1* Gene Expression in Prostate Cell Lines
Cell lines were grown in 6 well plates in supplemented media and harvested via RNA extraction at 100 % confluence. Data shown are the means of three independent experiments and error bars show SEM. *HAVCR1* mRNA expression was assessed using **A** PCR or **C** qPCR. **B** Graph shows band intensity as quantified by ImageJ software. **B** and **C** *HAVCR1* mRNA expression was normalised to *GAPDH* and is shown as fold change relative to HECV positive control (not shown on graph). Student's t-tests were performed and significance is indicated by * and **, which signify p<0.05 and p<0.01 respectively.

3.4 Discussion and Conclusion

This study commenced with the investigation of serum HAVcR-1 ectodomain levels in prostate cancer; which showed a decreased serum HAVcR-1 ectodomain levels in comparison to healthy control levels. Furthermore, decreases in serum HAVcR-1 ectodomain levels between Gleason score 6, 7, 8, 9 and 10 prostate and healthy controls presents HAVcR-1 as a potential diagnostic biomarker, which would be of particular interest in prostate cancer where the current biomarker (PSA) is highly nonspecific [329]. However, there were limitations with this study with low numbers of control serum samples reducing reliability of these conclusions. In addition, healthy control samples were not aged matched and therefore does not rule out the possibility of the decreasing in HAVcR-1 ectodomain levels being attributed to age rather than the presence of prostate cancer. Therefore, further study with increased n numbers and age matched controls should be undertaken. It is also currently it is not known whether changes in serum levels would be unique to prostate cancer and due to changes in expression levels of HAVcR-1 in other cancers as well as in other disease, it may be unlikely that serum HAVcR-1 levels are a prostate cancer specific biomarker [283, 298, 314, 315, 319, 320]. It is possible that serum levels decrease in a variety of cancer types and thus HAVcR-1 may need to be used in conjunction with other biomarkers, such as PSA in the instance of prostate cancer or be followed by further testing to determine cancer/ disease type.

Prostate cancer is an age-related disease, however despite the high incidence the associated mortality rate is relatively low [8]. This is due to the majority of prostate cancer cases remaining a localised disease and not progressing to the metastatic disease responsible for the related lethality [331]. Amongst others, the recent

ProtecT randomised trial highlights the amount of potentially unnecessary treatment given [334]. In conjunction with the side effects of such treatments, the treatment of localised prostate cancer may in fact be more harmful than beneficial [334]. Due to the alternatives to treatment (active surveillance and watchful waiting) relying on the non-cancer specific PSA test as well as the more invasive prostate biopsy there is a requirement for less invasive but more specific testing to determine disease progression as well as a biomarker for prostate cancer that is more likely to progress to metastatic disease [332]. It was due to this that links between Gleason score and HAVcR-1 ectodomain levels were investigated. However, there was no change in levels with increasing Gleason score or between low Gleason score and high Gleason score prostate cancer. It is therefore possible that serum HAVcR-1 ectodomain levels are of little or no clinical benefit in the monitoring of prostate cancer progression Gleason score is only one prognostic indicator and therefore it may be of use to investigate levels in relation invasiveness and metastasis. In ccRCC a link between HAVcR-1 ectodomain shedding and invasiveness and tumour malignancy, it would therefore be interesting to investigate if a similar effect is seen in prostate cancer [317]. Unfortunately, information into cancer metastasis in terms of TNM staging was either unavailable or incomplete for many serum samples used in the study and therefore future study would investigate any correlation between metastasis and serum HAVcR-1 ectodomain levels.

This study also aimed to assess total HAVcR-1 expression in prostate cancer, which revealed a significant increase in HAVcR-1 protein expression in prostate cancer tissue samples in comparison to normal control samples. This result was unsurprising as it has been previously documented that there is increased HAVcR-1 staining in

prostate cancer tissue samples [335]. Furthermore, using GEO DataSets HAVcR-1 overexpression in prostate cancer was also shown at gene level. HAVcR-1 overexpression has been previously observed in breast cancer, ovarian cancer and renal cell carcinoma therefore providing further evidence that HAVcR-1 is not specific to a certain cancer type [317, 336]. Interestingly, this increase in total HAVcR-1 protein expression is the opposite of the observed decreased serum HAVcR-1 ectodomain levels. Two possible explanations for this are that either the cleavage event that results in the release of the ectodomain is decreased in prostate cancer or that there is decreased entry of the HAVcR-1 ectodomain into the circulation in prostate cancer. Decreased cellular cleavage appears unlikely due to a previously documented increased urinary HAVcR-1 levels with the occurrence of prostate cancer [315]. In regards to decreased entry into the circulation as HAVcR-1 is expressed in prostate glandular epithelial cells it would be expected that, similarly to PSA, the disruption of the normal prostate architecture that occurs with prostate cancer progression would cause an increased entry into the circulation [298]. A possible explanation as to why this is not the case is that the HAVcR-1 ectodomain is sequestered within the tumour. HAVcR-1 is expressed on the surfaces of CDK4+ T cells, CDK8+ T cells, natural killer (NK) cells, NKT cells, dendritic cells, B cells and mast cells [85, 86]. HAVcR-1 is a co-stimulatory molecule with ligand binding resulting in the activation, proliferation and cytokine production of T cells and the activation of NKT cells [85, 86, 337]. HAVcR-1 ligands include TIM-4 and phosphatidylserine (PS) [86, 337]. The HAVcR-1 can bind PS and thus, it is possible that the released HAVcR-1 ectodomain is sequestered within the tumour, binding to TIM-4 and PS preventing the activation of infiltrating immune cells [86]. If this is the case the release of the

HAVcR-1 ectodomain may contribute to the non-responsiveness of many tumour infiltrating immune cells and would be of interest for future study.

HAVcR-1 is overexpressed in prostate cancer and therefore the staining of prostate biopsies could be used to aid in prostate cancer diagnosis however it would be of interest to investigate whether there is any correlation with total HAVcR-1 expression and disease prognosis as this would have more clinical benefit. Furthermore, as HAVcR-1 is a transmembrane protein it may be possible for HAVcR-1 to be a target for an antibody-drug complex (ADC) in the treatment of prostate cancer. Intriguingly, the CDX-014 ADC which targets HAVcR-1 is currently in phase I and II clinical trials for advanced or metastatic renal carcinoma [338]. Although this trial is not expected to be completed until August 2020 it may result in a viable treatment for other cancers of which HAVcR-1 is overexpressed including prostate cancer.

Depending on the function of HAVcR-1 in prostate cancer there may also be the possibility of a HAVcR-1 targeted therapy however further study is required to assess the role of HAVcR-1 in cancer development and progression. Therefore, various prostate cell lines were assessed to determine whether they were suitable models for further HAVcR-1 study. PC-3, Du145 and LNCaP were assessed to model metastatic disease, CA-HPV-10, to model localised disease, and PZ-HPV-7 to model normal prostate epithelia. *HAVCR1* gene expression was increased in PC-3, Du145, LNCaP and CA-HPV-10 cell lines in comparison to PZ-HPV-7 with this change being significant in PC-3 cells in comparison to LNCaP, CA-HPV-10 and PZ-HPV-7 cells. There was also consistent increased total HAVcR-1 protein expression in PC-3, Du145, LNCaP and CA-HPV10 cells in comparison to PZ-HPV-7 cells. Therefore, a similar trend was seen in cell lines as in the clinical samples; that HAVcR-1 is overexpressed at

protein and gene level in prostate cancer. Furthermore, there was no change in HAVcR-1 ectodomain levels found in cell media between cell lines thus conferring with the clinical data theory that the variation in serum HAVcR-1 ectodomain levels with the occurrence of prostate cancer is not due to a variation on the amount of HAVcR-1 cleavage. Cell line expression therefore agreed with clinical data to a suitable degree that they would be used for further study into the effect of HAVcR-1 in prostate cancer.

Chapter IV:

HAVcR- 1 Overexpression

and Knockdown in PC-3

Cells

4.1 Introduction

Prostate cancer is extremely prevalent in the western world and the majority of prostate cancer mortality is associated with cancer metastasis. Advanced metastatic disease accounts for 90 % of cancer deaths [49, 339]. There has been extensive study into metastasis with the hopes of improving therapeutics and therefore lowering mortality. However, metastasis is extremely complex involving a multitude of signalling cascades, the variations of which are still not fully understood [50]. Treatment and management of metastatic prostate cancer relies heavily upon androgen deprivation therapy (ADT) which, although initially effective, resistance to treatment and disease progression inevitably occurs [87]. It is therefore important for the continuation of research into the deregulated proteins associated with prostate cancer metastasis as well as the signalling pathways they are involved in. This would provide a greater understanding of the processes that occur with the overall aim of identifying novel biomarkers for prostate cancer progression as well as novel targets for prevention and treatment of metastatic disease.

For metastasis to occur a cancer cell must undergo an evolutionary series of mutations resulting in alterations in cell characteristics including cell growth, apoptosis, migration and dissemination [87]. Research into the role of HAVcR-1 in these characteristics is limited however, in colorectal cancer HAVcR-1 has been demonstrated to affect cell invasion and adhesion [320]. Furthermore, dissemination and migration require disordered adhesion and decreased TJ integrity leading to cancer invasion and metastasis [87]. In endothelial cells HAVcR-1 expression reduces TJ integrity and was found to precipitate with key TJ proteins ZO-1, ZO-2 and the TJ regulatory protein RhoC; an important protein in the migration of cancer cells

especially from a primary tumour [340-342]. Therefore, the interaction between HAVcR-1 and TJs in prostate cancer may aid in the understanding of cancer metastasis and provide a novel target for metastatic prostate cancer treatment.

The increase in *HAVCR1* gene and protein expression in prostate cancer and cell models as shown in Chapter III presents HAVcR-1 as important in prostate cancer development and progression. Therefore, HAVcR-1 could prove a therapeutic target for prostate cancer therapeutics. This chapter aimed to establish HAVcR-1 overexpressing and HAVcR-1 knockdown *in vitro* cell models, based on the metastatic prostate cancer PC-3 cell line. Then to use these cell models to assess the effects HAVcR-1 have on cell behaviours that are important for metastasis to occur. It also aimed to utilise these generated cell models to assess the effect of HAVcR-1 on the integrity of cell-cell contacts as well as the expression of TJ proteins to examine whether HAVcR-1 may be an important regulator of junctional complexes.

4.2 Materials and Methods

4.2.1 Mammalian Cell Culture

All cell lines were obtained from the ATCC (Middlesex, UK), maintained in recommended media (See Table 2.1) as described in Section 2.2.1.

4.2.2 Generation of Plasmids

HAVcR-1 ribozyme inserts were amplified as detailed in Section 2.2.2.1 via 2 X GoTaq G2 GREEN master mix (Promega, Southampton, UK) PCR. The ribozyme sequence was then cloned into the PEF6/V5-His TOPO TA plasmid to produce the HAVcR-1KD plasmid utilising the PEF6/V5-His TOPO TA expression kit (Invitrogen, Life technologies, Paisley, UK) as detailed in Section 2.2.2.2. This was then used to transform One Shot TOP10 Chemically Competent *E. coli* (Thermo Fisher Scientific, Cramlington, England, UK) as detailed in Section 2.2.2.3. Colonies for amplification and purification were selected as detailed in Section 2.2.2.4 and were subject to plasmid purification via the GenElute Plasmid Miniprep Kit (Sigma-Aldrich, Gillingham, Dorset, UK) as detailed in Section 2.2.2.5.

PEF6/V5-His TOPO TA control plasmid (termed pEF6 control) and HAVcR-1 overexpression PEF6/V5-His TOPO TA plasmid (termed HAVcR-1EXP) was obtained courtesy of Dr T.A. Martin (as described in [340]). Amplification of plasmids was achieved via transformation of One Shot TOP10 Chemically Competent *E. coli* (Invitrogen, life technologies, Paisley, UK) (detailed in Section 2.2.2.3) and plasmid purification using the GenElute Plasmid Miniprep Kit (Sigma Life Sciences, Dorset, UK) as detailed in Section 2.2.2.5. Purified plasmids were then stored at -20°C.

The PC-3 cell line was then transformed with pEF6 control, HAVcR-1EXP or HAVcR- 1KD plasmid via electroporation as detailed in Section 2.2.2.6.

4.2.3 RNA Extraction, PCR and qPCR

Cells were grown in 6 well plates until confluent, total RNA was then extracted using the EZ-RNA kit (Geneflow, Staffordshire, UK) as detailed in Section 2.2.3.1. Five hundred nanograms of total RNA was then used to synthesise cDNA using Primer Design Precision Nanoscript 2 Reverse Transcription kit (Primer Design, Southampton, UK) as detailed in Section 2.2.3.2. Polymerase chain reaction (PCR) was then carried out, as detailed in Section 2.2.3.3, using GoTaq G2 Green master mix (Promega) and primers detailed in Table 4.1. Products were then subjected to gel electrophoresis as described in Section 2.2.3.4. cDNA was also used for qPCR, using Precision FAST 2 X qPCR Master Mix with ROX (Primer Design, Southampton, UK). qPCR methodology is detailed in Section 2.2.3.5 and primers used within this chapter are detailed in Table 4.1.

4.2.4 ImmunoFluorescence (IF) Staining

Cells were seeded at $5X10^4$ cells per well of a Millicell EZ-8-well chamber slide until confluent prior to being subject to IF staining as detailed in Section 2.2.4.9. Primary and secondary antibodies used are described in Table 4.2.

4.2.5 Cell Growth Assay

Growth assays were carried out as described in Section 2.2.5.1 and cells were stained with crystal violet as described in Section 2.2.5.4.

4.2.6 Cell Adhesion Assay

Adhesion assays were carried out as described in Section 2.2.5.2 and stained with crystal violet as described in Section 2.2.5.4.

4.2.7 Cell Invasion Assay

Invasion assays were carried out as described in Section 2.2.5.3 and cells were stained with crystal violet as described in Section 2.2.5.4.

4.2.8 Cell Migration Assay

Migration assays were performed as detailed in Section 2.2.5.7.

4.2.9 Transepithelial Resistance (TER)

TERs were measured as described in Section 2.2.5.5.

4.2.10 Paracellular Permeability (PCP)

PCPs were performed as described in Section 2.2.5.6.

4.2.11 Electric Cell-Substrate Impedance Sensing (ECIS)

ECIS experiments were performed as described in Section 2.2.5.8.

4.2.12 Statistical Analysis

PCR and western blot analysis bands were quantified using Image J software, with data such as qPCR, cell growth, adhesion, invasion and TER was statistically analysed to assess for changes from PC-3^{pEF6} control using the Microsoft Excel Student's t-test. Wound area was quantified using Image J software and this data as well as data from other assays whereby time points were assessed, which included: ECIS and PCP, was

statistically analysed to assess changes from PC-3^{pEF6} control using the IBM SPSS

Statistics 24 mixed-design ANOVA.

Table 4.1. Chapter IV Primers used in PCR and qPCR

	Target		Sequence 5'-3'	Number of Cycles	Product Size (bp)
PCR	Plasmid correct orientation	T7F	TTAATACGCTCACTATAGGG	30	400
		RB BMR	TTCGTCCTCACGGACTCATCAG		
	Plasmid incorrect orientation	T7F	TTAATACGCTCACTATAGGG	30	400
		RB TPF	TTCGTCCTCACGGACTCATCAG		
	HAVCR1	F:	CAACAACAAGTGTTCCAGTG	35	436
		R:	GCATTTTGCAAAGCTTTAAT		
	GAPDH	F:	GGCTGCTTTTAACTCTGGTA	25	475
		R:	GACTGTGGTCATGAGTCCTT		
	ZO1	F:	CCACATACAGATACGAGTCCTC	30	533
		R:	TGGCTTATGCTGAGATGAAGG		
	ZO2	F:	CTGACATGGAGGAGCTGA	30	844
		R:	GAGACCATACTCTTCGTTCG		
	CLDN1	F:	ATGGCCAACGCGGGGC	30	636
		R:	TCACACGTAGTCTTTCC		
	CLDN2	F:	TATAGCACCCTTCTGGGCCT	30	432
		R:	CCTTGGAGAGCTCCTTGTGG		
	CLDN3	F:	ATGCAGTGAAGGTGTACGA	30	403
		R:	TGGTGGCCGTGTACTTCTTC		
	CLDN4	F:	TGGGAGGGCCTCTGGATGAA	30	422
		R:	TGGTGGCCGTGTACTTCTTC		
	CLDN7	F:	ATAACCCTTTGATCCCTACC	30	113
		R:	ACTGAACCTGACCGTACAACAGG		
	CLDN9	F:	CTTCATCGGCAACAGCATCG	30	339
		R:	AAGTCCTGGATGATGGCGTG		
	JAMA	F:	AACAAGATCACAGCTTCCTA	30	600
		R:	CTTACTCGAAGTCCCTTTCT		
	OCLN	F:	ATGTCATCCAGGCCTC	30	579
		R:	ATAGACAATTGTGGCA		
qPCR	*HAVCR1*	F:	GACAATGTTTCAACGA	100	99
		ZR:	**ACTGAACCTGACCGTACA** TGGAGGAACAAA		
	GAPDH	F:	CTGAGTACGTCGTGGAGTC	100	93
		ZR:	**ACTGAACCTGACCGTACA** CAGAGATGATGACCCTTTTG		

Table 4.2 Chapter IV Antibodies used in Immunofluorescence

Antibody	Animal Source	Company	Concentration
HAVcR-1	Rabbit	Abnova, Heyford, Oxfordshire, UK	2 µg/mL
TIM-1 (N-13)	Goat	Santa Cruz, Insight Biotechnology Limited, Middlesex UK	2 µg/mL
Cld-1	Goat	Santa Cruz, Insight Biotechnology Limited, Middlesex UK	2 µg/mL
Cld-7	Goat	Santa Cruz, Insight Biotechnology Limited, Middlesex UK	2 µg/mL
Occludin	Goat	Santa Cruz, Insight Biotechnology Limited, Middlesex UK	2 µg/mL
ZO-1	Goat	Santa Cruz, Insight Biotechnology Limited, Middlesex UK	2 µg/mL
Anti-Goat AlexaFluor 594	Donkey	Thermo Fisher Scientific, Cramlington, England, UK	1:500
Anti-Goat AlexaFluor 488	Donkey	Thermo Fisher Scientific, Cramlington, England, UK	1:500
Anti-Rabbit AlexaFluor 594	Donkey	Thermo Fisher Scientific, Cramlington, England, UK	1:500

4.3 Results

4.3.1 Generation and Validation of Plasmids

The *HAVcR-1* targeting ribozyme insert was created using PCR methods prior to being cloned into the pEF6/V5-HISTOPO TA vector and then transformed into *E.coli*. To ensure purification of plasmids that had incorporated this ribozyme insert in the correct orientation five colonies were checked for orientation analysis. This was achieved by utilising two sets of primers: one for correct orientation and one for incorrect orientation. All five colonies contained plasmids containing the ribozyme insert of the correct orientation (See Figure 4.1A). Colony 1 was chosen for plasmid purification.

HAVcR-1EXP plasmids were amplified using *E.coli* and to ensure *HAVCR1* gene was inserted into the plasmid PCR was performed alongside the HECV RNA positive control. This confirmed the plasmid contained the *HAVCR1* gene insert (See Figure 4.1B). The pEF6 control plasmid was also amplified purified and validated via a PCR alongside the original pEF6 plasmid (See Figure 4.1C).
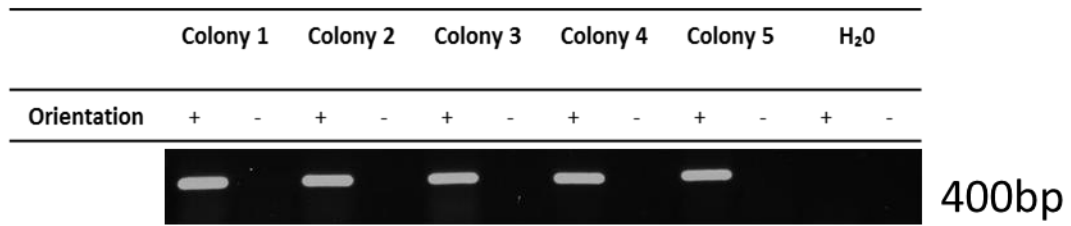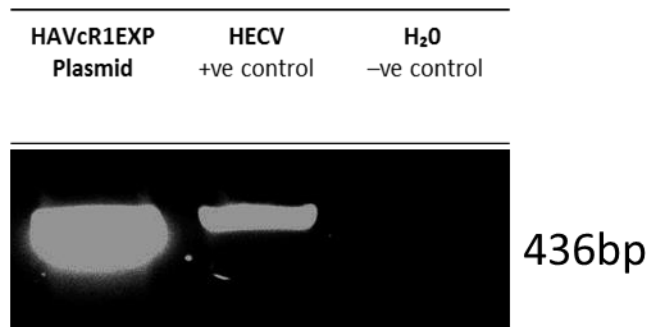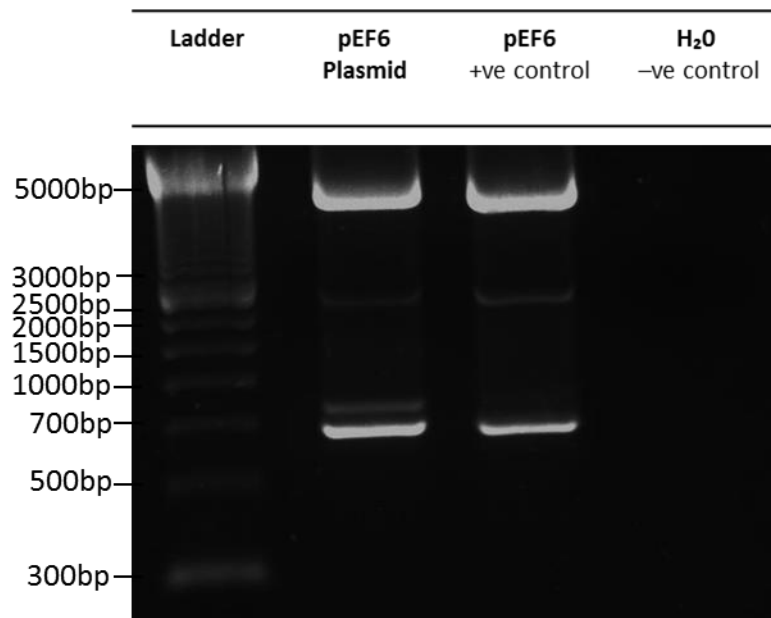
Figure 4.1 Generation of Plasmids
A Post transformation with ribozyme containing plasmid five colonies were checked for plasmids containing ribozyme of correct orientation. Positive orientation was shown via the use of T7F and RB BMR primers (indicated by +) and negative orientation was shown via the use of T7F and RB TPF primers (as indicated by -). **B** PCR of *HAVCR-1* to ensure gene was inserted. **C** PCR using T7F and RB BGH to ensure pure pEF6 plasmid with MidRanger 1 kb DNA Ladder.

4.3.2 *HAVCR1* Gene Expression Validated PC-3 Cell Models

PC-3 cells were transfected via electroporation with plasmids: pEF6 control (termed PC-3^{pEF6}), HAVcR-1EXP plasmid (termed PC-3$^{HAVcR-1EXP}$) or HAVcR-1KD plasmid (termed PC-3$^{HAVcR-1KD}$). The success of these transfections was assessed at mRNA level via PCR and qPCR. PCR band intensity as representative of mRNA expression was quantified via ImageJ software and analysed as fold change relative to the PC-3^{pEF6} (See Figure 4.2).

The PC-3^{pEF6} cell model was verified as a suitable control with PCR showing that there was no significant variation in *HAVCR1* gene expression between PC-3^{WT} and PC-3^{pEF6} with fold change from PC-3^{pEF6} being 1.46±0.50; p=0.25. This was also shown with qPCR with fold change from PC-3^{pEF6} being 1.32±0.64; p=0.66.

PCR showed a 4.55±2.19 fold increase in *HAVCR-1* expression in PC-3$^{HAVcR-1EXP}$ compared to PC-3^{pEF6} however this was not significant (p=0.25). qPCR however did show a significant increase with a 75.26±15.91 fold increase (p=0.043).

PCR showed a 0.37±0.299 fold decrease of *HAVCR1* expression in PC-3$^{HAVcR-1KD}$ in comparison to PC-3^{pEF6} and qPCR showed a 0.51±0.22 fold decrease however results were not significant in either case (p=0.17 and p=0.16 respectively).
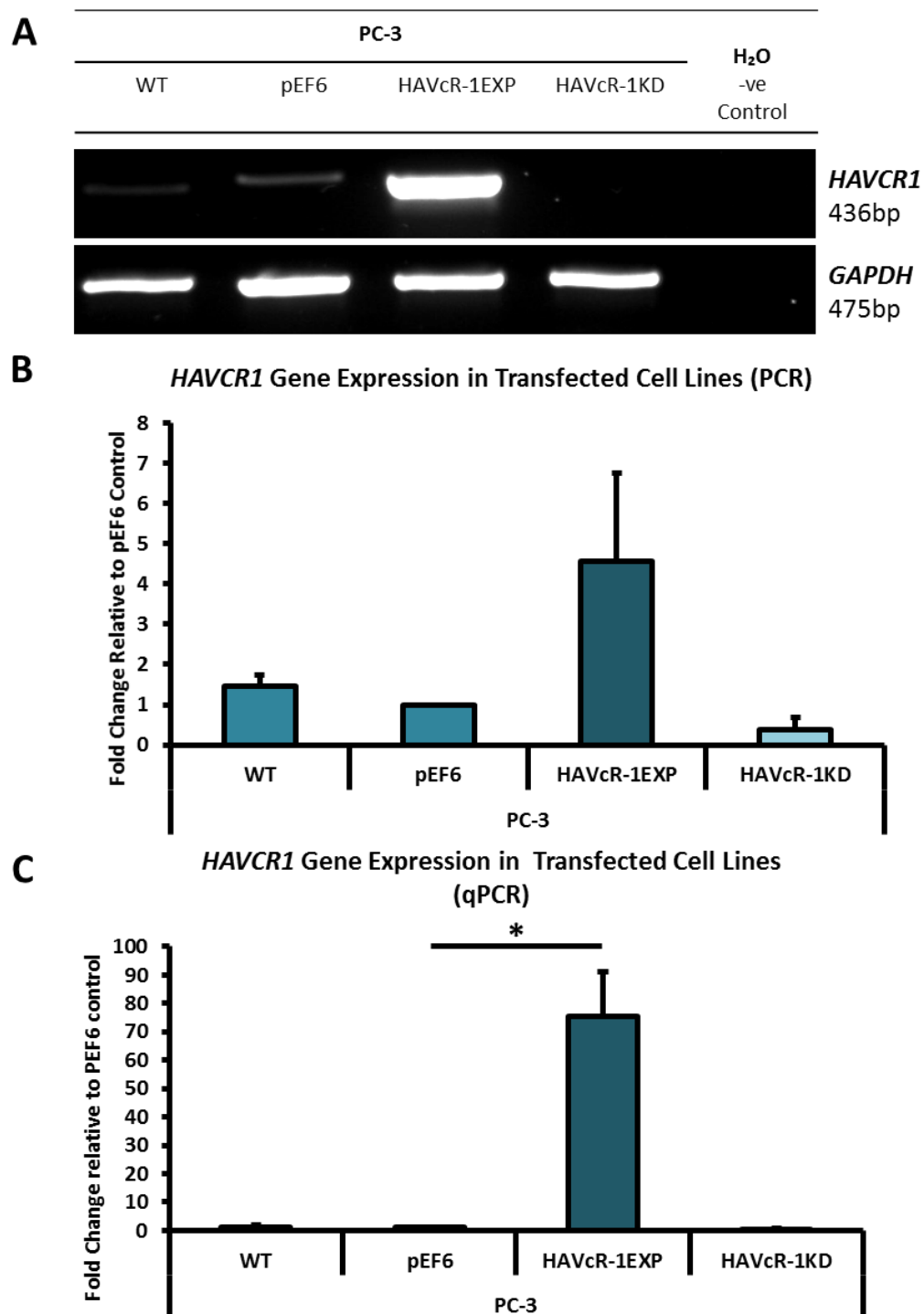
Figure 4.2 Validation of PC-3 *HAVCR1* Overexpression and Knockdown at Gene Level

Cells were grown in 6 well plates in supplemented media and harvested via RNA extraction at 100 % confluence. Data shown are the means of three independent experiments and error bars show SEM. *HAVCR1* mRNA expression was assessed using **A** PCR or **C** qPCR. **B** Graph shows band intensity as quantified by ImageJ software. **B and C** *HAVCR1* mRNA expression was normalised to *GAPDH* and is shown as fold change relative to pEF6 control. Student's t-tests were performed and significance of $p < 0.05$ is represented by *.

4.3.3 HAVcR-1 Protein Expression Validated PC-3 Cell Models

IF staining was utilised to validate successful cell transfection at protein level (See Figure 4.3 A) and the amount of fluorescence as representative of protein expression was quantified using ImageJ software (See Figure 4.3 B).

There was no change in HAVcR-1 expression in PC-3^{WT} from PC-3^{pEF6} (0.86±0.22 fold; p=0.600). Increased expression of HAVcR-1 in PC-3$^{HAVcR-1EXP}$ (2.32±0.25 fold; p=0.033) was observed compared to the expression inPC-3^{pEF6}. The protein expression of HAVcR-1 in PC-3$^{HAVcR-1KD}$ was decreased 0.82±0.05 fold from that of PC-3^{pEF6}, however this was not significant (p=0.079). Staining of HAVcR-1 was diffuse throughout the cell. Within PC-3$^{HAVcR-1EXP}$ HAVcR-1 staining was increased within the cytoplasm and nucleus.
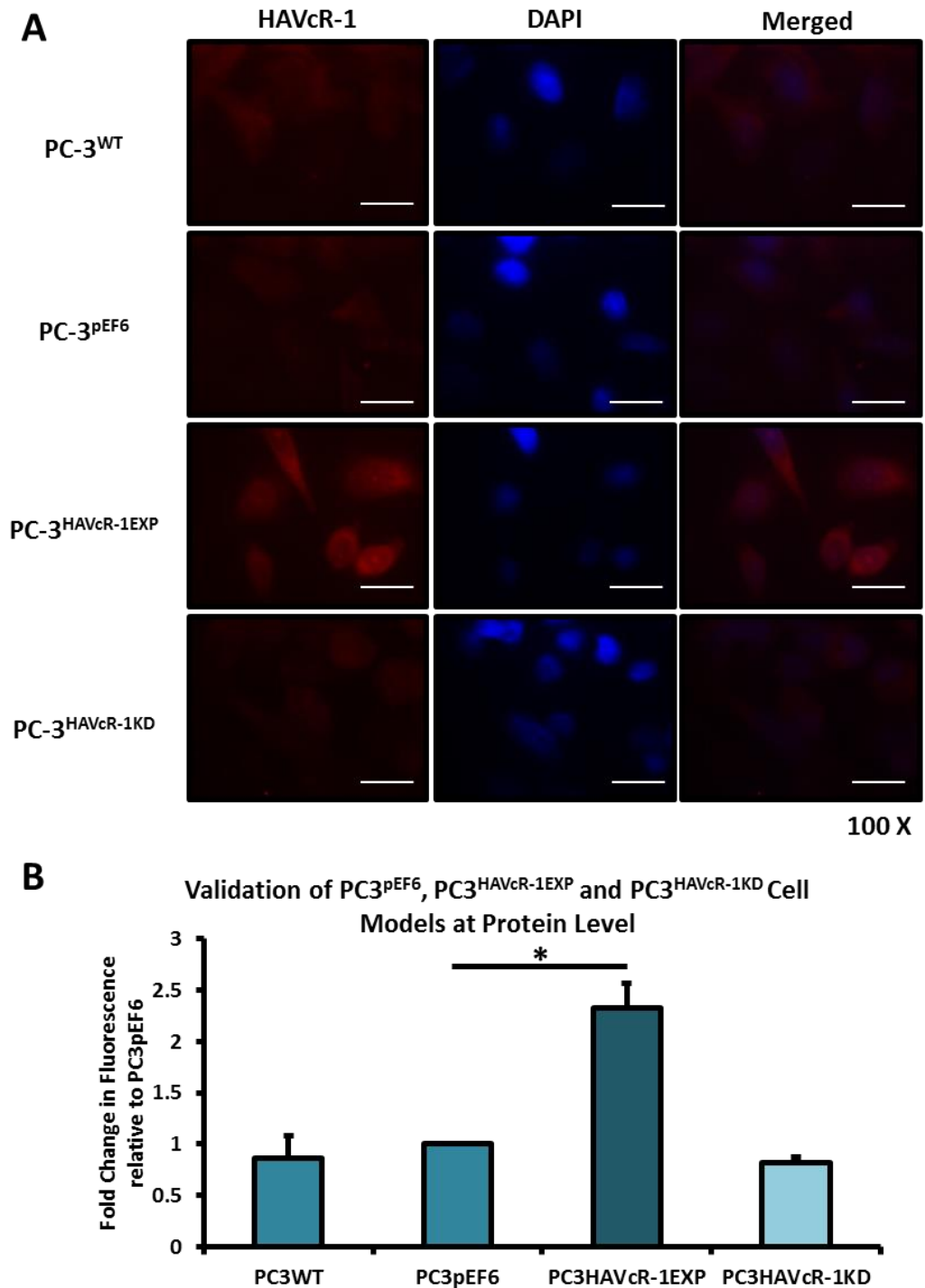
Figure 4.3 Protein Validation of HAVcR-1 Overexpression and Knockdown PC-3 Cell Lines Using Immunofluorescence

Cell were grown in 8 well chamber slides in supplemented media and subjected to immunofluorescence at 100 % confluence with HAVcR-1 and nuclear staining. **A** Images show fluorescence emission at 100 X magnification correlating to HAVcR-1 expression or nuclear staining and a merged image of both. Images are representative of three independent experiments. Scale bars represent 20 μm. **B** Graph shows quantitative analysis of immunofluorescent staining of HAVcR-1 (mean +SEM, n=3, * represents p<0.05)

4.3.4 HAVcR-1 Levels Have no Effect on Cell Growth

PC-3 transfected cell lines were then used to assess the influence if any of HAVcR-1 on cell growth via an *in vitro* cell growth assay.

This revealed that there was no significant change in cell growth in PC-3$^{HAVcR-1EXP}$ in comparison to PC-3^{pEF6} at Day 3 (2.50±0.66 vs 1.52±0.20: p=0.40) or at Day 5 (7.61±0.81 vs 5.67±0.20: p=0.185). It also showed no significant change in growth between HAVcR-1 PC-3$^{HAVcR-1KD}$ and PC-3^{pEF6} at Day 3 (3.15±1.00 vs 1.52±0.20: p=0.29) or Day 5 (10.71±2.30 vs 5.67±0.20: p=0.15) (See Figure 4.4).
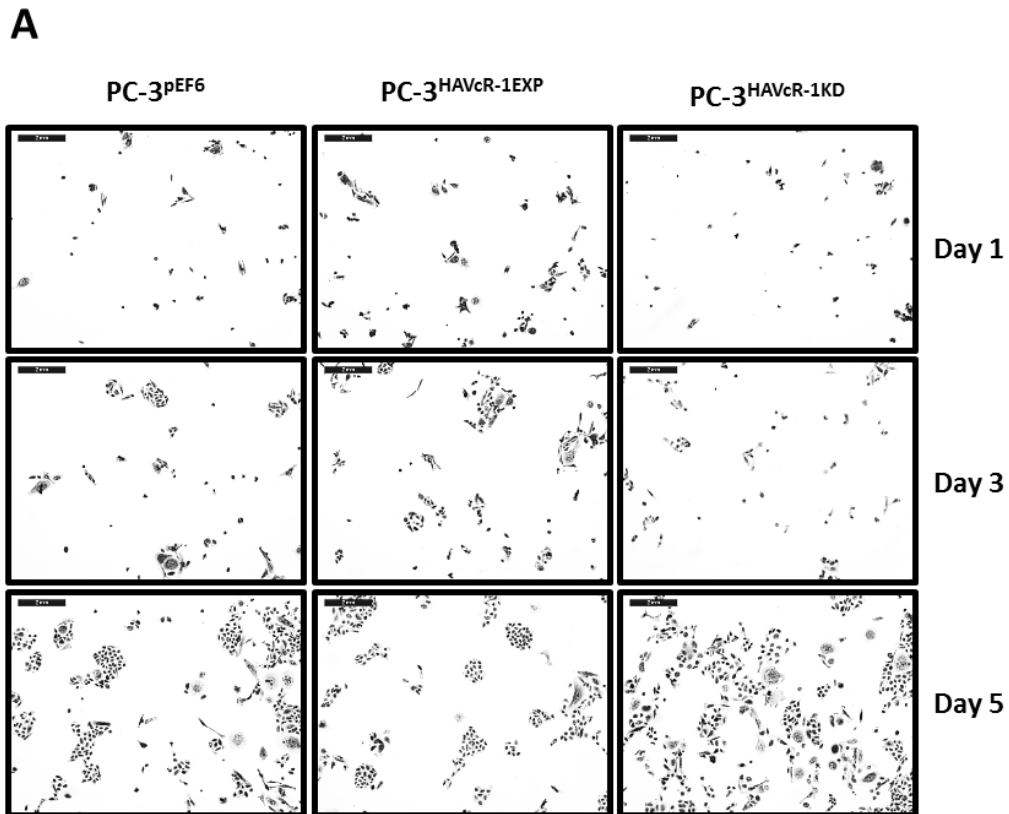
Figure 4.4 The Effect of HAVcR-1 Overexpression and Knockdown on PC-3 Cell Growth.

Cells were seeded into 24 well plates at 1×10^4 cells per well in triplicate and incubated for 1, 3 or 5 days. Post incubation cells were fixed, stained with crystal violet and images were taken at 5 X magnification. **A** Images are representative of three independent experiments. Scale bars represent 2 mm **B** Cells were counted and graph shows the means of three independent experiments as fold change relative to the cell count at day 1 with error bars showing SEM. Statistical analysis was performed at each time point via the Student's t-test using Microsoft Excel and significant of $p < 0.05$ was not reached.

4.3.5 HAVcR-1 Levels have no Effect on PC-3 Cell Invasion

The influence of HAVcR-1 on cell invasion was assessed utilising *in vitro* transwell Matrigel™ invasion assay. This assay analysed the number of cells which could invade though Matrigel™ in a 8 µm pore insert after 3 days with the amount of crystal violet staining being used as representative of cellular invasion.

This revealed no significant change in cell invasion with PC-3$^{HAVcR-1EXP}$ in comparison to PC-3^{pEF6} with a 2.58±1.017 fold increase (p=0.26). PC-3$^{HAVcR-1KD}$ also showed no significant increase in invasion in comparison to PC-3^{pEF6} with a 1.69±0.41 fold increase (p=0.24) (See Figure 4.5).
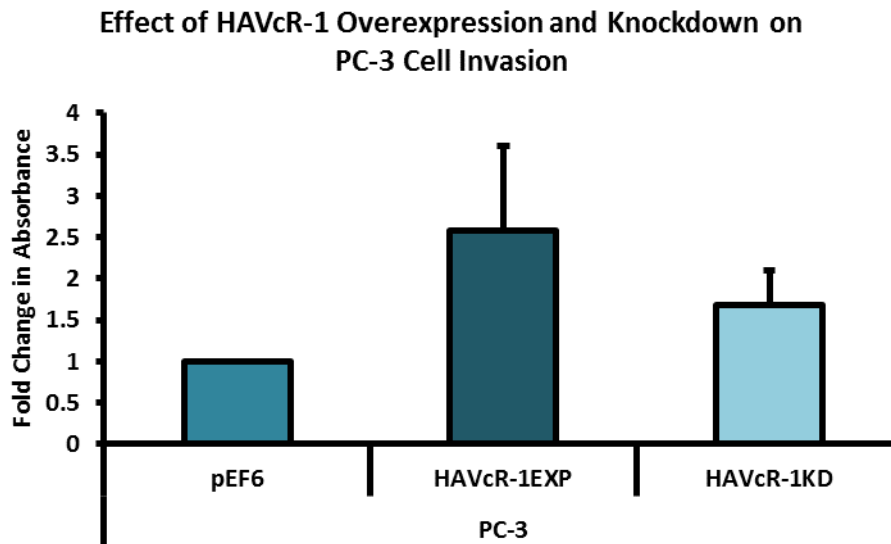
Figure 4.5 The Effect of HAVcR-1 Overexpression and Knockdown on PC-3 Cell Invasion

Cells seeded in triplicate into 8 μm size pore inserts coated in 200 μl of 500 μg/mL Matrigel™ in at 24 well plate at $3X10^4$ cells per insert and incubated for 3 days. Post incubation cells were fixed, stained with crystal violet which was then dissolved and absorbance readings taken. Graph shows the means of three independent experiments as fold change relative to the absorbance of the pEF6 control with error bars showing SEM. Statistical analysis was performed via the Student's t-test using Microsoft Excel and significance of $p<0.05$ was not reached.

190

4.3.6 HAVcR-1 Levels Have no Effect on PC-3 Cell Adhesion

To assess the importance of HAVcR-1 on cell adhesion an *in vitro* Matrigel™ adhesion assay was carried out. This assay analysed the amount of cell adhesion to Matrigel™ in 30 min there was relative to the pEF6 control (See Figure 4.6).

There was no significant change cell adhesion from to PC-3[pEF6] and PC-3[HAVcR-1EXP] (2.24±0.67 fold; p=0.207) or PC-3[HAVcR-1KD] (1.67±0.41 fold; p=0.250).

A

B
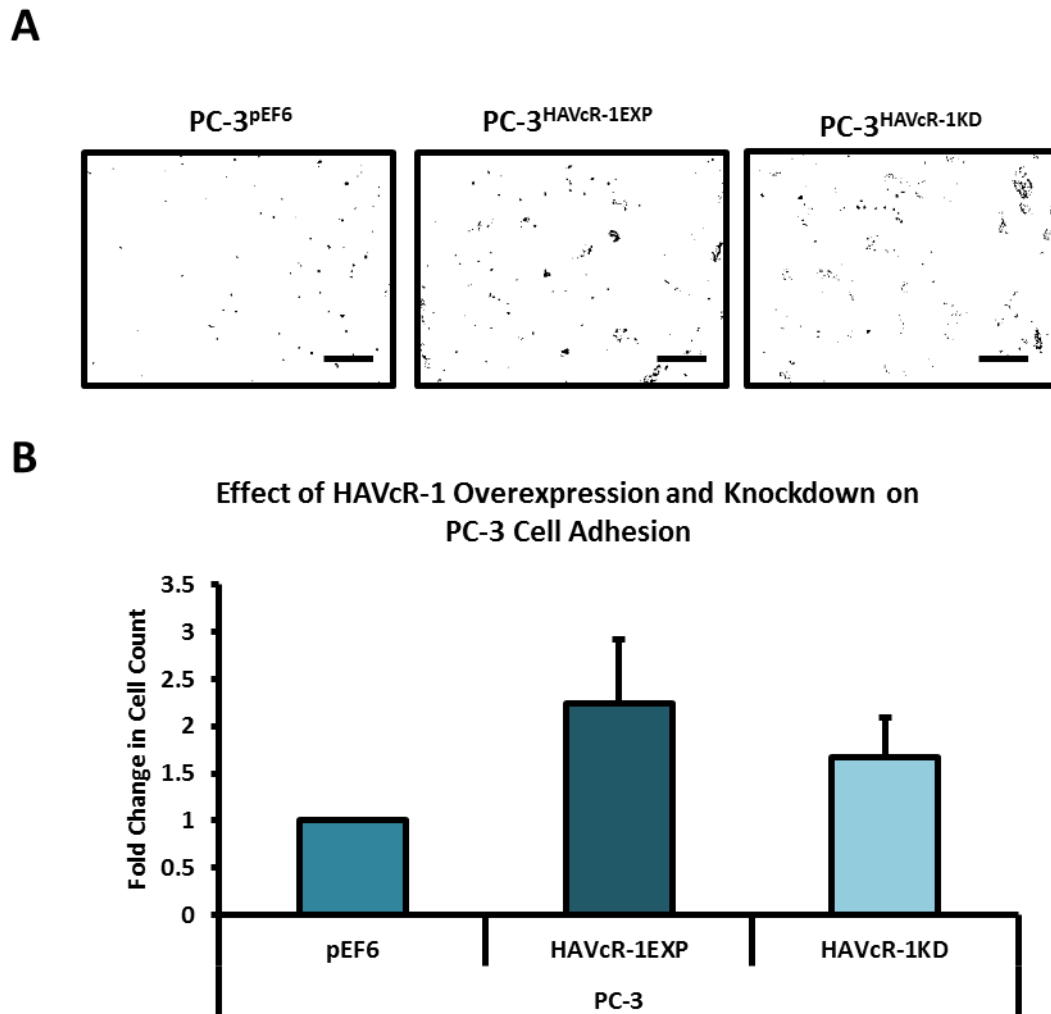
Figure 4.6 The Effect of HAVcR-1 Overexpression and Knockdown on PC-3 Cell Adhesion

Cells seeded into 96 well plates coated in 200 µl of 50 µg/mL Matrigel™ at $5X10^3$ cells per well in triplicate and incubated for 30 min. Post incubation cells were fixed, stained with crystal violet and images were taken at 5 X magnification. **A** Images are representative of three independent experiments. Scale bars represent 2 mm. **B** Cells were counted and graph shows the means of three independent experiments as fold change relative to the cell count of the pEF6 control with error bars showing SEM. Statistical analysis was performed via the Student's t-test using Microsoft Excel and significance of $p < 0.05$ was not reached.

4.3.7 HAVcR-1 Impacts PC-3 Barrier Resistance During Initial Attachment and Spreading

ECIS was used to investigate the effect of HAVcR-1 on cell attachment and spreading of PC-3 cells. Capacitance at 64 kHz was assessed as at this frequency the flow of current is mainly flowing through the cells thus it is representative of the amount of cell coverage on the electrode. There was no change in capacitance of PC-3$^{HAVcR-1EXP}$ in comparison to PC-3^{pEF6} (F(22,88)=0.159, p=1.000). There was also no change in capacitance of PC-3$^{HAVcR-1KD}$ in comparison to PC-3^{pEF6} (F(22,88)=0.116, p=1.000) (See Figure 4.7A). Resistance at 1 kHz was also assessed as at this frequency the current is mainly flowing outside of the cell and therefore is representative of cellular interactions with both the electrode as well as with adjacent cells. This revealed no change in resistance of PC-3$^{HAVcR-1EXP}$ in comparison to PC-3^{pEF6} (F(22,88)=0.194, p=1.000) or in PC-3$^{HAVcR-1KD}$ in comparison to PC-3^{pEF6} (F(22,88)=0.108, p=1.000) during PC-3 initial attachment and spreading (See Figure 4.7B).

The ECIS mathematical model was used to gain a greater understanding of the changes occurring to these cells as they attach and spread. Here the barrier function resistance (R_b) can be assessed thus giving an insight as to cellular junctional structures between cells. This showed a significant decrease in the R_b of PC-3$^{HAVcR-1EXP}$ in comparison to PC-3^{pEF6} (F(22,88)=2.341, p=0.003) as well as in the R_b of PC-3$^{HAVcR-1KD}$ in comparison to PC-3^{pEF6} (F(22,88)=1.750, p=0.035) (See Figure 4.8A). The adhesion to the electrode was also assessed via alpha (constraint on current flow beneath the cells) which showed no significant change in PC-3$^{HAVcR-1EXP}$ in comparison

to PC-3^{pEF6} (F(22,88)=0.033, p=1.000) or PC-3$^{HAVcR-1KD}$ in comparison to PC-3^{pEF6} (F(22,88)=1.619, p=0.060) (See Figure 4.8B).

A

Effect of HAVcR-1 on PC-3 Capacitance at 64kHz During Initial Attachment

B

Effect of HAVcR-1 on PC-3 Resistance at 1kHz During Initial Attachment
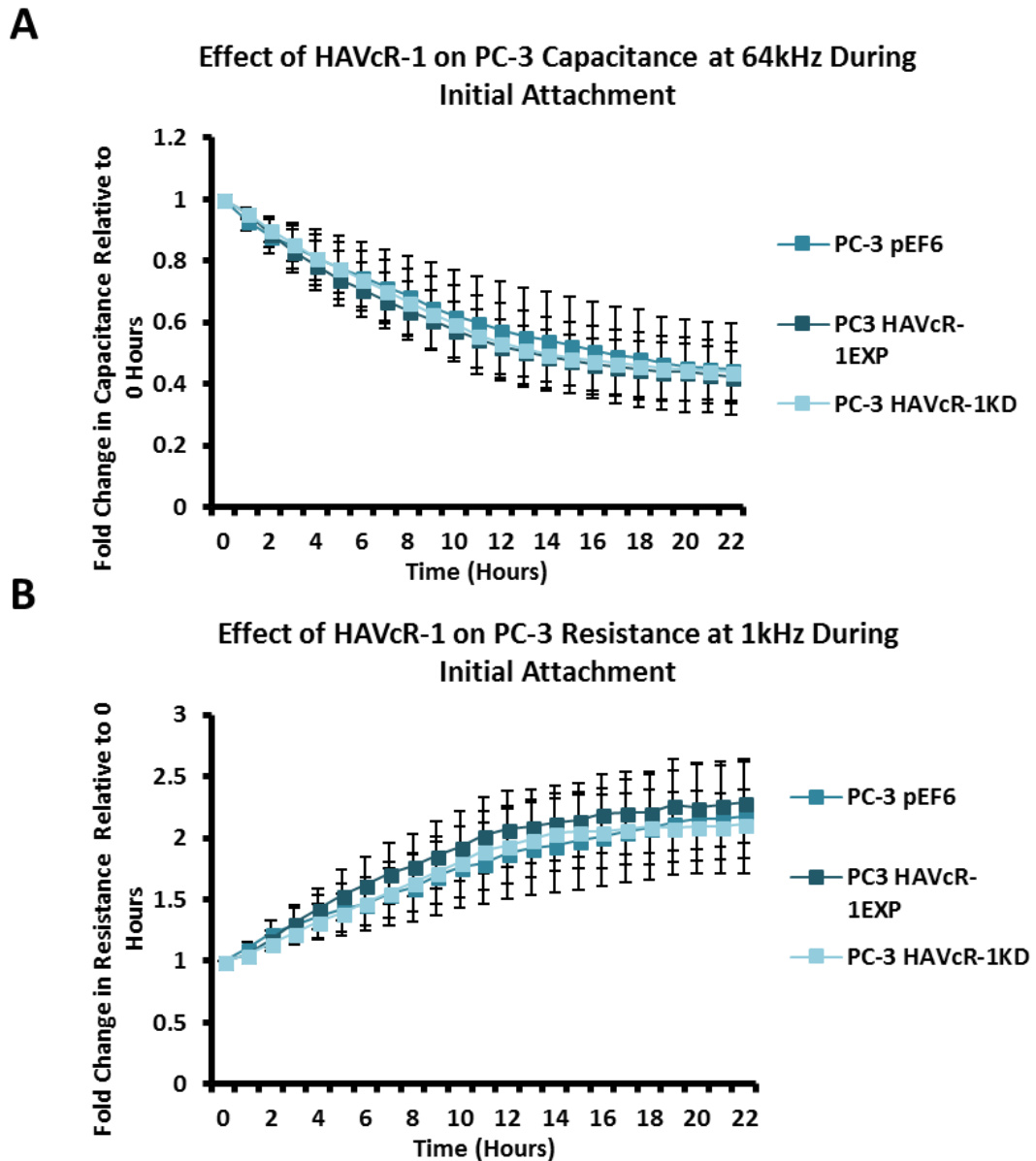
Figure 4.7 The Effect of HAVcR-1 Overexpression and Knockdown on PC-3 Initial Attachment and Spreading.

Cells seeded in octuplicate into 96W1E+ plates at 5×10^4 cells per well and resistance, capacitance and impedance were monitored for 22 hours post seeding at varying frequencies ranging from 1-64 kHz. Graphs show the means of three independent experiments as fold change relative to 0 hours with error bars showing SEM for **A** capacitance at 64 kHz and **B** resistance at 1 kHz. Statistical analysis was performed at each hour time point via IBM SPSS Statistics 24 Mixed ANOVA and p values of <0.05 were considered significant; significance was not reached.

A

B
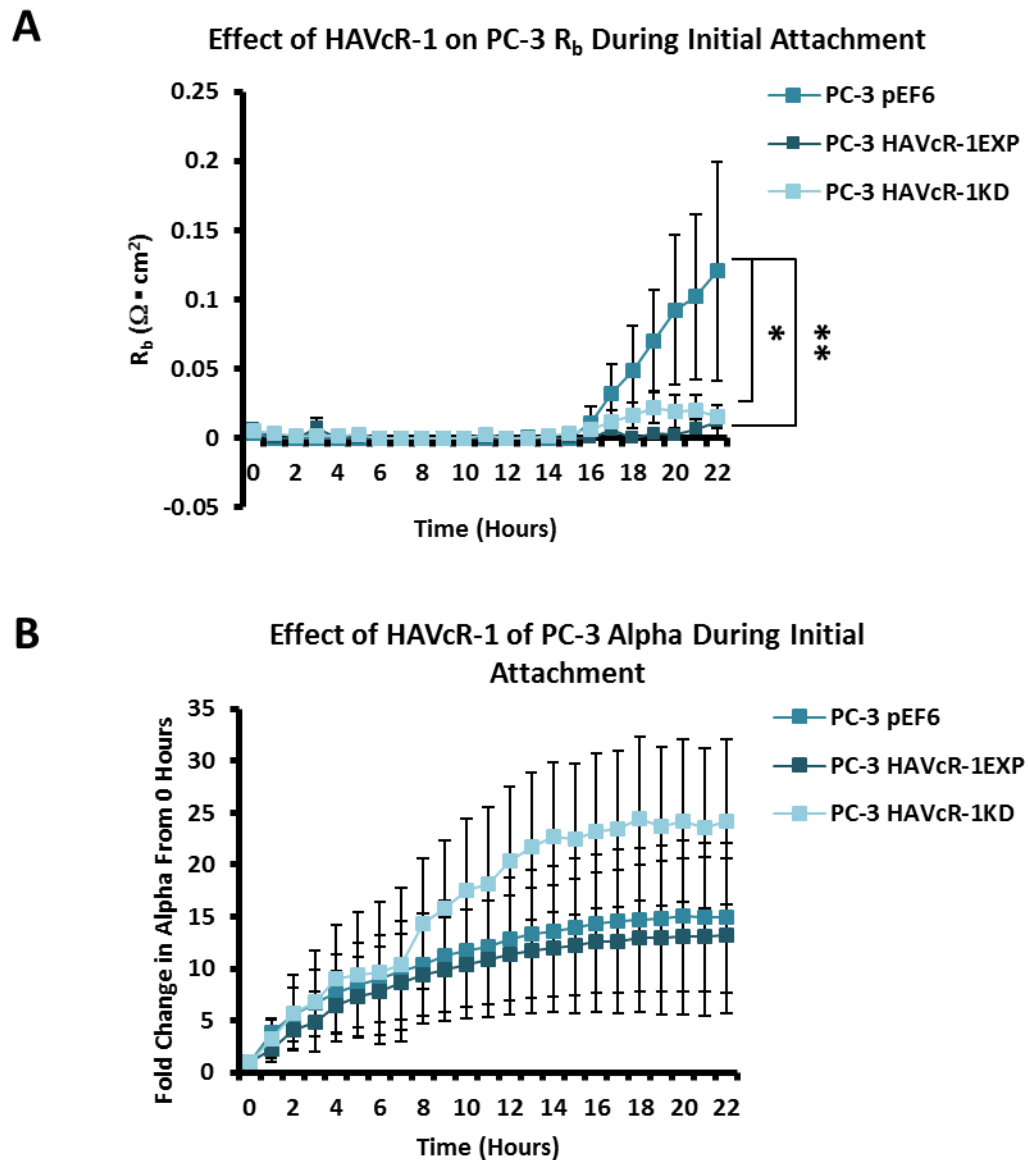
Figure 4.8 The Effect of HAVcR-1 Overexpression and Knockdown on PC-3 Barrier Function and Constraint on Current Flow Beneath Cells During Initial Attachment and Spreading.

Using the ECIS software the ECIS™ Model was applied to initial attachment data to give R_b (barrier function resistance) and alpha (constraint on current flow beneath the cells) values. Graph show then means of three independent experiments with error bars showing SEM for **A** R_b and **B** alpha shown as fold change relative to 0 hours. Statistical analysis was performed using IBM SPSS Statistics 24 Mixed ANOVA and $p < 0.05$ was considered significant ($p < 0.05$ and $p < 0.01$ are represented by * and ** respectively.

4.3.8 HAVcR-1 Decreases PC-3 Wound Healing

To assess the importance of HAVcR-1 on PC-3 cell migration an *in vitro* scratch assay was performed whereby cells grown in 24 well plates were scratched once a confluent monolayer was formed. Images were taken every hour (See Figure 4.9A), the area of the scratch at each time point was calculated via ImageJ and percentage wound closure was calculated from area at 0 hours.

This revealed that there was a significant decrease in wound healing of PC-3$^{HAVcR-1EXP}$ in comparison to PC-3^{pEF6} ($F_{(10,40)}$=3.436, p=0.003) however there was no difference in healing rate with PC-3$^{HAVcR-1EXP}$ closing 4.68 ±0.57 %/hr and PC-3^{pEF6} closing 5.01±1.24 %/hr (p=0.830) (See Figure 4.9)

There was no significant change in wound healing of PC-3$^{HAVcR-1KD}$ in comparison to PC-3^{pEF6} ($F_{(10,40)}$=0.135, p=0.999) and no significant difference in healing rate with PC-3$^{HAVcR-1KD}$ closing 5.88 ±0.73 %/hr and PC-3^{pEF6} closing 5.01±1.24 %/hr (p=0.730) (See Figure 4.9).
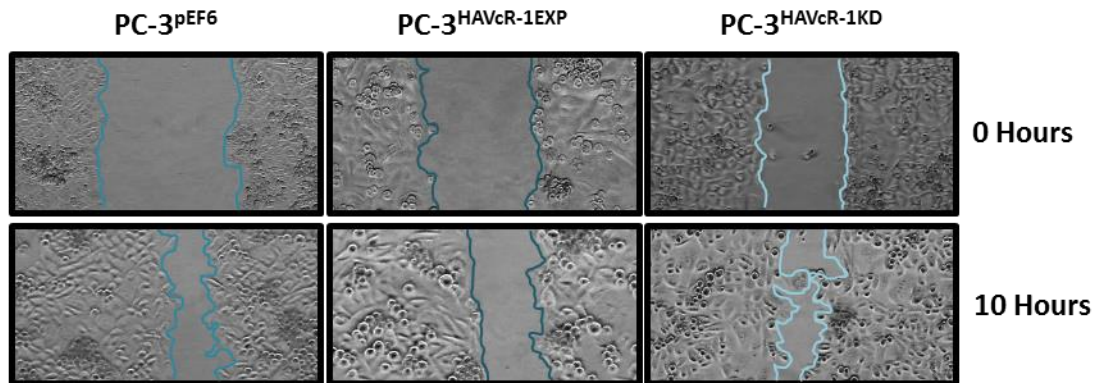
Figure 4.9 The Effect of HAVcR-1 Overexpression and Knockdown on PC-3 Cell Migration

Cells seeded into 24 well plates in quadruplicate and scratched once confluent layer formed. Images were taken at 5 X magnification immediately afterward and every hour thereafter. **A** Images shown are representative of three independent experiments. **B** Wound area was measured using ImageJ software and percentage wound closure was calculated as relative to 0 hour time point. Data shown are the means of three independent experiments and error bars represent SEM. Statistical analysis was performed using IBM SPSS Statistics 24 utilising a Mixed ANOVA and $p < 0.05$ was considered significant and represented by * (** represents $p < 0.01$).

4.3.9 HAVcR-1 Impacts PC-3 Constraint on Current Flow Beneath Cells During Electrical Wound Healing

ECIS was used to further investigate cell migration, whereby an electrical wound was applied to cells after initial attachment and spreading had concluded. Capacitance at 64 kHz was measured for 17 hours post wounding as indicative of cell coverage. This showed no change with PC-3$^{HAVcR-1EXP}$ ($F_{(17,68)}$=0.148, p=1.000) or PC-3$^{HAVcR-1KD}$ ($F_{(17,68)}$=0.120, P=1.000) in comparison to PC-3^{pEF6} during wound healing (See Figure 4.10A). Resistance at 1 kHz was also measured for 17 hours post wounding to investigate cell-cell and cell-plate interactions. There was no change in resistance with PC-3$^{HAVcR-1EXP}$ ($F_{(17,68)}$=0.203, p=1.000) and PC-3$^{HAVcR-1KD}$ ($F_{(17,68)}$=0.056, p=1.000) in comparison to PC-3^{pEF6} during wound healing (See Figure 4.10B).

ECIS mathematical modelling of this data to look at barrier function resistance (R_b) and constraint on current flow beneath the cells (alpha) revealed no significant difference in R_b with either PC-3$^{HAVcR-1EXP}$ ($F_{(17,68)}$=0.627, p=0.859) or PC-3$^{HAVcR-1KD}$ ($F_{(17,68)}$=1.105, p=0.368) in comparison to PC-3^{pEF6} (See Figure 4.11A). However there were significant increases in alpha of both PC-3$^{HAVcR-1EXP}$ ($F_{(17,68)}$=6.808, p<0.0001) and PC-3$^{HAVcR-1KD}$ ($F_{(17,68)}$=2.056, p=0.019) in comparison to PC-3^{pEF6} (See Figure 4.11A).

A Effect of HAVcR-1 on PC-3 Capacitance at 64kHz During Wound Healing

B Effect of HAVcR-1 on PC-3 Resistance at 1kHz During Wound Healing
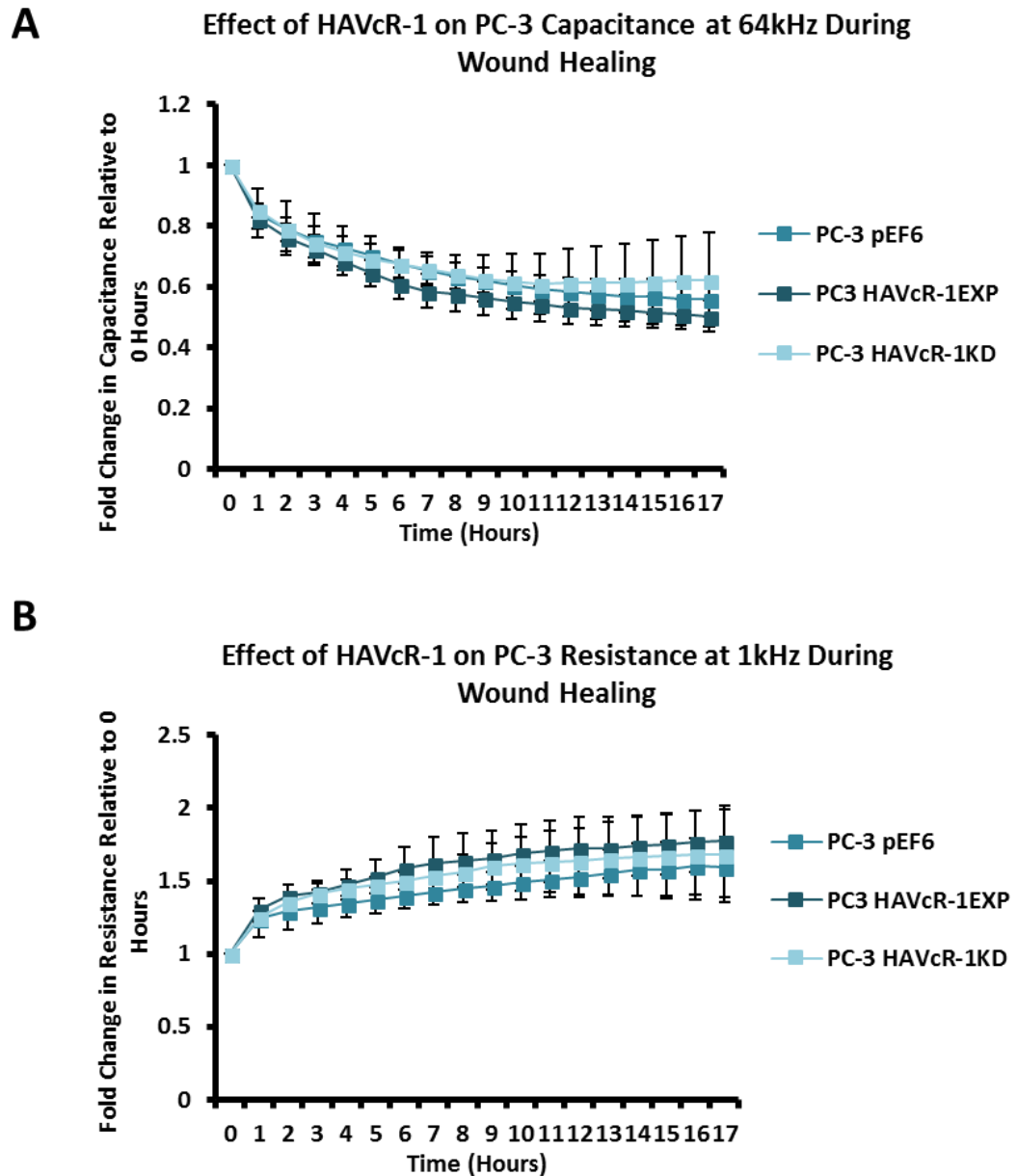
Figure 4.10 The Effect of HAVcR-1 Overexpression and Knockdown on PC-3 Electrical Wound Healing
Post initial attachment and spreading cells were electrically wounded at 6000 Hz and 3000 µA for 30 seconds. Resistance, capacitance and impedance were then monitored at varying frequencies (1-64 kHz) for 17 hours. Graphs shows the means of three independent experiments as fold change relative to 0 hours with error bars showing SEM for **A** capacitance at 64 kHz and **B** resistance at 1 kHz. Statistical analysis was performed at each hour time point via Mixed ANOVA using IBM SPSS Statistics 24 and p values of <0.05 were considered significant; significance was not reached.
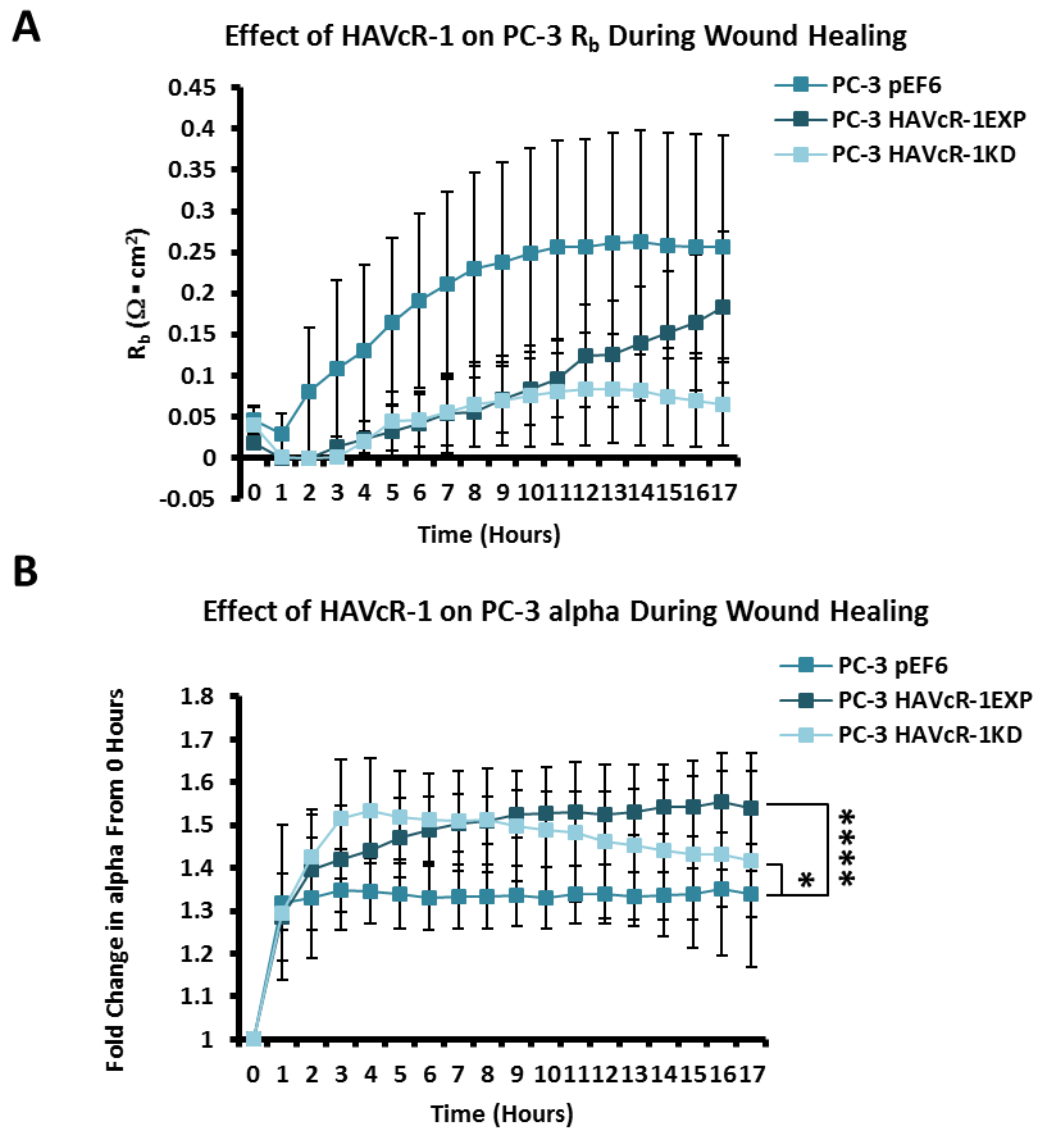
Figure 4.11 The Effect of HAVcR-1 Overexpression and Knockdown on PC-3 Barrier Function and Constricted Current Flow Beneath Cells During Initial Attachment and Spreading.

Using the ECIS software the ECIS™ Model was applied to electrical wound healing data to give R_b (barrier function resistance) and alpha (constraint on current flow beneath the cells) values. Graph show then means of three independent experiments with error bars showing SEM for **A** R_b and **B** alpha shown as fold change relative to 0 hours. Statistical analysis was performed using IBM SPSS Statistics 24 Mixed ANOVA and $p < 0.05$ was considered significant; $p < 0.05$ and $p < 0.0001$ were represented by * and **** respectively.

4.3.10 Effect of HAVcR-1 on the Gene Expression of PC-3 TJ Components

To begin exploring the potential relationship between HAVcR-1 and TJs in PC-3 cells a PCR screening to investigate gene expression of ten TJ proteins was undertaken. Changes in the gene expression of these ten TJ proteins in PC-3$^{HAVcR-1EXP}$and PC-3$^{HAVcR-1KD}$ were investigated in relation to expression in PC-3^{pEF6} (See Figure 4.12). From these ten gene, eight encoded integral membrane proteins (Claudin -1, -2, -3, -4, -7, and -9, Occludin, and JAM-A and two encoded plaque anchoring proteins (ZO -1 and ZO-2).

There was no significant change in the gene expression in PC-3$^{HAVcR-1EXP}$ in comparison to PC-3^{pEF6} of *CLDN1* (1.07±0.09 fold; p=0.503), *CLDN2* (0.98±0.46 fold; p=0.962), *CLDN3* (1.07±0.09 fold; p=0.536), *CLDN4* (0.86±0.09 fold; p=0.245), *CLDN7* (0.12±0.12 fold; p=0.272), *CLDN9* (0.71±0.20 fold; p=0.280), *JAMA* (1.02±0.29 fold; p=0.945), *OCLN* (0.96±0.09 fold; p=0.718), *ZO1* (1.02±0.11 fold; p=0.848) or *ZO2* (0.87±0.10 fold; p=0.334). There was also no significant change in gene expression in PC-3$^{HAVcR-1KD}$ in comparison to PC-3^{pEF6} of *CLDN1* (1.01±0.09 fold; p=0.909), *CLDN2* (1.81 ±1.15 fold; p=0.553), *CLDN3* (1.01±0.09 fold; p=0.909), *CLDN4* (0.80±0.13 fold; p=0.263), *CLDN7* (0.93±0.11 fold; p=0.602), *CLDN9* (0.63±0.20 fold; p=0.207), *JAMA* (1.11±0.55 fold; p=0.866), *OCLN* (1.01±0.0.8 fold; p=0.872), ZO1 (0.95±0.12 fold; p=0.734) or ZO2 (0.90±0.12 fold; p=0.493).
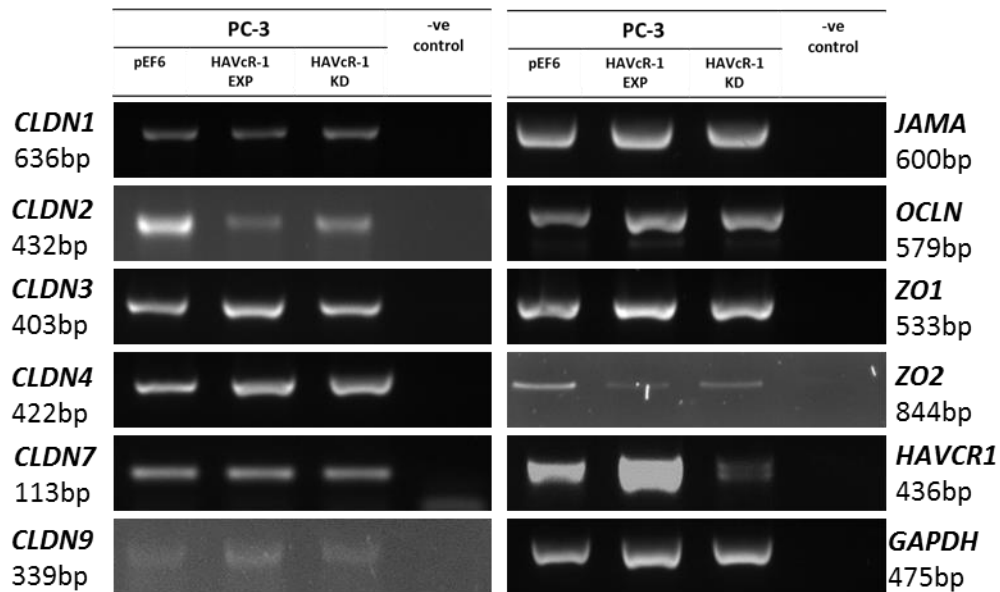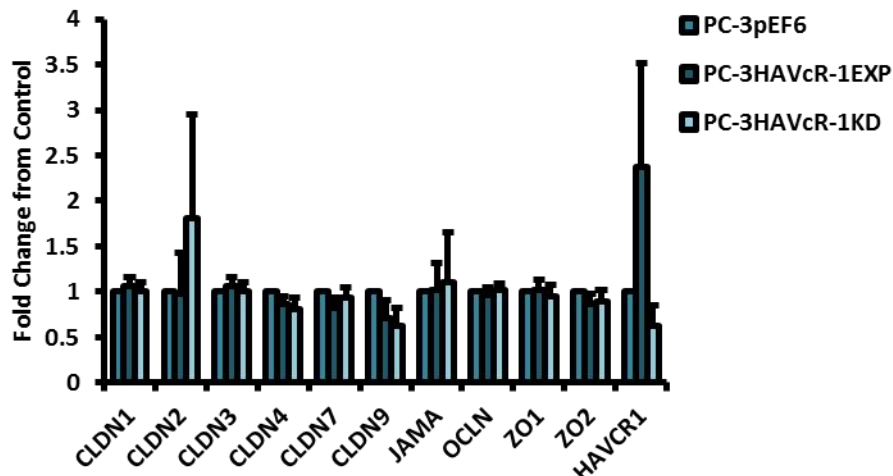
Figure 4.12 The Effect of HAVcR-1 Overexpression and Knockdown on Gene Expression of TJ Proteins
Cell were grown in 6 well plates in supplemented media and harvested via RNA extraction at 100 % confluence. Data shown are the means of three independent experiments and error bars show SEM. **A** Gene expression was assessed using PCR. **B** Graph shows band intensity as quantified by ImageJ software. Expression was normalised to *GAPDH* and is shown as fold change relative to pEF6 control. Student's t-tests were performed and significance of p<0.05 was not reached.

4.3.11 Effect of HAVcR-1 on PC-3 Protein Expression and Localisation of TJ Components

Preliminary investigations into Claudin1, Occludin, ZO-1 and RhoC protein expression and localisation were assessed using immunofluorescence.

Claudin 1 staining was slightly increased in PC-3$^{HAVcR-1EXP}$ and PC-3$^{HAVcR-1KD}$ in comparison to PC-3^{pEF6} cells with staining intensity being 1.12 fold and 1.19 fold increased respectively. Staining of Claudin 1 was highly localised within the cytoplasm with a minority of staining at the cell membrane. Staining was diffuse throughout the cell and showed no change with manipulation of HAVcR-1 expression (See Figure 4.13 A and E)

Occludin staining intensity decreased in PC-3$^{HAVcR-1EXP}$ cells and increased in PC-3$^{HAVcR-1KD}$ cells with 0.88 fold and 1.09 fold change from PC-3^{pEF6} cells. PC-3^{pEF6} and PC-3$^{HAVcR-1KD}$ cells showed diffuse staining through the cell. However, within PC-3$^{HAVcR-1EXP}$ although staining intensity was decreased, there was clear staining at the cell membrane (See Figure 4.13 B and E).

ZO-1 staining intensity decreased in both PC-3$^{HAVcR-1EXP}$ and PC-3$^{HAVcR-1KD}$ cells with a 0.66 fold change and 0.60 fold change respectively from PC-3^{pEF6} cells. Staining was diffuse throughout the cell in all cases however there appeared to be decreased nuclear staining within PC-3$^{HAVcR-1EXP}$ cells (See Figure 4.13 C and E).

RhoC staining intensity was also decreased in both PC-3$^{HAVcR-1EXP}$ and PC-3$^{HAVcR-1KD}$ cells with a 0.34 fold and 0.57 fold change from PC-3^{pEF6} cells. Expression of HAVcR-1 had no effect on the localisation of RhoC (See Figure 4.13 D and E)
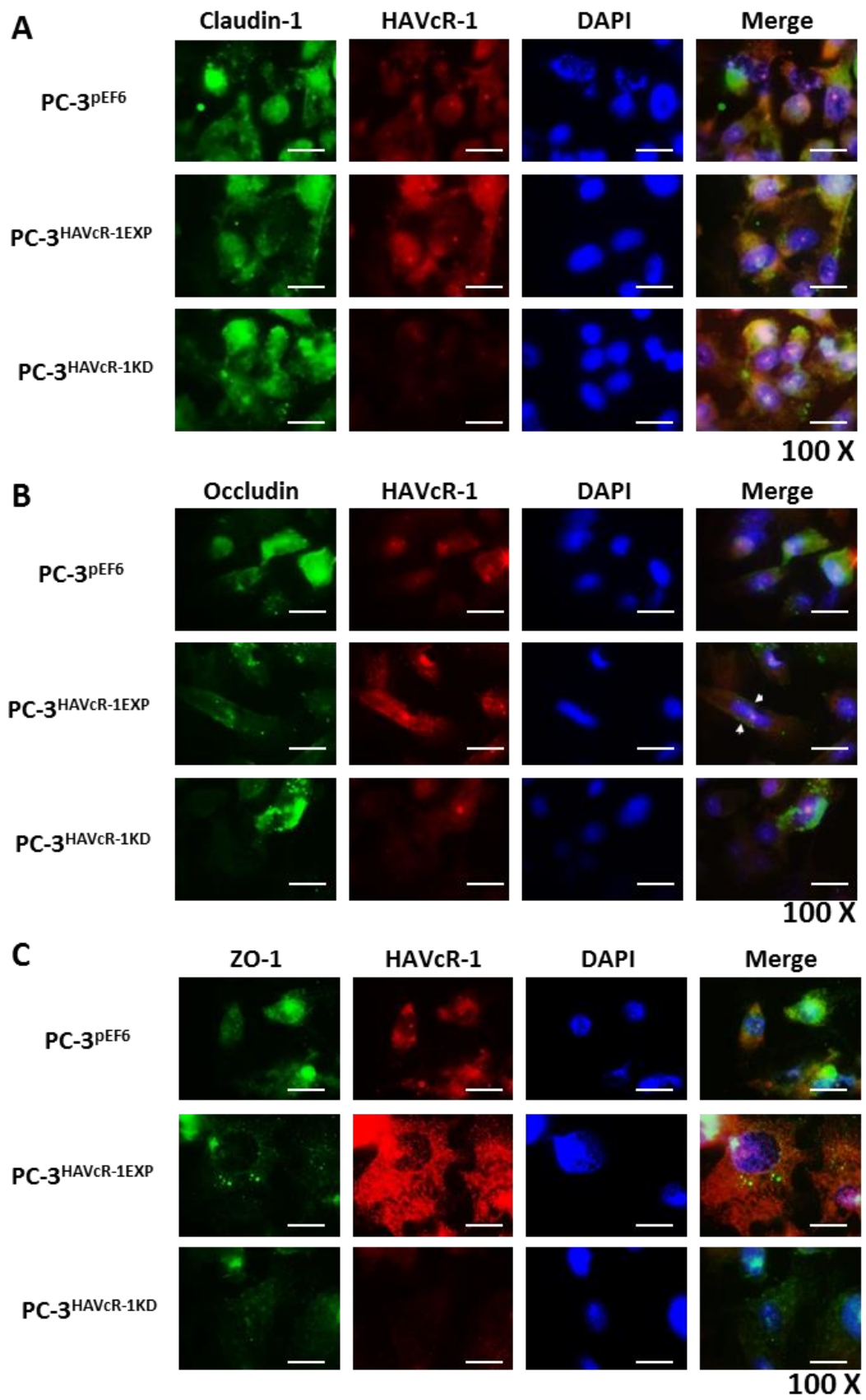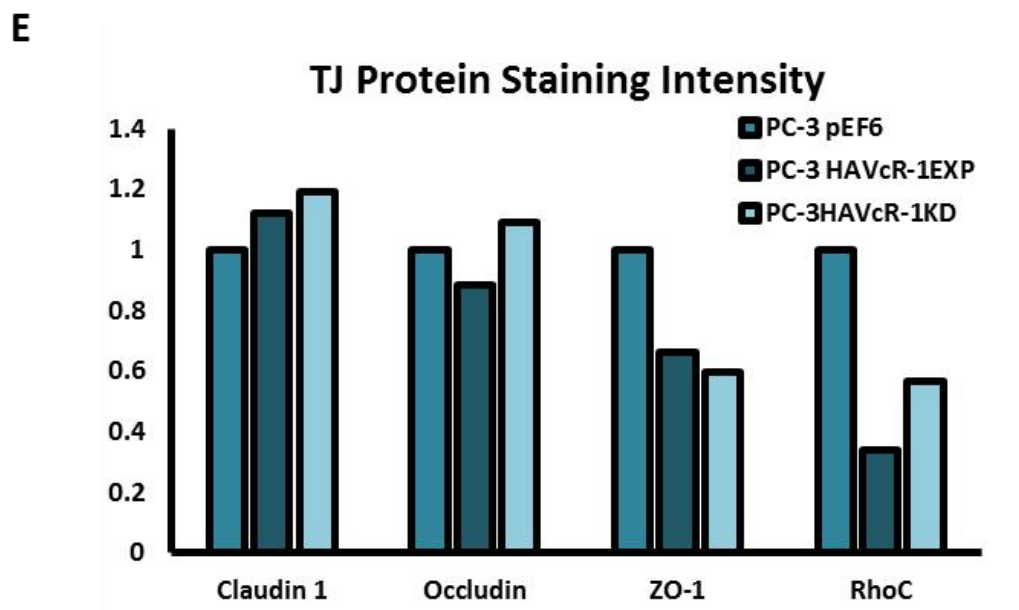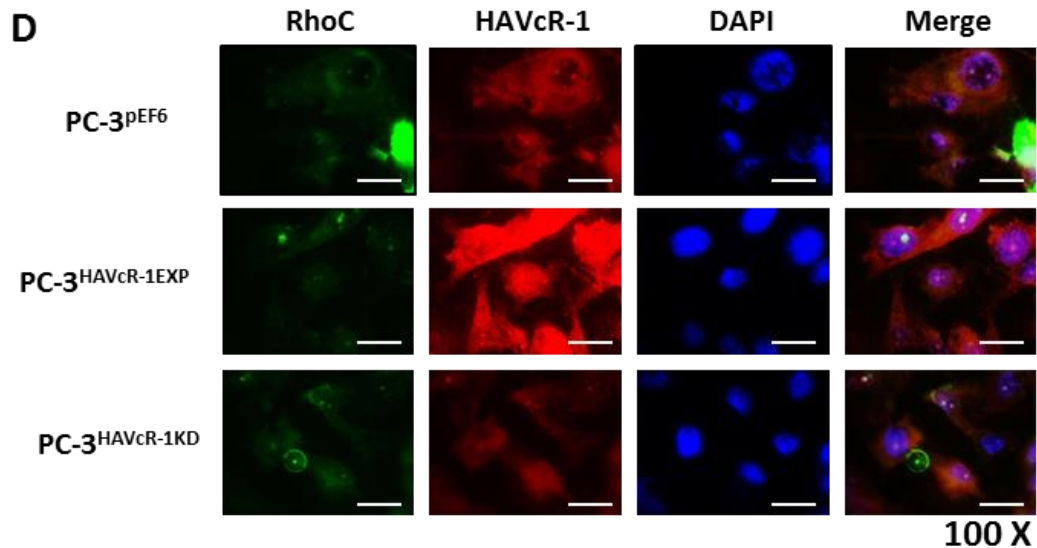
Figure 4.13 Effect of HAVcR-1 on TJ Protein Expression and Localisation
Cell were grown in 8 well chamber slides in supplemented media and subjected to immunofluorescence at 100 % confluence with antibodies specific for the protein of interest and nuclear staining. Data shown are of n=1. **A-D** Images show fluorescence emission correlating to protein expression (**A**:Claudin 1, **B**:Occludin, **C**:ZO-1 and **D**:RhoC),HAVcR-1 expression, DAPI nuclear staining and a merged image of both. Images were taken at 100 X magnification and scale bars represent 20 μm. **E** Graph shows quantitative analysis of immunofluorescent staining of proteins. White arrows highlight membranous staining.

4.3.12 PC-3 Transepithelial Resistance is Independent of HAVcR-1

The assess whether HAVcR-1 influenced PC-3 TER an *in vitro* TER assay was performed on transfected PC-3 cells. Resistance across a monolayer grown on a transwell insert was measured. Data was then analysed as change from PC-3^{pEF6}.

There was no significant change in TER of PC-3$^{HAVcR-1EXP}$, with a 1.02 ± 0.05 fold change from the PC-3^{pEF6} control (p= 0.706) (See Figure 4.14). The was also no significant change in TER of PC-3$^{HAVcR-1KD}$, with a 1.00 ± 0.02 fold change from the PC-3^{pEF6} control (p= 0.999) (See Figure 4.14).
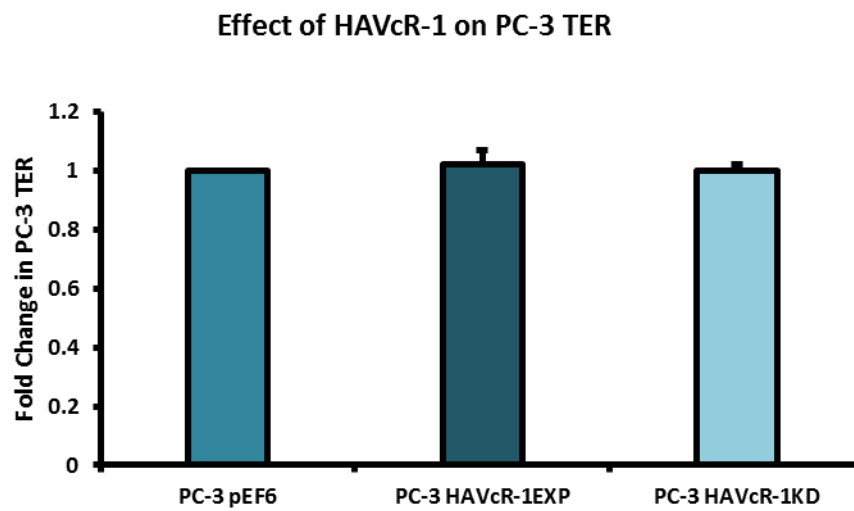
Figure 4.14 The Effect of HAVcR-1 Overexpression and Knockdown on PC-3 Transepithelial Resistance.

Cells seeded in triplicate into 0.4 μm size pore inserts $5X10^4$ cells per insert and incubated until confluent. Post incubation resistance across the membrane was measured immediately after media change. Graph shows the means of three independent experiments as fold change relative to the resistance of PC-3^{pEF6}. Error bars show SEM. Statistical analysis was performed via the Student's t-test using Microsoft Excel and $p<0.05$ was considered significant.

4.3.13   PC-3 Paracellular Permeability is Independent of HAVcR-1

To assess the effect if any HAVcR-1 has on PC-3 paracellular permeability an *in vitro* PCP assay was performed on PC-3^{pEF6}, PC-3$^{HAVcR-1EXP}$ and PC-3$^{HAVcR-1KD}$ cells.

This assay revealed no change in the amount of 40 kDa TRITC-dextran conjugate able to pass through PC-3$^{HAVcR-1EXP}$ monolayers in comparison to PC-3^{pEF6} monolayers ($F_{(10, 40)}=0.552$, $p=0.842$) (See Figure 4.15A). There was also no change in the amount of paracellular movement of 40 kDa TRITC-dextran conjugate able to pass through PC-3$^{HAVcR-1KD}$ monolayers in comparison to PC-3^{pEF6} monolayers ($F_{(10, 40)}=0.470$, $p=0.900$) (See Figure 4.15A).

Furthermore, there was no change in the passage of a smaller 10 kDa FITC-dextran conjugate through PC-3$^{HAVcR-1EXP}$ monolayers in comparison to PC-3^{pEF6} monolayers ($F_{(10, 40)}=0.259$, $p=0.987$), (See Figure 4.15B). There was also no change in the passage of 10 kDa FITC dextran conjugate through the PC-3$^{HAVcR-1KD}$ monolayers in comparison to PC-3^{pEF6} monolayers ($F_{(10, 40)}=0.488$, $p=0.888$) (See Figure 4.15B).

A

B
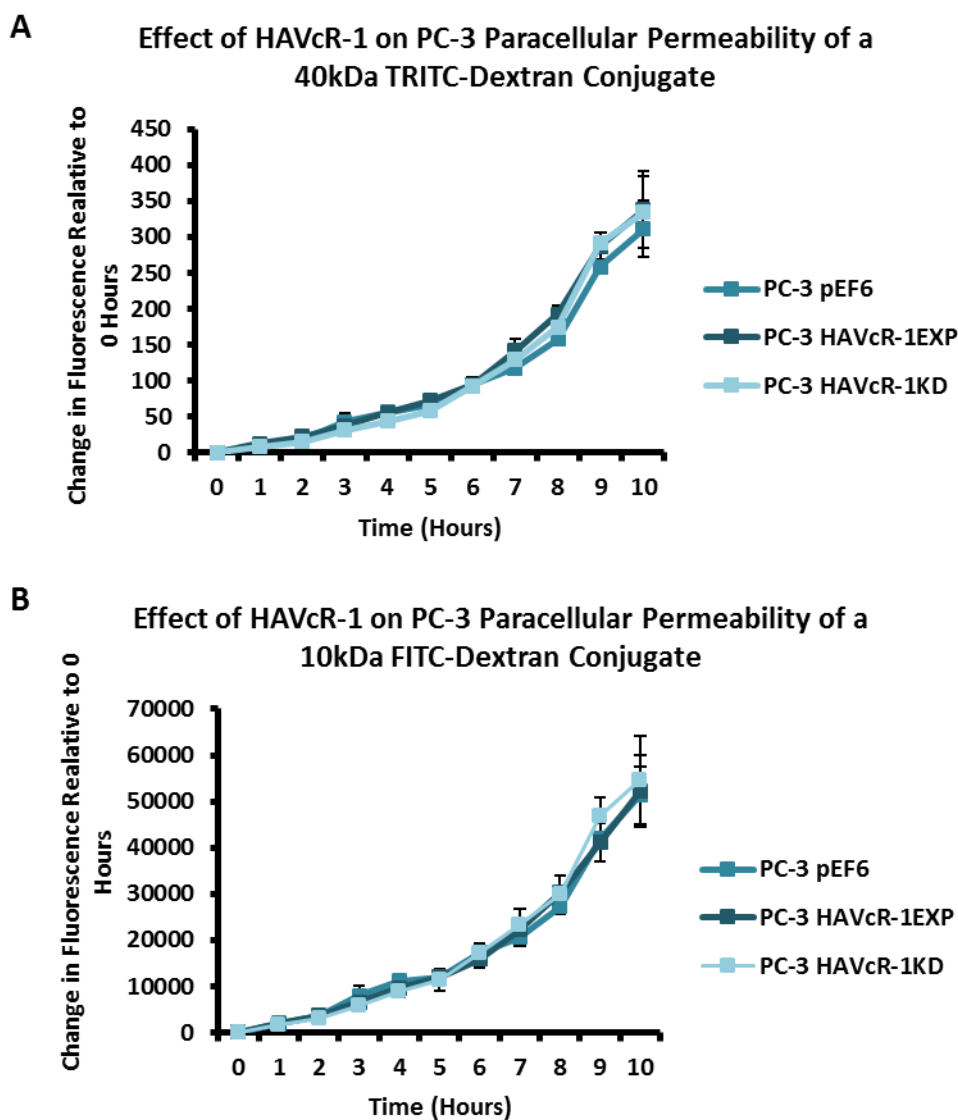
Figure 4.15 The Effect of HAVcR-1 Overexpression and Knockdown on PC-3 Paracellular Permeability

Cells seeded in triplicate into 0.4 μm size pore inserts 5×10^4 cells per insert and incubated until confluent. Post incubation cell media inside of the inserts were changed to media containing 0.2 mg/mL of 40 kDa TRITC-dextran conjugate and 0.2 mg/mL of 10 kDa FITC-dextran conjugate. Samples were then taken of medium outside of the insert were then taken every hour and fluorescence measured. Graph shows the means of three independent experiments as change to fluorescence from 0 hours for **A** the 40 kDa TRITC-dextran conjugate and **B** the 10 kDa FITC-dextran conjugate. Error bars show SEM. Statistical analysis was performed via Mixed ANOVAs using IBM SPSS Statistics 24 and significance of $p < 0.05$ was not reached.

4.4 Discussion

This chapter set out to evaluate the effect of HAVcR-1 on prostate cancer cell behaviours that are imperative to allow for disease progression to metastatic. To accomplish this cell models were created based on the PC3 cell line due to the consistent high protein and gene expression of HAVcR-1 as shown in Chapter III. These cell models were verified at gene and protein level and used for a variety of functional assays. Consistent with HAVcR-1 studies in colorectal cancer HAVcR-1 had no significant effect on cell growth [320]. However, unlike the colorectal study which showed that increased HAVcR-1 decreased invasion and adhesion this chapter showed no significant change in either with HAVcR-1 overexpression or knockdown. Furthermore HAVcR-1 overexpression in colorectal cells resulted in no change in cell migration, however overexpression in PC-3 showed decrease in wound healing and may therefore propose HAVcR-1 as a tumour suppressor [320].

The second area of interest of this chapter was the effect of HAVcR-1 on intercellular interactions, with a specific interest on TJs. PC-3$^{HAVcR-1EXP}$ and PC-3$^{HAVcR-1KD}$ cell models were utilised in a series of assays to assess this, the first being TER, a quantitative technique for the measurement of TJ integrity, which showed no change in resistance with PC-3$^{HAVcR-1EXP}$ or PC-3$^{HAVcR-1KD}$ [343]. Therefore, suggesting that HAVcR-1 has no effect on tight junction integrity and is inconsistent with the hypothesis that the increased HAVcR-1 expression seen in prostate cancer is important for metastasis to occur via the decreased integrity of TJs. The effect of HAVcR-1 on paracellular permeability was also assessed due to TJs being the primary determinant of epithelial permeability with Claudin expression patterns in particular being responsible for pore selectivity [344]. However, HAVcR-1 appeared to have no effect on PC-3

permeability and thus further suggesting that HAVcR-1 expression has no bearing on the integrity of TJ within PC-3 cells or on the composition of TJs within PC-3 cells. The compositional stability of PC-3 TJs with manipulated HAVcR-1 expression was further validated with gene expression of all TJ proteins investigated remaining constant. Preliminary investigations into TJ protein expression showed minute changes in expression and localisation of occludin and ZO-1. Decreased occludin staining in PC-3$^{HAVcR-1EXP}$ and increased staining in PC-3$^{HAVcR-1KD}$ suggests that overexpression of HAVcR-1 would decrease TJ integrity and that targeting HAVcR-1 could therefore be a potential therapeutic target for prostate cancer. However contradictory to this, there was also an increase in occludin membranous staining with HAVcR-1 overexpression suggesting an increase in TJs. Furthermore, in PC-3 cells that overexpressed HAVcR-1 there was a decreased nuclear staining of ZO-1. ZO-1 contains both NLS and NES thus scan shuttle between TJs and the cell nucleus [129]. Nuclear levels are generally associated with decreased TJ integrity being found in proliferating low confluent cells [176]. Therefore, low ZO-1 nuclear staining further suggests an increased junctional stability with HAVcR-1 overexpression.

To gain further insight into the effect of HAVcR-1 on cellular interactions during cell attachment and wound healing ECIS experiments were carried out. Results from which were inconsistent with previous assays, whereby HAVcR-1 expression had no impact on TER and PCP. There was a decrease in barrier resistance with HAVcR-1 overexpression and knockdown during cell adhesion and spreading indicating a decrease in cell-cell junction integrity. TER results suggested that junctional integrity remained constant regardless of HAVcR-1 expression, thus it is possible that HAVcR-1 levels effect the initiation of junction assembly however, do not affect the integrity

of junctions once formed. The cell adhesion assay as well as ECIS initial attachment experiment showed no change in cell adhesion with manipulated HAVcR-1 expression. However, there was an increased constraint under cells with both increased and decreased HAVcR-1 expression suggesting decreased focal adhesion. To validate changes to focal adhesion further analysis is required such as a dynamic culture cell adhesion assay would be required [345].

The lack of significance within this chapter suggests that the HAVcR-1 overexpression seen in prostate cancer does not decrease TJ integrity and may therefore not be involved in the process of metastasis. However, it is also possible that due to the PC-3 cell line being highly mutated from that of the normal prostate and being a metastatic prostate cancer cell line that these cells are no longer reliant on HAVcR-1. It is therefore possible that HAVcR-1 overexpression may be an initiation step for tumorigenesis or metastasis of which PC-3 have succeeded. It would therefore be of interest to investigate the effect of HAVcR-1 overexpression in a prostate cancer cell line which is closer to that of the normal prostate. It is also possible that HAVcR-1 overexpression alone is not responsible for cellular changes but the combination of HAVcR-1 overexpression and HAVcR-1 activation. There has been some research to indicate that HGF is important in HAVcR-1 activation and therefore it would be interesting to investigate the effect of a combination of HGF and HAVcR-1 on cell behaviours and TJ integrity [340].

Chapter V:

HAVcR- 1 Overexpression

in PZ-HPV-7 Cells

5.1 Introduction

The majority of prostate cancers originate from glandular epithelial cells, with 99 % being adenocarcinomas [346, 347]. Therefore, understanding the regulation of normal epithelial architecture and the mechanisms by which they are disturbed is critical in the understanding of carcinogenesis of prostate cancers [348]. Intercellular junctions are important in the homeostasis of epithelial sheets maintaining tissue integrity and cellular polarity as well as regulating paracellular transport and signalling events. The dysregulation of these junctions correlates with a loss in cell-cell adhesion and an increase in migratory potential and thus, are important in malignant transformation and progression [346, 349, 350].

AJs, key intercellular junctions, are composed of three main protein families: transmembrane cadherins, armadillo proteins and plakins. E cadherin is the predominant transmembrane protein in epithelial cell AJs and is responsible for cell-cell adhesion via homotypic binding to E-cadherin on neighbouring cells. Armadillo proteins, including α- and β- catenin, facilitate the interaction between the cytoplasmic tail of E-cadherin and the actin cytoskeleton. As well as the role in cellular adhesion, AJs are also important in the regulation of the actin cytoskeleton, signalling and transcriptional processes [346, 348]. Tumours originating from epithelial cells acquire alterations in cellular adhesion and cytoskeleton dynamics. These changes have the capacity to transduce intracellular signals which act to promote cell proliferation and survival as well as regulate cell motility and invasion. Thus, the dysregulation of AJs can play an important role in carcinogenesis [346, 349].

Changes in the expression and localisation of junctional proteins such as cadherin-switching are important in cancer progression. One of the most frequent is the loss

of E-Cadherin which has a role in the transformation from the normal epithelial morphology toward an invasive and less differentiated mesenchymal phenotype, known as EMT [346, 349, 351]. EMT is a natural process, seen in embryogenesis (type I) and wound healing (type II), which becomes pathological in the case of cancer. EMT is also characterised by the loss of other epithelial markers, including β-catenin, and the simultaneous increase of mesenchymal markers including N-cadherin and vimentin. EMT results in decreased adhesion, increased migration and the initiation of invasion and metastasis [209, 349]. Cancer cells that undergo EMT are therefore more invasive and are more likely to metastasise [346, 349]. EMT has been shown to be important in prostate cancer progression. Decreased E-cadherin and increased N-cadherin have been found in more aggressive prostate cancer cell lines and have been associated with cancer stage, progression and cancer-specific death [5, 209, 351, 352].

Cell adhesion complexes transduce signalling between cells and are critical for regulating cellular processes including gene expression, cell cycle and programmed cell death [6]. Dissociation of β-catenin from E-cadherin and the actin cytoskeleton enables its translocation to the nucleus where it can bind to transcription factors to promote gene expression including genes involved in cell proliferation [348]. Reduced membranous β-catenin and increased nuclear β-catenin have therefore been associated with aggressive prostate cancer [353].

HAVcR-1 expression is increased in prostate cancer therefore, to evaluate whether this increase is implicated in the development and progression of prostate cancer this section of my study aimed to create a HAVcR-1 overexpression cell model using the PZ-HPV-7 cell line. Utilising this cell model this chapter aimed to evaluate the

effect manipulated HAVcR-1 expression had on the expression and phosphorylation

of signalling molecules using the Kinex™ Antibody Microarray, validating and further

exploring the potential signalling pathways presented. Furthermore, this chapter set

out to assess the effect HAVcR-1 had on cell behaviours crucial for prostate cancer

development and progression to metastatic disease using *in vitro* functional assays.

5.2 Materials and Methods

5.2.1 Mammalian Cell Culture

The PZ-HPV-7cell line was purchased from ATCC (Middlesex, UK) and maintained in supplemented Keratinocyte-SFM medium (Sigma, Dorset). PZ-HPV-7^{pEF6} and PZ-HPV-7$^{HAVcR-1EXP}$ were maintained in maintenance Keratinocyte-SFM medium. Routine cell culture was carried out as described in Section 2.2.1

5.2.2 Generation of Plasmids

PEF6/V5-His TOPO TA control plasmid (termed pEF6 control) and HAVcR-1 overexpression PEF6/V5-His TOPO TA plasmid (termed HAVcR-1EXP) was obtained courtesy of Dr T.A. Martin. Amplification of plasmids was achieved via transformation of One Shot TOP10 Chemically Competent *E.coli* (Invitrogen, life technologies, Paisley, UK) (detailed in Section 2.2.2.3) and plasmid purification using the GenElute Plasmid Miniprep Kit (Sigma-Aldrich, Gillingham, Dorset, UK) as detailed in Section 2.2.2.5. Purified plasmids were then stored at -20 °C.

The PZ-HPV-7 cell line was then transformed with pEF6 control or HAVcR-1EXP plasmid via electroporation as detailed in Section 2.2.2.6

5.2.3 RNA Extraction, PCR and qPCR

Cells were grown in 6 well plates until confluent, total RNA was then extracted using the EZ-RNA kit (Geneflow, Staffordshire, UK) as detailed in 2.2.3.1. Five hundred nanograms of total RNA was used to synthesise cDNA using the GoScript™ Reverse Transcription System (Promega, Southampton, UK) as detailed in Section 2.2.3.2. Polymerase chain reaction (PCR) was carried out, as detailed in Section 2.2.3.3, using

GoTaq G2 Green master mix (Promega, Southampton, UK) and primers detailed in Table 4.1. Products were subjected to gel electrophoresis as described in Section 2.2.3.4. cDNA was also used for qPCR, using Precision FAST 2 X qPCR Master Mix with ROX (Primer Design, Southampton, UK) as detailed in Section 2.2.3.5 using the primers listed in Table 4.1.

5.2.4 Protein Extraction and SDS PAGE and Western Blotting Analysis

Cells were seeded at $3X10^4$ per well of a 6 well plate and incubated until confluent, total cellular protein was extracted using western blotting lysis buffer and denatured using laemmli 2 X concentrate (Sigma-Aldrich, Gillingham, Dorset, UK) and boiling at $100°C$ for 10 min. Samples were resolved using a polyacrylamide gel, consisting of a 4 % (v/v) stacking component and 10 % (v/v) running component. Resolved proteins were transferred to a PVDF membrane (Merck Millipore, Sigma-Aldrich, Gillingham, Dorset, UK). PVDF membranes were blocked using 5 % (w/v) milk. Primary antibodies and HRP-conjugated secondary antibodies diluted in 1 % (w/v) milk were used for immunoblotting (See Table 5.2). Proteins were detected using EZ-ECL Chemiluminescent Detection (Geneflow, Staffordshire, UK) and visualized using the G:Box Chemi RxQ Imaging System (Syngene, Cambridge, UK). Protein detection methodology is described in Section 2.2.4.

5.2.5 ImmunoFluorescence (IF) Staining

Cells were seeded at 5 $X10^4$ cells per well of an 8 well glass Millicell EZ slides (Merck Millipore, Sigma-Aldrich, Gillingham, Dorset, UK) and left to reach confluency prior

to being subjected to IF staining as detailed in Section 2.2.4.9. Primary and secondary

antibodies used are described in Table 5.2.

5.2.6 Cell Growth Assay

Growth assays were carried out as described in Section 2.2.5.1 and cells were stained

with crystal violet as described in 2.2.5.4

5.2.7 Cell Adhesion Assay

Adhesion assays were carried out as described in Section 2.2.5.2 and stained with

crystal violet as described in Section 2.2.5.4.

5.2.8 Cell Invasion Assay

Invasion assays were carried out as described in Section 2.2.5.3 and cells were

stained with crystal violet as described in Section 2.2.5.4.

5.2.9 Cell Migration Assay

Migration assays were performed as detailed in Section 2.2.5.7.

5.2.10   Transepithelial Resistance (TER)

TERs were measured as described in Section 2.2.5.5.

5.2.11   Paracellular Permeability (PCP)

PCPs were performed as described in Section 2.2.5.6.

5.2.12   Electric Cell-Substrate Impedance Sensing (ECIS)

ECIS experiments were performed as described in Section 2.2.5.8.

5.2.13   Kinex™ Antibody Microarray

Further detailed in Section 2.2.4.7, cells were cultured in 10 cm dishes and protein was extracted using Kinex™ Antibody Microarray lysis buffer. Protein was then quantified using fluorescamine and diluted in Kinex™ Antibody Microarray lysis buffer to 4 mg/mL and shipped to Kinex Bioinformatics, Vancouver, Canada for the Kinex™ Antibody Microarray.

5.2.14   Statistical Analysis

PCR and western blot analysis bands were quantified using Image J software, and with data from qPCR, cell growth, adhesion and invasion assays was statistically analysed to assess for changes from PZ-HPV-7^{pEF6} control using the Microsoft Excel Student's t-test. Wound area was quantified using Image J software and this data as well as data from other assays whereby time points were assessed, which included: ECIS and PCP, were statistically analysed to assess changes from PZ-HPV-7^{pEF6} control via two way mixed ANOVAs using IBM SPSS Statistic 24 software.

Table 5.1. Chapter V Primers used in PCR and qPCR screening of PZHPV-7 cells

	Target		Sequence 5'-3'	Number of Cycles	Product Size (bp)
PCR	*HAVCR1*	F:	CAACAACAAGTGTTCCAGTG	35	436
		R:	GCATTTTGCAAAGCTTTAAT		
	GAPDH	F:	GGCTGCTTTTAACTCTGGTA	25	475
		R:	GACTGTGGTCATGAGTCCTT		
	CTNNA1	F:	CACAGAGAAGGTTCTGGAAG	30	518
		R:	CCGATGTATTTTTGAGTGGT		
	CTNNA1	F:	AAAGGCTACTGTTGGATTGA	30	649
		R:	TCCACCAGAGTGAAAAGAAC		
	CCND1	F:	CGGTGTCCTACTTCAAATGT	30	721
		R:	ACCTCCTCCTCCTCCTCT		
	EPLIN	F:	TCAAACTAAGATTCTCCGGG	30	875
		R:	TCGGGGCATCTTCTACC		
	GSK3β	F:	ATGTTTCGTATATCTGTT	30	534
		R:	GGTGGAGTTGGAAGCTGATG		
qPCR	*HAVCR1*	F:	GACAATGTTTCAACGA	100	99
		ZR:	**ACTGAACCTGACCGTACA** TGGAGGAACAAA		
	GAPDH	F:	CTGAGTACGTCGTGGAGTC	100	93
		ZR:	**ACTGAACCTGACCGTACA** CAGAGATGATGACCCTTTTG		

Table 5.2 Chapter V Antibodies used in the screening of PZHPV-7 cells

Antibody	Animal Source	Company	Concentration
HAVcR-1	Rabbit	Abnova, Heyford, Oxfordshire, UK	2 µg/mL-IF 1:200-WB
TIM-1 (N-13)	Goat	Santa Cruz, Insight Biotechnology Limited, Middlesex UK	2 µg/mL-IF 1:100-WB
α-Catenin	Mouse	BD Transduction Laboratories, San Jose, CA, USA	2 µg/mL-IF 1:4000- WB
β-Catenin	Rabbit	Sigma-Aldrich, Gillingham, Dorset, UK	2 µg/mL-IF 1:4000- WB
E-Cadherin	Mouse	R & D Systems, Abingdon, Oxfordshire, UK	2 µg/mL-IF 1:200-WB
EPLIN	Rabbit	Bethyl Lab, Montgomery, TX, USA	1:1000- WB
PKM2	Goat	Santa Cruz, Insight Biotechnology Limited, Middlesex UK	1:200-WB
Cyclin D1	Rabbit	Santa Cruz, Insight Biotechnology Limited, Middlesex UK	1:200- WB
Anti-Goat AlexaFluor 594	Donkey	Santa Cruz, Insight Biotechnology Limited, Middlesex UK	1:500-IF
Anti-Mouse AlexaFluor 488	Donkey	Thermo Fisher Scientific, Cramlington, England, UK	1:500-IF
Anti-Rabbit AlexaFluor 488	Donkey	Thermo Fisher Scientific, Cramlington, England, UK	1:500-IF
Anti-Rabbit AlexaFluor 594	Donkey	Thermo Fisher Scientific, Cramlington, England, UK	1:500-IF
Anti-Mouse IgG (whole molecule)- Peroxidase	Goat	Sigma-Aldrich, Gillingham, Dorset, UK	1:1000 -WB
Anti-Rabbit IgG (whole molecule)- Peroxidase	Goat	Sigma-Aldrich, Gillingham, Dorset, UK	1:1000 -WB
Anti-Goat IgG (whole molecule)- Peroxidase	Rabbit	Sigma-Aldrich, Gillingham, Dorset, UK	1:1000 -WB

5.3 Results

5.3.1 *HAVCR1* Gene Expression Validated PZ-HPV-7 Cell Models

PZ-HPV-7 cells were transfected via electroporation with the pEF6 control plasmid to form PZ-HPV-7^{pEF6} or HAVcR-1EXP plasmid to form PZ-HPV-7$^{HAVcR-1EXP}$. Plasmid validation are shown in Section 4.3.1. The success of these transfections was then assessed using PCR and qPCR to investigate *HAVCR1* gene expression. PCR band intensity as representative of gene expression was then quantified via ImageJ software and PCR and qPCR data were analysed as fold change relative to PZ-HPV-7^{pEF6} (See Figure 5.1).

The PZ-HPV-7^{pEF6} cell model was verified as a suitable control with PCR showing that there was no significant variation in *HAVCR1* gene expression between PZ-HPV-7^{WT} and PZ-HPV-7^{pEF6} with fold change from PZ-HPV-7^{pEF6} being 0.71±0.28; p=0.41 (See Figure 5.1 A and B). This was also shown with qPCR with fold change from PZ-HPV-7^{pEF6} being 3.56±1.32; p=0.19 (Figure 5.1C).

The PZ-HPV-7$^{HAVcR-1EXP}$ cell model was also verified as a suitable HAVcR-1 overexpression model with PZ-HPV-7$^{HAVcR-1EXP}$ having a significant 3.63±0.26 fold increased in *HAVCR1* gene expression from PZ-HPV-7^{pEF6} as shown by PCR with p=0.010 (See Figure 5.1A and B). There was also a 109.10±44.93 fold increase via qPCR however this wasn't significant with p=0.14 (See Figure 5.1 C).

A
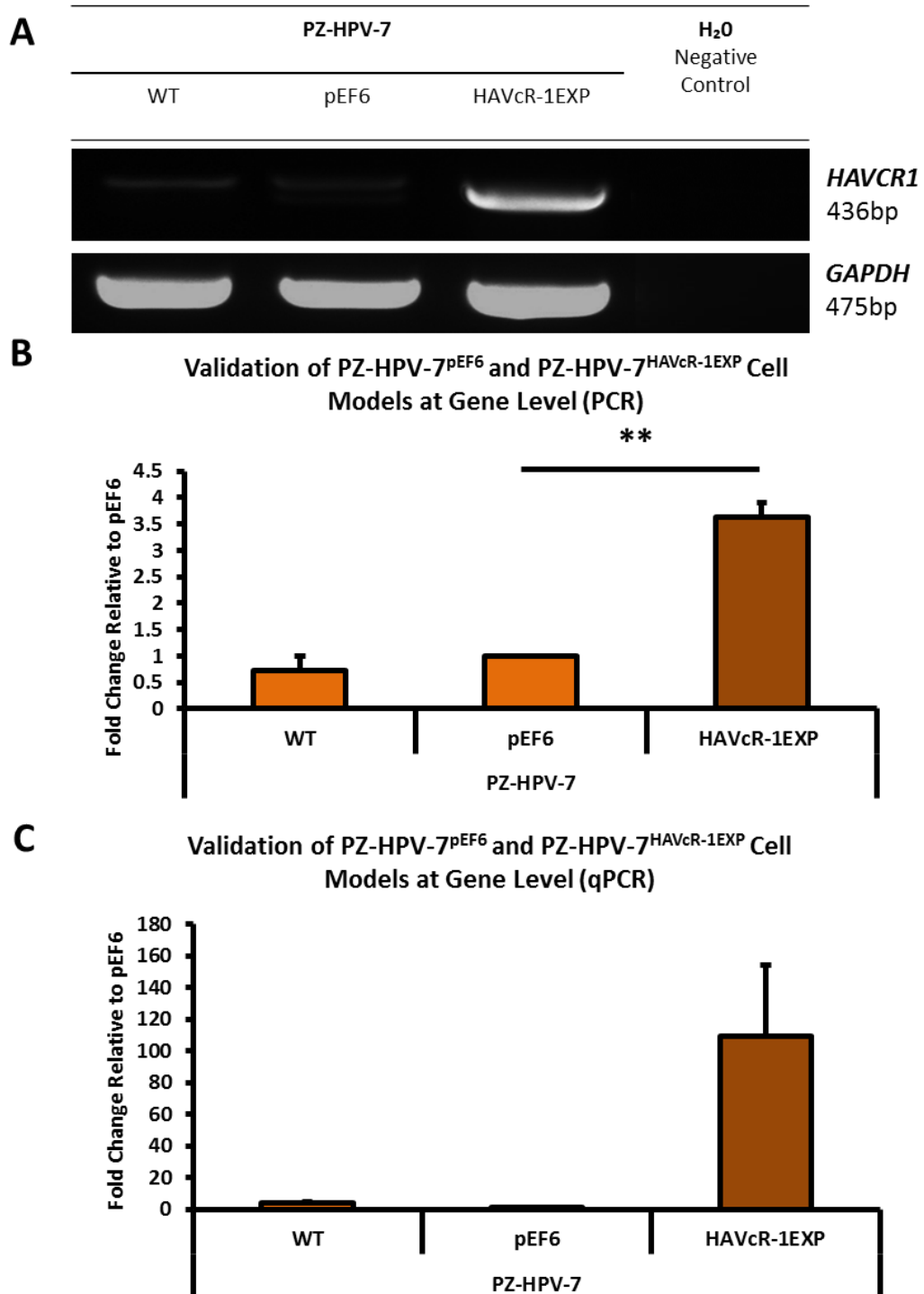
	PZ-HPV-7			H₂0

Figure 5.1 Gene Expression Validation of PZ-HPV-7^{pEF6} and PZ-HPV-7$^{HAVCR-1EXP}$
Cell were grown in 6 well plates in supplemented media and harvested via RNA extraction at 100 % confluence. Data shown are the means of three independent experiments and error bars show SEM. *HAVCR1* mRNA expression was assessed using **A** PCR or **C** qPCR. **B** Graph shows band intensity as quantified by ImageJ software. **B and C** *HAVCR1* mRNA expression was normalised to *GAPDH* and is shown as fold change relative to PZ-HPV-7^{pEF6}. Student's t-tests were performed and significance of $p<0.01$ is represented by **.

5.3.2 HAVcR-1 Protein Expression Validated PZ-HPV-7 Cell Models

Immunofluorescence was utilised to assess HAVcR-1 protein expression and therefore further validate PZ-HPV-7^{pEF6} and PZ-HPV-7$^{HAVcR-1EXP}$ cell models. Cells were stained for total HAVcR-1 as well as for the nucleus using DAPI staining (See Figure 5.2A). The amount of fluorescence as representative of protein expression was quantified using ImageJ software and analysed as fold change relative to PZ-HPV-7^{pEF6} HAVcR-1 expression (See Figure 5.2B).

Protein expression also verified PZ-HPV-7^{pEF6} as a suitable control with there being no variation in HAVcR-1 protein expression in PZ-HPV-7^{WT} from PZ-HPV-7^{pEF6} (0.72±0.17 fold; p=0.524).

PZ-HPV-7$^{HAVcR-1EXP}$ was also verified as a suitable HAVcR-1 overexpression cell model at protein level. There was a consistent increase in HAVcR-1 protein expression in PZ-HPV-7$^{HAVcR-1EXP}$ with a 1.86 ±0.58 fold increase from PZ-HPV-7^{pEF6} HAVcR-1 protein expression, although significance was not reached (p=0.375).
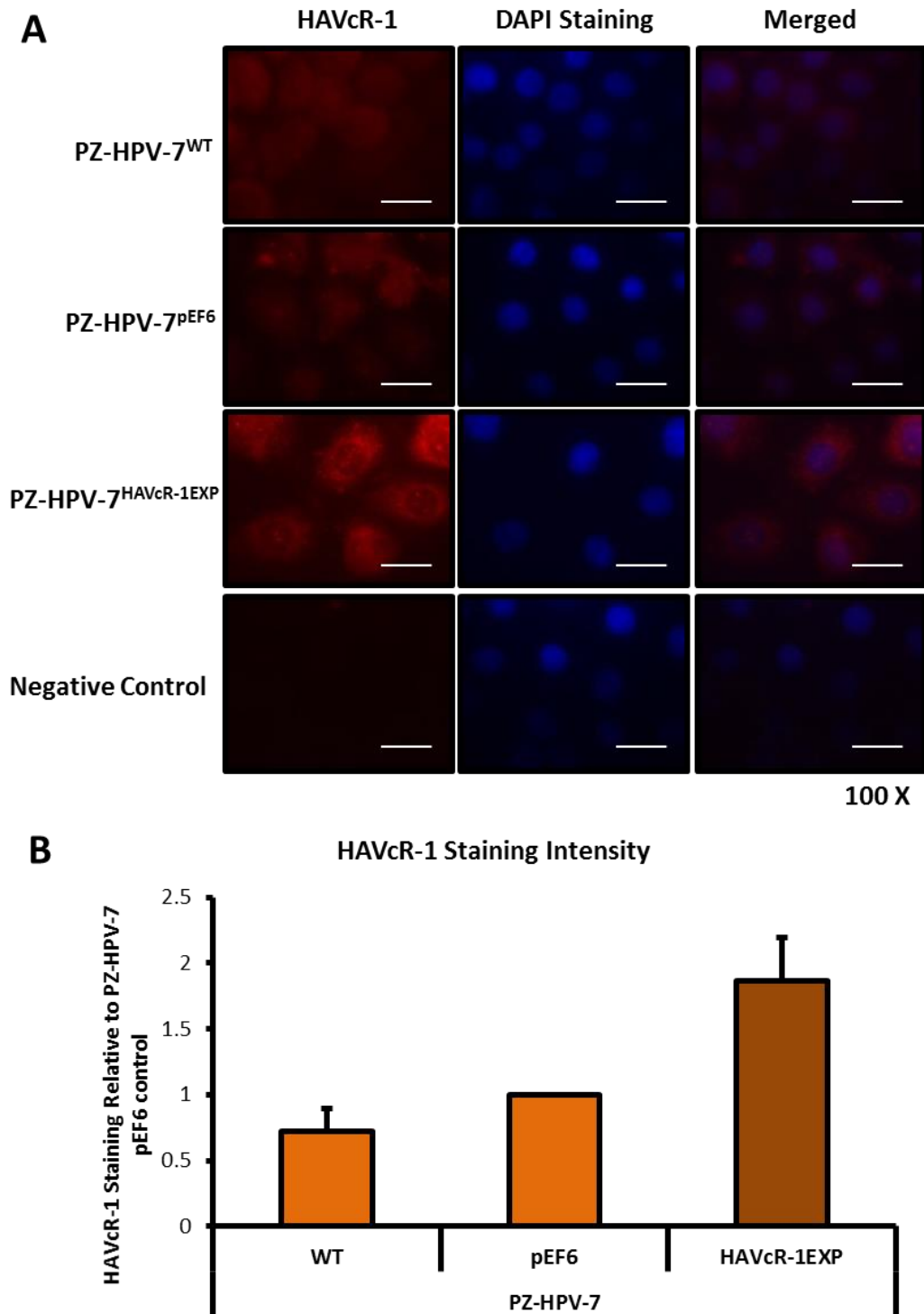
Figure 5.2 Protein Expression Validation of PZ-HPV-7^{pEF6} and PZ-HPV-7$^{HAVCR-1EXP}$
Cell were grown in 8 well chamber slides in supplemented media and subjected to immunofluorescence at 100 % confluence with HAVcR-1 and nuclear staining. **A** Images show fluorescence emission at 100 X magnification correlating to HAVcR-1 expression or nuclear staining and a merged image of both. Images are representative of three independent experiments. Scale bars represent 20 μm. **B** Graph shows quantitative analysis of immunofluorescent staining of HAVcR-1 (mean +SEM, n=3).

5.3.3 HAVcR-1 Overexpression Results in Significant Changes in Expression or Phosphorylation of Numerous Proteins

Protein lysates extracted from PZ-HPV-7^{pEF6} and PZ-HPV-7$^{HAVcR-1EXP}$ cell models were used to investigate changes in protein expression and phosphorylation levels using the Kinex™ KAM-880 Antibody microarray. The Kinex™ antibody microarray screens 877 antibodies, of which 518 were pan-specific and 359 were phosphosite-specific and thus was used to identify research leads. A data report was returned whereby every result that had a Z-ratio of ≤-1.65 or ≥1.65 was considered significant. This showed 20 significantly increased phosphorylation's at specific phosphosites in PZ-HPV-7$^{HAVcR-1EXP}$ in comparison to PZ-HPV-7^{pEF6} (See Figure 5.3A). It also showed the total expression of 12 proteins which were significantly increased (See Figure 5.3B). There were also 20 cases of decreased phosphorylation at specific phosphosites in PZ-HPV-7$^{HAVcR-1EXP}$ in comparison to PZ-HPV-7^{pEF6} (See Figure 5.4A). Furthermore, total protein expression was decreased in 12 cases (See Figure 5.4B).

A

B
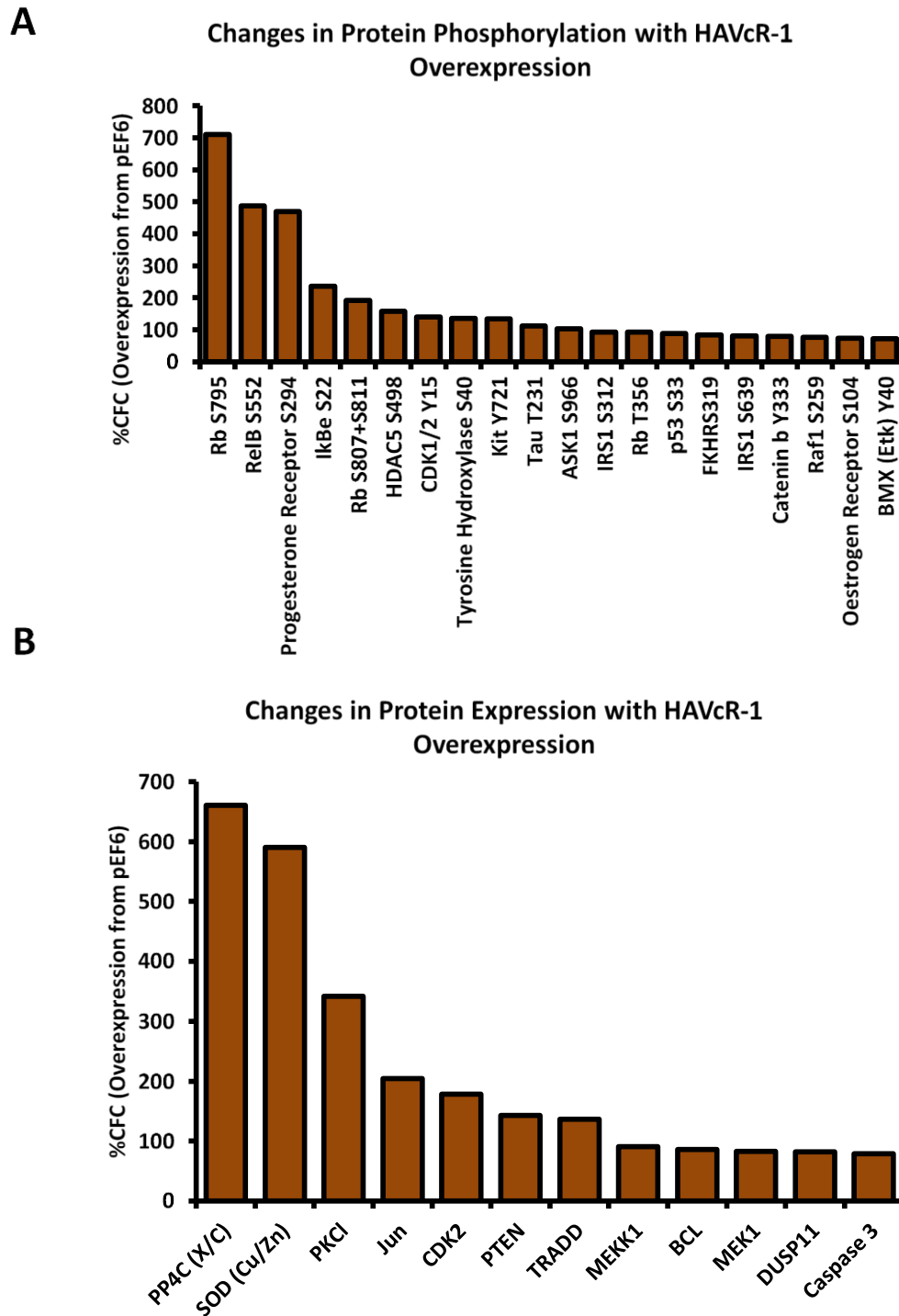
Figure 5.3 Protein Expression and Protein Phosphorylation That was Significantly Increased with HAVcR-1 Overexpression.
Protein was extracted from PZ-HPV-7^{pEF6} and PZ-HPV-7HAVcR-1^{EXP} and sent to Kinex Bioinformatics for a Kinex ™ antibody microarray. Graphs show the percentage change from control of **A** protein phosphorylation or **B** total protein expression for all significantly increased results (z value ≥1.65)

A

Changes in Protein Phosphorylation with HAVcR-1 Overexpression

B

Changes in Protein Expression with HAVcR-1 Overexpression
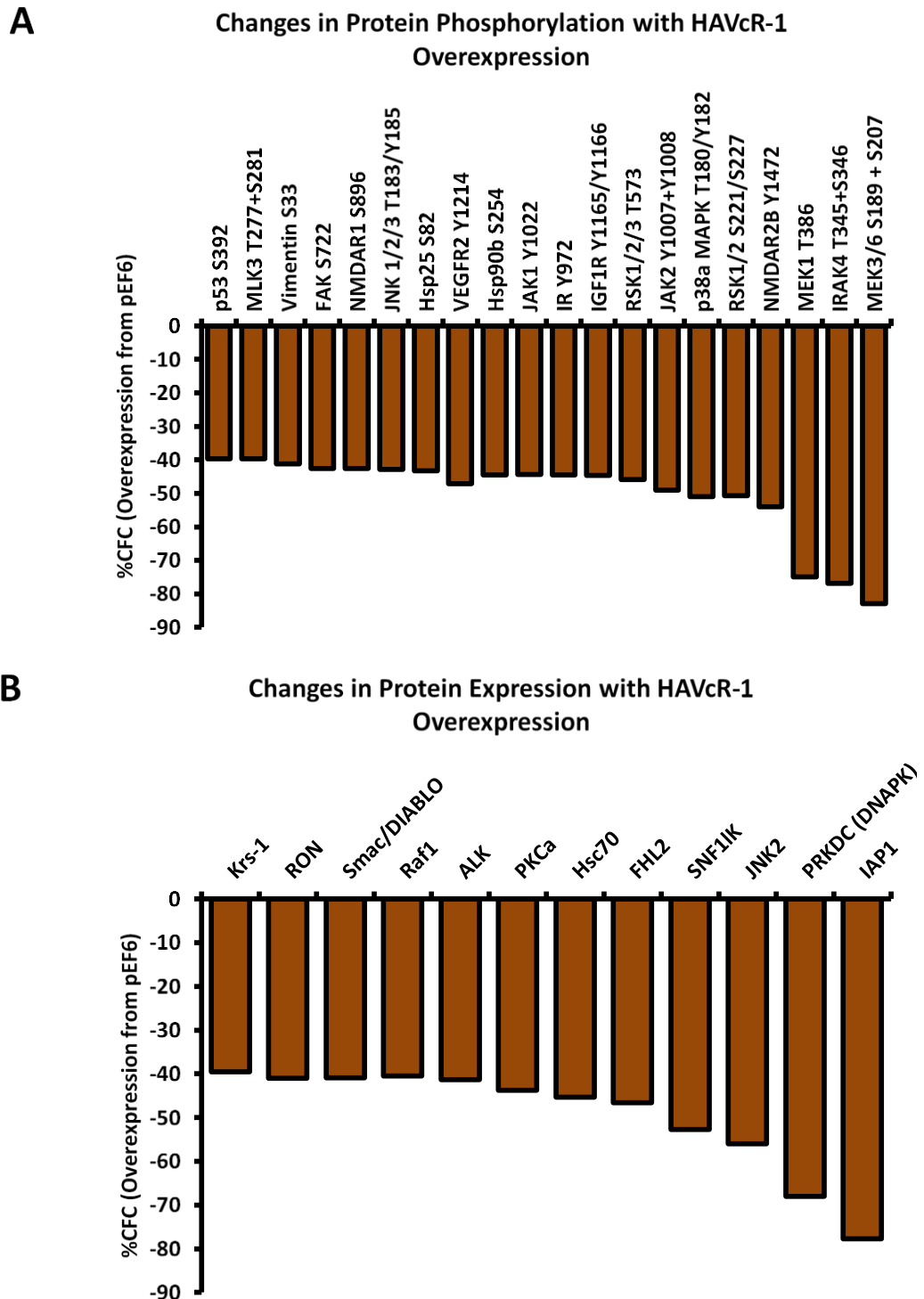
Figure 5.4 Protein Expression and Protein Phosphorylation That was Significantly Decreased with HAVcR-1 Overexpression.
Protein was extracted from PZ-HPV-7^{pEF6} and PZ-HPV-7$^{HAVcR-1EXP}$ and sent to Kinex Bioinformatics for a Kinex ™ antibody microarray. Graphs show the percentage change from control of **A** protein phosphorylation or **B** total protein expression for all significantly decreased results (z value ≤-1.65).

5.3.4 Significantly Increased β-CateninY333 in PZ-HPV-7^{HAVcR-1EXP} Cells

The changes to protein expression and phosphorylation that were seen from the Kinex™ antibody microarray as summarised in Figure 5.3 and Figure 5.4 were assessed for proteins of interest for immediate further study. β-catenin showed a 1.74 fold increase at the Y333 phosphorylation site in PZ-HPV-7[HAVcR-1EXP] when compared to levels in PZ-HPV-7[pEF6] (z value=1.77) and was chosen for further study. This interest was due to the involvement of β-catenin in AJs whereby β-catenin binds E-cadherin, which attaches to E-cadherins on adjacent cells, as well as binding to α-catenin which links the junction to the actin cytoskeleton, via EPLIN. Interestingly, phosphorylation of β-catenin at Y333 is WNT independent and is instead Src induced upon EGFR activation [354]. The phosphorylation of α-catenin is also induced via EGFR activation resulting in the activation of C2Kα via ERK. There was also a 1.63 fold increase in α-catenin S641 phosphorylation; however this was not significant with a z-value of 1.59. Phosphorylation of β-catenin at Y333 results in the dissociation of β-catenin from AJs and the translocation of β-catenin into the nucleus whilst phosphorylation of α-catenin at S641 also results in β-catenin dissociation and nuclear translocation. Within the nucleus β-catenin, in combination with other transcription factors such as PKM2 and the TCF/LEF family results in the transcription of certain genes including Cyclin D1 and c-Myc (See Figure 5.5B) [14, 354, 355].

Therefore, the data produced by the Kinex™ KAM-880 antibody microarray was subsequently assessed for proteins involved in the β-catenin Y333 signalling pathway. Along with α-catenin and β-catenin the microarray also screened Src, EGFR,

c-Myc and Cyclin D1. The fold change from PZ-HPV-7^{pEF6} are displayed from all on these proteins in Figure 5.5A however the only significant change was that of β-catenin Y333 phosphorylation.
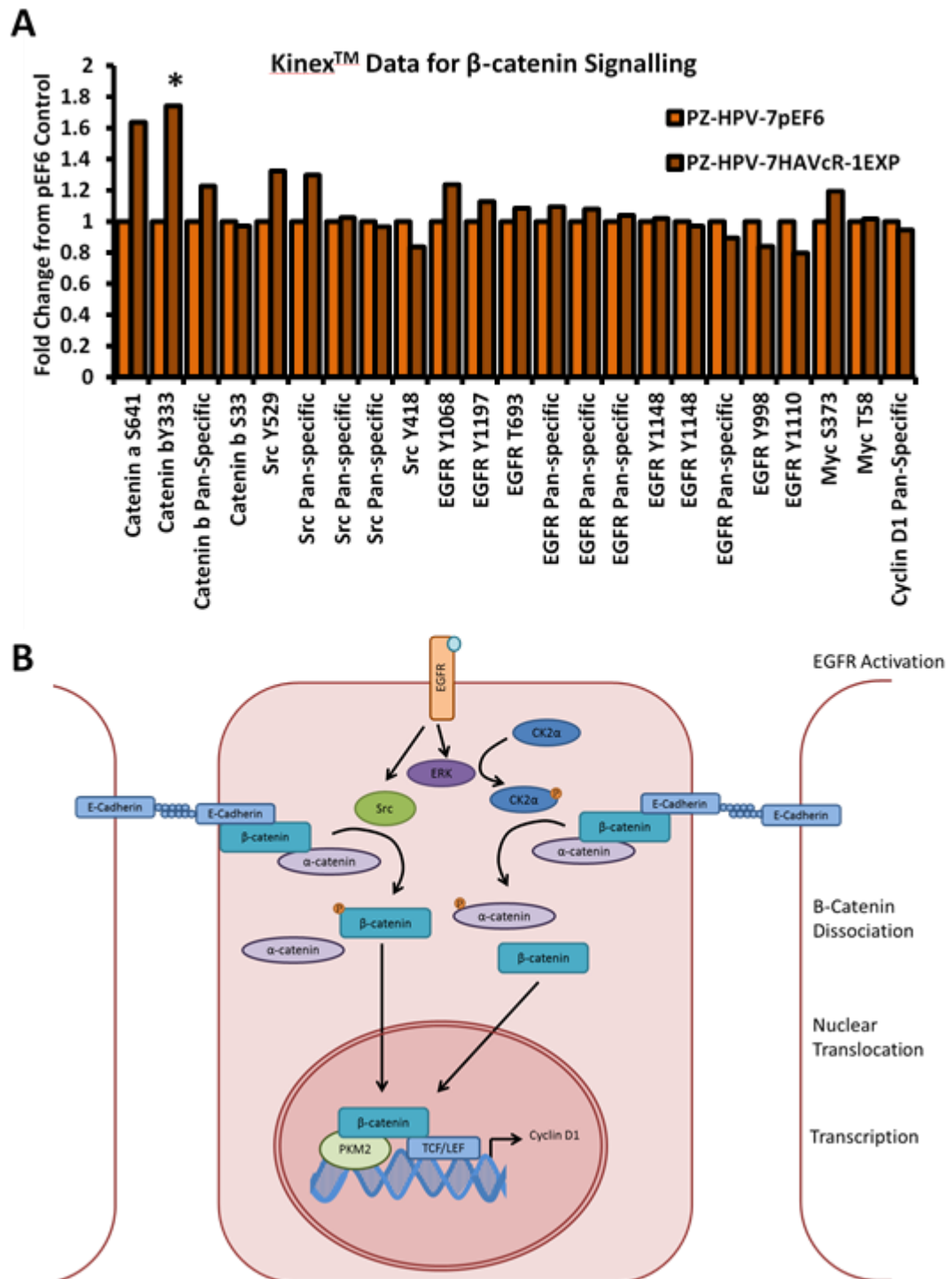
Figure 5.5 β-Catenin Y333 Signalling Changes with The Kinex™ Antibody Microarray A Graph shows fold change from PZ-HPV-7^{pEF6} control of all proteins and phosphosites involved with β-catenin signalling included within the Kinex™ antibody microarray. **B** Diagramatic representation of β-catenin Y333 and α-catenin S641 signalling (Amended from [354, 355]).

5.3.5 HAVcR-1 Overexpression Increases Cyclin D1 Expression

The Kinex™ KAM-880 Antibody microarray screens non-denatured proteins and therefore there is a possibility of false positives and negatives. Kinex states that in an internal study between 30-45 % of protein changes are reproducible by immunoblotting and 20-30 % could not be validated by immunoblotting due to the antibody microarray being 10-fold or more sensitive than standard western blotting. Therefore, it was imperative to verify Kinex™ KAM-880 Antibody microarray data. Furthermore, β-catenin signalling is complex and there was only a limited number of the potential proteins involved screened in the Kinex™ KAM-880 Antibody microarray, thus to further investigate the effect of HAVcR-1 on β-catenin signalling, gene and protein expression as well as localisation of proteins involved were screened using other *in vitro* techniques.

There was no significant change in the gene expression of *CTNNA1* (1.28±0.40;p=0.470), *CTNNB1* (0.78±0.15; p=0.177), *CCND1* (0.70±0.18; p=0.161), *EPLIN* (1.21±0.70; p=0.591) or *GSKβ* (1.30±0.51; p=0.541) between PZ-HPV-7$^{HAVcR-1EXP}$ and PZ-HPV-7^{pEF6} (See Figure 5.6).

There was no significant change in the protein expression of α-catenin (1.26±0.07; p=0.073), β-catenin (1.37±0.22; p=0.243), E-Cadherin (1.59±0.487; p=0.352), EPLIN-β (1.07±0.27; p=0.82), EPLIN-α (0.79±0.16; p=0.339) or PKM2 (2.00±0.53; p=0.199) between PZ-HPV-7$^{HAVcR-1EXP}$ and PZ-HPV-7^{pEF6}. However, there was a significant increase in Cyclin D1 protein expression by 1.74±0.13; p=0.030 in PZ-HPV-7$^{HAVcR-1EXP}$ in comparison to PZ-HPV-7^{pEF6} (See Figure 5.7)

The localisation of α- catenin, β-catenin and E-cadherin was also assessed via immunofluorescence. This showed a potential increased membrane localisation of α- catenin, although staining was discontinuous (See Figure 5.8.A), increased nuclear localisation of β-catenin (See Figure 5.8.B) and decreased membrane localisation of E-cadherin (See Figure 5.8.C)
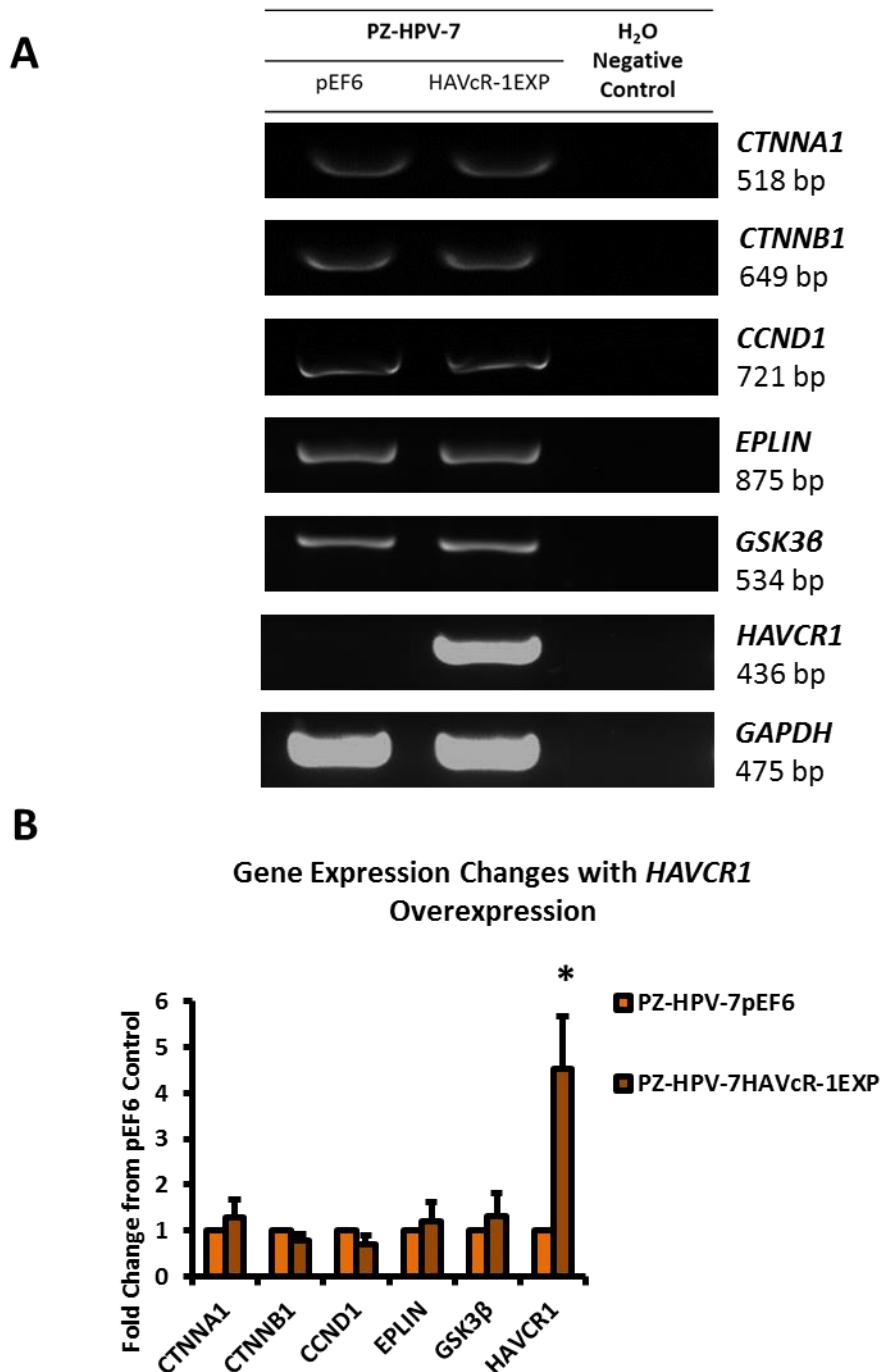
Figure 5.6 Changes to α- and β-Catenin Signalling Gene Expression

A to **C** Cell lines grown in 6 well plates and RNA extracted once confluent. *HAVCR1* mRNA expression was assessed using PCR. A. Figure is representative of three independent experiments. **B** Graph shows band intensity as quantified by ImageJ software. Data shown are the means of three independent experiments with gene expression shown as normalised to *GAPDH* and relative to PZ-HPV-7[pEF6] and error bars show SEM. Student's T tests were performed using Microsoft Excel and $p<0.05$ was significant and shown by *.
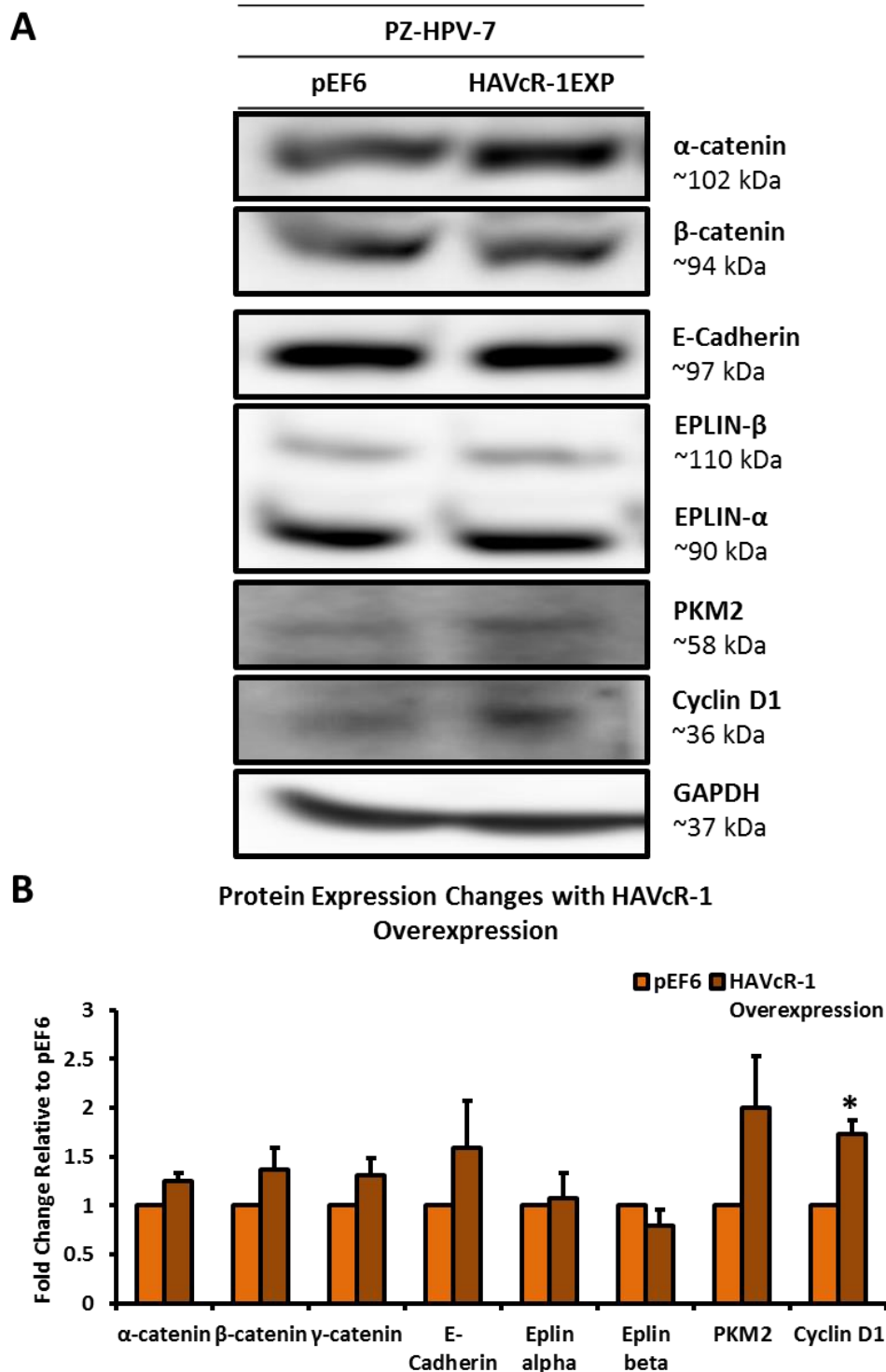
Figure 5.7 HAVcR-1 Induced Changes to β-Catenin Signalling Protein Expression
Cell lines grown in 6 well plates and harvested at 100 % confluency. Data shown are the means of three independent experiments and error bars show SEM. Protein expression was assessed using SDS PAGE and western blot analysis where **A** blots are representative images **B** Graph shows band intensity as quantified by ImageJ software and normalised to GAPDH and is shown as fold change relative to PZ-HPV-7^{pEF6}. Student's T tests were performed and significance of p<0.05 is represented by *.

A α-catenin   HAVcR-1   DAPI   Merged

PZ-HPV-7^{pEF6}

PZ-HPV-7^{HAVcR-1EXP}

100 X

B β-catenin   HAVcR-1   DAPI   Merged

PZ-HPV-7^{pEF6}

PZ-HPV-7^{HAVcR-1EXP}

100 X

C E-Cadherin   HAVcR-1   DAPI   Merged

PZ-HPV-7^{pEF6}

PZ-HPV-7^{HAVcR-1EXP}
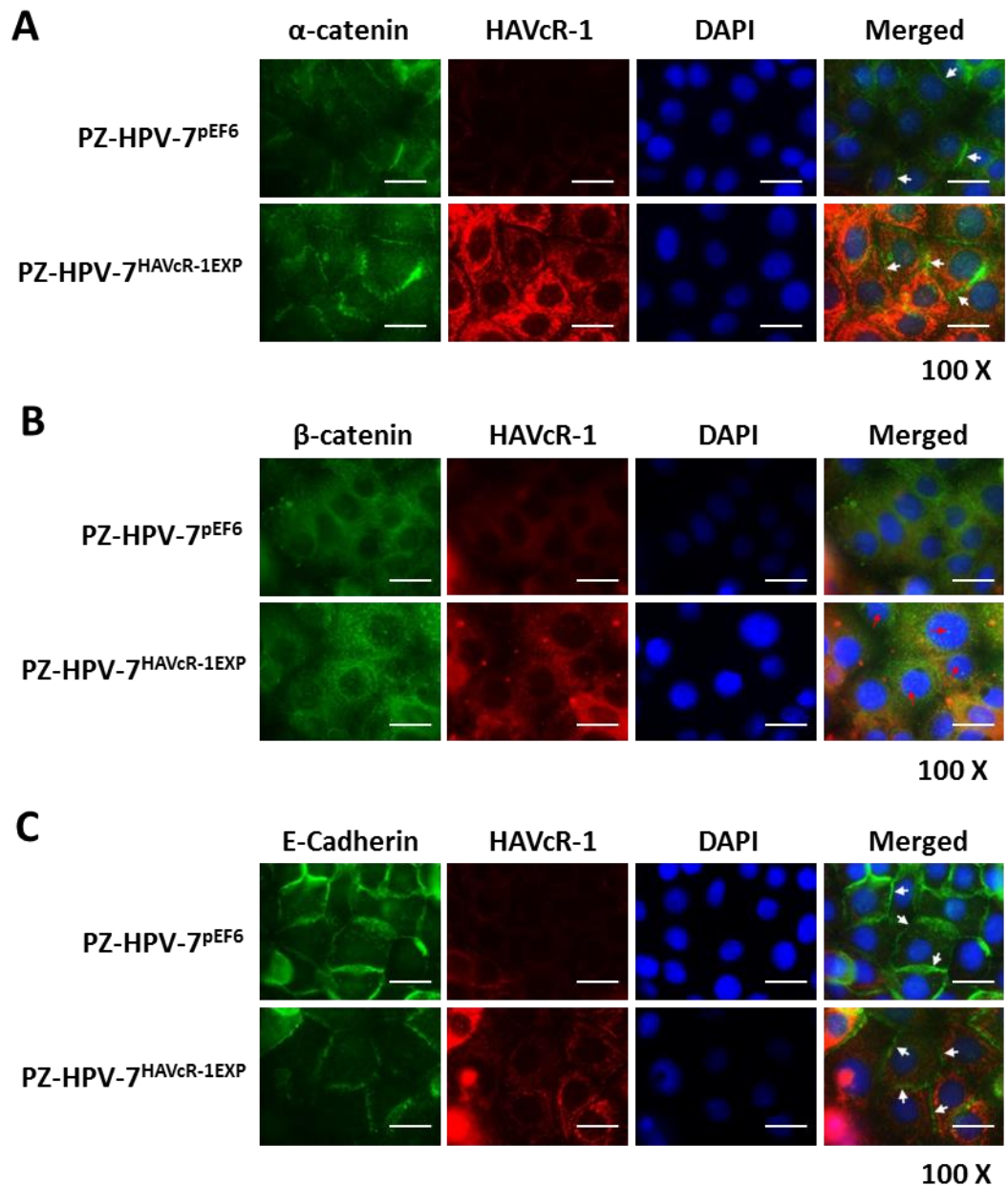
100 X

Figure 5.8 HAVcR-1 Induced Changes to α-Catenin, β-Catenin and E-Cadherin Protein Localisation
Cell were grown in 8 well chamber slides in supplemented media and subjected to immunofluorescence at 100 % confluence at 100 X magnification with **A** α-catenin, **B** β- catenin, or **C** E-cadherin alongside HAVcR-1 expression, nuclear staining and a merged image of both. Scale bars represent 20 μm and membranous staining and nuclear staining is highlighted by white and red arrows respectively

5.3.6 PZ-HPV-7 Cell Growth is Independent of HAVcR-1

Due to the link between β-catenin signalling and cell growth as well as increased cell growth being a phenotype of cancer, PZ-HPV-7$^{HAVcR-1EXP}$ and PZ-HPV-7^{pEF6} were used to assess the effect HAVcR-1 expression has on cell proliferation. An *in vitro* growth assay was performed whereby cells were seeded at the same time and cell count analysed after 3 or 5 days of growth relative to day 1 day of growth as a seeding control.

This showed no significant difference in cell growth with PZ-HPV-7$^{HAVcR-1EXP}$ in comparison to PZ-HPV-7^{pEF6} at Day 3 (2.47± 0.45 vs 3.10±0.36; p=0.34) or at Day 5 (7.00±0.8 vs 10.8±1.82; p=0.16) (See Figure 5.9).

A

B
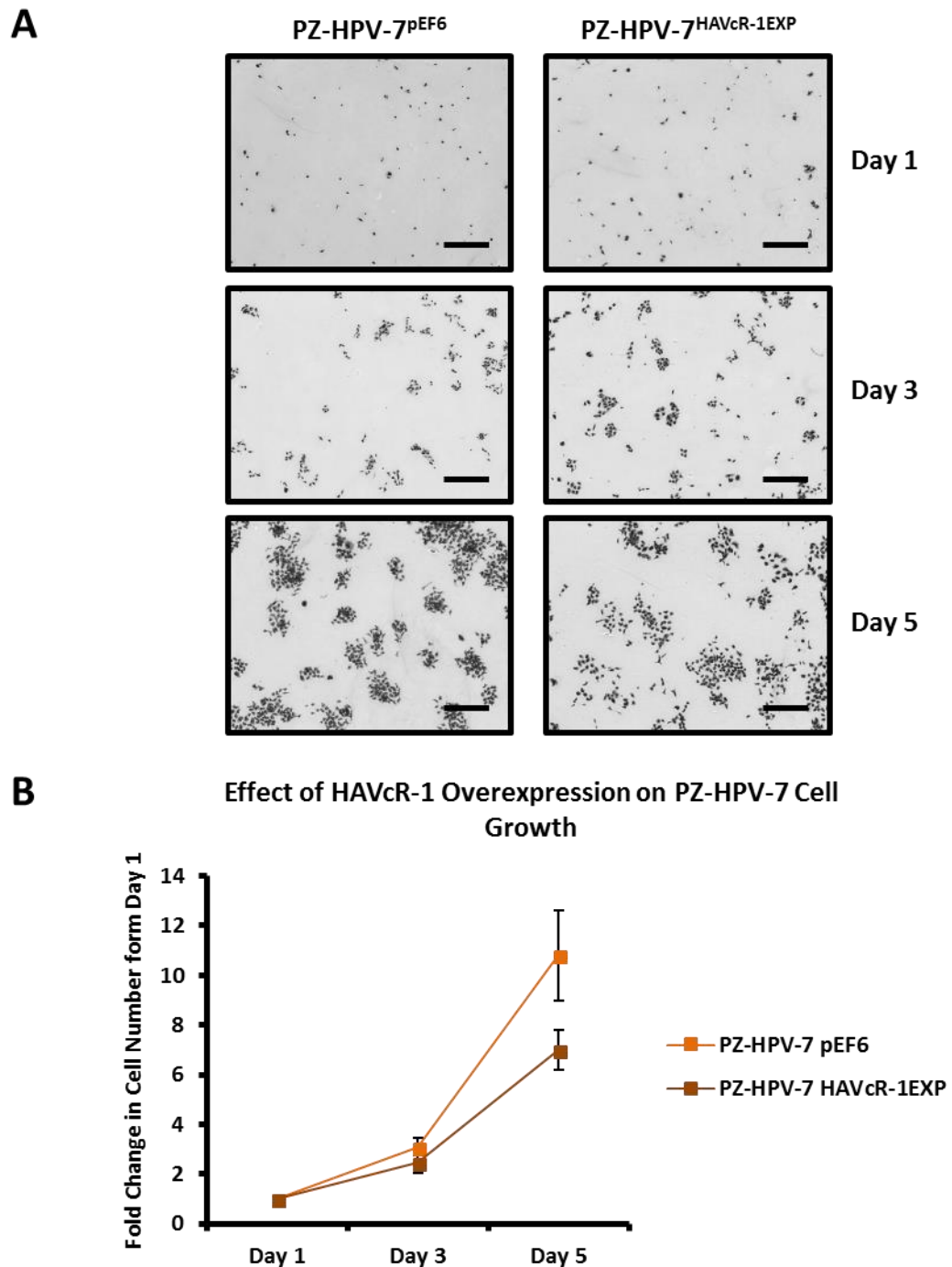
Figure 5.9 The Effect of HAVcR-1 Overexpression on PZ-HPV-7 Cell Growth.
Cells were seeded into 24 well plates at 1 X10^4 cells per well in triplicate and incubated for 1, 3 or 5 days. Post incubation cells were fixed, stained with crystal violet and images were taken at 5 X magnification. **A** Images are representative of three independent experiments. Scale bars represent 2 mm **B** Cells were counted and graph shows the means of three independent experiments as fold change relative to the cell count at day 1 with error bars showing SEM. Statistical analysis was performed at each time point via the Student's t-test using Microsoft Excel and significance of $p < 0.05$ was not reached.

5.3.7 HAVcR-1 Overexpression Increases PZ-HPV-7 Cell Invasion

An *in vitro* Matrigel™ transwell invasion assay was performed with PZ-HPV-7^{pEF6} and PZ-HPV-7^{HAVcR-1EXP} cell models to assess the effect of HAVcR-1 on PZ-HPV-7 cell invasion. This revealed an increase in cell invasion with PZ-HPV-7^{HAVcR-1EXP} in comparison to PZ-HPV-7^{pEF6} with a 1.95±0.07 fold increase in invaded cells. This difference was significant with p=0.006 (See Figure 5.10).

A PZ-HPV-7^pEF6   PZ-HPV-7^HAVcR-1EXP

B Effect of HAVcR-1 on PZ-HPV-7 Cell Invasion
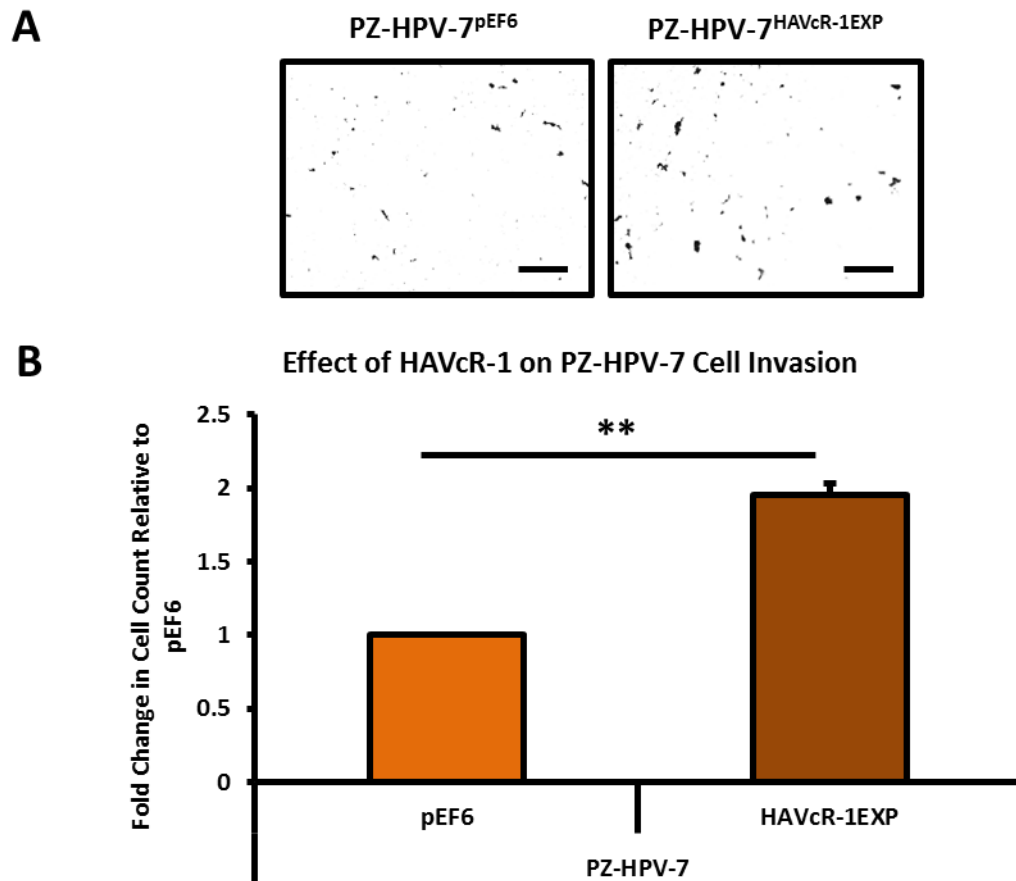
Figure 5.10 The Effect of HAVcR-1 Overexpression on PZ-HPV-7 Cell Invasion
Cells seeded in triplicate at 3×10^4 cells per 8 μm pore ThinCerts™ 24 well plate insert coated with 500 μg/mL Matrigel™ and incubated for 3 days. Post incubation cells were fixed, stained with crystal violet and images were taken at 5 X magnification. **A** Images are representative of three independent experiments. Scale bars are representative of 2 mm **B** Cells were counted and graph shows the means of three independent experiments as fold change relative to the cell count of PZ-HPV-7^pEF6 with error bars showing SEM. Statistical analysis was performed via the Student's t-test using Microsoft Excel and significance of $p < 0.05$ was reached. ** represents $p < 0.01$.

5.3.8 HAVcR-1 Overexpression Increases PZ-HPV-7 Cell Adhesion

PZ-HPV-7^{pEF6} and PZ-HPV-7$^{HAVcR-1EXP}$ cell models were used to assess the importance of HAVcR-1 on cell adhesion via an *in vitro* Matrigel™ adhesion assay. There was a significant 1.73±0.04 fold increase in adhered cells with PZ-HPV-7$^{HAVcR-1EXP}$ in comparison to PZ-HPV-7^{pEF6} with p=0.002 (See Figure 5.11).

A
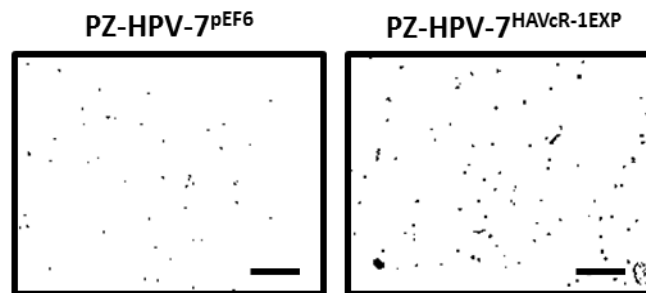
B

Effects of HAVCR-1 on PZ-HPV-7 Cell Adhesion
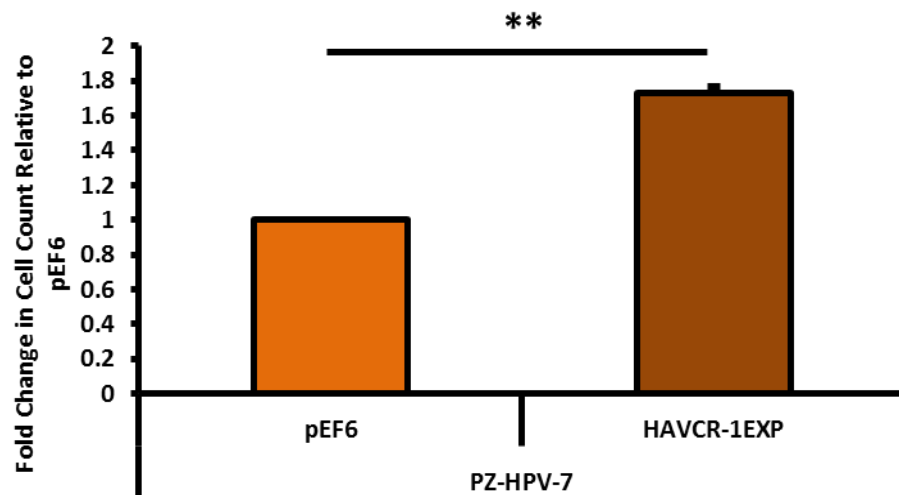
Figure 5.11 The Effect of HAVcR-1 Overexpression on PZ-HPV-7 Cell Adhesion
Cells seeded into 96 well plates coated in 200 μl of 50 μg/mL Matrigel™ at 5 X10^3 cells per well in triplicate and incubated for 30 min. Post incubation cells were fixed, stained with crystal violet and images were taken at 5 X magnification. **A** Images are representative of three independent experiments. Scale bars represent 2mm. **B** Cells were counted and graph shows the means of three independent experiments as fold change relative to the cell count of the PZ-HPV-7^{pEF6} control with error bars showing SEM. Statistical analysis was performed via the Student's t-test using Microsoft Excel and significance of p<0.05 was reached. ** represents p<0.01.

5.3.9 PZ-HPV-7 Initial Attachment and Spreading is Independent of HAVcR-1

ECIS was utilised to investigate the effect of HAVcR-1 on PZ-HPV-7 initial attachment and spreading. Capacitance at 64 kHz was assessed as at this frequency current is flowing through the cell thus capacitance at this frequency shows cell coverage of the electrode. HAVcR-1 had no impact on PZ-HPV-7 capacitance during initial attachment and spreading ($F_{(22, 88)}=0.488$, $p=0.971$) (See Figure 5.12A).

The resistance at 1 kHz was assessed due to current mainly flowing around the cell and it therefore indicative of junctional complexes. HAVcR-1 also had no impact on PZ-HPV-7 resistance during initial attachment and spreading ($F_{(22, 88)}=0.146$, $p=0.731$) (See Figure 5.12B).

The ECIS mathematical model was applied to this data to provide R_b (barrier function resistance) and alpha (constraint on current flow beneath cells). This model was unable to calculate R_b. However alpha was calculated and this showed that HAVcR-1 had no impact on PZ-HPV-7 alpha ($F_{(22, 88)}=0.615$, $p=0.903$) (See Figure 5.13).
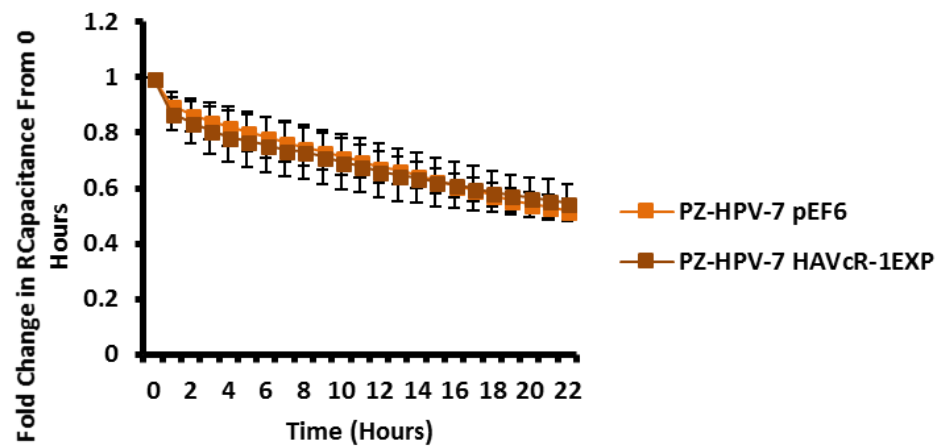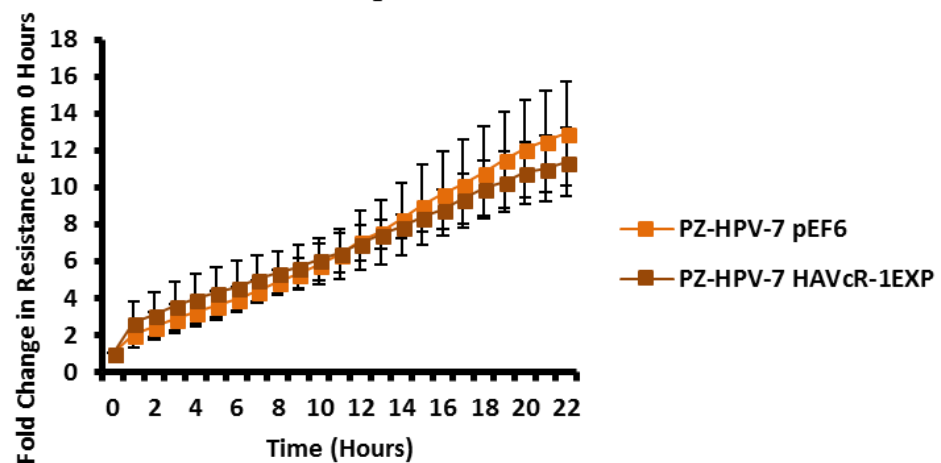
Figure 5.12 Effect of HAVcR-1 Overexpression on PZ-HPV-7 Initial Attachment and Spreading.
Cells seeded in octuplicate into 96W1E+ plates at 5 $\times 10^4$ cells per well and resistance, capacitance and impedance were monitored for 22 hours post seeding at varying frequencies ranging from 1-64 kHz. Graphs shows the means of three independent experiments as fold change relative to 0 hours with error bars showing SEM for **A** capacitance at 64 kHz and **B** resistance at 1 kHz. Statistical analysis was performed via IBM® SPSS Statistics 24 Mixed ANOVA and $p < 0.05$ were considered significant; significance was not reached.
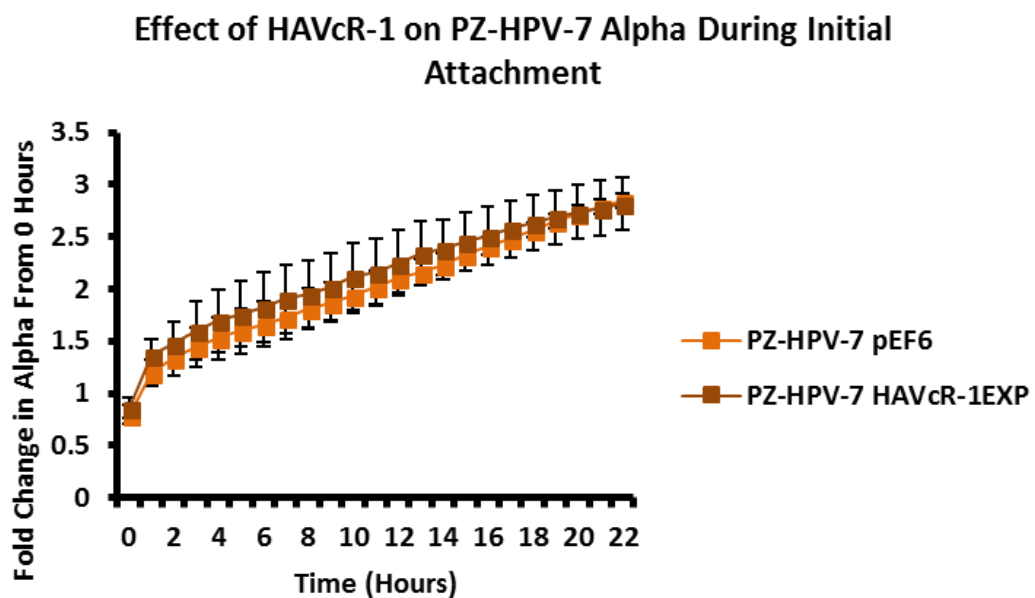
Figure 5.13 The Effect of HAVcR-1 Overexpression on the Constraint on Current Flow Beneath PZ-HPV-7 Cells During Initial Attachment and Spreading.
The ECIS™ Model was applied to initial attachment data using the ECIS software to give alpha (constraint on current flow beneath the cells) values. Graph shows the means of three independent experiments with error bars showing SEM for alpha shown as fold change relative to 0 hour. Statistical analysis was performed using IBM® SPSS Statistics 24 Mixed ANOVA and $p < 0.05$ was considered significant; significance was not reached.

5.3.10   PZ-HPV-7 Cell Migration is Independent of HAVcR-1

PZ-HPV-7^{pEF6} and PZ-HPV-7$^{HAVcR-1EXP}$ cell models were utilised to assess the importance of HAVcR-1 on cell migration. An *in vitro* scratch assay was performed and area of the wound was analysed every hour (up to 10 hours) in respect to the initial area. This showed that HAVcR-1 had no impact on PZ-HPV-7 cell migration ($F_{(10, 40)}=1.786$, $p=0.950$) (See Figure 5.14). There was also no significant difference in healing rate with PZ-HPV-7$^{HAVcR-1EXP}$ closing 3.53 ±0.42 %/hr in comparison to PZ-HPV-7^{pEF6} closing 4.64±0.70 %/hr ($p=0.262$).

A

B
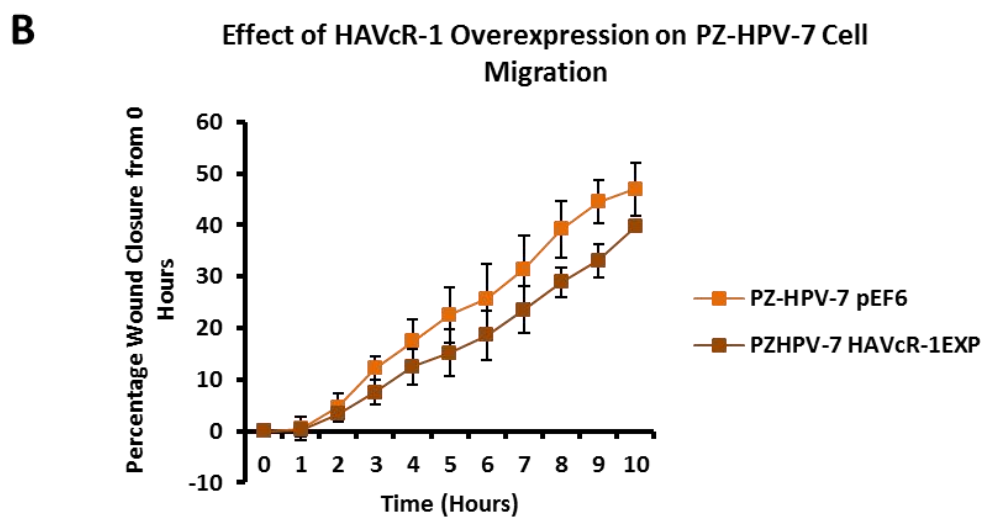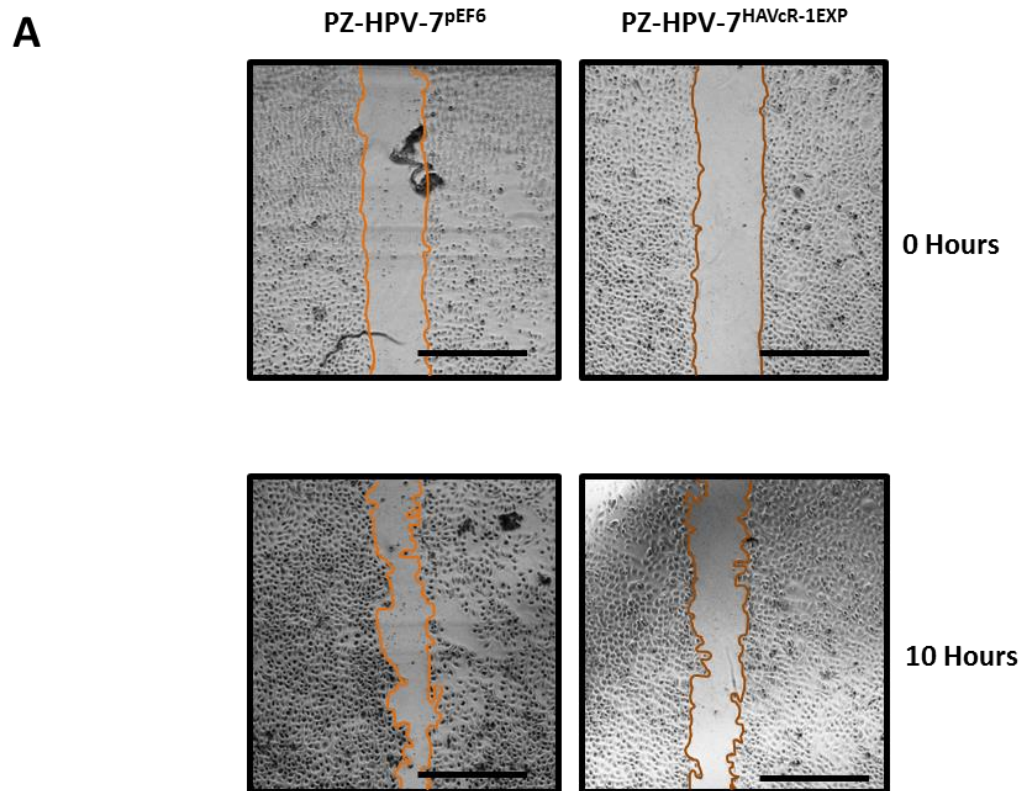
Figure 5.14 The Effect of HAVcR-1 Overexpression on PZ-HPV-7 Cell Migration
Cells seeded into 24 well plates in quadruplicate and scratched once confluent layer formed. Imaged were taken at 5 X magnification immediately afterward and every hour thereafter. **A** Images shown are representative of three independent experiments. Scale bars represent 2 mm **B** Wound area was measured using ImageJ software and percentage wound closure was calculated as relative to 0 hour time point. Data shown are the means of three independent experiments and error bars represent SEM. Statistical analysis was performed using IBM® SPSS Statistics 24 utilising the Mixed ANOVA significance of $p < 0.05$ was not reached.

5.3.11   PZ-HPV-7 Electrical Wound Healing is Independent of HAVcR-1

Post initial attachment and spreading of PZ-HPV-7 cells an electrical wound was applied and data was collected for 17 hours. Cell coverage of the electrode was assessed by assessing capacitance at 64 kHz and there was no difference in capacitance between PZ-HPV-7$^{HAVcR-1EXP}$ and PZ-HPV-7^{pEF6} ($F_{(17, 64)}=0.258$, p=0.998) (See Figure 5.15A). To give an insight into junctional complexes resistance at 1 kHz was assessed and there was no difference in resistance between PZ-HPV-7$^{HAVcR-1EXP}$ and PZ-HPV-7^{pEF6} ($F_{(17, 68)}=0.550$, p=0.916) (See Figure 5.15B).

The ECIS mathematical model was applied to gain further insight into cellular interactions via calculating alpha to assess cell-plate interactions and R_b to assess cell to cell interactions. HAVcR-1 had no impact on PZ-HPV-7 alpha during electrical wound healing ($F_{(17, 69)}=1.214$, P=0.278) (Figure 5.16A). HAVcR-1 also had no impact of PZ-HPV-7 R_b during electrical wound healing ($F_{(17, 68)}=0.798$, p=0.690) (Figure 5.16B).
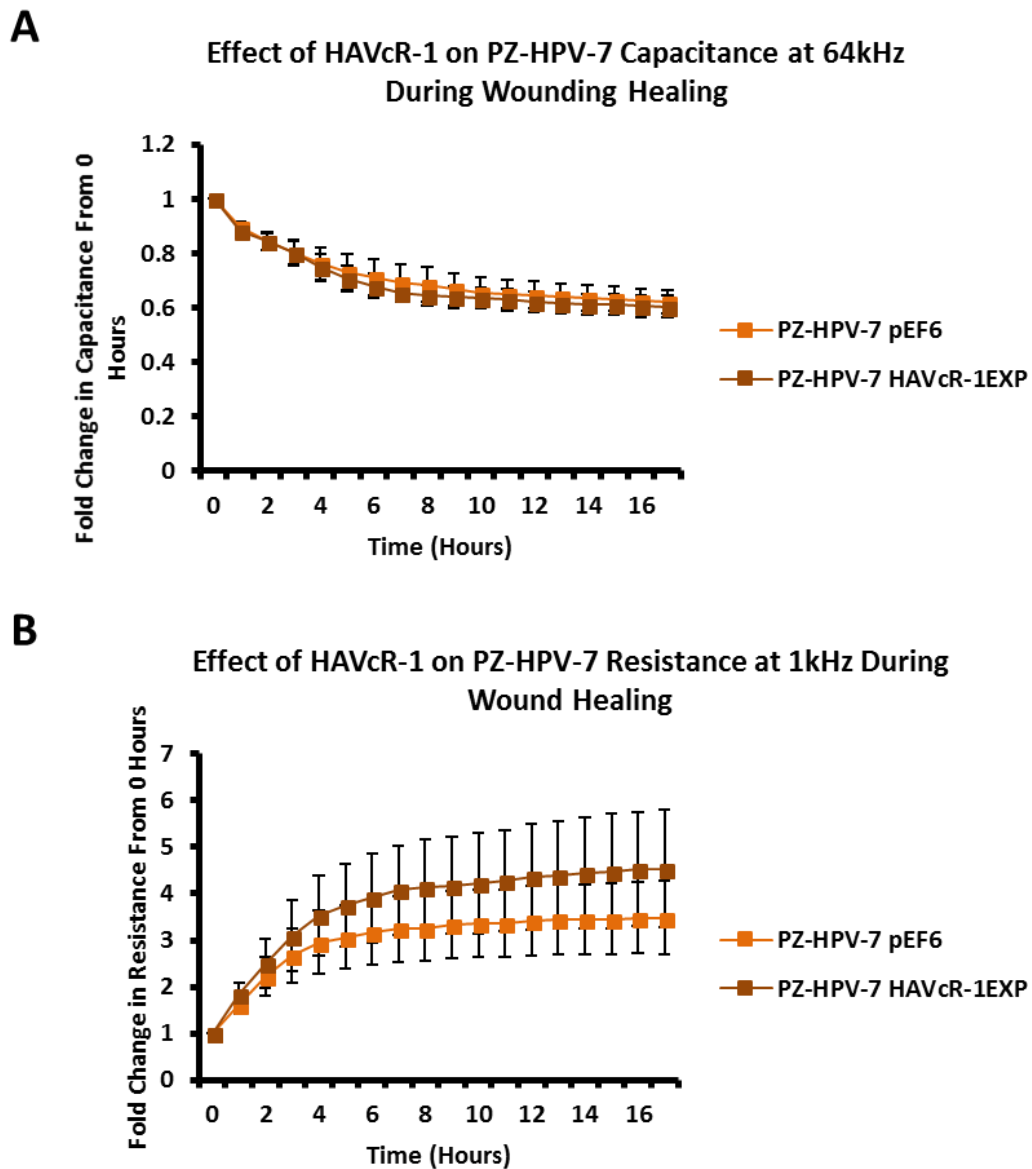
Figure 5.15 The Effect of HAVcR-1 Overexpression on PZ-HPV-7 Electrical Wound Healing
Post initial attachment and spreading cells were electrically wounded at 6000 Hz and 3000 µA for 30 seconds. Resistance, capacitance and impedance were then monitored at varying frequencies (1-64 kHz) for 17 hours. Graphs show the means of three independent experiments as fold change relative to 0 hours with error bars showing SEM for **A** resistance at 1 kHz and **B** capacitance at 64 kHz. Statistical analysis was performed at each hour time point via the IBM® SPSS Statistics 24 Mixed ANOVA and p values of <0.05 were considered significant; significance was not reached.
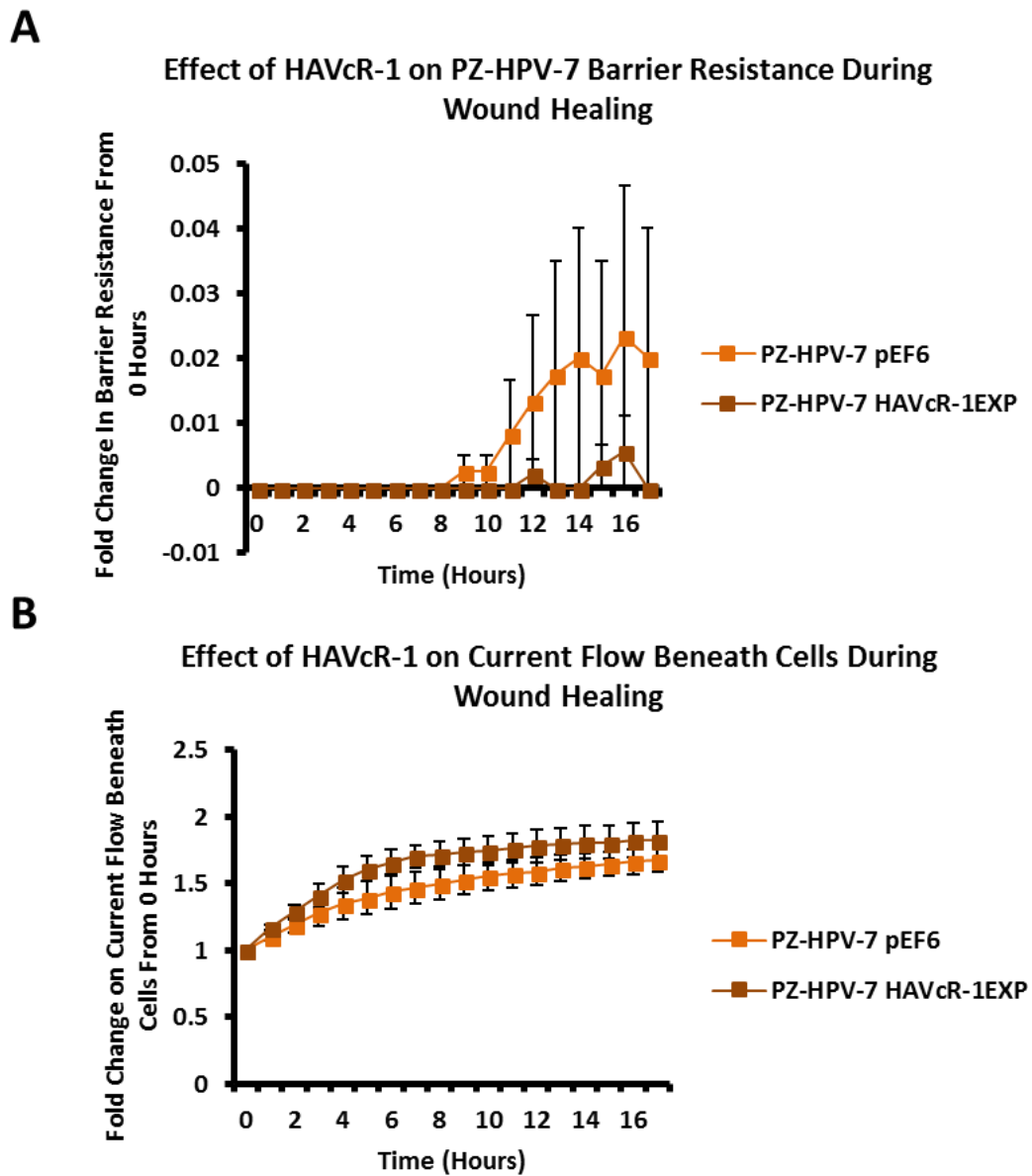
Figure 5.16 The Effect of HAVcR-1 Overexpression on the Constraint on Current Flow Beneath PZ-HPV-7 Cells and PZ-HPV-7 Barrier Resistance During Electrical Wound Healing.
The ECIS™ Model was applied to wound healing data using the ECIS software to give **A** R_b (Barrier Resistance) and **B** alpha (constraint on current flow beneath the cells) values. Graphs show the means of three independent experiments with error bars showing SEM shown as fold change relative to 0 hour. Statistical analysis was performed using IBM® SPSS Statistics 24 Mixed ANOVA and $p < 0.05$ was considered significant; significance was not reached.

PZ-HPV-7 Transepithelial Resistance is Independent of HAVcR-1

To assess whether HAVcR-1 influenced PZ-HPV-7 TER an *in vitro* TER assay was performed on transfected PZHPV-7 cells. Resistance across a confluent monolayer grown on a transwell insert was measured. Data was analysed as fold change from the PZ-HPV-7^{pEF6}.

There was no significant change in TER of PZ-HPV-7$^{HAVcR-1EXP}$, with a 0.81 ± 0.12 fold change in comparison to PZ-HPV-7^{pEF6} control (p=0.248) (See Figure 5.17).
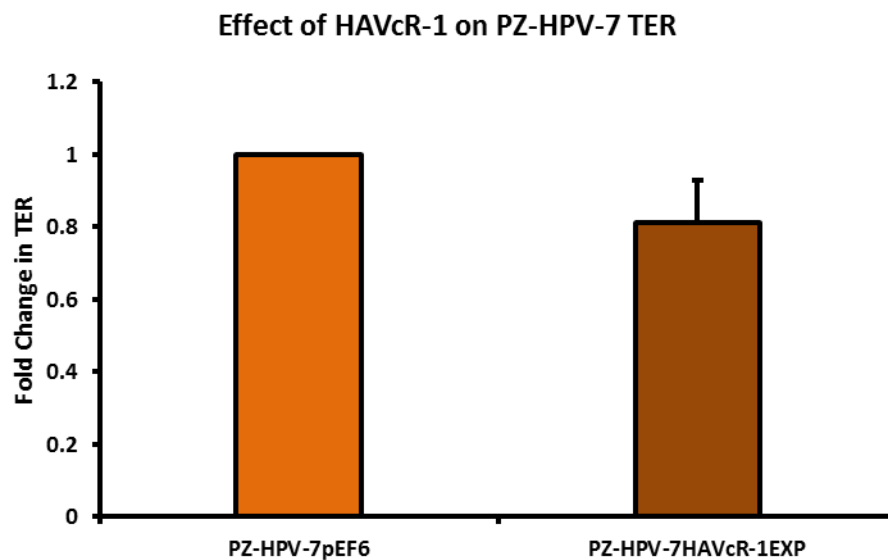
Figure 5.17 The Effect of HAVcR-1 Overexpression on PZ-HPV-7 Transepithelial Resistance
Cells seeded in triplicate into 0.4 μm size pore inserts 5 X10^4 cells per insert and incubated until confluent. Post incubation resistance across the membrane was measured immediately after media change. Graph shows the means of three independent experiments as fold change relative to PZ-HPV-7^{pEF6}. Error bars show SEM. Statistical analysis was performed via the Student's t-test using Microsoft Excel and p<0.05 was considered significant.

5.3.13   PZ-HPV-7 Paracellular Permeability is Independent of HAVcR-1

Junctional integrity is impetrative in the maintenance of paracellular permeability. Loss of junctional complexes between cancer cells is required for metastasis to occur thus an *in vitro* paracellular permeability assay was performed using the PZ-HPV-7^{pEF6} and PZ-HPV-7$^{HAVcR-1EXP}$ cell models to provide insight into the importance of HAVcR-1 in junctional integrity.

There was no significant difference between the paracellular permeability of PZ-HPV-7$^{HAVcR-1EXP}$ in comparison to PZ-HPV-7^{pEF6} of 40 kDa TRITC-dextran conjugate ($F_{(10, 40)}=0.960$, $p=0.492$) (See Figure 5.18A). There was also no significant difference in the paracellular permeability of 10 kDa FITC-dextran conjugate between PZ-HPV-7$^{HAVcR-1EXP}$ and PZ-HPV-7^{pEF6} ($F_{(10, 40)}=1.528$, $p=0.165$) (See Figure 5.18B).

A
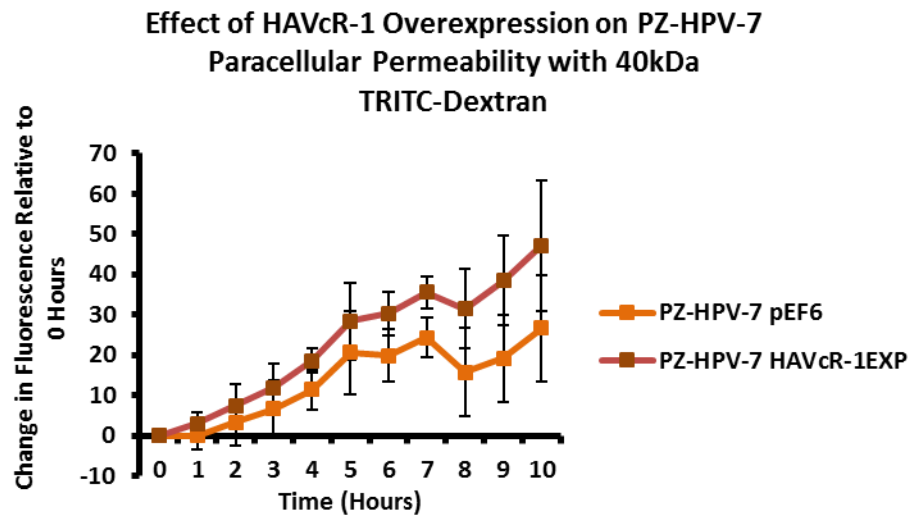
B
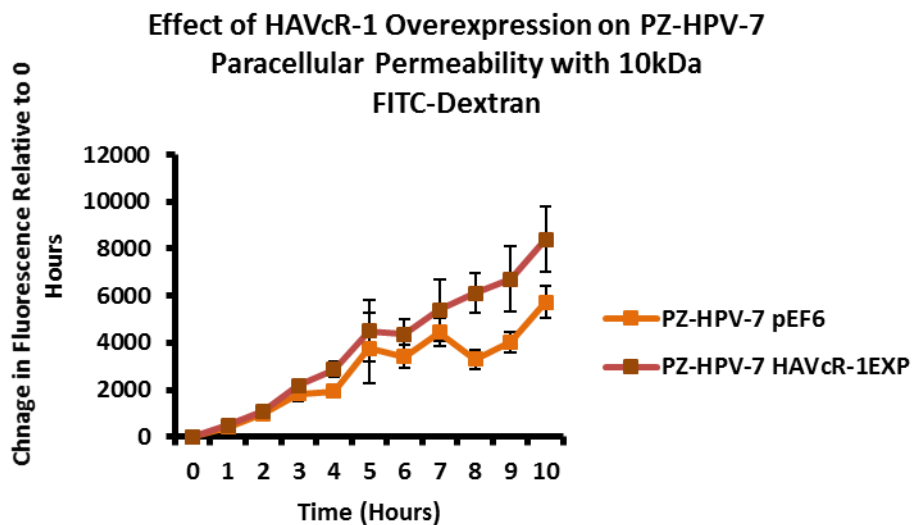
Figure 5.18 The Effect of HAVcR-1 Overexpression on PZ-HPV-7 Paracellular Permeability

Cells seeded in triplicate at 5×10^3 cells per 0.4 µm pore ThinCerts™ 24 well plate insert and incubated until confluent. Once confluent, 0.2mg/mL of both TRITC-dextran (40 kDa) and FITC-dextran (10 kDa) was added to each insert and samples were taken from outside of the insert to measure fluorescence immediately after and every hour thereafter for 10 hours. Graphs show the means of three independent experiments as change in fluorescence from 0 hours of **A** the 40 kDa TRITC-dextan conjugate and **B** the 10 kDa FITC-dextan conjugate. Error bars show SEM. Statistical analysis was performed via the IBM SPSS Startistics 24 Mixed ANOVA and significance of $p < 0.05$ was not reached.

5.4 Discussion

The chapter set out to identify potentially important signalling pathways responsible for the development and progression of prostate cancer that involve HAVcR-1. This was achieved by a commercially available Kinex™ KAM880 Protein array. After analysis 64 proteins were identified as being statistically altered either in expression or phosphorylation. Although there were numerous proteins that would be of interest for further study, β-catenin was chosen. β-catenin Y333 showed a significantly increased phosphorylation with HAVcR-1 overexpression. As well as β-catenin being an important structure component of AJs it also has a role in the de-differentiation process [19]. β-catenin has been shown to play a role in the tumorigenesis of numerous cancers with dysregulation being associated with prostate cancer progression however studies have generally focused on the Wnt/wingless cascade and activation mutations [7]. However, phosphorylation of β-catenin at residue Y333 has been shown to be due to EGFR signalling, thus identifying a novel area of interest in the study of prostate cancer research [354].

HAVcR-1 has no direct effect on total gene or protein expression of β-catenin in PZ-HPV-7 cells. However, HAVcR-1 overexpression alters the subcellular localisation of β-catenin which is an important indicator of signalling [7]. This chapter showed an increase in β-catenin nuclear staining and since nuclear staining is indicative of β-catenin activation, this therefore supports the Kinex™ KAM880 Protein array data and the theory that HAVcR-1 is involved in β-catenin signalling [14]. Interestingly nuclear accumulation of β-catenin has been associated with poorly differentiated and highly proliferative tumours with increased vascular invasion [6, 7]. As invasion

is a hallmark of malignancy and a prerequisite for cancer metastasis this proposes HAVcR-1 as a potential anti-metastatic target [356].

The Kinex™ KAM880 Protein array also revealed an increase in α-catenin S641 phosphorylation. Interestingly phosphorylation at this residue is also a result of EGFR activation and subsequently results in the dissociation of β-catenin from the membrane and its nuclear translocation [355]. Gene and protein analysis of α-catenin expression showed that HAVcR-1 had no effect on total expression levels. However, immunofluorescence showed a discontinuous staining of α-catenin at the cell membrane thus suggesting a breakdown of AJs, which was further shown by discontinuous membrane staining of E-cadherin with HAVcR-1 overexpression. These results therefore support the Kinex™ KAM880 Protein array and the theory that HAVcR-1 leads to the phosphorylation of α-catenin, which subsequently results in the disassociation of β-catenin from AJs and nuclear accumulation. However, further verification of this is necessary with co-immunofluorescence with β-catenin to assess disassociation of the two proteins as well as verifying the phosphorylation status of α-catenin at S641 and β-catenin at Y333. Junctional integrity was further investigated however no changes to paracellular permeability or transepithelial resistance were observed and therefore, conflict with the theory that HAVcR-1 affects junctional stability via β-catenin signalling. However, these assays primarily assess changes to TJs and although AJs have been shown to be important for the initialisation of TJs, once formed TJ stabilisation is independent of AJs. Therefore, further assays investigating junctional formation during initial attachment and spreading were carried out however no changes in resistance were observed. It may also be of

benefit to deplete and reintroduce calcium whilst performing a TER to gain further insight on the effect of HAVcR-1 on PZ-HPV-7 AJ stability.

Once accumulated in the nucleus, β-catenin binds PKM2 and this complex can be recruited to the CCND1 promoter leading to targeted gene transcription: including cyclin D1 [354, 357]. HAVcR-1 has no direct effect of PKM2 gene expression however this is unsurprising due to the localisation of PKM2 being important in β-catenin signalling. Thus, it would be of more interest to perform an immunoprecipitation to investigate whether HAVcR-1 influences the association of PKM2 and β-catenin and a co-immunofluorescence of PKM2 and β-catenin to investigate nuclear colocalization. CCND1 (Cyclin-D1) gene expression remained constant with HAVcR-1 overexpression however, the protein expression was significantly increased. It would be expected that activated β-catenin signalling would increase cyclin D1 transcription therefore increasing cyclin D1 gene expression and protein expression [99]. This therefore suggests that either PCR was not sensitive enough to identify these changes in gene expression or that the increase in expression was due to changes in the regulation of post-translational, transcriptional or degradational stages [12]. Cyclin-D1 is a cell cycle control protein and has been linked to the development and progression of cancer. Cyclin D1 is a regulator cell progression to the proliferation stage of cell cycle, in LNCaP cells cyclin D1 overexpression enhancing S-phase entry, increasing colony formation and tumour growth rate [11, 13, 99]. Interestingly cyclin D1 regulates of cell cycle progression via retinoblastoma protein phosphorylation and the Kinex™ KAM880 Protein array showed significant increases in retinoblastoma protein phosphorylation at S795, S807, S811 and T356 with HAVcR-1 overexpression [100]. Therefore, the increased cyclin D1 protein expression and

hyperphosphorylation of retinoblastoma protein with HAVcR-1 overexpression was predicted to increase cell growth however, there was no change in cell growth in PZ-HPV-7[HAVcR-1EXP] cells. It may however be of interest to investigate the cell cycle changes with HAVcR-1 overexpression.

EMT is a multi-step process involving the decreased integrity of junctional complexes [16]. As previously discussed, immunofluorescence showed as decreased integrity of AJs with E-cadherin, α-catenin and β-catenin membrane staining being disturbed after HAVcR-1 overexpression therefore it is possible that HAVcR-1 has an important role in the initiation of EMT. EMT is also characterised by an increased cellular invasion, modulation of cell-extracellular matrix adhesion and increased cellular migration [209, 349]. HAVcR-1 overexpression increased cellular invasion and adhesion thus supporting this theory. However, HAVcR-1 overexpression decreased cell migration and had no effect on the constraint on current flow beneath cells during initial attachment or wound healing, thus suggesting no change in focal adhesion. EMT is also characterised by the increase in mesenchymal markers and therefore it would be of interest to investigate whether HAVcR-1 expression has an effect on the expression or localisation of these markers, such as N-cadherin and vimentin [209, 349].

This chapter proposes HAVcR-1 as a potentially important protein in the regulation of AJs, β-catenin signalling and EMT and therefore prostate cancer development and progression. This makes HAVcR-1 a protein of interest in prostate cancer for future research.

Chapter VI:

HGF and HAVcR-1 in PC-3

and PZ-HPV-7 Cells

6.1 Introduction

The development and progression of cancer is controlled by variations in normal cellular signalling. These changes results in alterations in cellular behaviours described as cancer hallmarks, such as apoptosis, proliferation, survival and invasion as well as alterations in cellular architecture, including polarity and intercellular junctions [50, 92]. Signalling pathways are generally studied and described as independent cascades however they form a greater network intermingling with one-another. Therefore, the study of cellular signalling and the identification of dysregulated molecules is extremely complex with new interactions and the effect of these on cells being constantly discovered [92].

The HGF/*c*-met signalling cascade has been an area of interest in the study of cancer, with HGF activating a variety of signalling pathways that control cellular processes. These cellular processes are intrinsic to cancer development and progression including: cell proliferation, survival, motility and differentiation [245, 246, 253, 254]. HGF activation of the MAPK pathway results in changes to proliferation, differentiation, transformation and apoptosis. Whereas, HGF activation of the PI3K pathway results in changes in cell cycle regulation and invasion and the activation of the STAT pathway results in changes in proliferation, survival and differentiation [21, 252, 254]. HGF/ *c*-met signalling has also been shown to alter cellular architecture with HGF treatment dysregulating TJs, decreasing TER and decreasing cellular polarity [259]. It is therefore unsurprising that HGF/ *c*-met signalling has been linked to the development and progression of numerous cancers including prostate cancer [21, 22, 280]. High HGF plasma levels are associated with advanced stage and poor prognosis in patients with prostate cancer [93]. HGF has been shown to decrease

cellular junctions in prostate cancer cell lines, with HGF treatment decreasing TER and ZO-1, ZO-2 and ZO-3 expression levels at cell membranes as well as being shown to increase cell attachment [22, 281, 358]. Interestingly, knockdown of HAVcR-1 in HECV cells resulted in resistance to HGF mediated TJ disruption and decreased TER therefore suggesting a potential link between HAVcR-1 and HGF signalling [340]. However, the effect of HAVcR-1 and HGF in prostate cancer has not yet been studied. This chapter therefore aimed to evaluate the importance of HAVcR-1 in HGF/ *c*-Met signalling mediated cellular changes in prostate cancer cell lines. This is with the specific interest of identifying whether HAVcR-1 overexpression in prostate cancer cell lines (PC-3 and PZ-HPV-7) resulted in an increased sensitivity to HGF induced cellular changes. This chapter also set out to investigate whether knockdown of HAVcR-1 in the PC-3 prostate cancer cell line resulted in resistance to these changes with the hope that HAVcR-1 may be a promising molecule of interest in therapeutic development for prostate cancer.

6.2 Materials and Methods

6.2.1 Mammalian Cell Culture

The PC-3 and PZ-HPV-7cell lines was obtained from ATCC (LGC Standards, Middlesex, UK) and maintained in supplemented DMEM and Keratinocyte-SFM medium respectively. PC-3^{pEF6}, PC-3$^{HAVcR-1EXP}$ and PC-3$^{HAVcR-1KD}$ were maintained in maintenance DMEM medium. PZ-HPV-7^{pEF6} and PZ-HPV-7$^{HAVcR-1EXP}$ were maintained in maintenance Keratinocyte-SFM medium. Routine cell culture was carried out as described in Section 2.2.1.

6.2.2 Generation of Cell Lines

PC3^{pEF6}, PC-3$^{HAVcR-1EXP}$ and PC-3$^{HAVcR-1KD}$ were generated and validated in Chapter IV. PZ-HPV-7^{pEF6} and PZ-HPV-7$^{HAVcR-1EXP}$ were generated and validated in Chapter V.

6.2.3 Cell Growth Assay

Growth assays were carried out as described in 2.2.5.1. Cells were treated with 40 ng/mL HGF or an equal amount of 0.1 % BSA in PBS when being seeded. Cells were stained with crystal violet as described in 2.2.5.4

6.2.4 Cell Adhesion Assay

Adhesion assays were carried out as described in 2.2.5.2. Cells were treated with 40 ng/mL HGF or an equal amount of 0.1 % BSA in PBS when being seeded. Cells were stained with crystal violet as described in 2.2.5.4.

6.2.5 Cell Invasion Assay

Invasion assays were carried out as described in 2.2.5.3Cells were treated with 40 ng/mL HGF or an equal amount of 0.1 % BSA in PBS when being seeded. Cells were stained with crystal violet as described in 2.2.5.4.

6.2.6 Cell Migration Assay

Migration assays were performed as detailed in 2.2.5.7. At 0 hours cells were treated with 40 ng/mL HGF or an equal amount of 0.1 % BSA in PBS.

6.2.7 Transepithelial Resistance (TER)

TERs were measured as described in 2.2.5.5. At 0 hours cells were treated with 40 ng/mL HGF or an equal amount of 0.1 % BSA in PBS.

6.2.8 Paracellular Permeability (PCP)

PCPs were performed as described in 2.2.5.6. At 0 hours cells were treated with 40 ng/mL HGF or an equal amount of 0.1 % BSA in PBS.

6.2.9 Statistical Analysis

Cell growth, adhesion and invasion data were statistically analysed to assess for changes from control using the Microsoft Excel Student's t-test. TER assays were assessed as $\Omega . cm^2$ and PCP assays were assessed as fold change from 0 hours. Wound area was quantified using Image J software and this data, as well as data from other assays whereby time points were assessed, TER and PCP, was statistically analysed to assess changes from control using the IBM SPSS Statistics 24 Mixed ANOVA.

6.3 Results

6.3.1 Cell Growth Remains Constant with HGF Treatment Regardless HAVcR-1 Levels

PC-3^{pEF6}and PZ-HPV-7^{pEF6} cell models were utilised to assess the effect of HGF on cell growth. Furthermore PC-3$^{HAVcR-1EXP}$, PC-3$^{HAVcR-1KD}$ and PZ-HPV-7$^{HAVcR-1EXP}$ were used to assess whether HAVcR-1 influenced these HGF induced changes to cell growth. To achieve this, an *in vitro* growth assay was performed whereby cells were seeded and treated with either 40 ng/mL HGF or an equal volume of 0.1 % BSA in PBS. Cell counts were analysed after 3 or 5 days of growth relative to 1 day of growth as a seeding control.

This showed no significant difference in cell growth with HGF treatment of PC-3^{pEF6} cells in comparison to control at day 3 (14.70±4.13 vs 10.56± 3.93; p=0.508) or at day 5 (26.36±7.86 vs 21.65±5.55; p=0.652) (See Figure 6.1 A and D). HAVcR-1 overexpression had no effect on this with no significant difference in cell growth with HGF treatment of PC-3$^{HAVcR-1EXP}$ cells in comparison to control cells at day 3 (8.27±1.18 vs 9.85±2.16; p=0.567) or at day 5 (11.99±3.21 vs 20.07±9.11; p=0.476) (See Figure 6.1 B and E). HAVcR-1 knockdown also showed no effect with no significant difference in cell growth with HGF treatment of PC-3$^{HAVcR-1EXP}$ cells in comparison to control cells at day 3 (7.03±1.76 vs 11.23±4.50; p=0.457 or at day 5 (10.92±4.13 vs 17.00±5.10; p=0.409) (See Figure 6.1 C and F).

HGF treatment also had no effect on PZ-HPV-7^{pEF6} cell growth in comparison to control cells at day 3 (3.21± 0.02 vs 3.54±0.01; p=0.214) or at day 5 (7.42±0.73 vs 8.88±2.32; p=0.274) (See Figure 6.2A and C). HAVcR-1 overexpression in PZ-HPV-7

cells also had no effect on this with no significant difference in cell growth with HGF treatment of PZ-HPV-7$^{HAVcR-1EXP}$ cells in comparison to control cells at day 3 (3.04± 0.09 vs 3.10±0.18; p=0.789) or at day 5 (6.76±1.13 vs 6.55±1.16; p=0.905) (See Figure 6.2 B and D).
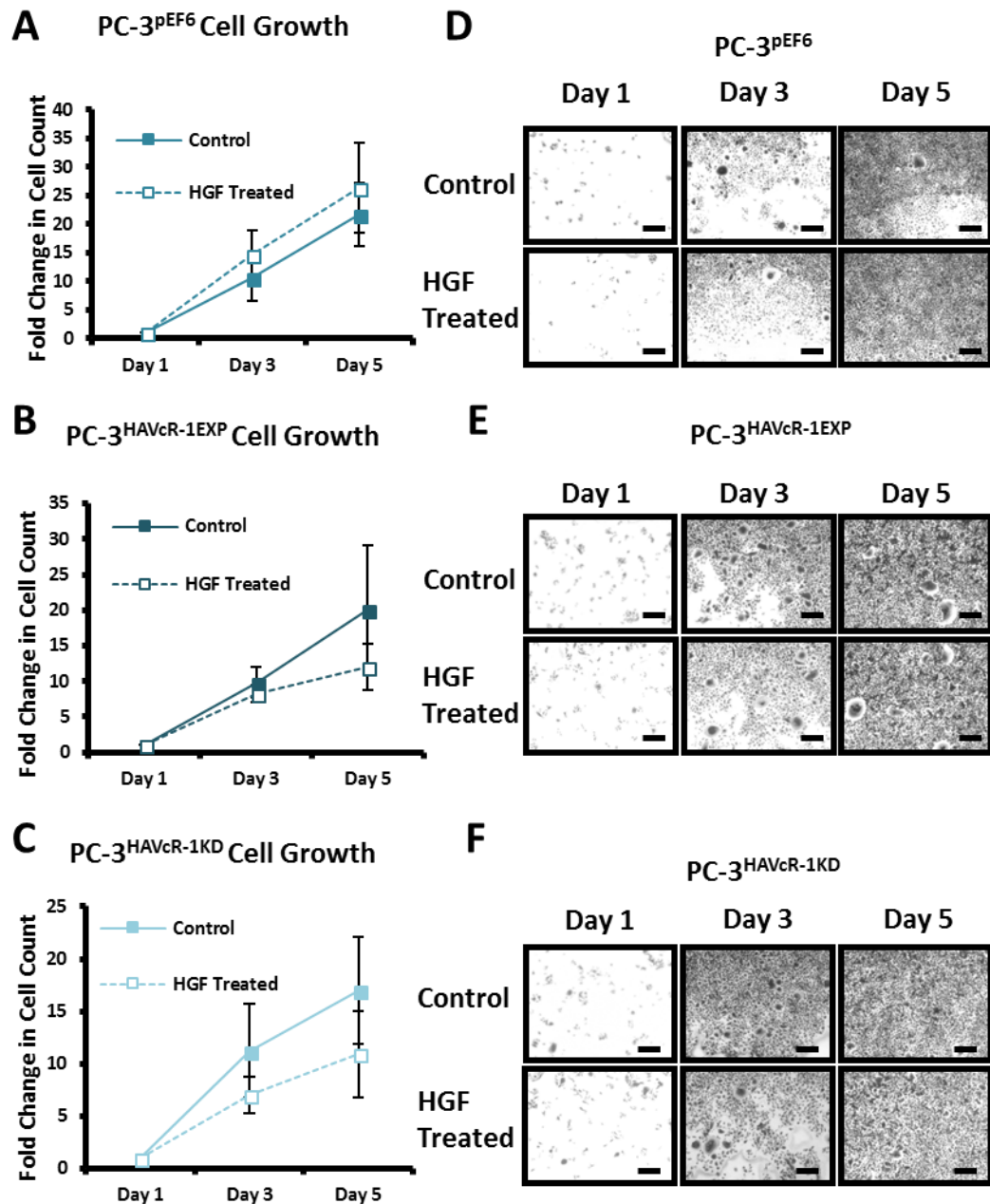
Figure 6.1 The Effect of HAVcR-1 in Combination with HGF on PC-3 Cell Growth.
Cells were seeded into 24 well plates at 1×10^4 cells per well in triplicate, treated with 40 ng/mL HGF or an equal volume of 0.1 % BSA in PBS and incubated for 1, 3 or 5 days. Post incubation cells were fixed, stained with crystal violet and images were taken at 5 X magnification. Scale bars are representative of 2 mm **A-C** Cells were counted and graphs show the means of three independent experiments as fold change relative to the cell count at day 1 with error bars showing SEM. Statistical analysis was performed at each time point via the Student's t-test using Microsoft Excel and significance of $p < 0.05$ was not reached. **D-F,** Images are representative of three independent experiments.
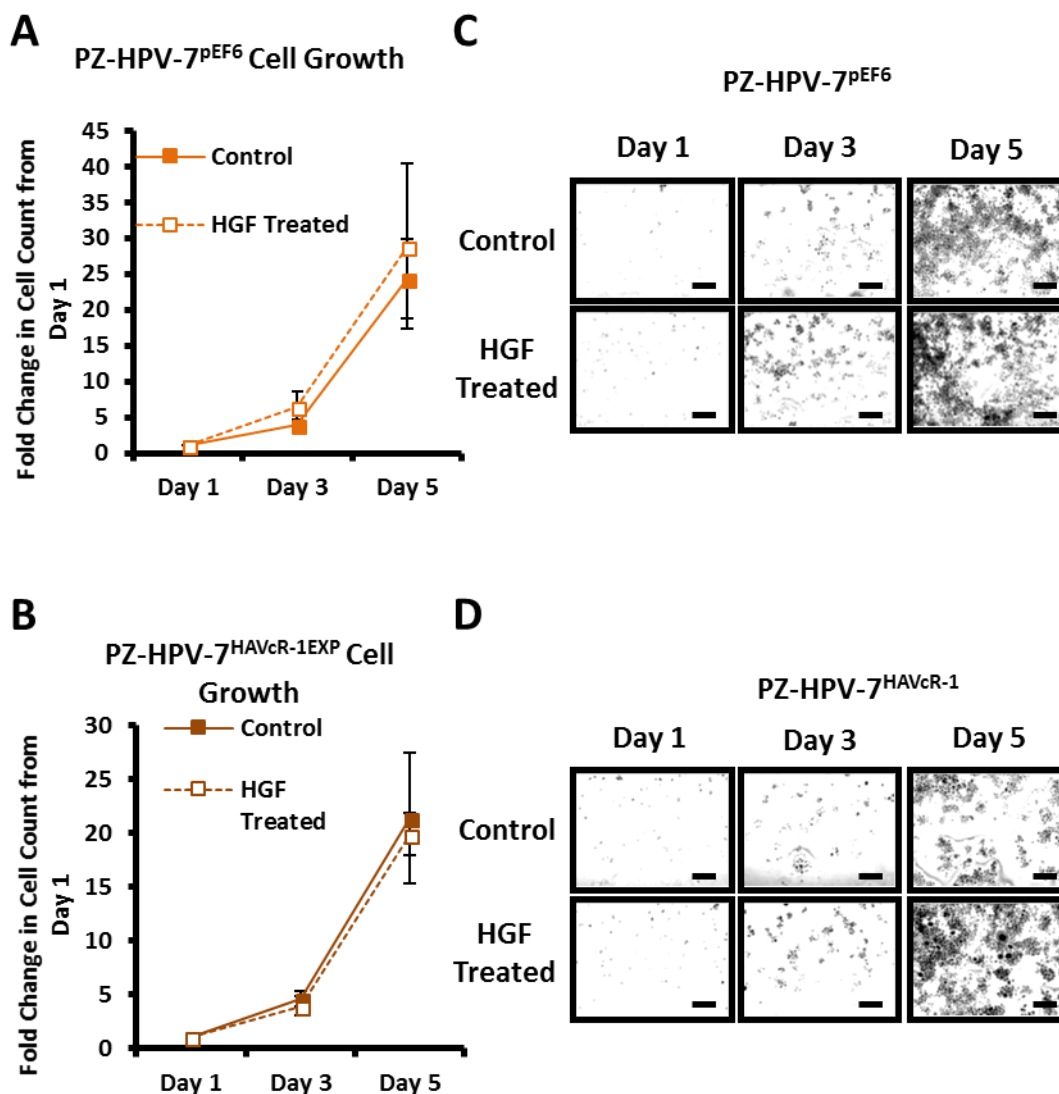
Figure 6.2 The Effect of HAVcR-1 in Combination with HGF on PZ-HPV-7 Cell Growth. Cells were seeded into 24 well plates at 1×10^4 cells per well in triplicate, treated with 40 ng/mL HGF or an equal volume of 0.1 % BSA in PBS and incubated for 1, 3 or 5 days. Post incubation cells were fixed, stained with crystal violet and images were taken at 5 X magnification. **A-C** Cells were counted and graphs show the means of three independent experiments as fold change relative to the cell count at day 1 with error bars showing SEM. Statistical analysis was performed at each time point via the Student's t-test using Microsoft Excel and significance of $p < 0.05$ was not reached. **D-F,** Images are representative of three independent experiments and scale bars are representative of 2 mm.

6.3.2 HGF Increases PZ-HPV-7 Cell Migration With HAVcR-1 Overexpression

To assess the effect of HGF on cell migration PC-3^{pEF6}and PZ-HPV-7^{pEF6} cell models were utilised. The effects of HAVcR-1 on HGF induced changes to cell migration were also assessed via the use of PC-3$^{HAVcR-1EXP}$, PC-3$^{HAVcR-1KD}$ and PZ-HPV-7$^{HAVcR-1EXP}$ cell models. To investigate these effects an *in vitro* scratch migration assay was performed whereby cells were seeded and incubated until confluent monolayers were formed. Cells were then scratched and treated with 40 ng/mL HGF or an equal volume of 0.1 % BSA in PBS. The wound area was then analysed every hour as percentage wound closure from the 0 hour time point.

This showed no significant difference in percentage wound closure of HGF treated PC-3^{pEF6} in comparison to control PC-3^{pEF6} ($F_{(10, 40)}$=1.202, p=0.319). There was also no change in healing rates of HGF treated PC-3^{pEF6} (7.19±0.78 %/hour) in comparison to control (6.92±0.63 %/hour) (p=0.79) (See Figure 6.3 A and D). HAVcR-1 overexpression had no effect on this with no significant difference in percentage wound closure of HGF treated PC-3$^{HAVcR-1EXP}$ and control PC-3$^{HAVcR-1EXP}$ ($F_{(10,40)}$=0.528, P=0.860). Healing rates also showed no change between PC-3$^{HAVcR-1EXP}$ with HGF treatment (5.24±0.25 %/hour) cells in comparison to control PC-3$^{HAVcR-1EXP}$ (5.19±0.63 %/hour) (p=0.943) (3.33 ± 0.27 vs 3.95 ± 0.39; p=0.191) (See Figure 6.3 B and E). HAVcR-1 knockdown also showed no significant impact change in percentage wound closure with HGF treatment in PC-3$^{HAVcR-1KD}$ cells in comparison to control cells ($F_{(10,40)}$=0.790, p=0.638). Healing rate also revealed no significant

effects between PC-3$^{HAVcR-1KD}$ with HGF treatment (7.20±0.59 %/hour) and control cells (5.08±0.63 %/hour :p=0.070) (See Figure 6.3 C and F).

HGF treatment also had no effect on PZ-HPV-7^{pEF6} percentage wound closure in comparison to control cells ($F_{(10,40)}$=0.079, p=1.000) or in healing rate with HGF treated closing 0.95±0.23 %/hour and control cells closing 0.76±0.33 %/hour (p=0.667) (See Figure 6.4 A and C). However, HGF treatment in PZ-HPV-7$^{HAVcR-1EXP}$ cells increased percentage wound closure in comparison to control PZ-HPV-7$^{HAVcR-1EXP}$ ($F_{(10,40)}$=4.315, p=0.00041). There was however no significant difference between the healing rates with HGF treated closing 1.39±0.28 %/hour and control cells closing 0.81±0.23 %/hour (p=0.181) (See Figure 6.4 B and D).
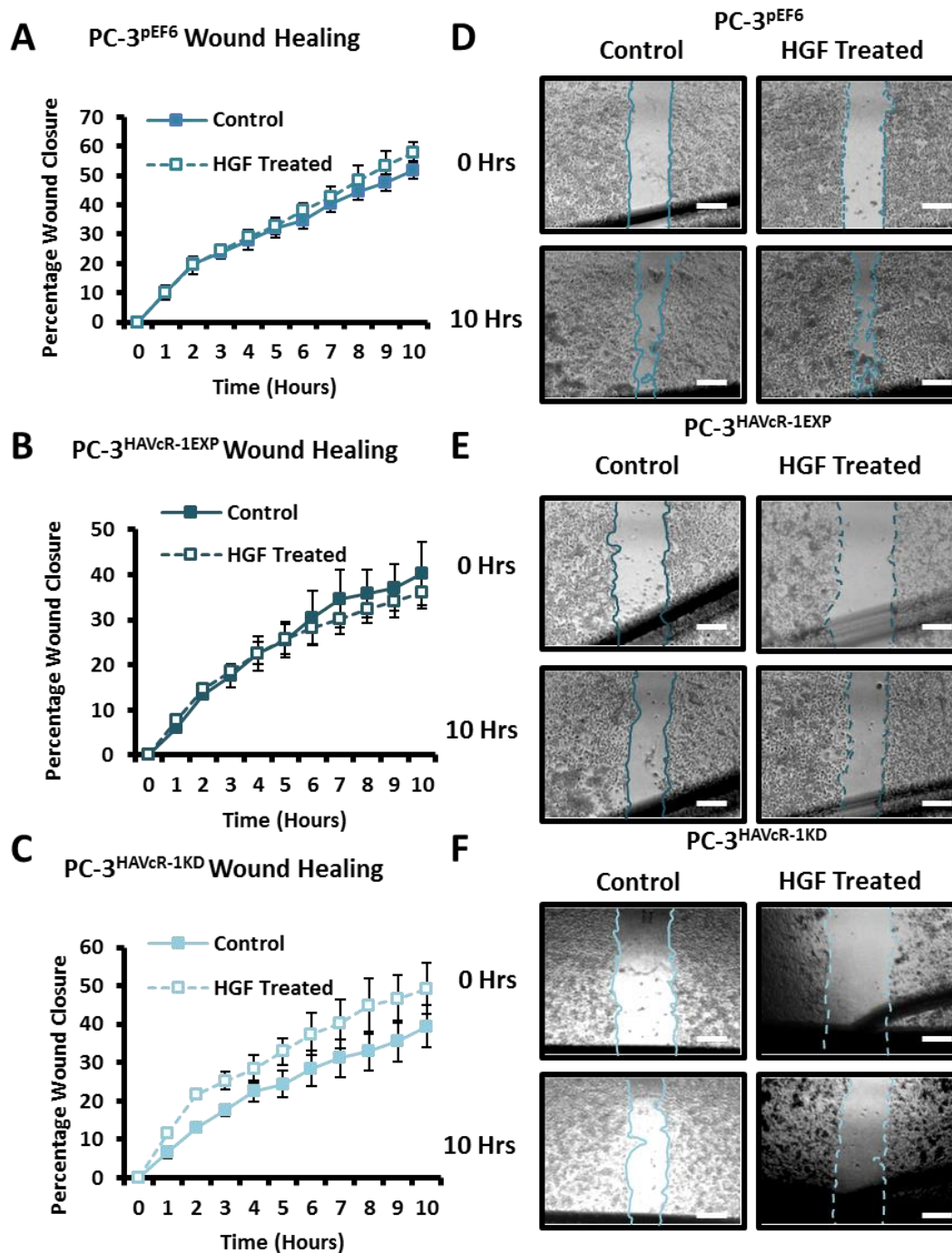
Figure 6.3 The Effect of HAVcR-1 in Combination with HGF on PC-3 Cell Migration
Cells seeded into 24 well plates in quadruplicate, scratched once confluent and treated with 40 ng/mL or equal volume 0.1 % BSA in PBS. Images were taken immediately afterward and every hour thereafter at 5 X magnification. **A-C** Wound area was measured using ImageJ software and percentage wound closures were calculated as relative to 0 hour time point. Data shown are the means of three independent experiments and error bars represent SEM. Statistical analysis was performed using IBM SPSS Statistics 24 utilising a Mixed ANOVA significance of $p < 0.05$ was not reached. **D-F,** Images shown are representative of three independent experiments and scale bars are representative for 2 mm.
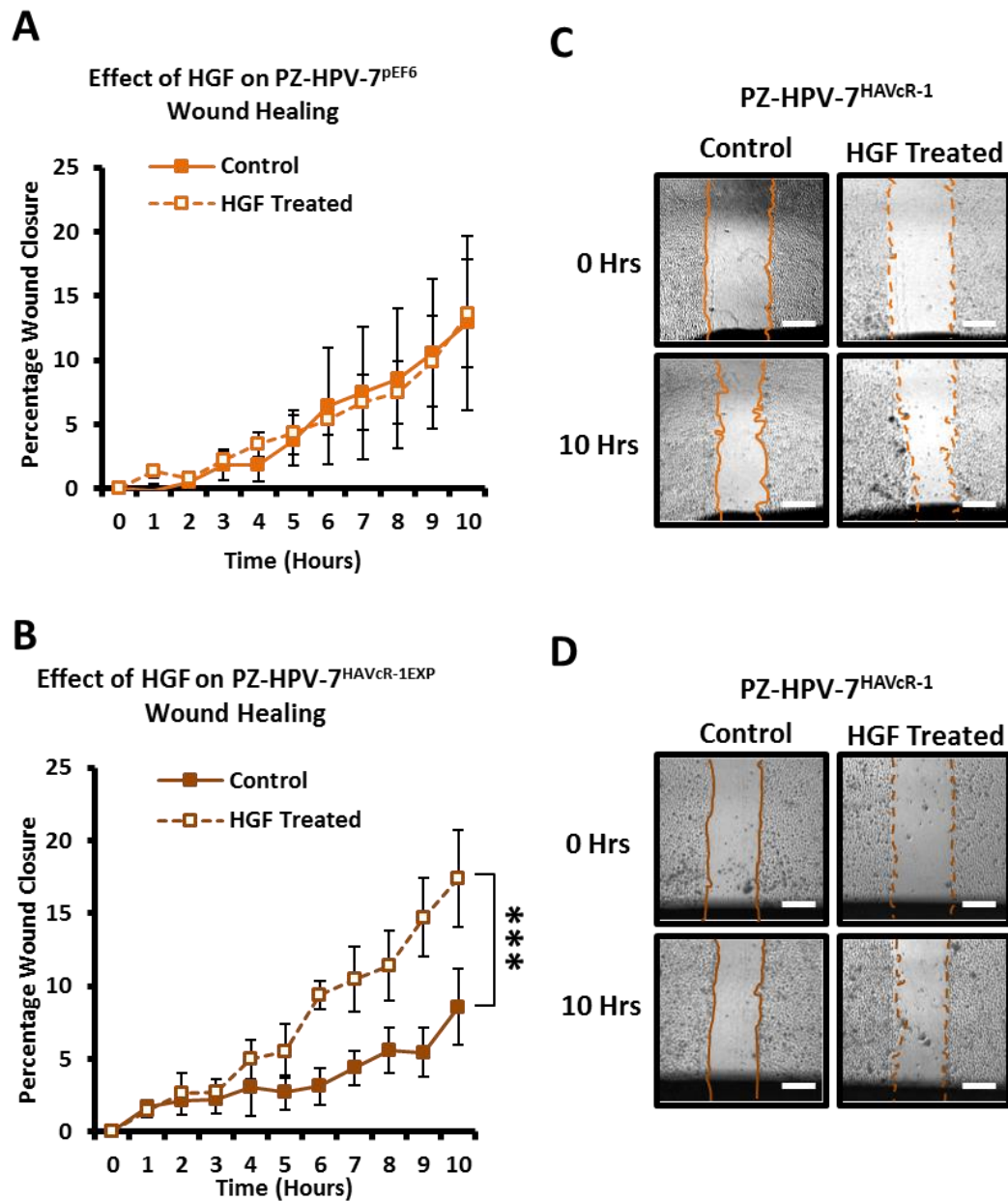
Figure 6.4 The Effect of HAVcR-1 in Combination with HGF on PZ-HPV-7 Cell Migration

Cells seeded into 24 well plates in duplicate, scratched once confluent and treated with 40 ng/mL or equal volume 0.1 % BSA in PBS. Images were taken immediately afterward and every hour thereafter at 5 X magnification. **A-C** Wound area was measured using ImageJ software and percentage wound closures were calculated as relative to 0 hour time point. Data shown are the means of three independent experiments and error bars represent SEM. Statistical analysis was performed using IBM SPSS Statistics 24 utilising the Mixed ANOVA $p < 0.05$ was considered significant and $p < 0.001$ is represented by ***. **D-F,** Images shown are representative of three independent experiments and scale bars are representative for 2 mm.

6.3.3 HGF Increases Cell Adhesion in PC-3 Cells With HAVcR-1 Knockdown and Decreases Cell Adhesion in PZ-HPV-7 Cells With HAVcR-1 Overexpression

The effect of HGF on cell adhesion was investigated via the use of PC-3^{pEF6}and PZ-HPV-7^{pEF6} cell. The effect of HAVcR-1 on HGF induced changes on cell adhesion was then investigated using the PC-3$^{HAVcR-1EXP}$, PC-3$^{HAVcR-1KD}$ and PZ-HPV-7$^{HAVcR-1EXP}$ cell models. These investigations utilised the *in vitro* Matrigel™ adhesion assay whereby cells were seeded in media containing 40 ng/mL HGF or an equal volume of 0.1 % BSA in PBS into a 96 well plate containing a Matrigel™ layer. Plates were then incubated for 30 min and the number of adhered cells counted and presented as fold change from 0.1 % BSA in PBS treated control cells.

There was no significant difference in cell adhesion with HGF treatment of PC-3^{pEF6} in comparison to the control (1.73±0.04 fold increase; p=0.875). HAVcR-1 overexpression in PC-3 cells had no effect on this result with no significant difference in cell adhesion with HGF treatment of PC-3$^{HAVcR-1EXP}$ resulting in a 1.28 ±0.68 fold increase from the control with p=0.724. However, HAVcR-1 knockdown in PC-3 resulted in cell adhesion being significantly increased by 2.05±0.21 fold with HGF treatment in comparison to control with p=0.039 (See Figure 6.5).

There was a significant decrease in cell adhesion with HGF treatment of PZ-HPV-7^{pEF6} in comparison to the control (0.60±0.02 fold change; p=0.002). HAVcR-1 overexpression also showed a significant decrease in cell adhesion with HGF treatment of PC-3$^{HAVcR-1EXP}$ resulting in a 0.45 ±0.05 fold change from the control with p=0.007 (See Figure 6.6).
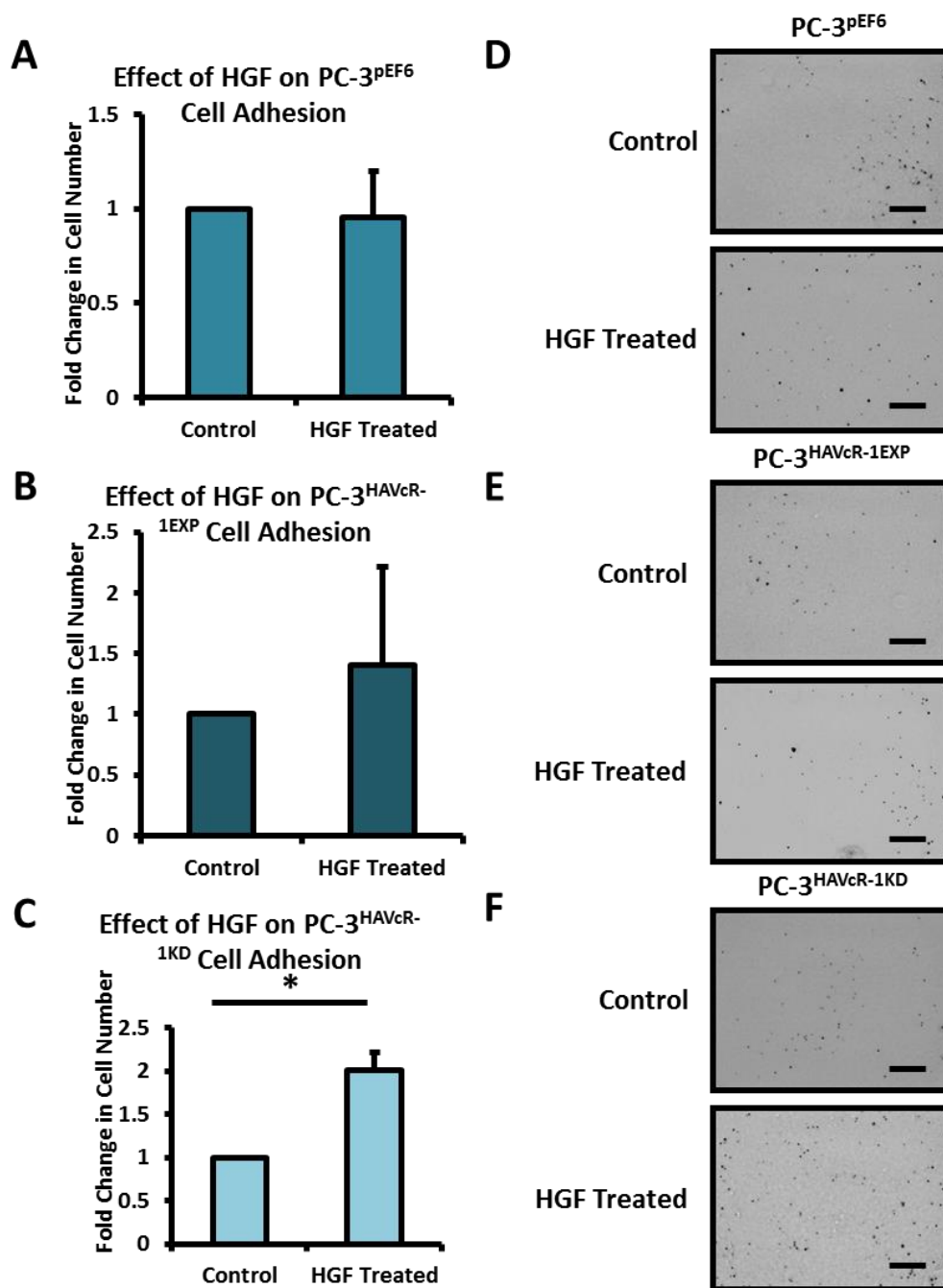
Figure 6.5 The Effect of HAVcR-1 in Combination with HGF on PC-3 Cell Adhesion
Cells seeded into 96 well plates coated in 200 µl of 50 ug/mL Matrigel™ at 5×10^3 cells per well in quadruplicate, treated with 40 ng/mL HGF or an equal volume 0.1 % BSA in PBS and incubated for 30 min. Post incubation cells were fixed, stained with crystal violet and images were taken at 5 X magnification. **A-C** Cells were counted and graphs show the means of three independent experiments as fold change relative to the cell count of the control with error bars showing SEM. Statistical analysis was performed via the Student's t-test using Microsoft Excel and significance of $p<0.05$ was reached. * represents $p<0.05$. **D-F,** Images are representative of three independent experiments. Scale bars are representative of 2 mm.
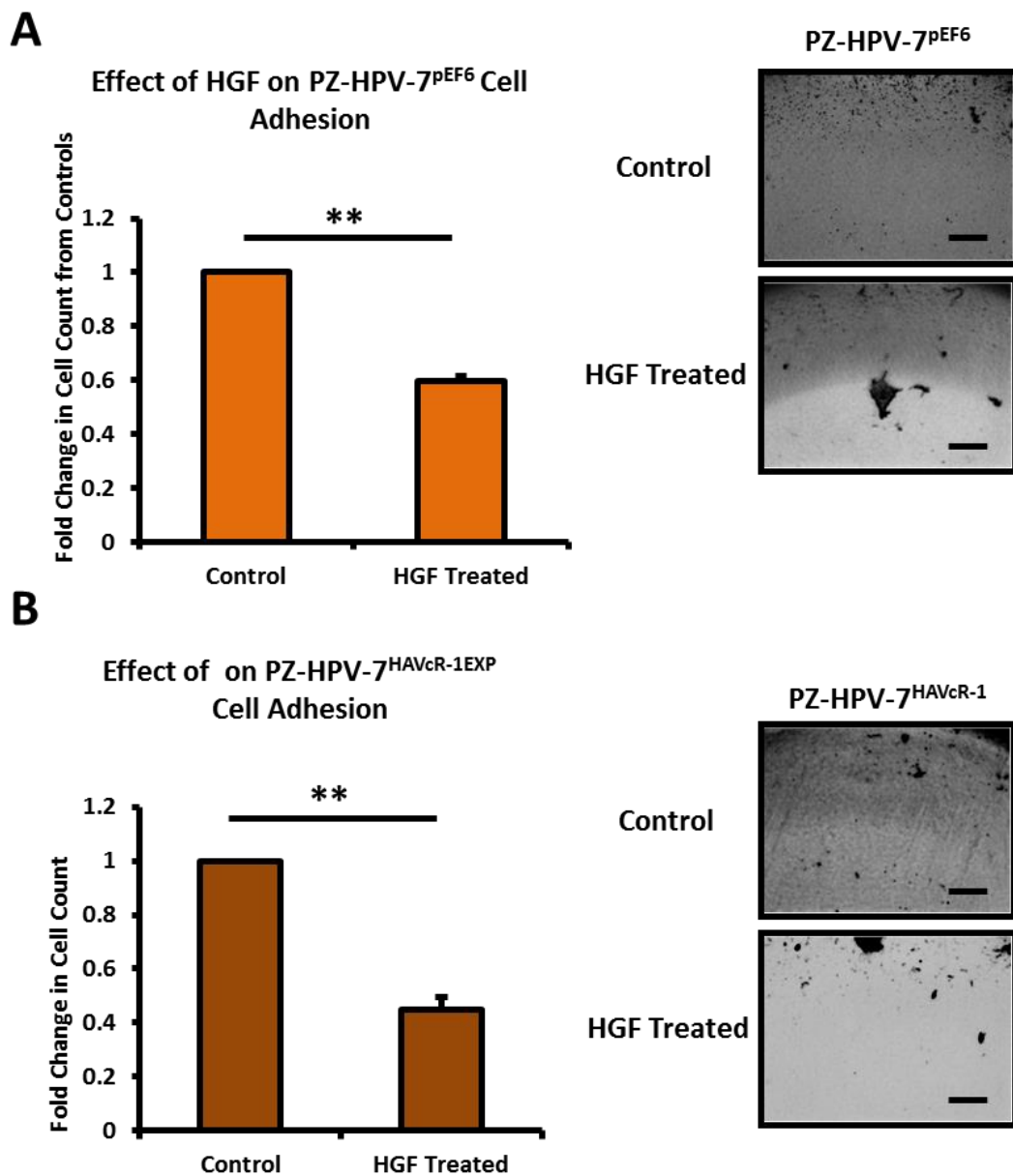
Figure 6.6 The Effect of HAVcR-1 in Combination with HGF on PZ-HPV-7 Cell Adhesion

Cells seeded into 96 well plates coated in 200 µl of 50 ug/mL Matrigel™ at $5x10^3$ cells per well in quadruplicate, treated with 40 ng/mL HGF or an equal volume 0.1 % BSA in PBS and incubated for 30 min. Post incubation cells were fixed, stained with crystal violet and images were taken at 5 X magnification. **A-C** Cells were counted and graphs show the means of three independent experiments as fold change relative to the cell count of the control with error bars showing SEM. Statistical analysis was performed via the Student's t-test using Microsoft Excel and significance of $p<0.05$ was reached. ** represents $p<0.01$. **D-F,** Images are representative of three independent experiments. Scale bars are representative of 2 mm.

6.3.4 Cell Invasion Remains Constant with HGF Treatment Regardless of HAVcR-1 Levels.

The effect of HGF on cell invasion was assessed via the use of PC-3^{pEF6} and PZ-HPV-7^{pEF6} cells. To assess the influence that HAVcR-1 has on this PC-3$^{HAVcR-1EXP}$, PC-3$^{HAVcR-1KD}$ and PZ-HPV-7$^{HAVcR-1EXP}$ were utilised. An *in vitro* Matrigel™ invasion assay was therefore carried out.

There was no significant difference in cell invasion in PC-3^{pEF6} with HGF treatment with a 0.77±0.16 fold change from control and p=0.283. HAVcR-1 overexpression had no significant effect on this with HGF treatment resulting in a 0.83±0.15 fold change from control with p=0.268 in PC-3$^{HAVcR-1EXP}$ cells. HAVcR-1 knockdown also had no significant effect on this with HGF treatment resulting in a 1.04±0.28 fold change (p=0.905) from control in PC-3$^{HAVcR-1KD}$ cells. (See Figure 6.7)

There was also no significant change in cell invasion of PZ-HPV-7^{pEF6} with HGF treatment resulting in a 0.77±0.08 fold change from the control with p=0.101. HAVcR-1 overexpression in PZ-HPV-7 cells has no effect on this with HGF treatment of PZ-HPV-7$^{HAVcR-1EXP}$ resulting in a 0.95±0.09 fold change in invasion from the control with p=0.645. (See Figure 6.8)
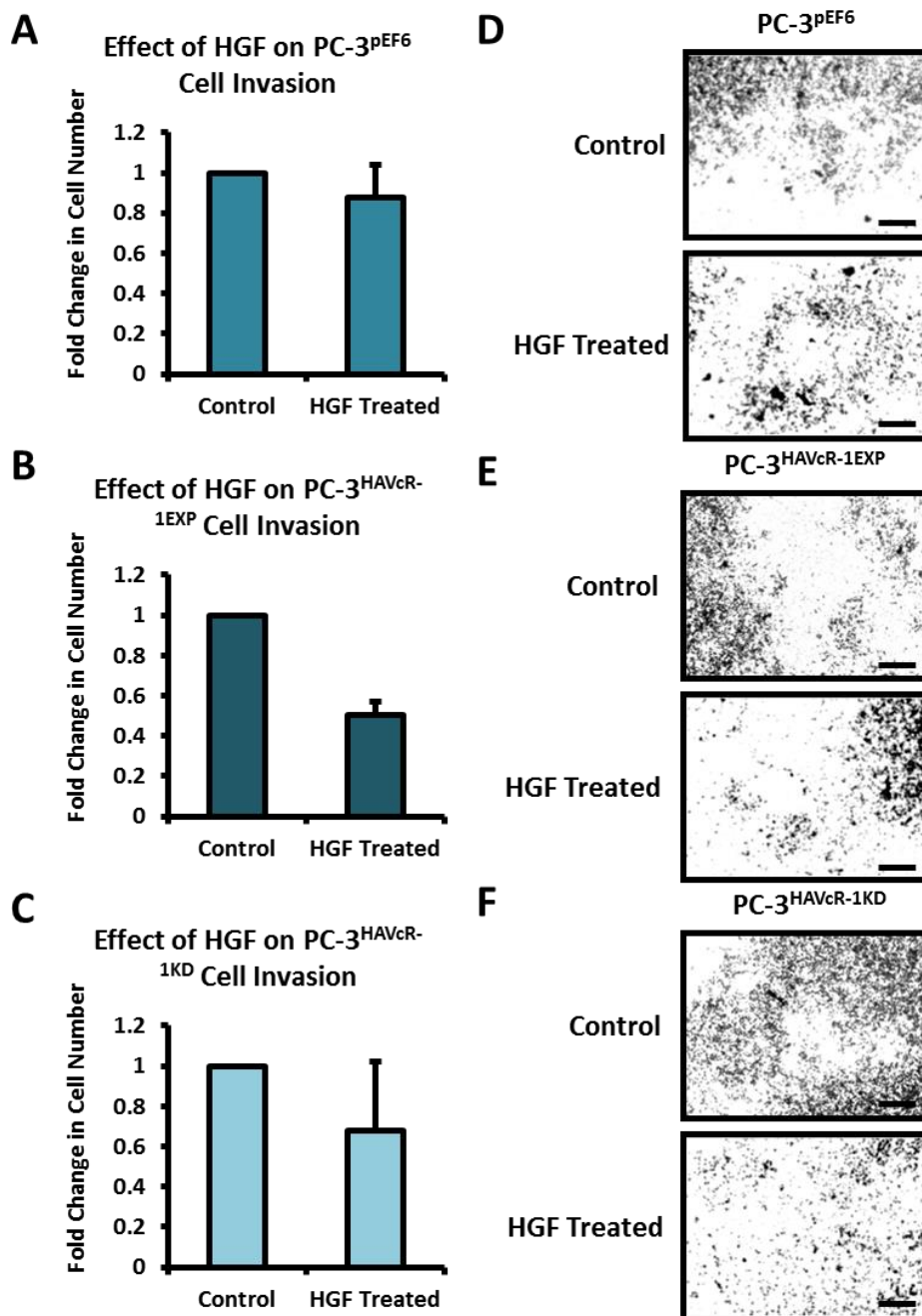
Figure 6.7 The Effect of HAVcR-1 in Combination with HGF Overexpression on PC-3 Cell Invasion

Cells seeded in triplicate into 8 µm size pore inserts coated in 200 µl of 500 µg/mL Matrigel™ in at 24 well plate at $3x10^4$ cells per insert, treated with 40 ng/mL HGF or an equal volume of 0.1 % BSA in PBS and incubated for 3 days. Post incubation cells were fixed, stained with crystal violet and images were taken at 5 X magnification. **A-C** Cells were counted and graphs show the means of three independent experiments as fold change relative to controls with error bars showing SEM. Statistical analysis was performed via the Student's t-test using Microsoft Excel and significance of $p<0.05$ was not reached. **D-F,** Images are representative of three independent experiments. Scales bars are representative of 2 mm.
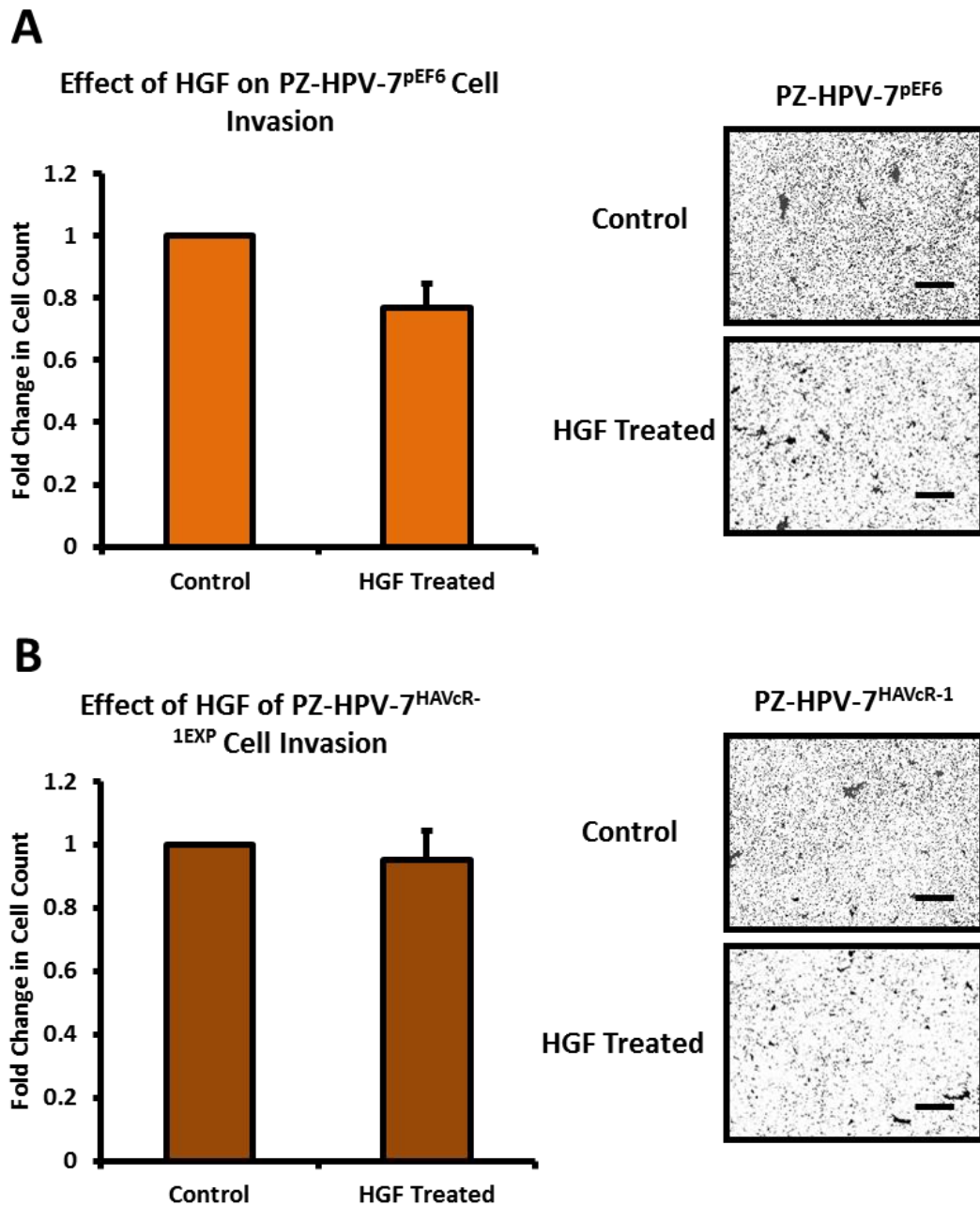
Figure 6.8 The Effect of HAVcR-1 in Combination with HGF Overexpression on PZ-HPV-7 Cell Invasion

Cells seeded in triplicate into 8 μm size pore inserts coated in 200 μL of 500 μg/mL Matrigel™ in at 24 well plate at $3x10^4$ cells per insert, treated with 40 ng/mL HGF or an equal volume of 0.1 % BSA in PBS and incubated for 3 days. Post incubation cells were fixed, stained with crystal violet and images were taken at 5 X magnification. **A-C** Cells were counted and graphs show the means of three independent experiments as fold change relative to controls with error bars showing SEM. Statistical analysis was performed via the Student's t-test using Microsoft Excel and significance of $p<0.05$ was not reached. **D-F,** Images are representative of three independent experiments. Scale bars are representative 2 mm.

6.3.5 TER Remains Constant with HGF Treatment Regardless of HAVcR-1 Levels.

To assess whether HGF had an effect of TER, PC-3^{pEF6} and PZ-HPV-7^{pEF6} cells were utilised. In addition, to assess the effect HAVcR-1 has on HGF induced changes in HGF PC-3$^{HAVcR-1EXP}$, PC-3$^{HAVcR-1KD}$ and PZ-HPV-7$^{HAVcR-1EXP}$ cell models were used. Cells were treated with 40 ng/mL HGF or equal volumes of 0.1 % BSA in PBS before resistance across a monolayer grown on a transwell insert was measured for 10 hours. Data was then analysed as Ω . cm^2 and normalised to 0 hours.

HGF had no significant effect on PC-3^{pEF6} TER (F(12,48)=0.456, p=0.930) (See A). HAVcR-1 overexpression in PC-3 cells had no effect on this with no significant difference in HGF treated PC-3$^{HAVcR-1EXP}$ in comparison to control PC-3$^{HAVcR-1EXP}$ (F(12,48)=0.828, p=0.621) (B). HAVcR-1 knockdown in PC-3 cells also had no effect with no change in TER in HGF treated PC-3$^{HAVcR-1KD}$ in comparison to control PC-3$^{HAVcR-1KD}$ (F(12,48)=1.081, p=0.397) (See C).

PZ-HPV-7^{pEF6} TER was also not effected by HGF treatment (F(12,48)=0.367, p=0.969) (See Figure 6.10A). HAVcR-1 overexpression in PZ-HPV-7 cells had no effect on this with no change in TER in HGF treated PZ-HPV-7$^{HAVcR-1EXP}$ in comparison to control PZ-HPV-7$^{HAVcR-1EXP}$ (F(12,48)=1.022, p=0.445) (See Figure 6.10B).
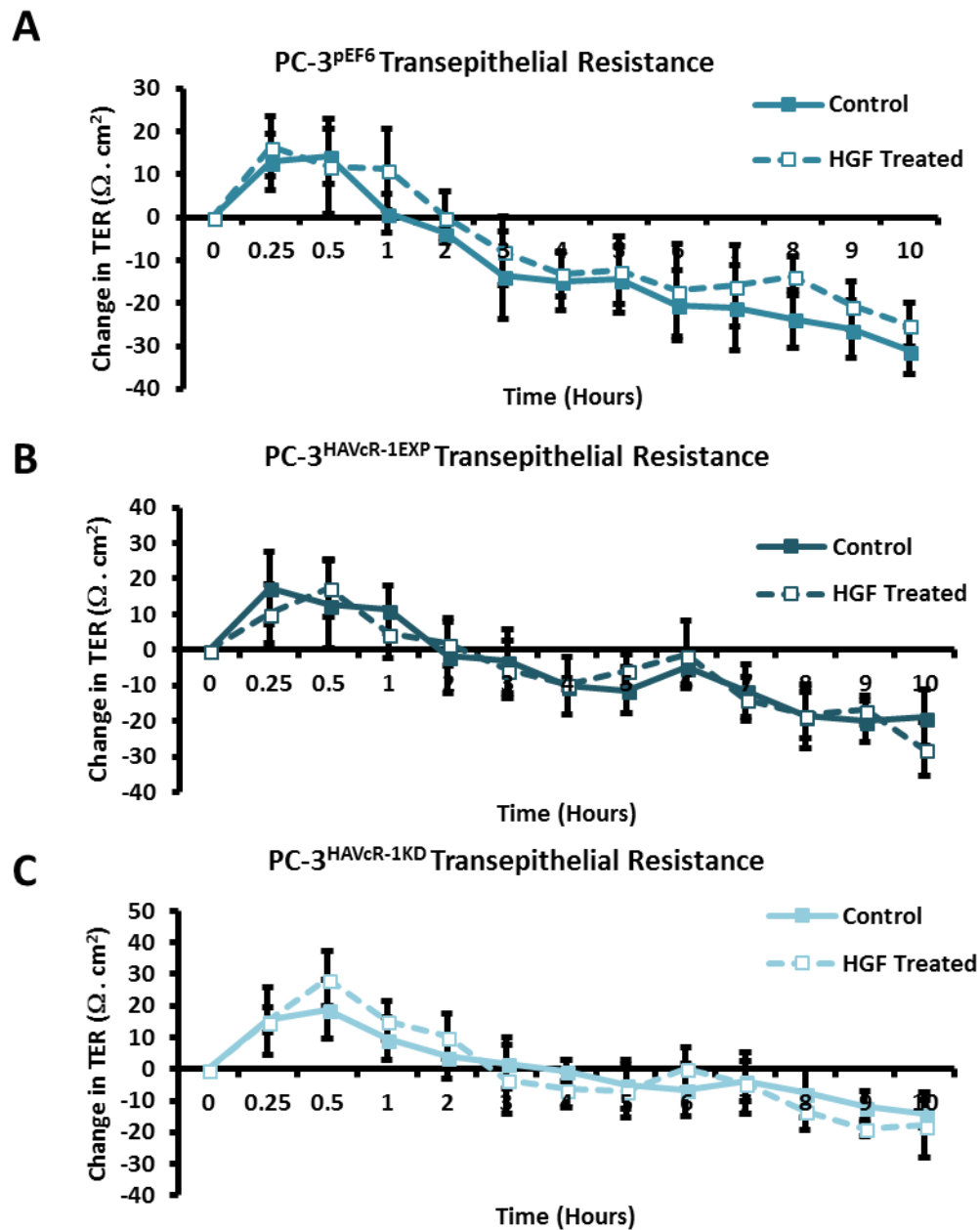
Figure 6.9 The Effect of HGF and HAVcR-1 on PC-3 Transepithelial Resistance
Cells seeded in triplicate into 0.4 µm size pore inserts 5x10^4 cells per insert and incubated until confluent. Post incubation cells were treated with either of 40 ng/mL HGF or equal volumes of 0.1 % BSA in PBS and resistance across the membrane was measured every hour for 10 hours. Graphs show the means of three independent experiments as change relative to the resistance at 0 hour for **A** PC3^{pEF6}, **B** PC-3$^{HAVcR-1EXP}$ and **C** PC-3$^{HAVcR-1KD}$. Error bars show SEM. Statistical analysis was performed via the Mixed ANOVA using IBM SPSS Statistics 24 and $p<0.05$ was considered significant. Significance was not reached.
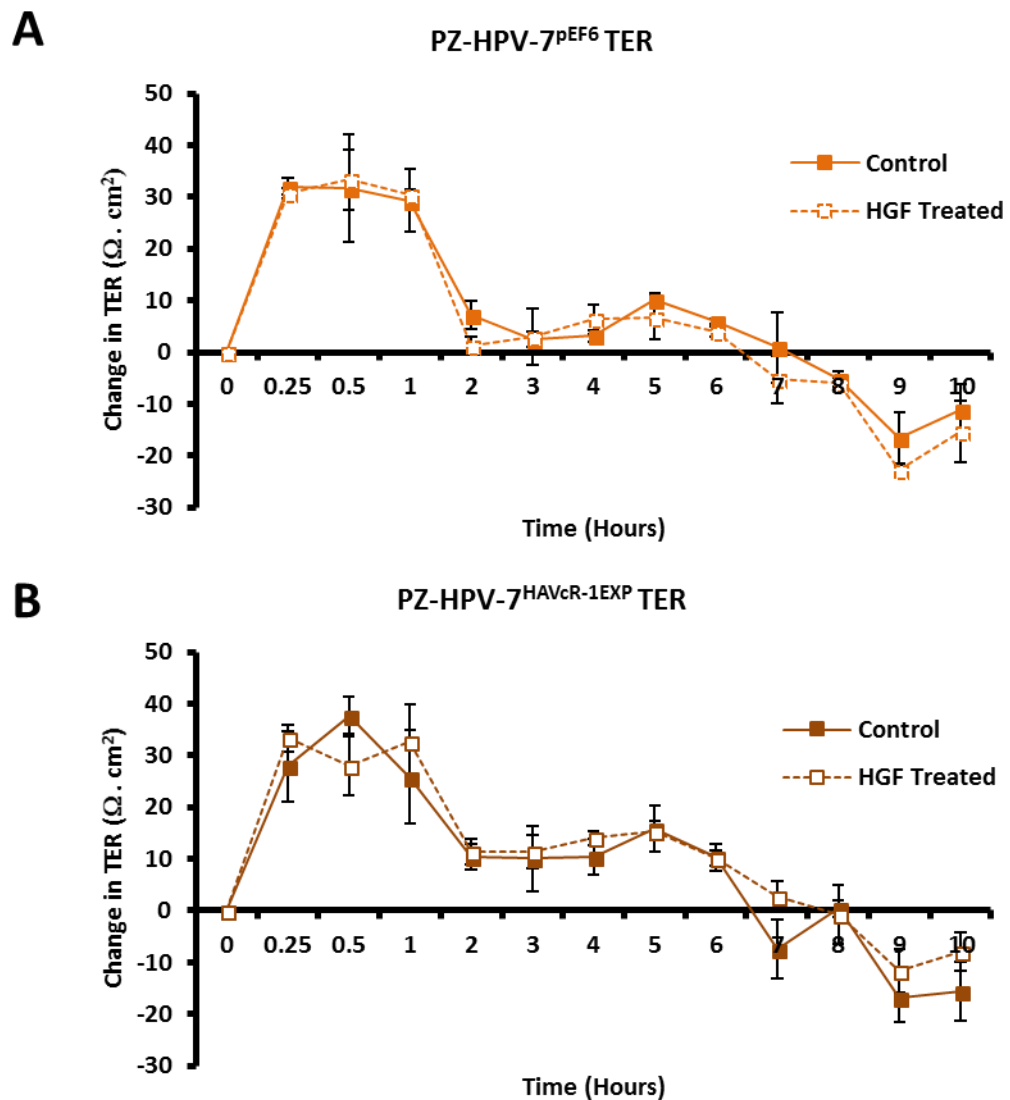
Figure 6.10 The Effect of HGF and HAVcR-1 on PZ-HPV-7 Transepithelial Resistance
Cells seeded in triplicate into 0.4 µm size pore inserts 5x10^4 cells per insert and incubated until confluent. Post incubation cells were treated with either of 40 ng/mL HGF or equal volumes of 0.1 % BSA in PBS and resistance across the membrane was measured every hour for 10 hours. Graphs show the means of three independent experiments as change relative to the resistance at 0 hour for **A** PZ-HPV-7^{pEF6} and **B** PZ-HPV-7$^{HAVcR-1EXP}$. Error bars show SEM. Statistical analysis was performed via the Mixed ANOVA using IBM SPSS Statistics 24 and p<0.05 was considered significant. Significance was not reached

6.3.6 PCP Remains Constant with HGF Treatment Regardless of HAVcR-1 Levels

To assess whether HGF had an effect of PCP, PC-3^{pEF6} and PZ-HPV-7^{pEF6} cells were utilised. To assess the effect HAVcR-1 has on HGF induced changes in PC-3$^{HAVcR-1EXP}$, PC-3$^{HAVcR-1KD}$ and PZ-HPV-7$^{HAVcR-1EXP}$ cells were used. Cells were treated with 40 ng/mL HGF or equal volumes of 0.1 % BSA in PBS prior with 40 kDa TRITC dextran and 10 kDa FITC dextran. The amount of fluorescence as representative of paracellular movement was then measured every hour and data was then analysed as change from 0 hour time point.

HGF has no effect on PCP of 40 kDa TRITC dextran conjugate in PC-3^{pEF6} in comparison to control ($F_{(12,48)}=0.022$, p=1.000) (See A). However, HGF significantly decreased the PCP of 10 kDa FITC dextran conjugate in PC-3^{pEF6} in comparison to control ($F_{(12,48)}=0.379$, P=0.965)(See D).

HGF treatment in PC-3$^{HAVcR-1EXP}$ cells also had no effect on the PCP of 40 kDa TRITC dextran conjugate with no significant difference shown in HGF treated PC-3$^{HAVcR-1EXP}$ in comparison to control PC-3$^{HAVcR-1EXP}$ ($F_{(12,48)}=0.010$, p=1.000) (See B).

HGF treatment in PC-3$^{HAVcR-1EXP}$ cells had no effect PCP of 10 kDa FITC dextran conjugate no significant difference in HGF treated PC-3$^{HAVcR-1EXP}$ in comparison to control PC-3$^{HAVcR-1EXP}$ ($F_{(12,48)}=0.109$, p=1.000) (See E).

Furthermore, HGF treatment in PC-3$^{HAVcR-1KD}$ cells also had no effect on PCP of 40 kDa TRITC dextran conjugate no significant difference in HGF treated PC-3$^{HAVcR-1KD}$ in comparison to control PC-3$^{HAVcR-1KD}$ ($F_{(12,48)}=0.033$, p=1.000) (See C). HGF treatment in PC-3$^{HAVcR-1KD}$ cells also had no effect on PCP of 10 kDa FITC dextran conjugate, no

significant difference shown in HGF treated PC-3$^{HAVcR-1KD}$ in comparison to control PC-3$^{HAVcR-1KD}$ (F(12,48)=0.248, p=0.994) (See F).

HGF has no effect on PCP of 40 kDa TRITC dextran conjugate in PZ-HPV-7^{pEF6} in comparison to control (F(12,48)=0.929, p=0.527) (See A). There was also no effect with HGF treatment on the PCP of 10 kDa FITC dextran conjugate in PZ-HPV-7^{pEF6} in comparison to control (F(12,48)=0.562, p=0.861) (See C).

HGF treatment in PZ-HPV-7$^{HAVcR-1EXP}$ cells resulted in no change in the PCP of 40 kDa TRITC dextran conjugate in comparison to the control (F(12,48)=0.929, p=0.526) (See B). However, HGF treatment in PZ-HPV-7$^{HAVcR-1EXP}$ cells had no effect PCP of 10 kDa FITC dextran conjugate no significant difference in HGF treated PC-3$^{HAVcR-1EXP}$ in comparison to control PC-3$^{HAVcR-1EXP}$ (F(12,48)=0.426, p=0.945) (See D).
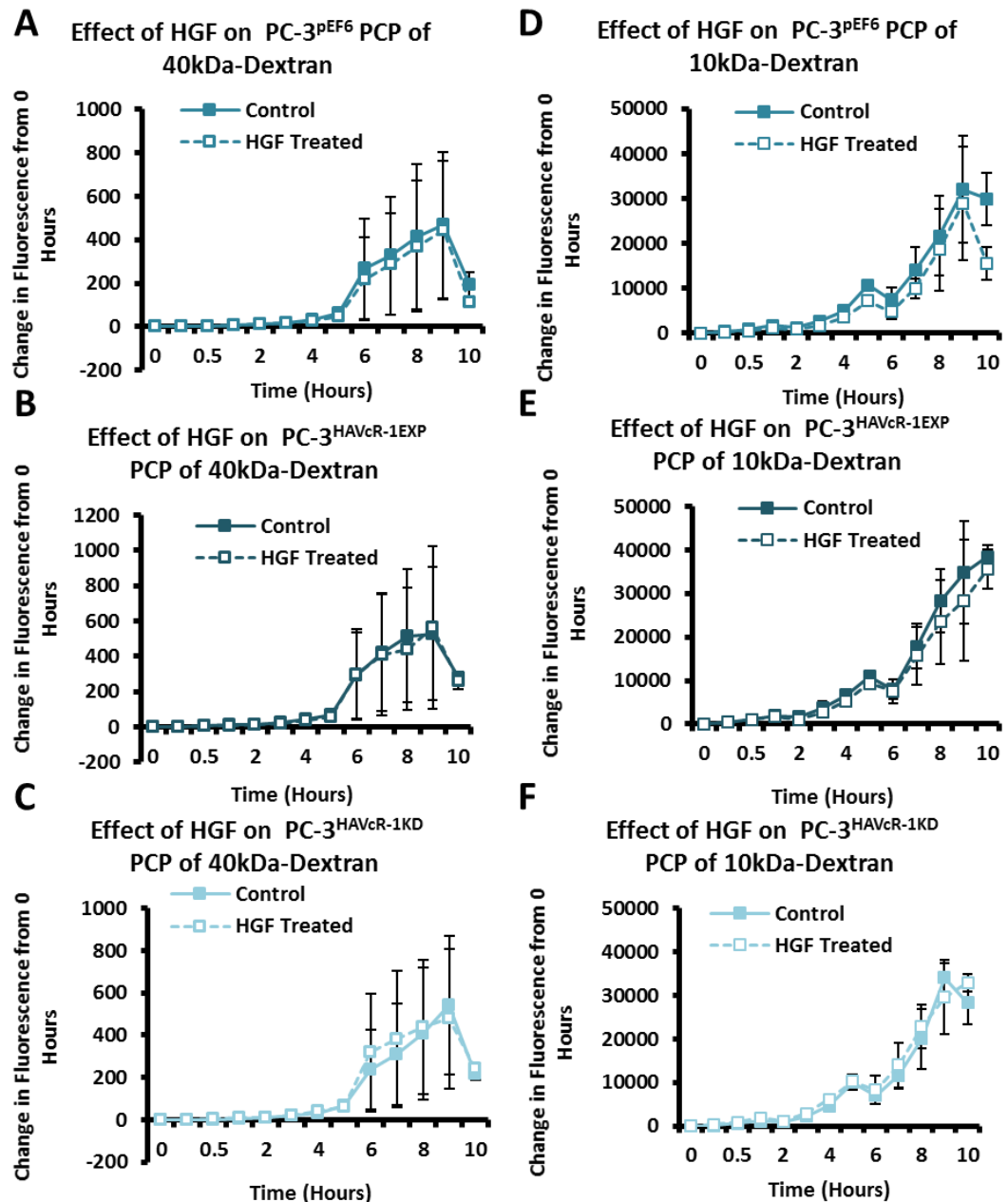
Figure 6.11 The Effect of HGF and HAVcR-1 on PC-3 Paracellular Permeability
Cells seeded in triplicate at 5×10^3 cells per 0.4 µm pore ThinCerts™ 24 well plate insert and incubated until confluent. Once confluent, 40 ng/mL HGF or equal volumes of 0.1 % BSA in PBS alongside 0.2mg/mL of both TRITC-dextran (40 kDa) and FITC-dextran (10 kDa) was added to each insert and samples were taken from outside of the insert to measure fluorescence immediately after and every hour thereafter for 10 Graphs show the means of three independent experiments as fold change relative to fluorescence at 0 hours of **A-C** the 40 kDa FITC-dextan conjugate and **D-F,** the 10 kDa TRITC-dextan conjugate of **A and D**, PC-3^{pEF6}, **B and E**, PC-3$^{HAVcR-1EXP}$ and **C and F**, PC-3$^{HAVcR-1KD}$. Error bars show SEM. Statistical analysis was performed via Mixed ANOVA using IBM SPSS Statistics 24 and significance of $p < 0.05$ was not reached.
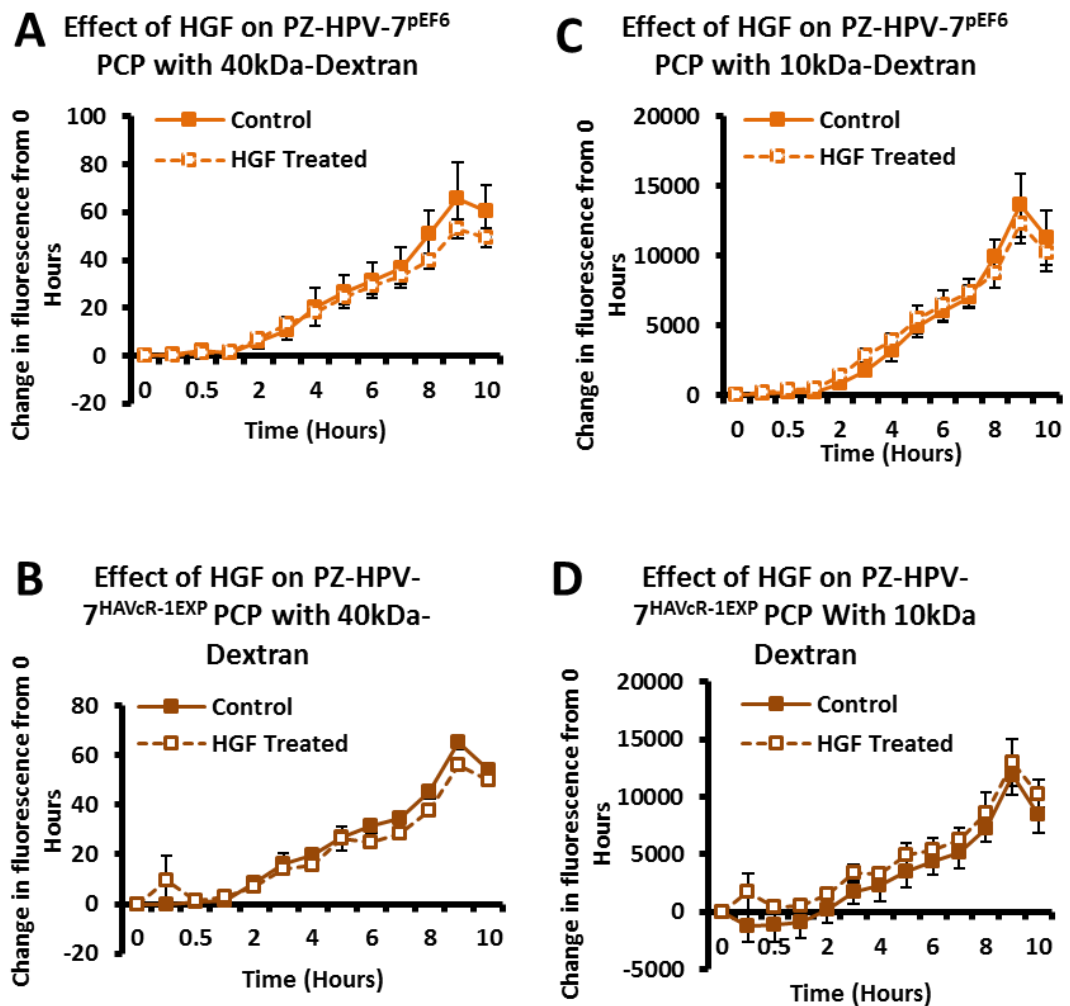
Figure 6.12 The Effect of HGF and HAVcR-1 on PZ-HPV-7 Paracellular Permeability
Cells seeded in triplicate at 5×10^3 cells per 0.4 μm pore ThinCerts™ 24 well plate insert and incubated until confluent. Once confluent, 40 ng/mL HGF or equal volumes of 0.1 % BSA in PBS alongside 0.2mg/mL of both TRITC-dextran (40 kDa) and FITC-dextran (10 kDa) was added to each insert and samples were taken from outside of the insert to measure fluorescence immediately after and every hour thereafter for 10 Graphs show the means of three independent experiments as fold change relative to fluorescence at 0 hours of **A-B** the 40 kDa FITC-dextan conjugate and **C-D,** the 10 kDa TRITC-dextran conjugate of **A and C** PZ-HPV-7^{pEF6} and **B and D**, PZ-HPV-7$^{HAVcR-1EXP}$. Error bars show SEM. Statistical analysis was performed via Mixed ANOVA using IBM SPSS Statistics 24 and significance of $p<0.05$ was not reached.

6.4 Discussion

HGF is known to be important in cancer aetiology. It is able to enhance the aggressiveness of cancer cells by promoting metastatic traits, including: mitogenesis, motogenesis, angiogenesis and morphogenesis [341, 359]. HGF treatment has been shown to increase cell growth of cancer cell lines (ovarian (KGN and HO8910) and prostate (PC-3)), increase cell migration of cancer cell lines (ovarian (HO8910), gastric (MKN1, MKN7 and MKN28) and prostate (PC-3)) and induce changes to cell invasion [90, 93, 94, 98, 360]. However, in contrast to the previous, within this study HGF treatment induced no changes to PC-3 or PZ-HPV-7 cell growth, cell migration or cell invasion. HGF has been extensively studied in prostate cancer and has been shown to have important roles in the progression of the disease [79, 279, 349]. Retrospectively, it is unlikely that these results show that HGF has no effect on these cell behaviours but instead that there were parts of this study that could have been improved. The growth assay utilised involves crystal violet staining of cells and relies on the detachment of dead cells prior to staining. It is therefore possible that the cell numbers are not accurately representing the number of live cells. It may be of more use to perform assays that can differentiate cell viability, such as MTT metabolic proliferation assays [345, 361]. Furthermore, HGF concentration and the HGF receptor c-Met expression were not validated in this study. A concentration of 40 ng/ml had been previously optimised in PC-3 cells and c-Met has been shown to be expressed in both PC-3 and PZ-HPV-7 cell lines [346, 359]. However, it may be of use to further validate this via examination of c-Met expression and phosphorylation post HGF treatment with varying concentrations to improve this study.

It is necessary for cancer cells to alter adhesion to a basement membrane to progress to invasive carcinoma, which in turn is a prerequisite of metastatic cancer [347]. HGF has been previously reported to increase PC-3 cell adhesion, however HGF had no impact on PC-3 cell adhesion in this study and decreased cell adhesion of PZ-HPV-7 [93]. These differences may be due to differences in cell lines PC-3 is a metastatic prostate cancer derived cell line whilst the PZ-HPV-7 cell line is immortalised normal prostate epithelia. HGF concentrations are increased in the prostate stroma with prostate cancer thus it is possible that these increases in HGF lead to changes in cell-ECM adhesion allowing for the process of dissemination of cancer cells from a primary tumour [48, 352]. Although c-Met expression has previously been shown in both PC-3 and PZ-HPV-7 cells, HGF signalling involves a myriad of different signalling proteins, the expression of which can explain the different responses to HGF of these cell lines [341, 359]. Cell to basement membrane interaction alterations are not solely responsible for dissemination, cell-cell interaction alterations are also important. Previous studies had demonstrated a decreased TER as well as decreased TJ protein expression and membrane localisation with HGF treatment, which are indicative of decreased junctional integrity [22, 281, 358]. However, HGF treatment had no impact on TER or PCP in PC-3 and PZ-HPV-7 cell lines and would suggest no changes to junctional integrity. This may further illustrate that HGF concentration requires optimisation.

The main focus of this study was to investigate the effect of HGF and HAVcR-1 on prostate cell line behaviour. It has previously been suggested that there may be a link between HAVcR-1 and HGF signalling in endothelial cells, with knockdown of HAVcR-1 in HECV cells impeding HGF induced decreased TER [340]. However, HGF

treatment of HAVcR-1 overexpression and knockdown cell models resulted in no change to cell growth, cell invasion, TER or PCP. Thus, either suggesting that HAVcR-1 is not linked to the HGF signalling pathways that influence these changes within prostate cancer, or that HGF optimization and different assay selection is required. This includes the utilisation of different growth assays as well as the calculation of apparent permeability coefficient (Papp) in PCP. Furthermore, there is a possibility that investigating cell models separately conceals overall changes thus it may be of benefit to compare HAVcR-1 overexpression and knockdown cell models with the control pEF6 cell models with and without HGF treatment. HGF treatment did however result in increased PZ-HPV-7 cell migration when HAVcR-1 was overexpressed and may support previous literature which propose the expression of HAVcR-1 as important for HGF signalling to occur. HGF treatment having no impact of HAVcR-1 overexpression and knockdown PC-3 cell models further highlights the differences in HGF signalling of PZ-HPV- 7 and PC-3 cells. Furthermore, HGF resulted in increased cell adhesion in the HAVcR-1 knockdown PC-3 cell model and decreased cell adhesion in the HAVcR-1 overexpression PZ-HPV-7 cell model. It is therefore possible that HAVcR-1 has a role in HGF signalling, however it is unclear to the extent of this role or how important this interaction is in prostate cancer development or progression. There is an increase of HGF in the serum and tumour tissues of patients with clinical prostate cancer. This as well as the association of HGF with advanced stage and decreased survival emphasize the importance of HGF in prostate cancer aetiology [342, 343]. Results from this preliminary study have potential shown an involvement of HAVcR-1 in HGF signalling, however, have not provided conclusive evidence of this. Nevertheless, it

would appear that future study into the role HAVcR-1 has in HGF signalling within the context of prostate cancer is worth pursuing. This may provide further insight into disease progression to the lethal metastatic stage and more importantly a potential novel therapeutic target.

Chapter VII:

Final Discussion

7.1 Thesis Aims

Prostate cancer is a significant problem in the UK and due to the high incidence rates can result in a large proportion of people burdened with the disease. Diagnostic testing fails to meet the requirements for effective screening. The lack of understating into disease progression to metastatic disease and the lack of accurate prognostics are major problems, especially when mortality rates significantly worsen in the case of metastatic prostate cancer. Therefore, there is a requirement for novel biomarkers to improve diagnosis and monitoring, prognostic indicators and increased understanding of progression with the hopes of developing therapeutic targets for the treatment or prevention of metastatic prostate cancer.

Therefore, this thesis aimed to assess the expression of HAVcR-1 in prostate cancer and the levels of HAVcR-1 ectodomain with patient serum samples. This thesis utilised overexpression and knockdown prostate cancer cell models to begin to examine understand the role of HAVcR-1 in prostate cancer aetiology. Initial steps have been taken towards investigating HAVcR-1 in the context of prostate cancer however, there are a myriad of unanswered questions that require further investigation and novel research areas that have been identified. The main findings of this study and areas of future study are summarised within the subsequent section.

7.2 The Potential Use of HAVcR-1 in a Clinical Setting for Human Prostate Cancer

7.2.1 HAVcR-1 In Prostate Cancer Diagnostics

Despite innovations and changes in practice, there is still no definitive test for detecting early prostate cancer. This thesis examined the expression profile and potential function of HAVcR-1 in human prostate cancer and demonstrated that the levels of the HAVcR-1 ectodomain in patient serum samples are diminished with prostate cancer. There is therefore an exciting potential for the use of HAVcR-1 in prostate cancer diagnostics and coincides with the current drive towards diagnostic techniques that are accurate but are minimally invasive. The current problems with prostate cancer diagnostic techniques are that they fail to meet both of these requirements. The DRE physical examination and the PSA blood test are minimally invasive however are inherently unreliable. DREs are unreliable due to results being dependent on the experience of the examiner as well as the location of the tumour [89, 91]. The PSA blood test has poor specificity due to PSA being prostate specific and not prostate cancer specific and therefore resulting in 67 % of false positive and 15 % false negatives [32, 33, 89]. Biopsies have numerous potential side effects, some of which are potentially debilitating or life threatening, and can also result in false negatives if the cancer is missed and false positive due to the ambiguity of prostate cells [362-364]. A blood test to identify levels of HAVcR-1 could therefore be used to improve the accuracy of diagnosis whilst enabling low invasive testing and reducing unwanted side effects. However, further research would have to be undertaken to prove the benefit of using HAVcR-1 ectodomain levels in this manner. Firstly,

improved control samples are required with larger n-numbers and that are age matched. Also, this study was retrospective and therefore a prospective study would have to be performed, such as a randomised control trial, to assess the reliability of HAVcR-1 ectodomain levels as a detection method for prostate cancer. Results from which would also have to be compared to the current standards to determine whether using HAVcR-1 ectodomain levels in this manner would be of clinical benefit. This study also didn't assess whether HAVcR-1 ectodomain levels were prostate cancer specific. Serum HAVcR-1 levels have not been assessed in other cancers or diseases thus there is the possibility that HAVcR-1 alone could not be used in the diagnosis of prostate cancer. However, if this is the case there would still be the potential to use HAVcR-1 alongside PSA to improve accuracy.

7.2.2 HAVcR-1 in Prostate Cancer Monitoring

Staging of prostate cancer is currently an issue with Gleason grading of a biopsy often not agreeing with the Gleason grading of the specimen removed via surgery [365]. Thus, this study set out to assess potential correlations in serum HAVcR-1 ectodomain levels and Gleason score, however this revealed that there was no correlation between HAVcR-1 ectodomain levels and prostate cancer Gleason score. Therefore, it is unlikely that HAVcR-1 ectodomain levels could be used to improve prostate cancer staging after diagnosis. However, it is important to note that Gleason grading system is based on the biopsy tissue architecture. Due to the importance of TNM staging in the indication of prognosis, it may be of use to investigate correlations between HAVcR-1 ectodomain levels and anatomic extent of the disease [348]. TNM staging information of serum samples obtained for this study were incomplete and

thus future study would be required to investigate this. It is important to improve prostate cancer staging and prognosis indication, with current studies are highlighting the current over treatment of prostate cancer and this over treatment is resulting in a worse quality of life of men suffering from the disease [82, 86, 88]. Watchful waiting and active surveillance are options to combat this problem whereby prostate cancer is monitored and treatment is given when the disease progresses [332-334]. Further study would assess whether serum HAVcR-1 ectodomain levels could be utilised to identify disease progression and be used to aid in the reduction of unnecessary treatment.

7.3 HAVcR-1 in Prostate Cancer Aetiology

7.3.1 HAVcR-1 and Cancer Cellular behaviour

Cancer development and progression can be characterised by certain hallmarks. These hallmarks include decreased apoptosis, increased proliferation, increased invasion and the alterations in cellular architecture [50]. Cellular architecture is controlled in part by junctional complexes and this study revealed HAVcR-1 potentially regulates AJ integrity. The effect of HAVcR-1 on other cancer hallmarks was also assessed within this study.

This study explored the importance of HAVcR-1 as a regulator of prostate cancer aetiology and cell behaviour and has added to the growing body of research that highlights HAVcR-1 as an important molecule in cell functions in a range of contexts. The involvement of HAVcR-1 on some cancer hallmarks (invasion, adhesion, cellular junctions) within the normal prostate epithelial cell lines (PZ-HPV-7) implicates HAVcR-1 in prostate cancer development. This provides a molecule of interest for

future study and a potential novel target for prostate cancer therapeutics. However, these changes were not replicated in the HAVcR-1 overexpression PC-3 cell model. This may be due to the vast differences between the two cell lines, with PZ-HPV-7 being immortalised normal prostate epithelial and PC-3 being metastatic prostate cancer derived. It is therefore possible that signalling pathways that HAVcR-1 are involved in differ in these cell lines. It is therefore important to identify these pathways to fully understand the differences between these cell lines and provide insight into the impact of HAVcR-1 in clinical prostate cancer.

The effect of HAVcR-1 on junctional complexes in prostate cancer was a major focus of this study. This was due to the importance of intercellular junctions in the process of metastasis in prostate cancer and the cancer specific mortality of metastatic disease. To metastasise epithelial derived cancers most overcome their restricted migratory capability and this is achieved with the loss of cell-cell junctions but also the increase in cell-ECM adhesion molecules [48, 53, 61, 62]. This study provides some evidence that HAVcR-1 has a role in junctional regulation. However, results were conflicting, during attachment and spreading barrier resistance decreased with both HAVcR-1 overexpression and knockdown in PC-3 cells suggesting decreased junctional integrity however other assays suggesting no change in PC-3 junctional integrity. Preliminary investigation suggest HAVcR-1 overexpression decreases PZ-HPV-7 AJ integrity but has no impact on PZ-HPV-7 TJ integrity. There is a possibility that HAVcR-1 is involved in the regulation of junctional integrity and in turn the dissemination of cancer cells from a primary tumour. HAVcR-1 has been shown important in the junctional regulation of endothelial cells with overexpression decreasing junctional integrity [340]. This also proposes the involvement of HAVcR-1

296

in cancer cell intravasation and extravasation. Due to these processes being critical in the metastatic process further investigations into the importance of HAVcR-1 in the regulation of junctional complexes as this study proposes HAVcR-1 as a potential novel target in the prevention of prostate cancer metastasis. Therefore, future study would also investigate the effect of HAVcR-1 inhibitors in prostate cancer and the effect of these on junctional integrity to assess the potential use of these in the prevention of metastasis.

7.3.2 HAVcR-1 and EMT

The dynamic transition between epithelial and mesenchymal states is essential during embryonic development. The shift towards the mesenchymal state termed EMT involves the loss of apico-basal polarity and the modification of cell adhesion resulting in migratory as well as invasive cellular behaviour [366]. These cellular behaviours are also important in tumorigenesis with EMT triggering dissociation of cancer cells from primary tumours and metastasis [366, 367]. EMT is initiated by multiple signalling pathways including that of HGF, EGF and Wnt [368]. These signalling pathways induce the expression of specific EMT transcription factor (EMT-TF) such as Snail, Zeb and Twist, miRNAs, epigenetic regulators and post-translational regulators [366].

Although the activation of EMT can differ, pathways generally converge at decreased E-cadherin at the plasma membrane and this is achieved by multiple mechanisms including the repression of transcription, promotion of endocytosis and the inhibition of transportation to the plasma membrane [368-370]. This loss of membranous E-cadherin is a fundamental event in EMT [368]. E-cadherin loss from the plasma

membrane is frequent in human cancer and it is considered crucial in the progression from adenoma to carcinoma [203]. Within this study the overexpression of HAVcR-1 in PZ-HPV-7 cells resulted in decreased membranous E-cadherin and therefore suggests that HAVcR-1 wasable to regulate EMT. HAVcR-1 has been shown to be overexpressed in numerous cancers and this could, at least in part, explain the loss of E-cadherin within the majority of cancer as well as proposing HAVcR-1 as an important protein in the switch from benign to malignant tumours [203, 283, 319, 320, 371]. Furthermore, the loss of E-cadherin promotes metastasis and therefore links HAVcR-1 to the progression of prostate cancer to a metastatic state [372].

HAVcR-1 overexpression in PZ-HPV-7 cells was also shown to potentially induce β-catenin Y333 phosphorylation and nuclear accumulation. Phosphorylation at this site is indicative of EGF signalling and membranous E-cadherin can be destabilised by phosphorylation of β-catenin [354, 373]. It is therefore possible that HAVcR-1 activates the EGF pathway resulting in the phosphorylation of β-catenin and this destabilizes and decreases membranous E-cadherin. This would explain why there were no significant changes in expression of E-cadherin with HAVcR-1 overexpression in PZ-HPV-7. Furthermore, it has been predicted that EGFR and HAVcR-1 could interact and thus there is a possibility that HAVcR-1 could directly activate EGFR, however further study would have to be undertaken to assess this such as an immunoprecipitation assay [374]. Further validation of β-catenin Y333 phosphorylation is also required via western blotting as there is a possibility of Kinex™ antibody microarray providing both false positives and negatives.

Other hallmarks of EMT include the increase in mesenchymal markers including N-cadherin and vimentin [151, 180]. Expression levels were not assessed within this

study and would therefore be of interest in the future. However, the Kinex™ antibody microarray revealed a significant decrease in vimentin s33 phosphorylation with HAVcR-1 overexpression. Phosphorylation and dephosphorylation of vimentin is crucial in its role in growth and motility and therefore there is the potential HAVcR-1 may have a role in integrin regulation and motility [375]. This is supported by HAVcR-1 altering adhesion of PZ-HPV-7 cells however contrary to HAVcR-1 having no impact on wound healing. Therefore, it may be of use to further investigation the impact of HAVcR-1 overexpression on vimentin phosphorylation.

EMT enables the degradation of the underlying basement membrane and the formation of a mesenchymal cells that has the ability to migrate away from the epithelium in which it originated [376]. Therefore cells that undergo EMT are more motile and invasive and these cellular behaviours are vital for metastasis to occur [180, 366, 377]. PZ-HPV-7 cells that had forced HAVcR-1 overexpression were more invasive and therefore support the theory that HAVcR-1 is involved in EMT. However, contradictory to this HAVcR-1 decreased PZ-HPV-7 motility EMT also involves the loss of cell-cell junctions, including AJs and TJs [378]. E-cadherin is the main transmembrane adhesion protein in AJs [134]. The loss of E-cadherin from PZ-HPV-7 cell membranes with HAVcR-1 overexpression is therefore indicative of decreased AJ integrity. However, there was no indication that HAVcR-1 had any impact on TJ stability in PZ-HPV-7 cells.

EMT has been linked to prostate cancer metastatic progression which is important due to the majority of prostate cancer associated morbidity being due to metastasis [379]. EMT may therefore be the differentiator between low-risk and high-risk prostate cancer. This study has potentially linked HAVcR-1 to EMT and due to the

importance of EMT and prostate cancer, it would be of interest to investigate this further.

7.3.3 HAVcR-1 in HGF Signalling

HGF has been proposed to be important in prostate cancer development and progression with treatment decreasing TER and increasing proliferation and scattering [279, 281]. A preliminary study using endothelial cells revealed a potential link between HAVcR-1 and HGF signalling thus this study hypothesised that HAVcR-1 expression was important for HGF induced junctional breakdown [143]. However, the results within this study did not confer with the literature and would therefore suggest problems with this study and thus validation of optimum HGF concentrations should be performed before further investigations of the potential links between HAVcR-1 and HGF signalling in prostate cancer aetiology.

7.4 Future Work

7.4.1 HAVcR-1 Signalling

This study has proposed a novel link between HAVcR-1 and EGF signalling within prostate cancer cells and may act to regulate EMT in prostate cancer. This highlights a new area of research to be pursued. How HAVcR-1 activates EGF signalling is yet to be addressed. There is a predicted interaction between HAVcR-1 and EGFR [374]. Thus, it would be of interest to assess if HAVcR-1 can interact and activate EGFR. It would also be of interest to assess inhibitors of HAVcR-1 in relation to EGF signalling in prostate cancer cells. As well as assessing whether inhibitors of EGFR affect HAVcR-1 overexpression induced changes to prostate cancer cells. These questions have not

been addressed in this study, however would be of interest in the future to elucidate a broader picture of signalling cascades that HAVcR-1 is involved in within prostate cancer.

7.4.2 HAVcR-1 in the Urine

This study investigated the levels of HAVcR-1 ectodomain within patient, however it would also of interest to investigate levels of the HAVcR-1 ectodomain secreted into the urine of prostate cancer patients. Urinary HAVcR-1 ectodomain levels have been showed to be increased in prostate cancer but there has at this time been no studies that have investigated the potential use of this is a clinical setting [315]. Furthermore, potential links between urinary HAVcR-1 levels and stage and prognosis have not been investigated. The development of the RenaStick™, a lateral flow detection system for urinary HAVcR-1, opens up the possibility for a non-invasive diagnostic and/or monitoring technique for prostate cancer [307].

7.4.3 HAVcR-1 as a Therapeutic Target

Inhibitors of HAVcR-1 have been created however were not tested within this study. Due to cell behavioural changes induced by HAVcR-1 and the involvement of HAVcR-1 in signalling pathways which have been linked to prostate cancer development and progression it is of interest to investigate HAVcR-1 as a novel target for the development of prostate cancer therapies. Furthermore, the identification that HAVcR-1 is overexpressed in prostate cancer proposes the potential use of an antibody-drug conjugated in the treatment of prostate cancer. This includes the CDX-014 ADC that is in phase I and II clinical trials for advanced or metastatic renal carcinoma [338]. This could have significant benefit in the treatment of metastatic

prostate cancer with current treatment, although initially effective, result in resistance and disease progression within 12-18 months [28, 37, 39].

7.4.4 HAVcR-1 as a Prognostic Indicator

This study did not assess HAVcR-1 levels or HAVcR-1 ectodomain levels and prostate cancer prognosis. However, did show that HAVcR-1 expression is increased in prostate cancer and investigated the effects of HAVcR-1 overexpression in the immortalised normal prostate epithelial cell line, PZ-HPV-7. HAVcR-1 was shown to decrease membranous E-cadherin and increase nuclear β-catenin both of which are indicative of EMT. With more aggressive prostate cancer cell lines E-cadherin expression is decreased and this decrease is associated with cancer grade, cancer progression and cancer specific death [5, 209, 351, 352]. Furthermore, increased nuclear β-catenin is found in aggressive prostate cancer and has been associated with poorly differentiated and highly proliferative tumours with increased vascular invasion [6, 7, 353]. Due to cell that undergo EMT being more likely to metastasise and the metastatic disease being responsible for 90 % of cancer specific death there is a potential link between HAVcR-1 and a worse prognosis [49, 209, 349]. This link is strengthened by PZ-HPV-7 cells that overexpress HAVcR-1 being more invasive and invasion being a hallmark of malignancy and a prerequisite for cancer metastasis [356].

The use of HAVcR-1 as an indicator of prostate cancer prognosis could have a great clinical benefit. Currently there is no way of differentiating low-risk and high-risk prostate cancer. This leads to under treatment of high-risk prostate cancer and an overtreatment of low-risk prostate cancer. Both of which are equally significant due

to the under treatment of high-risk prostate cancer potentially resulting in an increased mortality and overtreatment of low-risk prostate cancer potentially resulting in an increased morbidity [86]. Therefore, there may be benefit in further research to investigate the use of HAVcR-1 as a prognostic factor.

7.5 Final Conclusions

In summary, this study has shown that serum levels of the HAVcR-1 ectodomain are varied in prostate cancer and therefore identifies a novel area of study in prostate cancer diagnosis. Future study would assess the potential benefits of using serum levels in blood tests in a clinical setting as well as evaluating the variations in signalling pathways resulting in the release in HAVcR-1 from prostate cancer cells.

This work has also demonstrated that HAVcR-1 has the capacity to alter cell behaviour to promote phenotypes associated with cancer and cancer metastasis. Potential signalling pathways affected by HAVcR-1 have been identified. Future study is necessary to investigate the effect of HAVcR-1 inhibitors on HAVcR-1 induced cell behavioural changes and signalling pathways activity. Subsequently, this would assess the potential of HAVcR-1 inhibition as a treatment of prostate cancer and/or prevention of metastatic disease.

Chapter VIII:

Appendix

Table 8.1 Prostate Cancer Serum Sample Patient Information

WCB Number	Gleason Score	Tissue	Operation Date	Age at Collection	PSA	TNM Stage			Alive	Diead of Cancer
RWMBV0000009	3+3=6	Prostate	23/06/2005	66		T2	NX	MX	Yes	
RWMBV0000011	3+3=6	Prostate	24/06/2005	62		T2	NX	MX	Yes	
RWMBV0000021	3+3=6	Prostate	20/07/2005	69		T2	N0	MX	Yes	
RWMBV0000028	3+3=6	Prostate	18/08/2005	70		T2	N0	M0	Yes	
RWMBV0000030	3+3=6	Prostate	11/08/2005	62		T2	N0	M0	No	
RWMBV0000035	3+3=6	Prostate	16/09/2005	66		T2			Yes	
RWMBV0000046	3+3=6	Prostate	13/10/2005	57		T2	N0	M0	Yes	
RWMBV0000047	3+3=6	Prostate	20/10/2005	69		T2	N0	M0	Yes	
RWMBV0000065	3+3=6	Prostate	07/12/2006	64		T2	N0	M0	Yes	
RWMBV0000067	3+3=6	Prostate	15/12/2006	62		T2b			Yes	
RWMBV0000068	3+3=6	Prostate	22/12/2005	69		T2			Yes	
RWMBV0000081	3+3=6	Prostate	26/01/2006	60		T2	N0	M0	Yes	
RWMBV0000083	3+3=6	Prostate	03/02/2006	67		T2	NX	MX	Yes	
RWMBV0000095	3+3=6	Prostate	03/03/2006	63		T3a			Yes	
RWMBV0000097	3+3=6	Prostate	16/03/2006	60		T2			Yes	
RWMBV0000113	3+3=6	Prostate	04/05/2006	65		T3a			Yes	
RWMBV0000142	3+3=6	Prostate	11/01/2007	48		T2	NX	MX	Yes	
RWMBV0000155	3+3=6	Prostate	07/12/2006	58		T2	NX	MX	Yes	
RWMBV0000310	3+3=6	Prostate	22/10/2007	58		T2	NX	MX	Yes	
RWMBV0000384	3+3=6	Prostate	20/03/2008	67		T3a	N0	MX	No	
RWMBV0000552	3+3=6	Prostate	05/12/2008	59		T2	N0	MX	Yes	
RWMBV0000811	3+3=6	Prostate	03/03/2010	68		T2			Yes	
RWMBV0000827	3+3=6	Prostate	09/05/2010	69		T2			Yes	
RWMBV0000863	3+3=6	Prostate	13/08/2010	58		T3a	N0	MX	Yes	
RWMBV0000870	3+3=6	Prostate	18/11/2010	62		T2	NX		Yes	
RWMBV0000908	3+3=6	Prostate	17/12/2010	67		T1c	N0		Yes	
RWMBV0001115	3+3=6	Prostate	13/07/2011	64		T2	N0	M0	Yes	
RWMBV0001395	3+3=6	Prostate	04/01/2012	57		T1c			Yes	
RWMBV0001607	3+3=6	Prostate	04/04/2012	66		T3a	NX	M0	Yes	

RWMBV0001632	3+3=6	Prostate	19/04/2012	49	T2b	N0	M0	Yes	
RWMBV0001647	3+3=6	Prostate	23/05/2012	70	T2	NX	MX	Yes	
RWMBV0001689	3+3=6	Prostate	24/08/2012	47				Yes	
RWMBV0002081	3+3=6	Prostate	22/01/2013	73	T3a	N0	M0	Yes	
RWMBV0002095	3+3=6	Prostate	01/02/2013	64	T2a	N0	M0	Yes	
RWMBV0002520	3+3=6	Prostate	01/03/2013	51				Yes	
RWMBV0002585	3+3=6	Prostate	24/10/2013	57				Yes	
RWMBV0003339	3+3=6	Prostate	26/03/2014	61				Yes	
RWMBV0003370	3+3=6	Prostate	14/05/2014	73				Yes	
RWMBV0003392	3+3=6	Prostate	02/10/2014	59				Yes	
RWMBV0003397	3+3=6	Prostate	02/10/2014	65				Yes	
RWMBV0003398	3+3=6	Prostate	09/10/2014	58				Yes	
RWMBV0003399	3+3=6	Prostate	08/10/2014	71				Yes	
RWMBV0004204	3+3=6	Prostate	16/10/2014	67					
RWMBV0004236	3+3=6	Prostate	07/01/2015	71					
RWMBV0004247	3+3=6	Prostate	25/02/2015	67					
RWMBV0000017	4+3=7	Prostate	08/07/2005	66	T2	NX	MX	Yes	
RWMBV0000022	3+4=7	Prostate	20/07/2005	64	T3b	N0	M0	Yes	
RWMBV0000034	3+4=7	Prostate	15/09/2005	70	T3a	N0	M0	No	
RWMBV0000036	4+3=7	Prostate	16/09/2005	67				Yes	
RWMBV0000038	3+4=7	Prostate	22/09/2005	50	T3a	N0	MX	Yes	
RWMBV0000041	4+3=7	Prostate	29/09/2005	65	T2			Yes	
RWMBV0000043	3+4=7	Prostate	06/10/2005	63	T1			Yes	
RWMBV0000045	4+3=7	Prostate	13/10/2005	63	T3a	N0	M0	Yes	
RWMBV0000061	3+4=7	Prostate	10/11/2005	73	T2	N0	M0	Yes	
RWMBV0000080	3+4=7	Prostate	19/01/2006	57	T3a			Yes	
RWMBV0000093	3+4=7	Prostate	03/03/2006	70	T3	NX	M0	Yes	
RWMBV0000112	3+4=7	Prostate	27/04/2006	71	T3a				
RWMBV0000119	3+4=7	Prostate	08/06/2006	58	T3b	N0		Yes	
RWMBV0000121	3+4=7	Prostate	23/06/2006	61	T3a	N0	MX	Yes	
RWMBV0000248	3+4=7	Prostate	27/04/2007	51	T3b			Yes	
RWMBV0000348	3+4=7	Prostate	12/12/2007	68	T3b	N0	MX	Yes	

RWMBV0000363	7	Prostate	19/12/2007	67	T3	NX	M0	Yes
RWMBV0000374	4+3=7	Prostate	31/01/2008	61	T2	N0	M0	Yes
RWMBV0000376	4+3=7	Prostate	13/02/2008	66	T3a	N0	MX	Yes
RWMBV0000412	3+4=7	Prostate	11/04/2008	61	T3	N0	M0	Yes
RWMBV0000502	4+3=7	Prostate	15/10/2008	65	T3a	N0		Yes
RWMBV0000792	3+4=7	Prostate	21/01/2010	46	T3a	N0	M0	Yes
RWMBV0000815	4+3=7	Prostate	04/03/2010	69	T3a			Yes
RWMBV0000829	3+4=7	Prostate	07/04/2010	65	T3a	N0		Yes
RWMBV0000837	3+4=7	Prostate	21/04/2010	54	T2	N0		Yes
RWMBV0000838	4+3=7	Prostate	28/04/2010	56	T3a		MX	Yes
RWMBV0000862	4+3=7	Prostate	11/08/2010	65	T2	N0		Yes
RWMBV0000874	3+4=7	Prostate	10/09/2010	50	T2			Yes
RWMBV0000875	3+4=7	Prostate	29/09/2010	67	T3a	N0	M0	
RWMBV0000890	4+3=7	Prostate	20/10/2010	74	T3a	N0		
RWMBV0000892	4+3=7	Prostate	20/10/2010	65	T3b	N0		Yes
RWMBV0000907	4+3=7	Prostate	06/01/2011	67	T3a			Yes
RWMBV0000949	3+4=7	Prostate	07/04/2011	66	T3a			Yes
RWMBV0001035	3+4=7	Prostate	05/05/2011	67	T2	N0		Yes
RWMBV0001042	3+4=7	Prostate	12/05/2011	64	T3a	N0	M0	Yes
RWMBV0001133	3+4=7	Prostate	07/07/2011	59	T3a	N0	MX	Yes
RWMBV0001154	3+4=7	Prostate	18/08/2011	55	T2	N0	M0	
RWMBV0001161	4+3=7	Prostate	28/09/2011	53	T2	NX	MX	Yes
RWMBV0001174	3+4=7	Prostate	30/09/2011	54				Yes
RWMBV0001359	4+3=7	Prostate	19/10/2011	61	T3a		MX	Yes
RWMBV0001366	4+3=7	Prostate	21/11/2011	65	T3a	NX	MX	Yes
RWMBV0001377	4+3=7	Prostate	24/11/2011	68	T2	N0	M0	Yes
RWMBV0001388	3+4=7	Prostate	02/02/2012	64	T2	N0	M0	Yes
RWMBV0001610	4+3=7	Prostate	04/04/2012	68	T2a	NX	MX	Yes
RWMBV0001616	3+4=7	Prostate	21/03/2012	63	T3a	NX	MX	Yes
RWMBV0001618	3+4=7	Prostate	13/06/2012	54	T3b	N0	M0	Yes
RWMBV0001626	3+4=7	Prostate	16/03/2012	63	T2	N0	M0	Yes
RWMBV0001628	3+4=7	Prostate	29/02/2012	60				Yes

RWMBV0001634	3+4=7	Prostate	19/07/2012	60				Yes
RWMBV0001645	3+4=7	Prostate	21/06/2012	54				Yes
RWMBV0001648	4+3=7	Prostate	30/05/2012	70				Yes
RWMBV0001664	3+4=7	Prostate	19/07/2012	72				Yes
RWMBV0002061	3+4=7	Prostate	17/10/2012	72				Yes
RWMBV0002062	3+4=7	Prostate	08/11/2012	71	T2	N0	M0	Yes
RWMBV0002080	3+4=7	Prostate	31/10/2012	65				Yes
RWMBV0002084	4+3=7	Prostate	07/12/2012	66				Yes
RWMBV0002097	4+3=7	Prostate	06/02/2013	55	T3a	N0	M0	Yes
RWMBV0002512	3+4=7	Prostate	15/02/2013	59	T3b	N0	M0	Yes
RWMBV0002516	3+4=7	Prostate	07/03/2013	60				Yes
RWMBV0002535	3+4=7	Prostate	03/04/2013	68				Yes
RWMBV0002537	3+4=7	Prostate	03/04/2013	60				Yes
RWMBV0002560	3+4=7	Prostate	15/05/2013	71	T3a	N0	MX	Yes
RWMBV0002570	3+4=7	Prostate	20/06/2013	70	T3a	N0	MX	Yes
RWMBV0002586	4+3=7	Prostate	28/08/2013	67	T3a		MX	Yes
RWMBV0002596	3+4=7	Prostate	15/07/2013	53	T2	N0	M0	Yes
RWMBV0003303	4+3=7	Prostate	30/10/2013	58				Yes
RWMBV0003330	3+4=7	Prostate	22/01/2014	59				Yes
RWMBV0003335	3+4=7	Prostate	13/03/2014	75				Yes
RWMBV0003337	3+4=7	Prostate	21/03/2014	62				Yes
RWMBV0003340	3+4=7	Prostate	27/03/2014	63				Yes
RWMBV0003344	3+4=7	Prostate	27/03/2014	70				Yes
RWMBV0003348	3+4=7	Prostate	09/04/2014	55				Yes
RWMBV0003352	3+4=7	Prostate	09/04/2014	70				Yes
RWMBV0003359	3+4=7	Prostate	17/07/2014	72				Yes
RWMBV0003361	3+4=7	Prostate	17/07/2014	62				Yes
RWMBV0003365	3+4=7	Prostate	11/06/2014	69				Yes
RWMBV0003367	3+4=7	Prostate	23/05/2014	62				Yes
RWMBV0003371	3+4=7	Prostate	11/07/2014	69				Yes
RWMBV0003372	3+4=7	Prostate	03/07/2014	62				Yes
RWMBV0003377	3+4=7	Prostate	23/07/2014	64				Yes

ID	Gleason	Site	Date	Age	PSA	T	N	M	Outcome	Status
RWMBV0003379	3+4=7	Prostate	20/08/2014	71					Yes	
RWMBV0003384	3+4=7	Prostate	28/08/2014	75					Yes	
RWMBV0003385	3+4=7	Prostate	28/08/2014	64					Yes	
RWMBV0003395	3+4=7	Prostate	25/09/2014	55					Yes	
RWMBV0004200	3+4=7	Prostate	09/10/2014	63					Yes	
RWMBV0004221	4+3=7	Prostate	10/12/2014	67						
RWMBV0004222	3+4=7	Prostate	04/12/2014	69						
RWMBV0004225	3+4=7	Prostate	02/01/2015	65						
RWMBV0004235	3+4=7	Prostate	09/01/2015	67						
RWMBV0004241	3+4=7	Prostate	28/01/2015	61						
RWMBV0004251	3+4=7	Prostate	11/03/2015	58						
RT7AU0000397	3+5=8	Prostate	08/03/2010	66	6.7	T2b	NX		Yes	
RT7AU0000415	3+5=8	Prostate	10/05/2010	71	11.7		NX	MX	Yes	
RT7AU0000471	4+4=8	Prostate	13/09/2010	66	0.5	T2c	NX	MX	Yes	
RT7AU0000600	4+4=8	Prostate	12/03/2012	62	7.9	T3a	NX	MX	Yes	
RT7AU0000634	4+4=8	Prostate	23/04/2012	78	12.8	T3a	NX	MX	Yes	
RT7AU0000648	3+5=8	Prostate	21/05/2012	61	24	T2c	NX	MX	Yes	
RVCC40000278	8	Prostate	24/04/2006	65	7.1	T3a	N0	MX	Yes	
RVCC40000361	4+4=8	Prostate	11/07/2006	48	3.4	T2c	N0	MX	Yes	
RVCC40000377	3+5=8	Prostate	07/08/2006	59	4.7	T3			Yes	
RVCC40000564	4+4=8	Prostate	26/02/2007	67	8.5				Yes	
RVCC40000607	4+4=8	Prostate	27/03/2007	66	8.9	T3	N0	MX	Yes	
RVCC40000746	4+4=8	Prostate	06/08/2007	67	12	T2a	N0	MX	Yes	
RVCC40001023	8	Prostate	19/05/2008	71	6				Yes	
RVCC40001153	3+5=8	Prostate	11/11/2008	58	8.2				No	Unknown
RVCC40001319	4+4=8	Prostate	26/05/2009	63	7	T2c	N0	MX	Yes	
RVCC40001535	4+4=8	Prostate	23/02/2010	60	1.5	T3b	NX	MX	Yes	
RVCC40002387	4+4=8	Prostate	09/01/2012	69	10.1	T3a	N0	MX	Yes	
RVCC40002576	4+4=8	Prostate	24/07/2012	68	9	T3b	N0	MX	Yes	
RVCC40002590	4+4=8	Prostate	21/08/2012	64	6.9	T3a	N0	MX	Yes	
RVCC40002711	4+4=8	Prostate	10/09/2012	55	10.9	T3a	N0	M0	Yes	
RVCC40002723	4+4=8	Prostate	16/10/2012	69	10.3	T3b	N0	MX	Yes	

RVFAR0000124	3+5=8	Prostate	19/02/2008	61	14.2	T2a	N0	MX	Yes	
RVFAR0000234	8	Prostate	15/09/2009	57	7.4	T3a	N0	MX	Yes	
RVFAR0000294	3+5=8	Prostate	14/04/2010	54	3.9	T3	N0	MX	Yes	
RVFAR0000325	4+4=8	Prostate	29/07/2010	68	17.9	T3b	N0	MX	Yes	
RVFAR0000337	5+3=8	Prostate	15/09/2010	61	34.8	T3b	N0	MX	Yes	
RVFAR0000350	4+4=8	Prostate	14/10/2010	59	10.4	T3b	N0	MX	Yes	
RVFAR0000365	3+5=8	Prostate	04/11/2010	55	14	T3b	N0	MX	No	Yes
RVFAR0000393	4+4=8	Prostate	06/01/2011	61	6	T3b	N0	MX	Yes	
RVFAR0000399	5+3=8	Prostate	26/01/2011	60	11.3	T2	N0	MX	Yes	
RVFAR0000456	4+4=8	Prostate	18/05/2011	68	8.2	T2	N0	MX	Yes	
RVFAR0000474	5+3=8	Prostate	21/06/2011	65	6.4	T3b	N0	MX	Yes	
RVFAR0000476	3+5=8	Prostate	14/07/2011	52	9.7	T2	NX	MX	Yes	
RVFAR0000629	3+5=8	Prostate	09/05/2012	68	8.5	T2	N0	MX	Yes	
RVFAR0000645	5+3=8	Prostate	06/06/2012	57	9.1	T3	N0	MX	Yes	
RVFAR0000692	4+4=8	Prostate	15/08/2012	63	5.7	T3	N0	M0	Yes	
RVFAR0000728	4+4=8	Prostate	03/10/2012	65	17.7	T3	N0	M0	Yes	
RVFAR0000801	3+5=8	Prostate	17/01/2013	71	19.5	T2	N0	MX	Yes	
RWMBV0000062	3+5=8	Prostate	08/11/2005	78	96.3	T3	NX	M1	No	Yes
RWMBV0000120	3+5=8	Prostate	21/06/2006	68	8.2	T3a	N0	MX	Yes	
RWMBV0000272	4+4=8	Prostate	13/09/2007	61	8.5	T2	N0	MX	Yes	
RWMBV0000311	4+4=8	Prostate	19/10/2007	88	56.1	T4	NX	M0	No	Yes
RWMBV0000387	4+4=8	Prostate	15/07/2008	82	48.2	T4	NX	M0	No	No
RWMBV0001163	4+4=8	Prostate	15/09/2011	65		T2	N0	MX	Yes	
RWMBV0001370	4+4=8	Prostate	29/12/2011	61	3.6	T3b	N1	M0	Yes	
RWMBV0003331	3+5=8	Prostate	24/02/2014	66					Yes	
RWMBV0003336	4+4=8	Prostate	21/03/2014	52					Yes	
RT7AU0000417	5+4=9	Prostate	27/09/2010	76	35.9	T3b	NX	MX	No	Yes
RT7AU0000461	4+5=9	Prostate	06/09/2010	43	23.1	T3b	N1	MX	Yes	
RVCC40000650	4+5=9	Prostate	17/07/2007	56	18	T3a	N0	MX	Yes	
RVCC40001030	9	Prostate	11/06/2008	63	13.4				Yes	
RVCC40001180	4+5=9	Prostate	10/11/2008	53	5.1	T3a	N0	MX	Yes	
RVCC40001644	4+5=9	Prostate	08/06/2010	67	0.5	T3a	N0	MX	No	Yes

RVCC40002286	4+5=9	Prostate	29/10/2011	67	19	T3a	N0	MX	Yes	
RVFAR0000139	4+5=9	Prostate	21/05/2008	62	8.2	TX	NX	MX	No	Yes
RVFAR0000146	9	Prostate	11/06/2008	64	5.8	T3b	N0	MX	No	
RVFAR0000156	4+5=9	Prostate	29/07/2008	61	14.7	T2c	N0	MX	Yes	
RVFAR0000158	4+5=9	Prostate	05/08/2008	65	12.3	T3a	N0	MX	Yes	
RVFAR0000191	5+4=9	Prostate	03/03/2009	58	20.9	TX	NX	MX	Yes	
RVFAR0000209	5+4=9	Prostate	09/06/2009	57	8	T3b	N1	MX	Yes	
RVFAR0000210	4+5=9	Prostate	17/06/2009	61	8.9	T3b	N0	MX	Yes	
RVFAR0000305	4+5=9	Prostate	19/05/2010	67	7.9	T3	N0	MX	Yes	
RVFAR0000308	4+5=9	Prostate	26/05/2010	51	4.5	T2	N0	MX	Yes	
RVFAR0000309	4+5=9	Prostate	25/05/2010	61	24.7	T3b	N1	MX	Yes	
RVFAR0000318	4+5=9	Prostate	08/07/2010	65	7.9	T3b	N0	MX	Yes	
RVFAR0000427	4+5=9	Prostate	10/03/2011	59	14	T3a	N0	MX	Yes	
RVFAR0000451	5+4=9	Prostate	05/05/2011	70	5.2	T3	N0	M0	No	No
RVFAR0000468	4+5=9	Prostate	02/06/2011	67	20	T3b	N0	MX	Yes	
RVFAR0000509	4+5=9	Prostate	06/10/2011	69	8.6	T3	N0	MX	Yes	
RVFAR0000513	4+5=9	Prostate	26/10/2011	64	18.1	T3a	N1	MX	Yes	
RVFAR0000517	4+5=9	Prostate	20/10/2011	65	13.8	T3	N0	MX	Yes	
RVFAR0000523	4+5=9	Prostate	22/11/2011	66	2.9	T2	N1	MX	Yes	
RVFAR0000610	4+5=9	Prostate	04/04/2012	66	6.3	T3	N0	MX	Yes	
RVFAR0000640	4+5=9	Prostate	31/05/2012	68	6.5	T3	N0	M0	Yes	
RVFAR0000650	4+5=9	Prostate	21/06/2012	66	12.5	T3	N1	M0	Yes	
RVFAR0000712	4+5=9	Prostate	05/09/2012	68	9.3	T3a	N0	MX	Yes	
RVFAR0000752	4+5=9	Prostate	28/11/2012	61	12.8	T3a	N0	M0	Yes	
RVFAR0000809	4+5=9	Prostate	16/01/2013	58	18.5	T3b	N0	M0	Yes	
RVFAR0000822	5+4=9	Prostate	12/02/2013	54	11.5	T3	N1	MX	Yes	
RWMBV0000312	9	Prostate	23/03/2010	69	86	T4	NX	M1		Yes
RWMBV0000472	4+5=9	Prostate	17/07/2008	55	9.7	T3a	N0	MX	Yes	
RWMBV0000774	4+5=9	Prostate	03/12/2009	73		T2			Yes	
RWMBV0000844	4+5=9	Prostate	03/02/2011	73	8.5	T2b	N0	MX	No	Yes
RWMBV0000944	4+5=9	Prostate	29/03/2011	80		T3b	N0	M0	No	
RWMBV0001074	4+5=9	Prostate	19/05/2011	86	66.4	T2b	N0	M0	Yes	

RWMBV0001617	4+5=9	Prostate	23/03/2012	75	48.5	T3b	N1	M1	Yes	
RWMBV0001644	4+5=9	Prostate	16/05/2012	67	221.5	T4	NX	M1	Yes	
RWMBV0001659	5+4=9	Prostate	11/05/2012	67	23	T3b	N0	M0	Yes	
RWMBV0001674	5+4=9	Prostate	04/07/2012	73	50	T3b	N0	M0	Yes	
RWMBV0001694	4+5=9	Prostate	13/09/2012	53		T2a	N0	M0	Yes	
RWMBV0001699	4+5=9	Prostate	07/09/2012	83	20.6	T4	N1	M1	Yes	
RWMBV0002065	4+5=9	Prostate	07/09/2012	80	50.2	T3b	NX	M1	No	Yes
RWMBV0003356	4+5=9	Prostate	30/04/2014	51					Yes	
RWMBV0003357	4+5=9	Prostate	24/04/2014	68					Yes	
RVFAR0000303	5+5=10	Prostate	12/05/2010	55	9.8	T4	N1	MX	Yes	
RVFAR0000347	5+5=10	Prostate	30/09/2010	57	13.4	T3	N1	MX	No	Yes
RWMBV0000853	5+5=10	Prostate	08/07/2010	84		T3	N0	M0	No	
RWMBV0002551	5+5=10	Prostate	18/03/2013	85	74.6	T4	N0	MX	No	Yes
RWMBV0004284	3+7=10	Prostate	17/06/2015	66	4.7	T2	N0	MX		

Chapter IX:

References

1. Seeley, S.a.T., *Anatomy and Physiology*. 2nd ed. 1992, USA: Mosby.
2. Evans, C.P., *Prostate Cancer*, in *eLS*. 2001, John Wiley & Sons, Ltd.
3. Cunha, G.R., et al., *The endocrinology and developmental biology of the prostate.* Endocr Rev, 1987. **8**(3): p. 338-62.
4. Prostate.Cancer.UK. *Understading the prostate gland*. 2013 18/11/14]; Available from: http://prostatecanceruk.org/information/understanding-the-prostate-gland.
5. Smittenaar, C.R., et al., *Cancer incidence and mortality projections in the UK until 2035.* Br J Cancer, 2016. **115**(9): p. 1147-1155.
6. Patel, A.R. and E.A. Klein, *Risk factors for prostate cancer.* Nat Clin Pract Urol, 2009. **6**(2): p. 87-95.
7. National Collaborating Centre for, C., *National Institute for Health and Clinical Excellence: Guidance*, in *Prostate Cancer: Diagnosis and Treatment*. 2014, National Collaborating Centre for Cancer (UK) Copyright (c) National Collaborating Centre for Cancer.: Cardiff (UK).
8. CancerResearchUK. *Prostate cancer incidence by age*. 12/11/15 15/02/16]; Available from: http://www.cancerresearchuk.org/health-professional/prostate-cancer-incidence-statistics#heading-One.
9. CancerResearchUK. *Prostate cancer mortality by age*. 08/09/14 19/02/16]; Available from: http://www.cancerresearchuk.org/health-professional/prostate-cancer-mortality-statistics#heading-One.
10. CancerResearchUK. *Prostate cancer mortality trends over time*. 08/09/14 19/02/15]; Available from: http://www.cancerresearchuk.org/health-professional/prostate-cancer-mortality-statistics#heading-Two.
11. Ferlay, J., et al., *Cancer incidence and mortality patterns in Europe: Estimates for 40 countries and 25 major cancers in 2018.* Eur J Cancer, 2018. **103**: p. 356-387.
12. Hassanipour-Azgomi, S., et al., *Incidence and mortality of prostate cancer and their relationship with the Human Development Index worldwide.* Prostate Int, 2016. **4**(3): p. 118-24.
13. Jemal, A., et al., *Global cancer statistics.* CA Cancer J Clin, 2011. **61**(2): p. 69-90.
14. Bray, F., et al., *Global cancer statistics 2018: GLOBOCAN estimates of incidence and mortality worldwide for 36 cancers in 185 countries.* CA Cancer J Clin, 2018. **68**(6): p. 394-424.
15. CancerResearchUK. *Prostate Cancer Statistics*. 08/09/14 22/10/14]; Available from: http://www.cancerresearchuk.org/cancer-info/cancerstats/types/prostate/?script=true.
16. Lloyd, T., et al., *Lifetime risk of being diagnosed with, or dying from, prostate cancer by major ethnic group in England 2008-2010.* BMC Med, 2015. **13**: p. 171.
17. Elo, J.P. and T. Visakorpi, *Molecular genetics of prostate cancer.* Ann Med, 2001. **33**(2): p. 130-41.
18. Johns, L.E. and R.S. Houlston, *A systematic review and meta-analysis of familial prostate cancer risk.* BJU Int, 2003. **91**(9): p. 789-94.
19. Thompson, D. and D.F. Easton, *Cancer Incidence in BRCA1 mutation carriers.* J Natl Cancer Inst, 2002. **94**(18): p. 1358-65.

20.   Edwards, S.M., et al., *Two percent of men with early-onset prostate cancer harbor germline mutations in the BRCA2 gene.* Am J Hum Genet, 2003. **72**(1): p. 1-12.

21.   Kral, M., et al., *Genetic determinants of prostate cancer: a review.* Biomed Pap Med Fac Univ Palacky Olomouc Czech Repub, 2011. **155**(1): p. 3-9.

22.   Cancel-Tassin, G. and O. Cussenot, *Genetic susceptibility to prostate cancer.* BJU International, 2005. **96**(9): p. 1380-1385.

23.   Claessens, F., et al., *Diverse roles of androgen receptor (AR) domains in AR-mediated signaling.* Nucl Recept Signal, 2008. **6**: p. e008.

24.   Lonergan, P.E. and D.J. Tindall, *Androgen receptor signaling in prostate cancer development and progression.* J Carcinog, 2011. **10**: p. 20.

25.   Lu, C. and J. Luo, *Decoding the androgen receptor splice variants.* Translational Andrology and Urology, 2013. **2**(3): p. 178-186.

26.   Jenster, G., et al., *Identification of two transcription activation units in the N-terminal domain of the human androgen receptor.* J Biol Chem, 1995. **270**(13): p. 7341-6.

27.   Traish, A.M. and A. Morgentaler, *Epidermal growth factor receptor expression escapes androgen regulation in prostate cancer: a potential molecular switch for tumour growth.* Br J Cancer, 2009. **101**(12): p. 1949-56.

28.   Feldman, B.J. and D. Feldman, *The development of androgen-independent prostate cancer.* Nat Rev Cancer, 2001. **1**(1): p. 34-45.

29.   Gelmann, E.P., *Molecular biology of the androgen receptor.* J Clin Oncol, 2002. **20**(13): p. 3001-15.

30.   Tyagi, R.K., et al., *Dynamics of intracellular movement and nucleocytoplasmic recycling of the ligand-activated androgen receptor in living cells.* Mol Endocrinol, 2000. **14**(8): p. 1162-74.

31.   Gnanapragasam, V.J., et al., *Androgen receptor signalling in the prostate.* BJU Int, 2000. **86**(9): p. 1001-13.

32.   Lilja, H., D. Ulmert, and A.J. Vickers, *Prostate-specific antigen and prostate cancer: prediction, detection and monitoring.* Nat Rev Cancer, 2008. **8**(4): p. 268-78.

33.   Nash, A.F. and I. Melezinek, *The role of prostate specific antigen measurement in the detection and management of prostate cancer.* Endocr Relat Cancer, 2000. **7**(1): p. 37-51.

34.   Zou, J.X., et al., *ANCCA, an estrogen-regulated AAA+ ATPase coactivator for ERalpha, is required for coregulator occupancy and chromatin modification.* Proc Natl Acad Sci U S A, 2007. **104**(46): p. 18067-72.

35.   Revenko, A.S., et al., *Chromatin loading of E2F-MLL complex by cancer-associated coregulator ANCCA via reading a specific histone mark.* Mol Cell Biol, 2010. **30**(22): p. 5260-72.

36.   Zou, J.X., et al., *Androgen-induced coactivator ANCCA mediates specific androgen receptor signaling in prostate cancer.* Cancer Res, 2009. **69**(8): p. 3339-46.

37.   Heinlein, C.A. and C. Chang, *Androgen receptor in prostate cancer.* Endocr Rev, 2004. **25**(2): p. 276-308.

38. Ruizeveld de Winter, J.A., et al., *Androgen receptor status in localized and locally progressive hormone refractory human prostate cancer.* Am J Pathol, 1994. **144**(4): p. 735-46.

39. Chen, C.D., et al., *Molecular determinants of resistance to antiandrogen therapy.* Nat Med, 2004. **10**(1): p. 33-9.

40. Koivisto, P., et al., *Androgen receptor gene amplification: a possible molecular mechanism for androgen deprivation therapy failure in prostate cancer.* Cancer Res, 1997. **57**(2): p. 314-9.

41. Buchanan, G., et al., *Contribution of the androgen receptor to prostate cancer predisposition and progression.* Cancer Metastasis Rev, 2001. **20**(3-4): p. 207-23.

42. Gregory, C.W., et al., *Androgen receptor stabilization in recurrent prostate cancer is associated with hypersensitivity to low androgen.* Cancer Res, 2001. **61**(7): p. 2892-8.

43. Locke, J.A., et al., *Androgen levels increase by intratumoral de novo steroidogenesis during progression of castration-resistant prostate cancer.* Cancer Res, 2008. **68**(15): p. 6407-15.

44. Steinkamp, M.P., et al., *Treatment-dependent androgen receptor mutations in prostate cancer exploit multiple mechanisms to evade therapy.* Cancer Res, 2009. **69**(10): p. 4434-42.

45. Dehm, S.M., et al., *Splicing of a novel androgen receptor exon generates a constitutively active androgen receptor that mediates prostate cancer therapy resistance.* Cancer Res, 2008. **68**(13): p. 5469-77.

46. Jenster, G., et al., *Domains of the human androgen receptor involved in steroid binding, transcriptional activation, and subcellular localization.* Mol Endocrinol, 1991. **5**(10): p. 1396-404.

47. Hu, R., et al., *Ligand-independent androgen receptor variants derived from splicing of cryptic exons signify hormone-refractory prostate cancer.* Cancer Res, 2009. **69**(1): p. 16-22.

48. Arya, M., et al., *The metastatic cascade in prostate cancer.* Surg Oncol, 2006. **15**(3): p. 117-28.

49. Gupta, G.P. and J. Massague, *Cancer metastasis: building a framework.* Cell, 2006. **127**(4): p. 679-95.

50. Hanahan, D. and R.A. Weinberg, *The hallmarks of cancer.* Cell, 2000. **100**(1): p. 57-70.

51. Chiang, A.C. and J. Massague, *Molecular basis of metastasis.* N Engl J Med, 2008. **359**(26): p. 2814-23.

52. Bacac, M. and I. Stamenkovic, *Metastatic cancer cell.* Annu Rev Pathol, 2008. **3**: p. 221-47.

53. Jin, J.K., F. Dayyani, and G.E. Gallick, *Steps in prostate cancer progression that lead to bone metastasis.* Int J Cancer, 2011. **128**(11): p. 2545-61.

54. anatomychartpad.com. *https://anatomychartpad.com/cardiovascular-system-in-human-body/cardiovascular-system-in-human-body-gallery-full-body-circulatory-system-human-anatomy-diagram/.* 19/09/18]; Available from: https://anatomychartpad.com/cardiovascular-system-in-human-body/cardiovascular-system-in-human-body-gallery-full-body-circulatory-system-human-anatomy-diagram/.

55. anatomysciences.com. *Largest Cavity Is Abdominal Cavity Diagram Body Cavities And Membranes*. 2018 19/09/18]; Available from: http://anatomysciences.com/largest-cavity-is-abdominal-cavity-diagram/largest-cavity-is-abdominal-cavity-diagram-body-cavities-and-membranes-scientist-cindy/.

56. Chambers, A.F., A.C. Groom, and I.C. MacDonald, *Dissemination and growth of cancer cells in metastatic sites.* Nat Rev Cancer, 2002. **2**(8): p. 563-72.

57. Chung, A.S., J. Lee, and N. Ferrara, *Targeting the tumour vasculature: insights from physiological angiogenesis.* Nat Rev Cancer, 2010. **10**(7): p. 505-14.

58. Hoff, P.M. and K.K. Machado, *Role of angiogenesis in the pathogenesis of cancer.* Cancer Treat Rev, 2012. **38**(7): p. 825-33.

59. Li, W.W.L.a.V.W., *Angiogenesis in Wound Healing*, in *Contemporary surgery* 2003.

60. Coman, D.R., *Decreased mutual adhesiveness, a property of cells from squamous carcinomas* CancerRes, 1944. **4**(10): p. 625-629.

61. Birchmeier, W. and J. Behrens, *Cadherin expression in carcinomas: role in the formation of cell junctions and the prevention of invasiveness.* Biochim Biophys Acta, 1994. **1198**(1): p. 11-26.

62. Edlund, M., et al., *Integrin expression and usage by prostate cancer cell lines on laminin substrata.* Cell Growth Differ, 2001. **12**(2): p. 99-107.

63. Sahai, E. and C.J. Marshall, *Differing modes of tumour cell invasion have distinct requirements for Rho/ROCK signalling and extracellular proteolysis.* Nat Cell Biol, 2003. **5**(8): p. 711-9.

64. Friedl, P. and D. Gilmour, *Collective cell migration in morphogenesis, regeneration and cancer.* Nat Rev Mol Cell Biol, 2009. **10**(7): p. 445-57.

65. Reymond, N., B.B. d'Agua, and A.J. Ridley, *Crossing the endothelial barrier during metastasis.* Nat Rev Cancer, 2013. **13**(12): p. 858-70.

66. Ridley, A.J., et al., *The small GTP-binding protein rac regulates growth factor-induced membrane ruffling.* Cell, 1992. **70**(3): p. 401-10.

67. Amano, M., et al., *Formation of actin stress fibers and focal adhesions enhanced by Rho-kinase.* Science, 1997. **275**(5304): p. 1308-11.

68. Takai, Y., et al., *Rho as a regulator of the cytoskeleton.* Trends Biochem Sci, 1995. **20**(6): p. 227-31.

69. Wittekind, C. and M. Neid, *Cancer invasion and metastasis.* Oncology, 2005. **69 Suppl 1**: p. 14-6.

70. Anderberg, C., et al., *Deficiency for endoglin in tumor vasculature weakens the endothelial barrier to metastatic dissemination.* J Exp Med, 2013. **210**(3): p. 563-79.

71. Honn, K.V. and D.G. Tang, *Adhesion molecules and tumor cell interaction with endothelium and subendothelial matrix.* Cancer Metastasis Rev, 1992. **11**(3-4): p. 353-75.

72. Bubendorf, L., et al., *Metastatic patterns of prostate cancer: an autopsy study of 1,589 patients.* Hum Pathol, 2000. **31**(5): p. 578-83.

73. *Stephen Paget's paper reproduced from The Lancet, 1889.* Cancer and Metastasis Reviews. **8**(2): p. 98-101.

74. Ewing, J., *Neoplastic diseases; a treatise on tumours*. 2nd ed. 1922, Philadelphia and London: W.B Saunders company.

75. Jacob, K., et al., *Osteonectin promotes prostate cancer cell migration and invasion: a possible mechanism for metastasis to bone.* Cancer Res, 1999. **59**(17): p. 4453-7.

76. Festuccia, C., et al., *Osteoblast conditioned media contain TGF-beta1 and modulate the migration of prostate tumor cells and their interactions with extracellular matrix components.* Int J Cancer, 1999. **81**(3): p. 395-403.

77. Rajan, R., et al., *Epidermal growth factor (EGF) promotes chemomigration of a human prostate tumor cell line, and EGF immunoreactive proteins are present at sites of metastasis in the stroma of lymph nodes and medullary bone.* Prostate, 1996. **28**(1): p. 1-9.

78. Ritchie, C.K., et al., *The effects of growth factors associated with osteoblasts on prostate carcinoma proliferation and chemotaxis: implications for the development of metastatic disease.* Endocrinology, 1997. **138**(3): p. 1145-50.

79. Gmyrek, G.A., et al., *Normal and malignant prostate epithelial cells differ in their response to hepatocyte growth factor/scatter factor.* Am J Pathol, 2001. **159**(2): p. 579-90.

80. Cooper, C.R., et al., *Stromal factors involved in prostate carcinoma metastasis to bone.* Cancer, 2003. **97**(3 Suppl): p. 739-47.

81. Muller, A., et al., *Involvement of chemokine receptors in breast cancer metastasis.* Nature, 2001. **410**(6824): p. 50-6.

82. Lucia, M.S., et al., *Workgroup I: rodent models of prostate cancer.* Prostate, 1998. **36**(1): p. 49-55.

83. Namekawa, T., et al., *Application of Prostate Cancer Models for Preclinical Study: Advantages and Limitations of Cell Lines, Patient-Derived Xenografts, and Three-Dimensional Culture of Patient-Derived Cells.* Cells, 2019. **8**(1).

84. Sobel, R.E. and M.D. Sadar, *Cell lines used in prostate cancer research: a compendium of old and new lines--part 1.* J Urol, 2005. **173**(2): p. 342-59.

85. Rhim, J.S., *Human prostate epithelial cell cultures.* Methods Mol Biol, 2013. **946**: p. 383-93.

86. Rea, D., et al., *Mouse Models in Prostate Cancer Translational Research: From Xenograft to PDX.* Biomed Res Int, 2016. **2016**: p. 9750795.

87. Singh, A.S. and W.D. Figg, *In vivo models of prostate cancer metastasis to bone.* J Urol, 2005. **174**(3): p. 820-6.

88. Pavese, J., I.M. Ogden, and R.C. Bergan, *An orthotopic murine model of human prostate cancer metastasis.* J Vis Exp, 2013(79): p. e50873.

89. Kang, B.J., et al., *Diagnosis of prostate cancer via nanotechnological approach.* Int J Nanomedicine, 2015. **10**: p. 6555-69.

90. Quinn, J., et al., *Debate: the per rectal/digital rectal examination exam in the emergency department, still best practice?* Int J Emerg Med, 2018. **11**(1): p. 20.

91. Taneja, S.S., *Optimizing prostate biopsy strategies for the diagnosis of prostate cancer.* Rev Urol, 2003. **5**(3): p. 149-55.

92. Borley, N. and M.R. Feneley, *Prostate cancer: diagnosis and staging.* Asian J Androl, 2009. **11**(1): p. 74-80.

93. Rabbani, F., et al., *Incidence and clinical significance of false-negative sextant prostate biopsies.* J Urol, 1998. **159**(4): p. 1247-50.

94. Huang, S., et al., *Significant impact of transperineal template biopsy of the prostate at a single tertiary institution.* Urol Ann, 2015. **7**(4): p. 428-32.

95. Bhatt, N.R., et al., *Patient experience after transperineal template prostate biopsy compared to prior transrectal ultrasound guided prostate biopsy.* Cent European J Urol, 2018. **71**(1): p. 43-47.

96. Nakai, Y., et al., *Transperineal template-guided saturation biopsy aimed at sampling one core for each milliliter of prostate volume: 103 cases requiring repeat prostate biopsy.* BMC Urol, 2017. **17**(1): p. 28.

97. Logan, J.K., et al., *Current status of magnetic resonance imaging (MRI) and ultrasonography fusion software platforms for guidance of prostate biopsies.* BJU Int, 2014. **114**(5): p. 641-52.

98. Sogani, P.C., et al., *Gleason grading of prostate cancer: a predictor of survival.* Urology, 1985. **25**(3): p. 223-7.

99. Matoso, A. and J.I. Epstein, *Grading of Prostate Cancer: Past, Present, and Future.* Curr Urol Rep, 2016. **17**(3): p. 25.

100. Turkbey, B., et al., *Imaging localized prostate cancer: current approaches and new developments.* AJR Am J Roentgenol, 2009. **192**(6): p. 1471-80.

101. Cheng, L., et al., *Staging of prostate cancer.* Histopathology, 2012. **60**(1): p. 87-117.

102. Heidenreich, A., et al., *EAU guidelines on prostate cancer. part 1: screening, diagnosis, and local treatment with curative intent-update 2013.* Eur Urol, 2014. **65**(1): p. 124-37.

103. Kinsella, N., et al., *Active surveillance for prostate cancer: a systematic review of contemporary worldwide practices.* Transl Androl Urol, 2018. **7**(1): p. 83-97.

104. Herden, J. and L. Weissbach, *Utilization of Active Surveillance and Watchful Waiting for localized prostate cancer in the daily practice.* World J Urol, 2018. **36**(3): p. 383-391.

105. Chodak, G.W. and K.S. Warren, *Watchful waiting for prostate cancer: a review article.* Prostate Cancer Prostatic Dis, 2006. **9**(1): p. 25-9.

106. Neal, R.D., *NICE prostate cancer clinical guideline: implications for primary care.* Br J Gen Pract, 2008. **58**(554): p. 607-8.

107. Hugosson, J., J. Stranne, and S.V. Carlsson, *Radical retropubic prostatectomy: a review of outcomes and side-effects.* Acta Oncol, 2011. **50 Suppl 1**: p. 92-7.

108. Gomella, L.G., *Effective testosterone suppression for prostate cancer: is there a best castration therapy?* Rev Urol, 2009. **11**(2): p. 52-60.

109. Rud, O., et al., *Subcapsular orchiectomy in the primary therapy of patients with bone metastasis in advanced prostate cancer: an anachronistic intervention?* Adv Urol, 2012. **2012**: p. 190624.

110. Krupski, T.L., et al., *The relationship of palliative transurethral resection of the prostate with disease progression in patients with prostate cancer.* BJU Int, 2010. **106**(10): p. 1477-83.

111. Keyes, M., et al., *Treatment options for localized prostate cancer.* Can Fam Physician, 2013. **59**(12): p. 1269-74.

112. Chen, F.Z. and X.K. Zhao, *Prostate cancer: current treatment and prevention strategies.* Iran Red Crescent Med J, 2013. **15**(4): p. 279-84.

113. Board, P.D.Q.A.T.E., *Prostate Cancer Treatment (PDQ(R)): Health Professional Version*, in *PDQ Cancer Information Summaries*. 2002, National Cancer Institute (US): Bethesda (MD).

114. Goldstraw, M.A., *Prostate cancer treatment. The case for radical prostatectomy.* Ann R Coll Surg Engl, 2006. **88**(5): p. 439-42.

115. CancerResearchUK. *Radiotherapy for prostate cancer that has spread*. 25/02/16 27/04/16]; Available from: http://www.cancerresearchuk.org/about-cancer/type/prostate-cancer/treatment/radiotherapy/radiotherapy-for-prostate-cancer-that-has-spread.

116. Boyer, M.J., J.K. Salama, and W.R. Lee, *Palliative radiotherapy for prostate cancer.* Oncology (Williston Park), 2014. **28**(4): p. 306-12.

117. Spencer, K., et al., *Palliative radiotherapy.* Bmj, 2018. **360**: p. k821.

118. Dearnaley, D.P., et al., *Palliation of bone metastases in prostate cancer. Hemibody irradiation or strontium-89?* Clinical Oncology, 1992. **4**(2): p. 101-107.

119. Persson, B.E., T. Kold Olesen, and J.K. Jensen, *Degarelix: a new approach for the treatment of prostate cancer.* Neuroendocrinology, 2009. **90**(3): p. 235-44.

120. CancerResearchUK. *About hormone therapy for prostate cancer*. 25/02/16 [cited 28/04/16; Available from: http://www.cancerresearchuk.org/about-cancer/type/prostate-cancer/treatment/hormone/about-hormone-therapy-for-prostate-cancer#pitreg.

121. Rodriguez-Vida, A., et al., *Enzalutamide for the treatment of metastatic castration-resistant prostate cancer.* Drug Des Devel Ther, 2015. **9**: p. 3325-39.

122. Chen, Y., N.J. Clegg, and H.I. Scher, *Anti-androgens and androgen-depleting therapies in prostate cancer: new agents for an established target.* Lancet Oncol, 2009. **10**(10): p. 981-91.

123. CancerResearchUK. *About chemotherapy for prostate cancer*. 25/02/16 28/04/16]; Available from: http://www.cancerresearchuk.org/about-cancer/type/prostate-cancer/treatment/chemotherapy/about-chemotherapy-for-prostate-cancer.

124. CancerResearchUK. *Steroids for prostate cancer*. 25/02/14 28/04/16]; Available from: http://www.cancerresearchuk.org/about-cancer/type/prostate-cancer/treatment/steroids-for-prostate-cancer.

125. Rodriguez, S.A., et al., *Cryotherapy for primary treatment of prostate cancer: intermediate term results of a prospective study from a single institution.* Prostate Cancer, 2014. **2014**: p. 571576.

126. Sundaram, K.M., et al., *Therapeutic Ultrasound and Prostate Cancer.* Semin Intervent Radiol, 2017. **34**(2): p. 187-200.

127. Simons, K. and S.D. Fuller, *Cell surface polarity in epithelia.* Annu Rev Cell Biol, 1985. **1**: p. 243-88.

128. Giepmans, B.N. and S.C. van Ijzendoorn, *Epithelial cell-cell junctions and plasma membrane domains.* Biochim Biophys Acta, 2009. **1788**(4): p. 820-31.

129. Gonzalez-Mariscal, L., et al., *Tight junction proteins.* Prog Biophys Mol Biol, 2003. **81**(1): p. 1-44.

130. Brennan, K., et al., *Tight junctions: a barrier to the initiation and progression of breast cancer?* J Biomed Biotechnol, 2010. **2010**: p. 460607.

131. Bazzoni, G. and E. Dejana, *Endothelial cell-to-cell junctions: molecular organization and role in vascular homeostasis.* Physiol Rev, 2004. **84**(3): p. 869-901.

132. Niessen, C.M. and C.J. Gottardi, *Molecular components of the adherens junction.* Biochim Biophys Acta, 2008. **1778**(3): p. 562-71.

133. Farquhar, M.G. and G.E. Palade, *Junctional complexes in various epithelia.* J Cell Biol, 1963. **17**: p. 375-412.

134. Meng, W. and M. Takeichi, *Adherens junction: molecular architecture and regulation.* Cold Spring Harb Perspect Biol, 2009. **1**(6): p. a002899.

135. Vanneste, B.G., et al., *Prostate Cancer Radiation Therapy: What Do Clinicians Have to Know?* Biomed Res Int, 2016. **2016**: p. 6829875.

136. Drenckhahn, D. and H. Franz, *Identification of actin-, alpha-actinin-, and vinculin-containing plaques at the lateral membrane of epithelial cells.* J Cell Biol, 1986. **102**(5): p. 1843-52.

137. Fannon, A.M. and D.R. Colman, *A model for central synaptic junctional complex formation based on the differential adhesive specificities of the cadherins.* Neuron, 1996. **17**(3): p. 423-34.

138. Uchida, N., et al., *The catenin/cadherin adhesion system is localized in synaptic junctions bordering transmitter release zones.* J Cell Biol, 1996. **135**(3): p. 767-79.

139. Wuchter, P., et al., *Processus and recessus adhaerentes: giant adherens cell junction systems connect and attract human mesenchymal stem cells.* Cell Tissue Res, 2007. **328**(3): p. 499-514.

140. Niessen, C.M. and C.J. Gottardi, *Molecular components of the adherens junction.* Biochimica et Biophysica Acta (BBA) - Biomembranes, 2008. **1778**(3): p. 562-571.

141. Miyamoto, T., et al., *Tight junctions in Schwann cells of peripheral myelinated axons: a lesson from claudin-19-deficient mice.* J Cell Biol, 2005. **169**(3): p. 527-38.

142. Chasiotis, H., et al., *Tight junctions, tight junction proteins and paracellular permeability across the gill epithelium of fishes: a review.* Respir Physiol Neurobiol, 2012. **184**(3): p. 269-81.

143. Martin, T.A., *The role of tight junctions in cancer metastasis.* Semin Cell Dev Biol, 2014.

144. Gumbiner, B., *Structure, biochemistry, and assembly of epithelial tight junctions.* Am J Physiol, 1987. **253**(6 Pt 1): p. C749-58.

145. Garcia-Lozano, J.R., et al., *Identification of HAVCR1 gene haplotypes associated with mRNA expression levels and susceptibility to autoimmune diseases.* Hum Genet, 2010. **128**(2): p. 221-9.

146. Rindler, M.J., et al., *Biogenesis of epithelial cell plasma membranes.* Ciba Found Symp, 1982(92): p. 184-208.

147. Mitic, L.L. and J.M. Anderson, *Molecular architecture of tight junctions.* Annu Rev Physiol, 1998. **60**: p. 121-42.

148. Zegers, M.M. and D. Hoekstra, *Mechanisms and functional features of polarized membrane traffic in epithelial and hepatic cells.* Biochem J, 1998. **336 (Pt 2)**: p. 257-69.

149. Wallez, Y. and P. Huber, *Endothelial adherens and tight junctions in vascular homeostasis, inflammation and angiogenesis.* Biochim Biophys Acta, 2008. **1778**(3): p. 794-809.

150. Takeichi, M., *The cadherins: cell-cell adhesion molecules controlling animal morphogenesis.* Development, 1988. **102**(4): p. 639-55.

151. Hartsock, A. and W.J. Nelson, *Adherens and tight junctions: structure, function and connections to the actin cytoskeleton.* Biochim Biophys Acta, 2008. **1778**(3): p. 660-9.

152. Ferber, A., et al., *An octapeptide in the juxtamembrane domain of VE-cadherin is important for p120ctn binding and cell proliferation.* Exp Cell Res, 2002. **274**(1): p. 35-44.

153. Davis, M.A., R.C. Ireton, and A.B. Reynolds, *A core function for p120-catenin in cadherin turnover.* J Cell Biol, 2003. **163**(3): p. 525-34.

154. Noren, N.K., et al., *p120 catenin regulates the actin cytoskeleton via Rho family GTPases.* J Cell Biol, 2000. **150**(3): p. 567-80.

155. Huber, A.H. and W.I. Weis, *The structure of the beta-catenin/E-cadherin complex and the molecular basis of diverse ligand recognition by beta-catenin.* Cell, 2001. **105**(3): p. 391-402.

156. Lilien, J., et al., *Turn-off, drop-out: functional state switching of cadherins.* Dev Dyn, 2002. **224**(1): p. 18-29.

157. Hirokawa, N. and J.E. Heuser, *Quick-freeze, deep-etch visualization of the cytoskeleton beneath surface differentiations of intestinal epithelial cells.* J Cell Biol, 1981. **91**(2 Pt 1): p. 399-409.

158. Ozaki-Kuroda, K., et al., *Nectin couples cell-cell adhesion and the actin scaffold at heterotypic testicular junctions.* Curr Biol, 2002. **12**(13): p. 1145-50.

159. Mitchell, L.A., et al., *Junctional adhesion molecule A promotes epithelial tight junction assembly to augment lung barrier function.* Am J Pathol, 2015. **185**(2): p. 372-86.

160. Tornavaca, O., et al., *ZO-1 controls endothelial adherens junctions, cell-cell tension, angiogenesis, and barrier formation.* J Cell Biol, 2015. **208**(6): p. 821-38.

161. Furuse, M., et al., *Occludin: a novel integral membrane protein localizing at tight junctions.* J Cell Biol, 1993. **123**(6 Pt 2): p. 1777-88.

162. Powell, D.W., *Barrier function of epithelia.* Am J Physiol, 1981. **241**(4): p. G275-88.

163. Ando-Akatsuka, Y., et al., *Interspecies diversity of the occludin sequence: cDNA cloning of human, mouse, dog, and rat-kangaroo homologues.* J Cell Biol, 1996. **133**(1): p. 43-7.

164. Saitou, M., et al., *Occludin-deficient embryonic stem cells can differentiate into polarized epithelial cells bearing tight junctions.* J Cell Biol, 1998. **141**(2): p. 397-408.

165. Furuse, M., et al., *Claudin-1 and -2: novel integral membrane proteins localizing at tight junctions with no sequence similarity to occludin.* J Cell Biol, 1998. **141**(7): p. 1539-50.

166. Gunzel, D. and A.S. Yu, *Claudins and the modulation of tight junction permeability.* Physiol Rev, 2013. **93**(2): p. 525-69.

167. Mineta, K., et al., *Predicted expansion of the claudin multigene family.* FEBS Lett, 2011. **585**(4): p. 606-12.

168. Wu, J., et al., *Identification of new claudin family members by a novel PSI-BLAST based approach with enhanced specificity.* Proteins, 2006. **65**(4): p. 808-15.

169. Chiba, H., et al., *Transmembrane proteins of tight junctions.* Biochim Biophys Acta, 2008. **1778**(3): p. 588-600.

170. McNeil, E., C.T. Capaldo, and I.G. Macara, *Zonula occludens-1 function in the assembly of tight junctions in Madin-Darby canine kidney epithelial cells.* Mol Biol Cell, 2006. **17**(4): p. 1922-32.

171. Anderson, J.M. and C.M. Van Itallie, *Tight junctions and the molecular basis for regulation of paracellular permeability.* Am J Physiol, 1995. **269**(4 Pt 1): p. G467-75.

172. Stiffler, M.A., et al., *PDZ domain binding selectivity is optimized across the mouse proteome.* Science, 2007. **317**(5836): p. 364-9.

173. Gonzalez-Mariscal, L., A. Betanzos, and A. Avila-Flores, *MAGUK proteins: structure and role in the tight junction.* Semin Cell Dev Biol, 2000. **11**(4): p. 315-24.

174. Coyne, C.B. and J.M. Bergelson, *CAR: a virus receptor within the tight junction.* Adv Drug Deliv Rev, 2005. **57**(6): p. 869-82.

175. Balda, M.S. and K. Matter, *Tight junctions and the regulation of gene expression.* Biochim Biophys Acta, 2009. **1788**(4): p. 761-7.

176. Guillemot, L., et al., *The cytoplasmic plaque of tight junctions: a scaffolding and signalling center.* Biochim Biophys Acta, 2008. **1778**(3): p. 601-13.

177. Gonzalez-Mariscal, L., R. Tapia, and D. Chamorro, *Crosstalk of tight junction components with signaling pathways.* Biochim Biophys Acta, 2008. **1778**(3): p. 729-56.

178. McNeill, H., et al., *Spatial and temporal dissection of immediate and early events following cadherin-mediated epithelial cell adhesion.* J Cell Biol, 1993. **120**(5): p. 1217-26.

179. Micalizzi, D.S., S.M. Farabaugh, and H.L. Ford, *Epithelial-mesenchymal transition in cancer: parallels between normal development and tumor progression.* J Mammary Gland Biol Neoplasia, 2010. **15**(2): p. 117-34.

180. Talbot, L.J., S.D. Bhattacharya, and P.C. Kuo, *Epithelial-mesenchymal transition, the tumor microenvironment, and metastatic behavior of epithelial malignancies.* Int J Biochem Mol Biol, 2012. **3**(2): p. 117-36.

181. Huang, D. and X. Du, *Crosstalk between tumor cells and microenvironment via Wnt pathway in colorectal cancer dissemination.* World J Gastroenterol, 2008. **14**(12): p. 1823-7.

182. Tsukita, S. and M. Furuse, *Occludin and claudins in tight-junction strands: leading or supporting players?* Trends Cell Biol, 1999. **9**(7): p. 268-73.

183. Griepp, E.B., et al., *Participation of plasma membrane proteins in the formation of tight junctions by cultured epithelial cells.* J Cell Biol, 1983. **96**(3): p. 693-702.

184. Anderson, J.M. and C.M. Van Itallie, *Physiology and Function of the Tight Junction.* Cold Spring Harb Perspect Biol, 2009. **1**(2).

185. Forster, C., *Tight junctions and the modulation of barrier function in disease.* Histochem Cell Biol, 2008. **130**(1): p. 55-70.

186. Betanzos, A., et al., *The tight junction protein ZO-2 associates with Jun, Fos and C/EBP transcription factors in epithelial cells.* Exp Cell Res, 2004. **292**(1): p. 51-66.

187. Paris, L., et al., *Structural organization of the tight junctions.* Biochim Biophys Acta, 2008. **1778**(3): p. 646-59.

188. Getsios, S., D.P. Kelsell, and A. Forge, *Junctions in human health and inherited disease.* Cell Tissue Res, 2015. **360**(3): p. 435-8.

189. Mehta, S., et al., *Defects in the adherens junction complex (E-cadherin/ beta-catenin) in inflammatory bowel disease.* Cell Tissue Res, 2015. **360**(3): p. 749-60.

190. Samuelov, L., E. Sprecher, and R. Paus, *The role of P-cadherin in skin biology and skin pathology: lessons from the hair follicle.* Cell Tissue Res, 2015. **360**(3): p. 761-71.

191. Vite, A., J. Li, and G.L. Radice, *New functions for alpha-catenins in health and disease: from cancer to heart regeneration.* Cell Tissue Res, 2015. **360**(3): p. 773-83.

192. Elding, H., et al., *Dissecting the genetics of complex inheritance: linkage disequilibrium mapping provides insight into Crohn disease.* Am J Hum Genet, 2011. **89**(6): p. 798-805.

193. Gibson, P.R., et al., *Ulcerative colitis--a disease characterised by the abnormal colonic epithelial cell?* Gut, 1988. **29**(4): p. 516-21.

194. Gibson, P., et al., *Colonic epithelium is diffusely abnormal in ulcerative colitis and colorectal cancer.* Gut, 1995. **36**(6): p. 857-63.

195. Wyatt, J., et al., *Intestinal permeability and the prediction of relapse in Crohn's disease.* Lancet, 1993. **341**(8858): p. 1437-9.

196. Arnott, I.D., K. Kingstone, and S. Ghosh, *Abnormal intestinal permeability predicts relapse in inactive Crohn disease.* Scand J Gastroenterol, 2000. **35**(11): p. 1163-9.

197. Lai-Cheong, J.E., K. Arita, and J.A. McGrath, *Genetic diseases of junctions.* J Invest Dermatol, 2007. **127**(12): p. 2713-25.

198. Sprecher, E., et al., *Hypotrichosis with juvenile macular dystrophy is caused by a mutation in CDH3, encoding P-cadherin.* Nat Genet, 2001. **29**(2): p. 134-6.

199. Dusek, R.L. and L.D. Attardi, *Desmosomes: new perpetrators in tumour suppression.* Nat Rev Cancer, 2011. **11**(5): p. 317-23.

200. Okegawa, T., et al., *Cell adhesion proteins as tumor suppressors.* J Urol, 2002. **167**(4): p. 1836-43.

201. Knights, A.J., et al., *Holding Tight: Cell Junctions and Cancer Spread.* Trends Cancer Res, 2012. **8**: p. 61-69.
202. Strathdee, G., *Epigenetic versus genetic alterations in the inactivation of E-cadherin.* Semin Cancer Biol, 2002. **12**(5): p. 373-9.
203. Perl, A.K., et al., *A causal role for E-cadherin in the transition from adenoma to carcinoma.* Nature, 1998. **392**(6672): p. 190-3.
204. Bremnes, R.M., et al., *High-throughput tissue microarray analysis used to evaluate biology and prognostic significance of the E-cadherin pathway in non-small-cell lung cancer.* J Clin Oncol, 2002. **20**(10): p. 2417-28.
205. Yap, A.S., *The morphogenetic role of cadherin cell adhesion molecules in human cancer: a thematic review.* Cancer Invest, 1998. **16**(4): p. 252-61.
206. Arnes, J.B., et al., *Placental cadherin and the basal epithelial phenotype of BRCA1-related breast cancer.* Clin Cancer Res, 2005. **11**(11): p. 4003-11.
207. Jaggi, M., et al., *Aberrant expression of E-cadherin and beta-catenin in human prostate cancer.* Urol Oncol, 2005. **23**(6): p. 402-6.
208. Aaltomaa, S., et al., *Reduced alpha- and beta-catenin expression predicts shortened survival in local prostate cancer.* Anticancer Res, 2005. **25**(6c): p. 4707-12.
209. Perera, R. and B.D. Nicholson.
210. Gravdal, K., et al., *A switch from E-cadherin to N-cadherin expression indicates epithelial to mesenchymal transition and is of strong and independent importance for the progress of prostate cancer.* Clin Cancer Res, 2007. **13**(23): p. 7003-11.
211. Vermeer, P.D., et al., *Segregation of receptor and ligand regulates activation of epithelial growth factor receptor.* Nature, 2003. **422**(6929): p. 322-6.
212. Martin, T.A., M.D. Mason, and W.G. Jiang, *Tight junctions in cancer metastasis.* Front Biosci (Landmark Ed), 2011. **16**: p. 898-936.
213. Yoon, C.H., et al., *Claudin-1 acts through c-Abl-protein kinase Cdelta (PKCdelta) signaling and has a causal role in the acquisition of invasive capacity in human liver cells.* J Biol Chem, 2010. **285**(1): p. 226-33.
214. Li, J., et al., *Possible angiogenic roles for claudin-4 in ovarian cancer.* Cancer Biol Ther, 2009. **8**(19): p. 1806-14.
215. Osanai, M., et al., *Epigenetic silencing of claudin-6 promotes anchorage-independent growth of breast carcinoma cells.* Cancer Sci, 2007. **98**(10): p. 1557-62.
216. Lu, Z., et al., *Claudin-7 inhibits human lung cancer cell migration and invasion through ERK/MAPK signaling pathway.* Exp Cell Res, 2011. **317**(13): p. 1935-46.
217. Oshima, T., et al., *Reduced expression of the claudin-7 gene correlates with venous invasion and liver metastasis in colorectal cancer.* Oncol Rep, 2008. **19**(4): p. 953-9.
218. Lioni, M., et al., *Dysregulation of claudin-7 leads to loss of E-cadherin expression and the increased invasion of esophageal squamous cell carcinoma cells.* Am J Pathol, 2007. **170**(2): p. 709-21.
219. Tobioka, H., et al., *Occludin expression decreases with the progression of human endometrial carcinoma.* Hum Pathol, 2004. **35**(2): p. 159-64.

220. Osanai, M., et al., *Epigenetic silencing of occludin promotes tumorigenic and metastatic properties of cancer cells via modulations of unique sets of apoptosis-associated genes.* Cancer Res, 2006. **66**(18): p. 9125-33.

221. McSherry, E.A., et al., *JAM-A expression positively correlates with poor prognosis in breast cancer patients.* Int J Cancer, 2009. **125**(6): p. 1343-51.

222. Gutwein, P., et al., *Downregulation of junctional adhesion molecule-A is involved in the progression of clear cell renal cell carcinoma.* Biochem Biophys Res Commun, 2009. **380**(2): p. 387-91.

223. Ghislin, S., et al., *Junctional adhesion molecules are required for melanoma cell lines transendothelial migration in vitro.* Pigment Cell Melanoma Res, 2011. **24**(3): p. 504-11.

224. Laukoetter, M.G., et al., *JAM-A regulates permeability and inflammation in the intestine in vivo.* J Exp Med, 2007. **204**(13): p. 3067-76.

225. Nava, P., et al., *JAM-A regulates epithelial proliferation through Akt/beta-catenin signalling.* EMBO Rep, 2011. **12**(4): p. 314-20.

226. Cooke, V.G., M.U. Naik, and U.P. Naik, *Fibroblast growth factor-2 failed to induce angiogenesis in junctional adhesion molecule-A-deficient mice.* Arterioscler Thromb Vasc Biol, 2006. **26**(9): p. 2005-11.

227. Zhan, L., et al., *Deregulation of scribble promotes mammary tumorigenesis and reveals a role for cell polarity in carcinoma.* Cell, 2008. **135**(5): p. 865-78.

228. Long, H., et al., *Expression of Clostridium perfringens enterotoxin receptors claudin-3 and claudin-4 in prostate cancer epithelium.* Cancer Res, 2001. **61**(21): p. 7878-81.

229. Sheehan, G.M., et al., *Loss of claudins-1 and -7 and expression of claudins-3 and -4 correlate with prognostic variables in prostatic adenocarcinomas.* Hum Pathol, 2007. **38**(4): p. 564-9.

230. Soini, Y., *Expression of claudins 1, 2, 3, 4, 5 and 7 in various types of tumours.* Histopathology, 2005. **46**(5): p. 551-60.

231. Coutinho-Camillo, C.M., et al., *Claudin expression is dysregulated in prostate adenocarcinomas but does not correlate with main clinicopathological parameters.* Pathology, 2011. **43**(2): p. 143-8.

232. Bartholow, T.L., et al., *Immunohistochemical profiles of claudin-3 in primary and metastatic prostatic adenocarcinoma.* Diagn Pathol, 2011. **6**: p. 12.

233. Busch, C., et al., *Down-regulation of CEACAM1 in human prostate cancer: correlation with loss of cell polarity, increased proliferation rate, and Gleason grade 3 to 4 transition.* Hum Pathol, 2002. **33**(3): p. 290-8.

234. Shah, G.V., et al., *Cadherin switching and activation of beta-catenin signaling underlie proinvasive actions of calcitonin-calcitonin receptor axis in prostate cancer.* J Biol Chem, 2009. **284**(2): p. 1018-30.

235. Shah, G.V., et al., *Identification of a small molecule class to enhance cell-cell adhesion and attenuate prostate tumor growth and metastasis.* Mol Cancer Ther, 2009. **8**(3): p. 509-20.

236. Meng, J., et al., *Testosterone regulates tight junction proteins and influences prostatic autoimmune responses.* Horm Cancer, 2011. **2**(3): p. 145-56.

237. Zheng, J.Y., et al., *Regulation of the expression of the prostate-specific antigen by claudin-7.* J Membr Biol, 2003. **194**(3): p. 187-97.

238. Miyazawa, K., et al., *Molecular cloning and sequence analysis of the cDNA for a human serine protease reponsible for activation of hepatocyte growth factor. Structural similarity of the protease precursor to blood coagulation factor XII.* J Biol Chem, 1993. **268**(14): p. 10024-8.

239. Gohda, E., et al., *Purification and partial characterization of hepatocyte growth factor from plasma of a patient with fulminant hepatic failure.* J Clin Invest, 1988. **81**(2): p. 414-9.

240. Nakamura, T., et al., *Purification and subunit structure of hepatocyte growth factor from rat platelets.* FEBS Lett, 1987. **224**(2): p. 311-6.

241. Zarnegar, R. and G. Michalopoulos, *Purification and biological characterization of human hepatopoietin A, a polypeptide growth factor for hepatocytes.* Cancer Res, 1989. **49**(12): p. 3314-20.

242. Weidner, K.M., et al., *Evidence for the identity of human scatter factor and human hepatocyte growth factor.* Proc Natl Acad Sci U S A, 1991. **88**(16): p. 7001-5.

243. Tang, W., K. Miyazawa, and N. Kitamura, *Hepatocyte growth factor remains as an inactive single chain after partial hepatectomy or unilateral nephrectomy.* FEBS Lett, 1995. **362**(2): p. 220-4.

244. Naka, D., et al., *Activation of hepatocyte growth factor by proteolytic conversion of a single chain form to a heterodimer.* J Biol Chem, 1992. **267**(28): p. 20114-9.

245. Birchmeier, C., et al., *Met, metastasis, motility and more.* Nat Rev Mol Cell Biol, 2003. **4**(12): p. 915-25.

246. Organ, S.L. and M.S. Tsao, *An overview of the c-MET signaling pathway.* Ther Adv Med Oncol, 2011. **3**(1 Suppl): p. S7-s19.

247. Cooper, C.S., et al., *Molecular cloning of a new transforming gene from a chemically transformed human cell line.* Nature, 1984. **311**(5981): p. 29-33.

248. Epstein, J.A., et al., *Pax3 modulates expression of the c-Met receptor during limb muscle development.* Proc Natl Acad Sci U S A, 1996. **93**(9): p. 4213-8.

249. Gambarotta, G., et al., *Ets up-regulates MET transcription.* Oncogene, 1996. **13**(9): p. 1911-7.

250. Boccaccio, C., et al., *Hepatocyte growth factor (HGF) receptor expression is inducible and is part of the delayed-early response to HGF.* J Biol Chem, 1994. **269**(17): p. 12846-51.

251. Niemann, H.H., et al., *Structure of the human receptor tyrosine kinase met in complex with the Listeria invasion protein InlB.* Cell, 2007. **130**(2): p. 235-46.

252. Furge, K.A., Y.W. Zhang, and G.F. Vande Woude, *Met receptor tyrosine kinase: enhanced signaling through adapter proteins.* Oncogene, 2000. **19**(49): p. 5582-9.

253. Salgia, R., *Role of c-Met in cancer: emphasis on lung cancer.* Semin Oncol, 2009. **36**(2 Suppl 1): p. S52-8.

254. Trusolino, L., A. Bertotti, and P.M. Comoglio, *MET signalling: principles and functions in development, organ regeneration and cancer.* Nat Rev Mol Cell Biol, 2010. **11**(12): p. 834-48.

255. Jeffers, M., et al., *Degradation of the Met tyrosine kinase receptor by the ubiquitin-proteasome pathway.* Mol Cell Biol, 1997. **17**(2): p. 799-808.

256. Peschard, P., et al., *Mutation of the c-Cbl TKB domain binding site on the Met receptor tyrosine kinase converts it into a transforming protein.* Mol Cell, 2001. **8**(5): p. 995-1004.

257. Foveau, B., et al., *Down-regulation of the met receptor tyrosine kinase by presenilin-dependent regulated intramembrane proteolysis.* Mol Biol Cell, 2009. **20**(9): p. 2495-507.

258. Abella, J.V., et al., *Met/Hepatocyte growth factor receptor ubiquitination suppresses transformation and is required for Hrs phosphorylation.* Mol Cell Biol, 2005. **25**(21): p. 9632-45.

259. Balkovetz, D.F., et al., *Gene expression alterations during HGF-induced dedifferentiation of a renal tubular epithelial cell line (MDCK) using a novel canine DNA microarray.* Am J Physiol Renal Physiol, 2004. **286**(4): p. F702-10.

260. Lipschutz, J.H., et al., *Extracellular signal-regulated kinases 1/2 control claudin-2 expression in Madin-Darby canine kidney strain I and II cells.* J Biol Chem, 2005. **280**(5): p. 3780-8.

261. Martin, T.A., R.E. Mansel, and W.G. Jiang, *Antagonistic effect of NK4 on HGF/SF induced changes in the transendothelial resistance (TER) and paracellular permeability of human vascular endothelial cells.* J Cell Physiol, 2002. **192**(3): p. 268-75.

262. Jin, M., et al., *Regulation of RPE intercellular junction integrity and function by hepatocyte growth factor.* Invest Ophthalmol Vis Sci, 2002. **43**(8): p. 2782-90.

263. Muto, S., et al., *HGF/SF-induced spreading of MDCK cells correlates with disappearance of barmotin/7H6, a tight junction-associated protein, from the cell membrane.* Cell Biol Int, 2000. **24**(7): p. 439-46.

264. Hollande, F., et al., *HGF regulates tight junctions in new nontumorigenic gastric epithelial cell line.* Am J Physiol Gastrointest Liver Physiol, 2001. **280**(5): p. G910-21.

265. Martin, T.A., et al., *Hepatocyte growth factor disrupts tight junctions in human breast cancer cells.* Cell Biol Int, 2004. **28**(5): p. 361-71.

266. Miller, C.T., et al., *Genomic amplification of MET with boundaries within fragile site FRA7G and upregulation of MET pathways in esophageal adenocarcinoma.* Oncogene, 2006. **25**(3): p. 409-18.

267. Hara, T., et al., *Amplification of c-myc, K-sam, and c-met in gastric cancers: detection by fluorescence in situ hybridization.* Lab Invest, 1998. **78**(9): p. 1143-53.

268. Kuniyasu, H., et al., *Frequent amplification of the c-met gene in scirrhous type stomach cancer.* Biochem Biophys Res Commun, 1992. **189**(1): p. 227-32.

269. Houldsworth, J., et al., *Gene amplification in gastric and esophageal adenocarcinomas.* Cancer Res, 1990. **50**(19): p. 6417-22.

270. Tong, C.Y., et al., *Detection of oncogene amplifications in medulloblastomas by comparative genomic hybridization and array-based comparative genomic hybridization.* J Neurosurg, 2004. **100**(2 Suppl Pediatrics): p. 187-93.

271. Di Renzo, M.F., et al., *Expression of the Met/hepatocyte growth factor receptor in human pancreatic cancer.* Cancer Res, 1995. **55**(5): p. 1129-38.

272. Comoglio, P.M., S. Giordano, and L. Trusolino, *Drug development of MET inhibitors: targeting oncogene addiction and expedience.* Nat Rev Drug Discov, 2008. **7**(6): p. 504-16.

273. Olivero, M., et al., *Novel mutation in the ATP-binding site of the MET oncogene tyrosine kinase in a HPRCC family.* Int J Cancer, 1999. **82**(5): p. 640-3.

274. Schmidt, L., et al., *Novel mutations of the MET proto-oncogene in papillary renal carcinomas.* Oncogene, 1999. **18**(14): p. 2343-50.

275. Park, M., et al., *Mechanism of met oncogene activation.* Cell, 1986. **45**(6): p. 895-904.

276. Pennacchietti, S., et al., *Hypoxia promotes invasive growth by transcriptional activation of the met protooncogene.* Cancer Cell, 2003. **3**(4): p. 347-61.

277. Kitajima, Y., et al., *Induction of hepatocyte growth factor activator gene expression under hypoxia activates the hepatocyte growth factor/c-Met system via hypoxia inducible factor-1 in pancreatic cancer.* Cancer Sci, 2008. **99**(7): p. 1341-7.

278. Matsumoto, K. and T. Nakamura, *Hepatocyte growth factor and the Met system as a mediator of tumor-stromal interactions.* Int J Cancer, 2006. **119**(3): p. 477-83.

279. Humphrey, P.A., et al., *Hepatocyte growth factor and its receptor (c-MET) in prostatic carcinoma.* Am J Pathol, 1995. **147**(2): p. 386-96.

280. Fan, S., et al., *Role of NF-kappaB signaling in hepatocyte growth factor/scatter factor-mediated cell protection.* Oncogene, 2005. **24**(10): p. 1749-66.

281. Martin, T.A., M.D. Mason, and W.G. Jiang, *HGF and the regulation of tight junctions in human prostate cancer cells.* Oncol Rep, 2014. **32**(1): p. 213-24.

282. Feigelstock, D., et al., *The human homolog of HAVcr-1 codes for a hepatitis A virus cellular receptor.* J Virol, 1998. **72**(8): p. 6621-8.

283. Vila, M.R., et al., *Hepatitis A virus receptor blocks cell differentiation and is overexpressed in clear cell renal cell carcinoma.* Kidney Int, 2004. **65**(5): p. 1761-73.

284. Bailly, V., et al., *Shedding of kidney injury molecule-1, a putative adhesion protein involved in renal regeneration.* J Biol Chem, 2002. **277**(42): p. 39739-48.

285. Kuchroo, V.K., et al., *The TIM gene family: emerging roles in immunity and disease.* Nat Rev Immunol, 2003. **3**(6): p. 454-62.

286. Jentoft, N., *Why are proteins O-glycosylated?* Trends Biochem Sci, 1990. **15**(8): p. 291-4.

287. Waanders, F., et al., *Kidney injury molecule-1 in renal disease.* J Pathol, 2010. **220**(1): p. 7-16.

288. Hooper, N.M., E.H. Karran, and A.J. Turner, *Membrane protein secretases.* Biochem J, 1997. **321 (Pt 2)**: p. 265-79.

289. Zhang, Z., B.D. Humphreys, and J.V. Bonventre, *Shedding of the urinary biomarker kidney injury molecule-1 (KIM-1) is regulated by MAP kinases and juxtamembrane region.* J Am Soc Nephrol, 2007. **18**(10): p. 2704-14.

290. Kaplan, G., et al., *Identification of a surface glycoprotein on African green monkey kidney cells as a receptor for hepatitis A virus.* Embo j, 1996. **15**(16): p. 4282-96.

291. Weitz, M., et al., *Detection of a genome-linked protein (VPg) of hepatitis A virus and its comparison with other picornaviral VPgs.* J Virol, 1986. **60**(1): p. 124-30.

292. Probst, C., M. Jecht, and V. Gauss-Muller, *Intrinsic signals for the assembly of hepatitis A virus particles. Role of structural proteins VP4 and 2A.* J Biol Chem, 1999. **274**(8): p. 4527-31.

293. Wang, X., et al., *Hepatitis A virus and the origins of picornaviruses.* Nature, 2015. **517**(7532): p. 85-88.

294. Silberstein, E., G. Dveksler, and G.G. Kaplan, *Neutralization of hepatitis A virus (HAV) by an immunoadhesin containing the cysteine-rich region of HAV cellular receptor-1.* J Virol, 2001. **75**(2): p. 717-25.

295. Silberstein, E., et al., *Alteration of hepatitis A virus (HAV) particles by a soluble form of HAV cellular receptor 1 containing the immunoglobin-and mucin-like regions.* J Virol, 2003. **77**(16): p. 8765-74.

296. Thompson, P., J. Lu, and G.G. Kaplan, *The Cys-rich region of hepatitis A virus cellular receptor 1 is required for binding of hepatitis A virus and protective monoclonal antibody 190/4.* J Virol, 1998. **72**(5): p. 3751-61.

297. Sheridan, A.M. and J.V. Bonventre, *Cell biology and molecular mechanisms of injury in ischemic acute renal failure.* Curr Opin Nephrol Hypertens, 2000. **9**(4): p. 427-34.

298. Ichimura, T., et al., *Kidney injury molecule-1 (KIM-1), a putative epithelial cell adhesion molecule containing a novel immunoglobulin domain, is up-regulated in renal cells after injury.* J Biol Chem, 1998. **273**(7): p. 4135-42.

299. Ichimura, T., et al., *Kidney injury molecule-1 is a phosphatidylserine receptor that confers a phagocytic phenotype on epithelial cells.* J Clin Invest, 2008. **118**(5): p. 1657-68.

300. Kobayashi, N., et al., *TIM-1 and TIM-4 glycoproteins bind phosphatidylserine and mediate uptake of apoptotic cells.* Immunity, 2007. **27**(6): p. 927-40.

301. Yang, L., et al., *KIM-1-mediated phagocytosis reduces acute injury to the kidney.* J Clin Invest, 2015. **125**(4): p. 1620-36.

302. Zhang, Z. and C.X. Cai, *Kidney injury molecule-1 (KIM-1) mediates renal epithelial cell repair via ERK MAPK signaling pathway.* Mol Cell Biochem, 2016. **416**(1-2): p. 109-16.

303. Han, W.K., et al., *Urinary biomarkers in the early diagnosis of acute kidney injury.* Kidney Int, 2008. **73**(7): p. 863-9.

304. Han, W.K., et al., *Kidney Injury Molecule-1 (KIM-1): a novel biomarker for human renal proximal tubule injury.* Kidney Int, 2002. **62**(1): p. 237-44.

305. Vaidya, V.S., et al., *Kidney injury molecule-1 outperforms traditional biomarkers of kidney injury in preclinical biomarker qualification studies.* Nat Biotechnol, 2010. **28**(5): p. 478-85.

306. Tian, L., et al., *Kidney Injury Molecule-1 is Elevated in Nephropathy and Mediates Macrophage Activation via the Mapk Signalling Pathway.* Cell Physiol Biochem, 2017. **41**(2): p. 769-783.

307. Field, M., et al., *Urinary biomarkers of acute kidney injury in deceased organ donors--kidney injury molecule-1 as an adjunct to predicting outcome.* Clin Transplant, 2014. **28**(7): p. 808-15.

308. Vaidya, V.S., et al., *A rapid urine test for early detection of kidney injury.* Kidney Int, 2009. **76**(1): p. 108-14.

309. McIntire, J.J., et al., *Identification of Tapr (an airway hyperreactivity regulatory locus) and the linked Tim gene family.* Nat Immunol, 2001. **2**(12): p. 1109-16.

310. Wills-Karp, M., *Asthma genetics: not for the TIMid?* Nat Immunol, 2001. **2**(12): p. 1095-6.

311. Umetsu, S.E., et al., *TIM-1 induces T cell activation and inhibits the development of peripheral tolerance.* Nat Immunol, 2005. **6**(5): p. 447-54.

312. McIntire, J.J., et al., *Immunology: hepatitis A virus link to atopic disease.* Nature, 2003. **425**(6958): p. 576.

313. McIntire, J.J., D.T. Umetsu, and R.H. DeKruyff, *TIM-1, a novel allergy and asthma susceptibility gene.* Springer Semin Immunopathol, 2004. **25**(3-4): p. 335-48.

314. Morrissey, J.J., et al., *Sensitivity and specificity of urinary neutrophil gelatinase-associated lipocalin and kidney injury molecule-1 for the diagnosis of renal cell carcinoma.* Am J Nephrol, 2011. **34**(5): p. 391-8.

315. Han, W.K., et al., *Human kidney injury molecule-1 is a tissue and urinary tumor marker of renal cell carcinoma.* J Am Soc Nephrol, 2005. **16**(4): p. 1126-34.

316. Cohen, H.T. and F.J. McGovern, *Renal-cell carcinoma.* N Engl J Med, 2005. **353**(23): p. 2477-90.

317. Cuadros, T., et al., *Hepatitis A virus cellular receptor 1/kidney injury molecule-1 is a susceptibility gene for clear cell renal cell carcinoma and hepatitis A virus cellular receptor/kidney injury molecule-1 ectodomain shedding a predictive biomarker of tumour progression.* Eur J Cancer, 2013. **49**(8): p. 2034-47.

318. Shalabi, A., et al., *Urinary NGAL and KIM-1: potential association with histopathologic features in patients with renal cell carcinoma.* World J Urol, 2013. **31**(6): p. 1541-5.

319. Martin, T.A. and W.G. Jiang, *Loss of tight junction barrier function and its role in cancer metastasis.* Biochim Biophys Acta, 2009. **1788**(4): p. 872-91.

320. Wang, Y., T.A. Martin, and W.G. Jiang, *HAVcR-1 expression in human colorectal cancer and its effects on colorectal cancer cells in vitro.* Anticancer Res, 2013. **33**(1): p. 207-14.

321. Cuadros, T., et al., *HAVCR/KIM-1 activates the IL-6/STAT-3 pathway in clear cell renal cell carcinoma and determines tumor progression and patient outcome.* Cancer Res, 2014. **74**(5): p. 1416-28.

322. Kozarsky, K., D. Kingsley, and M. Krieger, *Use of a mutant cell line to study the kinetics and function of O-linked glycosylation of low density lipoprotein receptors.* Proc Natl Acad Sci U S A, 1988. **85**(12): p. 4335-9.

323. DeLoia, J.A., et al., *Regional specialization of the cell membrane-associated, polymorphic mucin (MUC1) in human uterine epithelia.* Hum Reprod, 1998. **13**(1o): p. 2902-9.

324. Komatsu, M., et al., *Reversible disruption of cell-matrix and cell-cell interactions by overexpression of sialomucin complex.* J Biol Chem, 1997. **272**(52): p. 33245-54.

325. Weltman, J.K., et al., *Rapid screening with indirect immunotoxin for monoclonal antibodies against human small cell lung cancer.* Cancer Res, 1987. **47**(21): p. 5552-6.

326. Heinrich, P.C., et al., *Interleukin-6-type cytokine signalling through the gp130/Jak/STAT pathway.* Biochem J, 1998. **334 (Pt 2)**: p. 297-314.

327. Jung, J.E., et al., *STAT3 is a potential modulator of HIF-1-mediated VEGF expression in human renal carcinoma cells.* Faseb j, 2005. **19**(10): p. 1296-8.

328. Molina, M.A., et al., *Trastuzumab (herceptin), a humanized anti-Her2 receptor monoclonal antibody, inhibits basal and activated Her2 ectodomain cleavage in breast cancer cells.* Cancer Res, 2001. **61**(12): p. 4744-9.

329. ProstateCancerUK. *The PSA Test*. November 2016 21/05/17]; Available from: https://prostatecanceruk.org/prostate-information/prostate-tests/psa-test#advantages-and-disadvantages-of-the-psa-test.

330. ProstateCancerUK. *Prostate Biopsy*. July 2016 21/05/17]; Available from: https://prostatecanceruk.org/prostate-information/prostate-tests/prostate-biopsy.

331. CancerResearchUK. *The stages of prostate cancer*. 17/02/14 21/04/16]; Available from: http://www.cancerresearchuk.org/about-cancer/type/prostate-cancer/treatment/the-stages-of-prostate-cancer.

332. ProstateCancerUK. *Active surveillance*. June 2014 26/04/16]; Available from: http://prostatecanceruk.org/prostate-information/treatments/active-surveillance.

333. ProstateCancerUK. *Watchful Waiting*. Jan 2014 26/04/16]; Available from: http://prostatecanceruk.org/prostate-information/treatments/watchful-waiting.

334. Hamdy, F.C., et al., *10-Year Outcomes after Monitoring, Surgery, or Radiotherapy for Localized Prostate Cancer.* New England Journal of Medicine, 2016. **375**(15): p. 1415-1424.

335. Harrison, G.M., et al., *Expression of HAVcR-1/TIM-1 (Hepatitis A virus cellular receptor) in human prostate cancer and its potential role in invasiveness of prostate cancer cells.* Cancer Research, 2005. **65**(9 Supplement): p. 1330-1331.

336. Thomas, L.J., et al., *Development of a Novel Antibody-Drug Conjugate for the Potential Treatment of Ovarian, Lung, and Renal Cell Carcinoma Expressing TIM-1.* Mol Cancer Ther, 2016. **15**(12): p. 2946-2954.

337. Meyers, J.H., et al., *TIM-4 is the ligand for TIM-1, and the TIM-1-TIM-4 interaction regulates T cell proliferation.* Nat Immunol, 2005. **6**(5): p. 455-64.

338. ClinicalTrails.gov. *A Dose Escalation, Safety and Activity Study of CDX-014 in Patients With Advanced or Metastatic Renal Cell Carcinoma*. 2017 05/07/2017 06/07/2017]; Available from: https://clinicaltrials.gov/show/NCT02837991.

339. CancerResearchUK. *Prostate cancer incidence in Europe and worldwide*. 11/06/14 15/02/16]; Available from:

http://www.cancerresearchuk.org/health-professional/prostate-cancer-incidence-statistics#heading-Five.

340.   Martin, T.A., et al., *HAVcR-1 reduces the integrity of human endothelial tight junctions.* Anticancer Res, 2011. **31**(2): p. 467-73.

341.   Sanders, A.J., et al., *Tumour angiogenesis and repulsive guidance molecule b: a role in HGF- and BMP-7-mediated angiogenesis.* Int J Oncol, 2014. **45**(3): p. 1304-12.

342.   Hashem, M. and T. Essam, *Hepatocyte growth factor as a tumor marker in the serum of patients with prostate cancer.* J Egypt Natl Canc Inst, 2005. **17**(2): p. 114-20.

343.   Humphrey, P.A., et al., *Prognostic significance of plasma scatter factor/hepatocyte growth factor levels in patients with metastatic hormone-refractory prostate cancer: results from cancer and leukemia group B 150005/9480.* Clin Genitourin Cancer, 2006. **4**(4): p. 269-74.

344.   Davies, G., et al., *The HGF/SF antagonist NK4 reverses fibroblast- and HGF-induced prostate tumor growth and angiogenesis in vivo.* Int J Cancer, 2003. **106**(3): p. 348-54.

345.   Adan, A., Y. Kiraz, and Y. Baran, *Cell Proliferation and Cytotoxicity Assays.* Curr Pharm Biotechnol, 2016. **17**(14): p. 1213-1221.

346.   Ye, L., et al., *HGF/SF up-regulates the expression of bone morphogenetic protein 7 in prostate cancer cells.* Urol Oncol, 2008. **26**(2): p. 190-7.

347.   Moro, L., et al., *Up-regulation of Skp2 after prostate cancer cell adhesion to basement membranes results in BRCA2 degradation and cell proliferation.* J Biol Chem, 2006. **281**(31): p. 22100-7.

348.   Brierley, J., M. Gospodarowicz, and B. O'Sullivan, *The principles of cancer staging.* Ecancermedicalscience, 2016. **10**: p. ed61.

349.   Varkaris, A., et al., *The role of HGF/c-Met signaling in prostate cancer progression and c-Met inhibitors in clinical trials.* Expert Opin Investig Drugs, 2011. **20**(12): p. 1677-84.

350.   Zhou, C.K., et al., *Prostate cancer incidence in 43 populations worldwide: An analysis of time trends overall and by age group.* Int J Cancer, 2016. **138**(6): p. 1388-400.

351.   Sci Rep.

352.   Liotta, L.A., *Adhere, Degrade, and Move: The Three-Step Model of Invasion.* Cancer Res, 2016. **76**(11): p. 3115-7.

353.   Oke, J.L. and J.W. O'Sullivan, *The mapping of cancer incidence and mortality trends in the UK from 1980-2013 reveals a potential for overdiagnosis.* 2018. **8**(1): p. 14663.

354.   Yang, W., et al., *Nuclear PKM2 regulates beta-catenin transactivation upon EGFR activation.* Nature, 2011. **480**(7375): p. 118-22.

355.   Lee, Y., et al., *WNT signaling in glioblastoma and therapeutic opportunities.* Lab Invest, 2016. **96**(2): p. 137-50.

356.   Kolonel, L.N., D. Altshuler, and B.E. Henderson, *The multiethnic cohort study: exploring genes, lifestyle and cancer risk.* Nat Rev Cancer, 2004. **4**(7): p. 519-27.

357. Rohrmann, S., et al., *Family history of prostate cancer and obesity in relation to high-grade disease and extraprostatic extension in young men with prostate cancer.* Prostate, 2003. **55**(2): p. 140-6.

358. Adjakly, M., et al., *Prostate cancer: The main risk and protective factors-Epigenetic modifications.* Ann Endocrinol (Paris), 2015. **76**(1): p. 25-41.

359. Jiang, W.G., et al., *Hepatocyte growth factor, its receptor, and their potential value in cancer therapies.* Crit Rev Oncol Hematol, 2005. **53**(1): p. 35-69.

360. Epstein, J.I., *An update of the Gleason grading system.* J Urol, 2010. **183**(2): p. 433-40.

361. Feoktistova, M., P. Geserick, and M. Leverkus, *Crystal Violet Assay for Determining Viability of Cultured Cells.* Cold Spring Harb Protoc, 2016. **2016**(4): p. pdb.prot087379.

362. Brewster, D.H., et al., *Risk of hospitalization and death following prostate biopsy in Scotland.* Public Health, 2017. **142**: p. 102-110.

363. ProstateCancerUK. *What tests will I have at the hospital?* Feb 2014 21/04/16]; Available from: http://prostatecanceruk.org/prostate-information/getting-diagnosed/what-tests-will-I-have-at-the-hospital?what-tests-will-.

364. CancerResearchUK. *Prostate cancer tests*. 20/02/14 [cited 21/04/16; Available from: http://www.cancerresearchuk.org/about-cancer/type/prostate-cancer/diagnosis/prostate-cancer-tests.

365. Algaba, F., *Pitfalls of Pathologic Staging in Prostate Cancer.* European Urology Supplements, 2008. **7**(1): p. 6-14.

366. Nieto, M.A., et al., *EMT: 2016.* Cell, 2016. **166**(1): p. 21-45.

367. Brabletz, T., et al., *EMT in cancer.* Nat Rev Cancer, 2018. **18**(2): p. 128-134.

368. Thiery, J.P., et al., *Epithelial-mesenchymal transitions in development and disease.* Cell, 2009. **139**(5): p. 871-90.

369. Gotzmann, J., et al., *A crucial function of PDGF in TGF-beta-mediated cancer progression of hepatocytes.* Oncogene, 2006. **25**(22): p. 3170-85.

370. Zhu, W., B. Leber, and D.W. Andrews, *Cytoplasmic O-glycosylation prevents cell surface transport of E-cadherin during apoptosis.* Embo j, 2001. **20**(21): p. 5999-6007.

371. Wagoner, M.P., K. Ling, and R.A. Anderson, *Tracking the transport of E-cadherin to and from the plasma membrane.* Methods Mol Biol, 2008. **457**: p. 267-78.

372. Onder, T.T., et al., *Loss of E-cadherin promotes metastasis via multiple downstream transcriptional pathways.* Cancer Res, 2008. **68**(10): p. 3645-54.

373. Yilmaz, M. and G. Christofori, *EMT, the cytoskeleton, and cancer cell invasion.* Cancer Metastasis Rev, 2009. **28**(1-2): p. 15-33.

374. UniversityOfDundee. *Human Protein-Protein Interaction Prediction*. 12/09/2008 14/06/18]; Available from: http://www.compbio.dundee.ac.uk/www-pips/evidence.jsp?Prot=IPI00018274&Prot1=2386&Prot2=13085&Interactions=Prot&LR=0.125&modules=on.

375. Cogli, L., et al., *Vimentin phosphorylation and assembly are regulated by the small GTPase Rab7a.* Biochim Biophys Acta, 2013. **1833**(6): p. 1283-93.

376.   Kalluri, R. and R.A. Weinberg, *The basics of epithelial-mesenchymal transition.* J Clin Invest, 2009. **119**(6): p. 1420-8.
377.   Heerboth, S., et al., *EMT and tumor metastasis.* Clin Transl Med, 2015. **4**: p. 6.
378.   Lamouille, S., J. Xu, and R. Derynck, *Molecular mechanisms of epithelial-mesenchymal transition.* Nat Rev Mol Cell Biol, 2014. **15**(3): p. 178-96.
379.   Montanari, M., et al., *Epithelial-mesenchymal transition in prostate cancer: an overview.* Oncotarget, 2017. **8**(21): p. 35376-35389.